UNIVERSITEIT·STELLENBOSCH·UNIVERSITY
jou kennisvennoot • your knowledge partner

Performance Characterization of Cement Treated Sand Base Material of Mozambique

by

Ebenhaezer Roux de Vos

Thesis presented at the University of Stellenbosch in partial fulfilment of the requirements for the degree of

Master of Science in Engineering

Study leader: Prof. F. Hugo Pr.Ing

March 2007

Declaration

I, the undersigned, hereby declare that the work contained in this thesis is my own original work and that I have not previously in its entirety or in part submitted it at any university for a degree.

Signature: . . . . . .

E.R. de Vos

Date: . . . . . .

Abstract

Mozambique is investing heavily in rehabilitating and upgrading the current roadway infrastructure. Investigation by the Mozambican roads authority found that some consulting engineers and contractors were not familiar with Mozambican conditions and materials. The World Bank sponsored a research project to support the roadway infrastructure preservation and maintenance efforts. The thesis work presented forms an integral part of the work conducted by the World Bank project research team. The objective of the thesis is to characterise cement stabilized sand bases in Mozambique under Accelerated Pavement Testing (APT) in terms of stiffness and deflection responses under load trafficking. This work forms the basis for developing guidelines for a mechanistic-empirical design method for Mozambican conditions and materials. Reported findings from initial MMLS3 testing conducted for the World Bank project were used to scope the full-scale research study and provided guidelines for the selection and construction of full scale test sections on natural subgrade. The APT presented encompass full-scale pavement testing including wet trafficking cycles to emulate environmental effects.

Pavement responses under traffic loading were monitored by deflection, seismic and surface rut measurements. Surface crack formation was photographically recorded and visually evaluated. Diagnostic evaluation of the pavement structure was conducted after test completion through trenching. The measured data was reduced, analysed and presented according to methodologies developed in this thesis.

Six test sections were comprehensively trafficked by the MLS10, responses monitored and diagnostically evaluated. A total of 1.51 million 60 kN and 1.93 million 70 kN axle loads was applied. The MLS10 APT program for trafficking selected test sections and Non-Destructive Test (NDT) methodologies used for response monitoring proved very effective in the characterization of stiffness and deflection trends for cement stabilized sand bases under repeated loading. Pavement distress mechanisms under APT were

found to be similar to that of in-service highways and mechanisms found in reported exploratory scaled APT studies. Three distress mechanisms were found to occur under traffic loading: (1) HMA-CTB interface distress, (2) in-plane horizontal shear at the midpoint of the combined pavement structure as well as (3) transverse and longitudinal flexural fatigue cracking of the CTB.

Stiffness performance functions for the different zones in which the failure mechanisms occur were developed through analysis of the dispersion curves from intermitted seismic testing. This enabled continuous stiffness characterization under traffic loading and subsequent enhanced pavement performance modelling. Performance trends in terms of and under load applications yielded sound information for establishment of exploratory transfer functions and material fatigue curves for two of the three principle distress mechanisms found. Pavement performance sensitivity to material shear and flexural strength parameters were illustrated. Subsequently CTB material and pavement structure critical parameters were established as the material shear and flexural strengths and traffic induced stresses respectively.

A material damage exponent n of 12.5 (in $F = [P/80]^n$) was determined for the thin 5 percent cement stabilized sand base pavement structures. From the responses monitored a stiffness – deflection relation was established which may be utilised for simple CTB condition evaluation during pavement management surveys.

Results reported in this thesis should serve to support the preservation, maintenance and upgrading efforts that are currently underway in Mozambique. The research study yielded a significant amount of invaluable findings which will provide the basis for development of the Mozambique Mechanistic Pavement Design Method (MMPDM). Successful implementation of the synthesis and recommendations of this study would lead to a total pavement engineering system if appropriately applied.

Opsomming

Mosambiek is tans besig met rehabilitasie en opgradering van hul padnetwerk. n Ondersoek deur die Mosambiek se padowerheid het getoon dat konsultant ingenieurs asook kontrakteurs nie vertroud is met die gebruik van Mosambiek se materiale en toestande nie. Die Wêreld Bank het n navorsings projek geborg met die doel om die huidige padnetwerk infrastruktuur onderhoud en instandhouding pogings te steun. Die doelstelling van die tesis is die karakterisering van sement gestabiliseerde sand kroonlae in Mosambiek deur middel van Versnelde Plaveisel Toetsing (VPT) in terme van styfheid en defleksie gedrag asook falings meganismes. Hierdie navorsing sal as basis dien vir die ontwikkeling van riglyne vir n meganisties – empieriese ontwerp metode vir Mosambiek se toestande en materiale.
Rapporteerde bevindings van geskaalde MMLS3 toetse ,gedoen as deel van die Wêreld Bank navorsingsprojek, op dieselfde materiale het as riglyne gedien vir seleksie en bepaling van die volskaalse toets seksies se konstruksie op natuurlike stutlae in Mosambiek. Die VPT wat voorgelê word sluit volskaalse plaveisel toetsing met nat lassiklusse om omgewings effekte te simuleer in.

Plaveisel gedrag onder verkeers belasting is gemonitor deur oppervlak defleksie, siesmiese en oppervlak sporing meetings. Oppervlak kraking is fotografies vasgelê en visueel ge-evalueer. Diagnostise evalueering van die plaveisel struktuur is na afloop van die toets deur middel van uitgrawings gedoen. Gemete plaveisel gedrags reaksie data is gereduseer, analiseer en voorgestel volgens metodologiee ontwikkel in hierdie tesis.

Ses toets seksies is volledig met die MLS10 (Volskaalse Mobiele Las Simuleerder) belas en ge-evalueer. In toetaal is daar 1.51 miljoen 60 kN en 1.93 mijoen 70 kN aslasse tydens die toetsprogram aangewend. Die VPT program van die MLS10 vir die

bepaalde toets seksies en Nie Destruktiewe Toets (NDT) methodologiëe aangewend was effektief ten opsigte van die karakteriseering van styfheid en defleksie neigings onder herhaalde belasting. Plaveisel falings meganismes gevind deur diagnostiese evalueering na afloop van VPT stem ooreen met die van hoofweë tans in gebruik asook die meganismis gerapporteer vanuit geskaleerde VPT studies. Drie plaveisel falings meganismes is gevind na herhaalde verkeers belasting:

(1) Faling van die Asphalt-Gestabiliseerde kroon kontakvlak
(2) In vlak horistontale skuifskeur by die middelpunt van die gekombineerde plaveisel struktuur, asook
(3) longitudinale en transverse buig vermoeiings kraaking van die sement gestabiliseerde kroonlaag.

Styfheids gedragsfunksies vir die verskillende sones waarin die verskeie falings meganismes voorkom is ontwikkel deur analise van seismiese despersie kruwes van tussentydse seismiese meetings. Hierdie styfheids gedragsfunksies het kontinue styfheids karakteriseering vir die plaveisels onderhewe aan herhaalde verkeers belasting bewerkstellig en sodoende plaveisel gedrags modelleering verbeter. Plaveisel gedrags neigings onder en in terme van asherhalings het goeie inligting geproduseer vir die ontwikkeling van voorlopige oordrags funksies en materiaal vermoeiings funksies vir bevinde falings meganismis. Die plaveisel se werksverrigting sensitiwiteit ten opsigte van materiaal skuif en buig sterkte parameters was hierdeur geillustreer. Gevolglik is die kritiese sement gestabiliseerde materiaal en plaveisel parameters as die materiaal skuif en buig sterktes asook verkeer geinduseerde spannings vasgestel.

n Materiaal skade eksponent n van 12.5 ($F = [P/80]^n$) is gevind vir 5 persent sement gestabiliseerde sand kroonlae. Styfheids-Defleksie gedrags verhoudings is ontwikkel en kan benut word as n plaveisel toestand peiling metodiek vir plaveisel bestuur stelsels.

Resultate gerapporteer moet die huidige onderhoud, opgradering en instandhouding pogins in Mosambiek ondersteun. Die navorsings studie het n beduidende hoeveelheid kosbare bevindings gelewer wat as die basis van die ontwikkeling van die Mosambiek Meganistiese Plaveisel Ontwerp Metode (MMPOM) sal dien. Suksesvolle

implimentering van die sintese en aanbevelings uit hierdie studie sal to n totale plaveisel ingenieurs bestuur stelsel lei as dit toepaslik aangewend word.

Acknowledgements

I would like to express my sincere gratitude to the following people and organizations who have contributed to making this work possible:

- To our Heavenly Father for the opportunities, gifts and strength.
- Supervisor and mentor Prof Fred Hugo, for the great privilege of studying and working under him. Invaluable lessons learned and skills acquired. Introducing me to different fields and levels of engineering.
- Mnr Johan Muller, MLS10 Design Engineer.
- Alett Slabbert, Institute of Transport Technology secretary.
- Student members of the MLS team Johan Gerber, Louis Maree, Carl Fredericks and Carlos of Mozambique.
- The Mozambican local team of Simbine, Focas, Augostino, Romeo and friend Vasco – obrigado.
- I am grateful for the opportunity that I had to be a part of a great team. The collective thinking, innovation, creativity and individualism made the team effort an invaluable learning experience.
- World Bank Mozambique research project team: Dr Pieter Strauss, Dr Jorge Prozzi, Ken Fults and Andre Smit
- MC Barnard and family, Resident Engineer in Mozambique at time of construction.
- Families De Vos, Schutte, Maree and friends for support, enthusiasm and encouragement.
- Steyn and Corrie de Vos, father and mother.
- The Institute of Transport Technology and the National Department of Transport for the financial support.
- The department of Civil Engineering Prof. Bester and his staff for the opportunity to study at Stellenbosch University

- The research that was reported in this thesis was done as an integral part of project,

206/CON/ES/DEN/2003 for the ANE. The funding was sponsored by the World Bank. The author gratefully acknowledges permission to publish the findings.

- Lucas-Jan Ebels, doctoral student
- The laboratory team: Colin Isaacs and Gavin Williams.
- The workshop personnel: Oom Andries, Dion Viljoen and Louis Fredericks

Contents

Declaration ii

Abstract iii

Opsomming v

Acknowledgements viii

Contents x

List of Tables xiv

List of Figures xx

Nomenclature xxi

1 Introduction **1**

1.1 Context of the problem 2

1.2 Scope of work 3

1.3 Objectives 8

1.4 Outline 8

2 Literature Review **9**

2.1 Accelerated Pavement Testing 10

2.1.1 Evaluation, Validation, and Improvement of Structural Designs 11

2.1.2 Vehicle–Pavement–Environment Interaction 12

2.1.3 Material characterization 13

2.1.4 Enhancement of Modelling in Pavement Engineering 13

2.1.5 Pavement Engineering Applications and Issues 15
2.2 Seismic Pavement Testing 17
2.3 Cement Treated Base Material 20
2.4 Pavement Deflection Measurements 20
2.5 Closure 21

3 Research Methodology for Accelerated Pavement Testing 22
3.1 Elements pertaining to pavement response generation 22
3.1.1 Material 22
3.1.1.1 Mozambique geology 25
3.1.1.2 Physical characteristics 25
3.1.1.3 Chemical characteristics 28
3.1.1.4 Stabilizing agents 29
3.1.1.5 Strength characteristics 29
3.1.2 Pavement design 31
3.1.3 Pavement Construction 34
3.1.4 Accelerated Pavement testing 37
3.1.4.1 MLS10 APT Device 37
3.1.4.2 Test Protocol 41
3.2 Data Acquisition 42
3.2.1 Recording equipment 43
3.2.2 Recording procedure 48
3.3 Data Processing 49
3.3.1 Seismic stiffness 49
3.3.1.1 Modulus plots 49
3.3.1.2 Layered extraction 50
3.3.1.3 Data interpretation 54
3.3.2 Dynamic Surface deflection 54
3.3.3 Transverse surface rutting 55
3.4 Data Presentation 55
3.5 Diagnostic Evaluation 57

4 Results and Findings of Applied Test Methodologies 60
4.1 Material strength tests 61

4.2 Deflection performance 65
4.3 Stiffness performance curves 70
4.4 Surface rut formation 74
4.5 Surface crack formation 75
4.6 Diagnostic evaluation 78

5 Synthesis 81
5.1 Mechanisms of failure 82
51.1 Shear failure at surface - CTB interface 82
5.1.2 Longitudinal en transverse flexural cracking 83
5.1.3 Formation of shear plane in CTB 85
5.2 Material Damage factor 90
5.3 Development of flexural fatigue transfer function 91
5.4 Development of interface shear performance and fatigue functions 92
5.5 Stiffness deflection relation 96
5.6 Comparison of findings to the SAMPD 97
5.7 Discussion of Synthesis 102

6 Conclusions, Recommendations for future research and closure 107
6.1 Conclusions 107
6.2 Recommendations for future research 110
6.3 Closure 112

References 113

Appendices

A: Accelerated and Seismic pavement testing 119

B: Deflection performance plots 210

C: Stiffness performance plots 213

D: Surface rutting performance plots 216

E: Pictorial overview Section 4A 222

F: Pictorial overview Section 4B 234

G: Pictorial overview Section 5A 242

H: Pictorial overview Section 5B 243

I: Pictorial overview Section 8 246

J: Pictorial overview Section 7 255

K: Stiffness – Deflection relation 259

List of Figures

2.1 Interrelationship between pavement engineering facets that collectively and individually contribute to knowledge (Hugo et al. 1991) 10

3.1a Flowchart overview of total research project 23
3.1b Methodology layout of pavement response generation, monitoring and evaluation 24
3.2 Wet and Dry Sieve analysis of Red and Yellow sand types 26
3.3 Electron microscope photos of Yellow sand vs. Red sand 27
3.4 Polished red sand disc for determining chemical composition of surface layer using backscatter detector (100µm) 28
3.5 Shear split test setup (side and frontal view) 30
3.6 Layout of test sections constructed adjacent to highway EN1 36
3.7 Schematic of MLS10 with Bogie Detail 39
3.8 View of the MLS10 trafficking on the test site at Manhiça in Mozambique 40
3.9 View of the MLS10 lifted in pavement monitoring and visual inspection configuration 40
3.10 Portable Seismic Pavement Analyser 43
3.11 Typical time records form PSPA and SPA Manager software detail 45
3.12 Typical dispersion curve obtained from time records in Figure 3.10 and phase spectra detail 45
3.13 Relationship between seismic and low-strain resilient moduli for granular base material (Nazarian et al., 2004) 46
3.14 View of the modified Benkelman Beam setup under the MLS10 47
3.15 MLS10 APT test section layout 49
3.16 Typical seismic stiffness vertical profiles with axle load applications 50
3.17a Plan View of the CTB slab extracted from 5 percent cement stabilized full scale test section 4 after 340 00 60 kN load repetitions for diagnostic investigation (550 x 1200 mm length and width as indicated by the white arrows) 52
3.17b Elevation View of the CTB slab extracted from 5 percent cement stabilized full-scale test section 4 after 340 000 load repetitions for diagnostic investigation (160 x 1200 mm height and width as indicated by the white arrows) 52
3.17c View of underside of HMA extracted from full scale test section 4 after 340 000

	load repetitions for diagnostic investigation showing marked positions of cracks	53
3.17d	Side view of beams taken from scaled 3 percent cement stabilized section after 150 000 2.7 kN load repetitions. Note progressive phases of failure	53
3.17e	Close-up of 3 percent cement base with seal, shear plane on neutral axis of the 3 percent cement stabilized 50 mm scaled pavement clearly visible after 150 000 2.7 kN axle load repetitions	54
3.18	Weibull probability of failure distribution for different β–values	56
3.19a	Removed HMA after dual box cut by diamond blade grinder	58
3.19b	CTB block ready for removal all surrounding CTB material	58
3.19c	Shifting of CTB block with hydraulic jack to prevent formation of non-traffic related fractures	59
4.1	General pavement structure and compostion of sections tested	60
4.2	Indirect tensile strength growth chart for cemented material tested	62
4.3	Influence of age on compressive strength of cemented materials (Croney and Croney, 1991)	65
4.4a	Initial unftrafficked deflection bowls for sections tested with 60 kN axle load	66
4.4b	Initial unftrafficked deflection bowls for sections tested with 70 kN axle load	67
4.5	Deflection profiles for Section 5A monitored at intervals during axle load trafficking	68
4.6	Maximum deflection growth trends with axle load applications for respective test sections (Axle load 60 kN and 70 kN indicated with *)	68
4.7	Comparative Stiffness Performance Chart for Top of CTB in Longitudinal Direction	71
4.8	Comparative Stiffness Performance Chart for Middle of CTB in Longitudinal Direction	71
4.9	Comparative Stiffness Performance Chart for Bottom of CTB in Longitudinal Direction	72
4.10	Comparative Stiffness Performance Chart for Top of CTB in Transverse Direction	72
4.11	Comparative Stiffness Performance Chart for Middle of CTB in Transverse Direction	73
4.12	Comparative Stiffness Performance Chart for Bottom of CTB in Transverse Direction	73
4.13	Transverse surface rut profiles with load applications for Section 5	74
4.14	Cumulative maximum rut depth for sections tested	75

4.15a	Isometric views of cracked surface at different stages of traffic loading Transverse shear crack initiation at 270 000 60 kN load applications - Section 4	76
4.15b	Transverse propagation of shear cracks at 285 000 60 kN load applications -	76
4.15c	Continuous transverse cracks and longitudinal crack formation after 320 000 60 kN load applications - Section 4	77
4.15d	Plan view of cracking pattern after 1 million 70 kN load applications on Section 7	77
4.15e	Overview of Section 7 after 1 million 70 kN load applications	78
5.1a	Pictorial view of HMA-CTB interface distress surfaces, Section 8 (note longitudinal shear markings) Underside of HMA	83
5.1b	Top of CTB	83
5.2a	Plan and side views of CTB block extracted from 5 percent cement stabilized Section 4B after 150 000 70 kN load applications Side view – note two longitudinal cracks and in-plane shear crack (direction of traffic indicated with arrow)	84
5.2b	Plan view (direction of traffic indicated with arrow)	85
5.3	Shear stress plots for 5 percent CTB under 60 kN axle load	86
5.4a	Front, plan and rear views of fractured CTB extracted form Section 4B Front view - note horizontal shear plane and longitudinal cracks	87
5.4b	Plan view – note transverse crack	87
5.4c	Rear view – note horizontal shear plane	88
5.5	Stiffness – Deflection performance of 2.5 % cement and 2.5 % lime stabilized red base material under 60 kN axle loading	89
5.6	Relationship between traffic induced stress and wheel loads trafficked for flexural fatigue	92
5.7	Flexural fatigue of 5 percent cement stabilized sand	92
5.8	Shear interface failure performance curve for sand cement stabilized bases	94
5.9	Interface shear fatigue curves for cement stabilized sand bases	95
5.10	Stiffness - Deflection relations for cement treated base materials tested	96
5.11	Stiffness deflection trends for percentage binder and corresponding axle load	97
5.12	Long-term behavior of lightly cemented material	99
5.13	Crush initiation and advanced crushing for lightly cemented layers	101
5.14	Design flow diagram for interface distress mechanism	105
5.15	Design flow diagram for flexural fatigue failure mechanism	106
A.1	Interrelationship between pavement engineering facets that collectively and individually contribute to knowledge (Hugo et al. 1991)	120
A.2	Effect of speed on pavement deflection (Lourens 1995)	127

A.3 Effects of wheel load and temperature on permanent deformation 129
A.4 Impact of water ingress on pavement performance (Rust et al. 1997) 132
A.5 Schematic outline depicting the interaction between SA–HVS APT results and real-life Implementation and pavement performance (De Beer et al. 2001) 144
A.6 The final result from surface wave or deflection based testing of pavements is a stiffness modulus profile of the test section (Rydèn 2004) 155
A.7 Schematic illustration showing shear modulus stress and strain dependency (Rydèn 2004) 156
A.8 A plane wave in space and time. The phase velocity vector is indicated with an arrow. 158
A.9 Result from the steady state vibration method on a pavement profile. The depth to each layer interface has been correlated with the wavelength divided by 2, from Heukelum and Foster (1960). 161
A.10 Schematic of experimental arrangement for SASW tests, from Rix et al. (1991). 162
A.11 Example from SASW field plots received instantly on site. In (a) time signals from both receivers, (b) the coherence function of the recorded signals, and (c) the wrapped phase of the cross power spectrum. The example is taken from a SASW test on a pavement construction with receiver spacing, D=1.3 meters. 164
A.12 Calculated dispersion curve from data in Figure A.6, (a) wavelength domain and (b) frequency domain. Marked line shows the usable range according to the wave filter criteria presented by Heisey et al. (1982). 165
A.13 SASW flow chart, from Wu et al., (2002). 166
A.14 Illustration of whole space, half space and layered half space concepts 181
A.15 Illustration of a sinusoidal waveform 182
A.16 Rayleigh wave amplitude as a function of depth for various values of Poisson's ratios (from Richart et al, 1970) 186
A.17 Major types of seismic waves and their respective motions (from Braile, 2003) 187
A.18 Wave field generated due to a harmonic vertical point source acting on a homogenous isotropic, elastic halfspace (from Richard et al, 1970) 190
A.19 Lamb's solution for a vertical point or line source acting on a homogenous, isotropic, elastic half space. Both radial motion (top) and vertical motion (bottom) are shown (from Richart et al, 1970, after Lamb 1904) 191
A.20 Representation of a waveform in (a) time domain view, (b) 3-D view, and (c) frequency domain view (From Agilent Technologies, 2000) 192
A.21 A transient signal shown in time and frequency domains (From Agilent Technologies Application note 243, 2000) 193
A.22 Phasor model of signal (From Marven, 1996) 193
A.23 Idealized linear system (a) and actual linear system (b) 197

A.24 Response of a linear network to a single sine wave input signal (From Agilent Technologies, 2000) 200
A.25 Frequency response components of a linear network (From Agilent Technologies, 2000) 201
A.26 Effect of wavelength in a layered medium (from Foti, after Rix 1988) 204
A.27 Typical shape of dispersion curves obtained from normally and inversely dispersive profiles (From Foti, after Rix 1988) 206
A.28 Concept of the steady state vibration technique to construct a dispersion curve (from Das, 1992) 207

B.1 Maximum Deflection at Slow Speed vs. Axle Load Application for Section 4B – 70 kN Axle Load 210
B.2 Maximum Deflection at Slow Speed vs. Axle Load Application for Section 5A – 60 kN Axle Load 210
B.3 Maximum Deflection at Slow Speed vs. Axle Load Application for Section 5B – 60 kN Axle Load 211
B.4 Maximum Deflection at Slow Speed vs. Axle Load Application for Section 8 – 70 kN Axle Load 211
B.5 Maximum Deflection at Slow Speed vs. Axle Load Application for Section 7 – 70 kN Axle Load 212
B.6 Maximum Deflection Growth Trends with Equivalent 60 kN Axle Load Applications for Respective Test Sections 212

C.1 Comparative Stiffness Performance Chart for Top of CTB in Longitudinal Direction for Equivalent 60 kN axle loads 213
C.2 Comparative Stiffness Performance Chart for Middle of CTB in Longitudinal Direction for Equivalent 60 kN axle load 213
C.3 Comparative Stiffness Performance Chart for Bottom of CTB in Longitudinal Direction for Equivalent 60 kN axle loads 214
C.4 Comparative Stiffness Performance Chart for Top of CTB in Transverse Direction for Equivalent 60 kN axle loads 214
C.5 Comparative Stiffness Performance Chart for Middle of CTB in Transverse Direction for Equivalent 60 kN axle loads 215
C.6 Comparative Stiffness Performance Chart for Bottom of CTB in Transverse Direction for Equivalent 60 kN axle loads 215

D.1 Transverse rut profiles with load applications for Test Section 4A 216
D.2 Cumulative maximum rut depth for Test Section 4A 216
D.3 Transverse rut profiles with load applications for Test Section 4B 217

D.4 Cumulative maximum rut depth for Test Section 4B 217
D.5 Transverse rut profiles with load applications for Test Section 5A 218
D.6 Cumulative maximum rut depth for Test Section 5A 218
D.7 Transverse rut profiles with load applications for Test Section 5B 219
D.8 Cumulative maximum rut depth for Test Section 5B 219
D.9 Transverse rut profiles with load applications for Test Section 8 220
D.10 Cumulative maximum rut depth for Test Section 8 220
D.11 Transverse rut profiles with load applications for Test Section 7 221
D.12 Cumulative maximum rut depth for Test Section 7 221

K.1 Stiffness Deflection relations for base materials tested (Deflection in mm) 259
K.2 Stiffness Deflectoin performacne of 5 % Cement stabilized Red base material under 60 kN axle laoding 259
K.3 Stiffness Deflectoin performacne of 5 % Cement stabilized Red base material under 70 kN axle laoding 260
K.4 Stiffness Deflectoin performacne trends of 2.5 % Cement and 2.5 % Lime stabilized Red base material under 60 kN axle laoding 260
K.5 Stiffness Deflectoin performacne of 2.5 % Cement and 2.5 % Lime stabilized Red base material under 60 kN axle laoding 261
K.6 Stiffness Deflectoin performacne trends of 7 % Cement stabilized Red base material under 70 kN axle laoding 261

List of Tables

3.1	Summary of hydrometer test results	26
3.2	Quantative Analysis of Major Elements in Red and Yellow sands particles	28
3.3	Chemical composition of surfaces coatings for red and yellow sands	29
3.4	Composition of full-scale test sections	32
3.5	Summary of Construction Test Results at Manhiça Mozambique	35
3.6	MLS10 APT machine parameters	38
3.7	Average test surface temperatures during full-scale APT study	41
4.1	Summary of MLS10 tests	61
4.2	Summary of material test results conducted on laboratory prepared specimens	62
4.3	Summary of test results obtained from tested full-scale field test section cores at an age of 1.5 years	63
4.4	Summary of ITS test results of cores taken from scaled laboratory test sections at an age of 1.5 years	63
4.5	Initial untrafficked modified Benkelman beam deflection bowls (µm)	66
4.6	Summary of Deflection Data for Full-Scale Test Sections	69
4.7	Summary of rut depths at termination of testing for respective test sections	75
5.1	Stress to strength ratios for the interface and shear plane failure mechanisms	88
5.2	Results from pavement shear stress analysis and reported by de Beer et al. (2002)	94

Nomenclature

AASHTO	American Association of State Highway and Transportation Officials
ALF	Accelerated Loading Facility
ANE	National Administration of Roads
APT	Accelerated Pavement Testing
ARRB	Australian Road Research Board
BB	Benkelman Beam
CAPTIF	Canterbury Accelerated Pavement Testing Indoor Facility
CEDEX	Spanish Centro De Estudios De Carreteras test facility
CSIR	Council for Scientific and Industrial Research Organization
CTB	Cement Treated Base
CTCR	Cement-Treated Crushed Rock
FWD	Falling Weight Deflectometer
GEMs	Granular Emulsion Mixes
HMA	Hot-Mix Asphalt
HVS	Heavy Vehicle Simulator
ITS	Indirect Tensile Strength
LAMBs	Large Aggregate Mixes for Bases
LTPP	Long-Term Pavement Performance
LVDT	Linear Variable Differential Transducer
MAASHTO	Modified AASHTO
MBB	Modified Benkelman Beam
MLS10	Full-Scale Mobile Load Simulator
MMLS3	One-Third Scale Mobile Load Simulator
MMPAM	Mozambique Mechanistic Pavement Design Method
NDT	Non-Destructive Testing
PMS	Pavement Management System
PSPA	Portable Seismic Pavement Analyzer
SABS	South African Bureau of Standards
SASW	spectral analysis of surface waves
SAMDM	South African Mechanistic Design Method
TRH	Technical Recommendations for Highways
TRL	Transport Research Laboratory (United Kingdom)
US	University of Stellenbosch
VRSPTA	Vehicle–Road Surface Pressure Transducer Array

Symbols:

A	Amplitude
C	Carbon
E	Elastic modulus, Young's Modululs
G	Shear Modulus
N	Number of axles
O	Oxygen
T	Period
V	Velocity
Al	Aluminum
Fe	Iron
Ti	Titanium
ρ	Mass Density of Material
V	Poisson's Ratio
β	Beta
σ	Stress
ε	Strain
τ	Shear Stress
γ	Shear Strain
f	Frequency
λ	Wavelength
$\prod$	Pi
V_p	Raleigh Wave Speed
V_s	Shear Wave Speed
ω	Angular frequency
r	Raduis

Chapter 1

Introduction

Mozambique is investing heavily in rehabilitating and upgrading their current roadway infrastructure. Coastal sands are being used extensively as a base material when stabilized with cement. In the past extensive use has been made of design consulting engineers as well as contractors that were not necessarily familiar with Mozambican conditions and materials. Insufficient knowledge regarding marginal pavement material, related construction techniques and long term pavement performance of these materials resulted in premature pavement failures. Discussions with role players such as the National Administration of Roads - ANE (Administracao Nacional de Estradas), design consultants and contractors, revealed that bases built with stabilized fine grained materials and, specifically, sand materials of the coastal plains normally showed distress in the form of disintegration of the surface of the base at the contact zone with the surfacing. Furthermore, a high incidence of shrinkage cracking in cement stabilized fine grained bases leads to reflection cracking, the entrance of water and failures in the form of potholes, which are difficult to repair in remote areas. The World Bank sponsored a research project, Contract 206/CON/ES/DEN/2003: Evaluation of Long Term Behavior of Pavement Layered Materials by Means of Accelerated Pavement and Supplementation/Verification Testing in Mozambique, to support the roadway preservation and maintenance efforts currently underway in Mozambique. The objective of the World Bank Project is to develop guidelines for a mechanistic-empirical pavement design method for cement stabilized sand bases in Mozambique based on *Accelerated Pavement Testing (APT)* technology. The APT program encompasses both scaled (one

third) and full-scale APT using mobile load simulator technology: Model Mobile Load Simulator (MMLS3) and Full-Scale Mobile Load Simulator (MLS10). The relation between the Word Bank research project and the thesis are presented further under the scope of work, Section 1.2.

1.1 Context of the problem

Mozambique generally lacks suitable base and sub base road building materials and special efforts need to be made by ANE, the design consulting engineers and the contractors to:

- appraise as well as evaluate the performance of different pavement designs and construction techniques;
- investigate alternative pavement designs using available but sometimes substandard road building materials;
- adhere to project specifications and perform appropriate quality control to avoid unnecessary and costly repairs to prematurely damage areas after construction or rehabilitation.

A number of pavement and rehabilitation design methods being used worldwide are being used in Mozambique as well. Some are not necessarily applicable to Mozambican conditions resulting in the implementation of inappropriate designs and construction techniques leading to poor performance. The South African Mechanistic Design Procedure (SAMDP) is extensively used in Mozambique. However, the SAMDP is based on performance transfer functions developed for South African materials and conditions that have been found inappropriate for Mozambican conditions.

The lack of knowledge about the appropriate engineering properties of locally available road building materials, mostly sands but also finely graded material is the main cause of unsuccessful projects. Main contributors to the premature failures of pavements appear to be:

(i) specification of incorrect stabilizer or incorrect stabilizer content;
(ii) inappropriate construction practices;
(iii) lack of understanding of behaviour and the long term performance of these

materials;

(iv) very high axle loads and extreme climatic conditions;

(v) inability to maintain roads due to lack of funds and skills.

There is a great need to understand the performance of this substandard material under traffic loading and to evaluate critical pavement parameters relating to mechanisms of failure. Accelerated Pavement Testing (APT) using not only full scale loading on real pavements but also scaled testing in the laboratory is considered to be an appropriate testing technique to simulate the material properties and to evaluate the performance of different pavement structures in a short period of time. Scaled APT in the laboratory using the MMLS3 provides a comparison, in terms of pavement behavior and performance, between alternative materials under the same environmental and subgrade conditions.

APT of materials under these conditions of loading together with the experience and information obtained on the performance of pavement sections that were built, provide opportunity for development of appropriate transfer functions for mechanistic design of pavements in Mozambique.

1.2 Scope of work

The research presented in this thesis was conducted as an integral part of The World Bank sponsored Contract 206/CON/ES/DEN/2003: Evaluation of Long Term Behavior of Pavement Layered Materials by Means of Accelerated Pavement and Supplementation/ Verification Testing in Mozambique. The employer being ANE, primary consultant The University of Texas at Austin, subcontracted consultant MLS Test Systems (Pty) Ltd.

The thesis research forms an integral part of the work conducted by the research team under The World Bank contract and reported as mentioned under Phases 1 and 2 that are presented subsequently. The author acted as the principle investigator and performed the leading roll in the monitoring, analysis and synthesis of the pavement response data. The stiffness performance characterization methodology followed and subsequent deductions were solemnly developed by the author. Research team members' input is noted and referenced where applicable. A great deal of input

information (Phase 1) came from the reported contract research and is referenced accordingly. The scope of the contract research provided the guidelines for establishing the objectives for the research presented in this thesis. The opinions expressed in this thesis are therefore that of the author and do not necessarily reflect those of the research team members.

The sandy materials used in this research study are those most commonly used by local consultants and the most abundant material available in the coastal plains of the southern region. These are the reddish and yellowish coloured sands. Mentioned sands were fine in particle size, rounded to semi-rounded in texture and have a single sized particle distribution. These sands were used for rehabilitation of the national road by the contractor and consultant that facilitated the construction of the full-scale test sections on the same road section.

The research contract comprises four phases, each will be described briefly to give an overview of the input into the research conducted for this thesis and illustrate the relevant guidelines for development of the objectives thereof:

Phase 1 : Problem identification and pre-APT study

The objective of the first phase was to maximize the impact of the research and was aimed at identification of the areas where research was required. Problem areas regarding:

(a) modes of failure,
(b) material behavior and performance under traffic loading,
(c) deficiencies in current testing methods and
(d) the lack of identifying pavement behavior through laboratory testing were discussed with the client, design consultants and contractors.

Construction methods that lead to failures and deficiencies in specifications that resulted in unacceptable performance were addressed.

A number of tasks were completed. These include:

(1) Materials were characterized by supplementary laboratory testing and
(2) Exploratory MMLS3 testing were conducted on scaled laboratory pavements.
(3) The framework for development of the final MMPDM was developed.
(4) Specifications for the construction of field test sections for conduction of full-scale and model APT studies were developed based on results from preliminary scaled laboratory APT and material tests.

Information obtained through Phase 1 and findings reported were used for the establishment of the guidelines and background elements for this thesis (points 2, 3 and 4 above). Supplementary/verification testing conducted in Phase 1 forms part of the work presented in the thesis.

Phase 2: Accelerated pavement testing (APT) and Supplementation/Verification Testing (SVT)

The objective of this phase was the adaptation and completion of the exploratory laboratory testing program, interactively with the experience gained from Phase 1; construction of the field test sections; full-scale and model field APT by means of full-scale Mobile Load Simulator (MLS10) and MMLS3. The outcome of this phase is the performance characterization of the selected pavement materials for establishment of appropriate transfer functions and related design parameters.

The bulk of the full-scale APT testing as set out under Phase 2 above will be reported in this thesis. Pavement response monitoring under full-scale traffic loading in terms of CTB stiffness, pavement deflection and surface crack formation responses as well as subsequent deductions and synthesis pertaining to pavement performance forms the core of the thesis work presented. Details pertaining to the

construction of the full-scale test sections are also presented to provide background information pertaining to the elements of the full-scale APT.

Phase 3: Development of Transfer Functions and Estimation of Life Cycle Costs

The objectives of this phase are the validation and calibration of transfer functions, development of viable maintenance and rehabilitation strategies and life cycle cost analysis. The transfer functions to be developed will be based on the background from the SAMDP, the AASHTO 2002 Guide for the Design of New and Rehabilitated Pavement Structures and work carried out by the Transportation Research Laboratory (TRL) of the United Kingdom. Viable maintenance and rehabilitation strategies will be selected and probabilities associated with each strategy estimated. Life cycle cost analysis will be aimed at determination of optimum pavement design strategy.

Preliminary transfer functions developed by the author based on the synthesis of the measured pavement responses, findings from diagnostic evaluation and CTB material testing are presented in the thesis.

Phase 4: Compilation of the Mozambican Mechanistic Pavement Design Method (MMPDM)

A pavement design method for Mozambique along the lines of the South African Mechanistic Pavement Design and Analysis Method will be documented.

Phases 1 and 2 have been completed and reported to ANE (Strauss et al. 2005; 2006). An academic paper comparing the performance of scaled MML3 tests vs. full-scale MLS10 tests under Mozambican conditions (De Vos et al. 2006) has been presented at the Transportation Research Board General Meeting in January 2007 and accepted for publication on the proceedings CD-Rom. The research paper provides an overview of the scaled laboratory APT program and subsequent findings. It should be noted that the

paper was submitted in August 2006 and presents research finished up to that point in time.

The scope of work presented in this thesis will be the aspects pertaining only to the response characterization of the full-scale APT tests conducted with the MLS10. Response performance measures addressed includes CTB stiffness loss, surface deflection, surface deformation and surface crack formation monitoring under trafficking. The reason for focusing on the CTB stiffness performance under traffincking is to enhance the modelling of pavement performance for mechanistic design of these pavement structures with thin cement treated bases. Diagnostic evaluation of the pavement structures after completion of APT testing for characterization of failure mechanisms is also reported. Characterization of pavement failure mechanisms are important for establishing the critical pavement parameters to be considered during design. Background information will be presented regarding the material characteristics, pavement design (inputs from Phase 1) and construction as well as the APT device and test methodology (inputs from Phase 2 and research presented by De Vos (2004)). Response measurement, analysis, results and subsequent synthesis of full-scale test conducted will be discussed in greater depth.

The research study was limited with regard to the following aspects:

- Materials used for construction of the full-scale test sections were representative of the greater geographical area of coastal plains and dunes. The study was focused only on the single sized sands found in the southern part of Mozambique. Subsequently findings are applicable to materials conforming to the same standards and not a greater material range.
- Full-scale APT was limited to the application of 6 million equivalent 60 kN axles only. Not all sections constructed could be tested and only selected ones of the sections tested were trafficked up to terminal pavement condition.
- Full-scale APT traffic loading was applied in the channelized method; this was due to the limitation on the total number of axle loads applied for the research contract. Lateral wander during load application was subsequently outside the scope of the work. This limited the research with regard to establishment of the relationship between the channalized and transverse loading methodologies.

The World Bank research project started in November 2004 with the scaled laboratory APT testing in Stellenbosch. Construction of full-scale test sections in Mozambique was carried out in June 2005. Full-scale field APT in Mozambique started in April 2006 and was carried on to January 2007 with some intermediate stoppages.

1.3 Objectives of this study

The objective of this research study is to characterize the performance of thin cement stabilized sand bases under loading through accelerated pavement testing in terms of:

- stiffness performance;
- surface deflection under loading;
- pavement failure mechanisms manifested during full-scale traffic loading.

The ultimate objective is the subsequent development of general performance trends pertaining to specific failure mechanisms and pavement responses derived from synthesis of the above mentioned pavement performance and responses.

1.4 Outline of this study

Chapter 2 gives a background study on the philosophy and fundamentals of APT and Non-Destructive Testing (NDT). A literary review of work done in the field of CTB performance characterization by means of APT is also presented in this chapter.
In Chapter 3 the various methodologies developed for data generation, acquisition, processing and presentation of pavement response monitoring under repeated full-scale loading are discussed and presented. Chapter 4 is the exposition of the respective results and findings of material tests and pavement response monitoring methodologies proposed in Chapter 3. Results presented in Chapter 4 are synthesized and discussed in Chapter 5. This thesis is concluded and recommendations are made in Chapter 6.

Chapter 2

Literature review

Short overviews of accelerated and seismic pavement testing fundamentals are presented in this chapter. The reader is referred to Appendix A for excerpts from a synthesis on accelerated pavement testing and literature reviews on non-destructive testing and the physical fundamentals thereof.

The focus of the presented literature review on APT is the elements and the factors thereof that should be considered during the evaluation of APT results. The basic fundamentals of seismic NDT are shortly presented since this form the basis for the primary findings and the results presented in this study. The primary objectives of this literature review are to illustrate:

- The roles that APT and NDT fulfill in the process of pavement design;
- The appropriateness of the research methodology followed for characterization of the CTB with NDT under APT conditions;
- The current status of the art regarding the fields covered.

The reader is further referred to supplementary information pertaining to cement treated base material and the performance thereof in Southern Africa as well as pavement deflection measurements. Performance of the thin sandy cement treated bases in Mozambique has been found not to conform to the models of South African cement treated materials and conditions. A short overview of cement treated base performance according to the SAMPD system is presented in Chapter 5.

2.1 Accelerated Pavement Testing

The objectives of this subsection are to provide the reader with an broad overview of the important elements of APT and to highlight the respective elements and factors that needs to be considered during the evaluation of APT test results. The primary focus will be on the elements affecting CTB performance under traffic loading. This subsection is supplemented with relevant extracts from NCHRP Synthesis 325: Significant Findings from Full-Scale Accelerated Pavement Testing (Hugo and Epps, 2004) presented in Appendix A.

The definition of APT according to Hugo and Epps (2004) are as follow:

> "*Accelerated pavement testing is defined as the controlled application of wheel loading to pavement structures for the purpose of simulating the effects of long-term in-service loading conditions in a compressed time period. APT is a facet of pavement engineering and generates knowledge over a wide spectrum.*"

Figure 2.1 from Hugo et al. (1991) in Hugo and Epps (2004) places APT programs in context to the broad basis of pavement engineering.

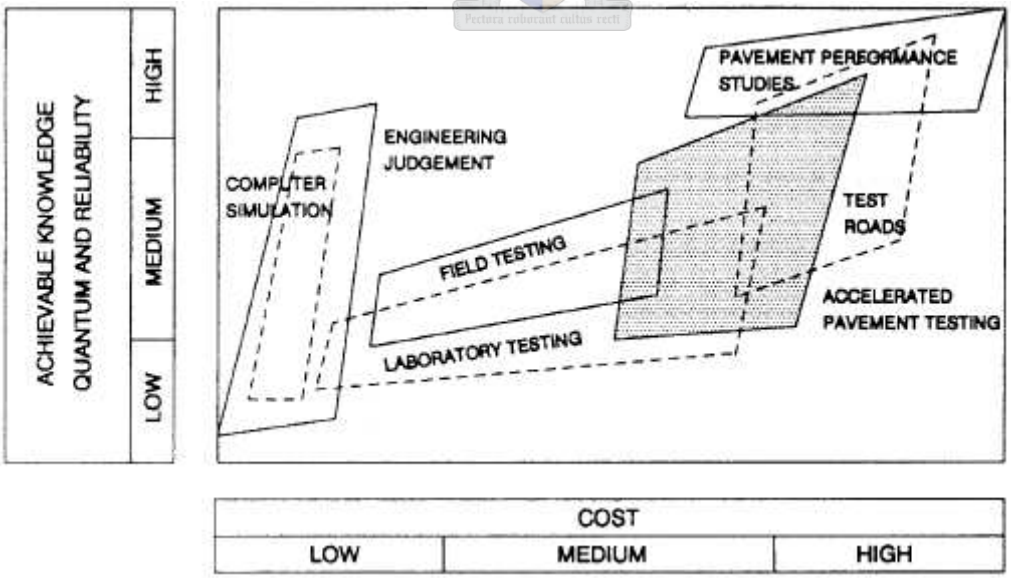

Figure 2.1: Interrelationship between pavement engineering facets that collectively and individually contribute to knowledge (Hugo et al. 1991)

APT programs provide significant insight into pavement performance and are usually supplemented with laboratory testing programs to gain more benefit thereof. Environmental conditioning during APT is very important since material performance could be significantly influenced by the environmental conditions prevalent during testing.

APT is briefly discussed under the following topics that relate to elements of the pavement system:

- Evaluation, validation, and improvement of structural designs;
- Vehicle–pavement–environment interaction;
- Evaluation of materials and tests;
- Enhancement of modelling in pavement engineering;
- Pavement engineering applications and issues.

2.1.1 Evaluation, Validation, and Improvement of Structural Designs

APT research is used to enhance structural design of pavements. Structural design of pavements should be considered together with other fields of pavement engineering such as materials and vehicle-pavement-environment interaction for evaluation of the pavement system as a whole. Reported applications of accelerated pavement testing to asphalt pavement designs and composite pavement structures in South Africa are cited and discussed.

In South Africa the Heavy Vehicle Simulator (HVS) testing program has been instrumental in the development of the South African Mechanistic Design Method (SAMDM). According to Theyse et al. (1996) in Hugo and Epps (2004) results of HVS testing were used to develop transfer functions for the mechanistic-empirical modelling of the permanent deformation of unbound pavement layers in pavements with asphalt and granular base layers as well as stabilized and granular subbase layers. Catalogued standard pavement structures has been validated and refined in the field using HVS testing. Pavement design confidence levels were established from extensive testing on a range of pavement structures to assess the reliability of design methodologies.

The effectiveness of the inverted pavement structure, used extensively throughout South Africa, has also been validated by HVS testing. APT has further contributed to advances made in stabilization of marginal materials for strengthening of pavements. Road agency structural design guidelines have also been refined and validated through APT, discussed in more detail in Appendix A.

2.1.2 Vehicle–Pavement–Environment Interaction

The structural pavement system, comprising the pavement design and materials used, is subjected to traffic loading under the prevailing environmental conditions that affect the pavement system's performance. These environmental conditions are time dependent and have variable levels of control to a greater or lesser degree. Overall pavement performance is dependent on the interaction of these environmental factors. The following elements and factors thereof need to be considered during the development and selection of accelerated pavement testing protocols:

- Axle load trafficking
    - Wheel load compositions, e.g. single or multiple axle
    - Nature of the wheel load, e.g. static of dynamic
    - Nature of wheel load application, e.g. channelized trafficking or lateral wander
    - Type of suspension system used
    - Tyre type, pressure and contact stress
    - Speed of trafficking

- Environmental impact
    - Temperature
    - Surface and subsurface water and or moisture
    - Wind and solar radiation.

It is imperative that the environmental factors influencing pavement performance under load application should be addressed in development of the test methodology and controlled during testing. Proper incorporation of vehicle-pavement–environment interaction should benefit the quality and applicability of APT results. Findings reported from studies conducted on the above mentioned factors are quoted from the synthesis on APT reported by Hugo and Epps (2004) in Appendix A.

2.1.3 Material characterization

Evaluation of pavement material response and performance is the primary objective of many full-scale APT programs. These performance characterization programs are often related to material characterization and testing in the laboratory. When evaluating APT and laboratory test results it is very important to consider the differences in terms of loading and environmental conditions, failure definitions as well as techniques and analysis of measurement.

Pavement performance monitoring generally involves measurement of:

- transverse and longitudinal profiles;
- pavement deformation and deflection in response to a moving wheel load or falling weight at the pavement surface or with depth;
- in situ material densities;
- environmental conditions e.g. temperature and moisture;
- visual surface distress;
- and in situ stresses and strains.

Seismic wave and in situ permeability testing as well as diagnostic trenching after test completion have been reported. Simultaneous testing by scaled and full-scale APT for the evaluation of different environmental conditions has also been reported by Walubita et al. (2000). Different effects of environmental conditioning could also be assed through laboratory testing and modelling.

Numerous APT tests have been conducted to evaluate the performance of stabilized granular or unbound materials used as base or subbase pavement materials. Test programs conducted and findings reported by the Australian Loading Facility (ALF), the SA – HVS, CSIR, CAPTIF, LA ALF and CEDEX are cited and discussed in Appendix A1.

2.1.4 Enhancement of Modelling in Pavement Engineering

Pavement performance and performance modelling as described by Hugo and Epps (2004) are as follow:

> *"Pavement performance is a measure of the extent to which a pavement fulfils its principal objective. Performance models are tools to predict performance; they may ultimately be used in pavement management systems, in the structural design of pavements, and in the development of performance-related specifications."*

APT provides a window on pavement performance which could be used to predict how the pavement will perform under real traffic as reported by Jooste et al. (1997) in Hugo and Epps (2004).

One of the immediate benefits of APT is that pavement performance can be modelled directly. This is possible through control of performance influencing variables such as wheel loads and tire pressures, pavement structures, layer thicknesses and materials as well as environmental conditions like temperature and moisture conditions.

According to Hugo and Epps (2004) models developed as part of APT research include:

- *"Pavement damage*
- *Subgrade rutting performance*
- *Asphalt rutting performance*
- *Asphalt cracking and fatigue performance and*
- *Elasto-plastic behaviour of unbound materials."*

Pavement performance modelling through APT is also limited. Limitations include:

(1) The inability of APT to account for time related factors that influence distress e.g. environmental and traffic related influences.
(2) The relation between APT performance and performance under conventional traffic
(3) The applicability of localized models to other sites.

The limitations of APT have necessitated the normalization of data to reference parameters. The limitations also motivated development of models based on probabilistic approaches.

2.1.5 Pavement Engineering Applications

The relationship of accelerated pavement testing to in-service pavements with conventional trafficking as well as rutting, fatigue and cracking failure criteria's will be touched upon in this subsection.

The question is often asked: Why is there a difference between APT and conventional traffic? There are two reasons according to Metcalf (1996) as presented in Hugo and Epps (2004):

> • *"Environmental effects, especially long-term aging, are difficult to capture in APT. (The combined effect of environment and time difference is not simulated.)*
> • *A full spectrum of in-service wheel loads are not applied in APT."*

APT programs have to consider these two factors when developing methodologies to utilizing the APT results optimally. Formal *Long Term Pavement Performance* LTPP studies usually feature during development of the methodologies to optimize APT research output. The relationship between APT and in-service highway performance is an important aspect of the evaluation and application APT results. An overview by Hugo and Epps (2004) of the South African approach to this issue are quoted in Appendix A. Generally APT findings are transformed in various ways to enable usage of the results for the specific purposes.

An issue relating to the comparability of APT and conventional in-service pavement performances is the selection of appropriate pavement failure criteria. This should be done to define the benchmarks for performance evaluation comparison of APT and in-service pavement structures.

Factors that should be taken into account are the:

- size of the test sections;
- differences in the nature of traffic loading;
- differences in the pavement performance time scale;
- limited number of experiments and
- limited ability to determine pavement condition non-destructively.

Rutting and fatigue cracking are the two types of load related distress generally considered for the definition of pavement failure criteria.

Rutting is the distress form which is easier to monitor and evaluate. Measured rut performance of the section tested is generally used as the representative of the in-service road that it presents. The averaged maximum rut recorded at a cross section in the test section is generally reported.

Pavement fatigue performance relates to the stiffness loss and cracking of pavement layers. According to Bhario et al. (1998) in Hugo and Epps (2004) it is generally accepted that pavement layer failure has occurred once the in situ stiffness has lowered to a level of 50 percent of the initial untrafficked pavement layer stiffness. Monitoring of surface crack development under full-scale APT is therefore necessary. According to Hugo and Epps (2004) various methodologies for monitoring and recording of crack orientation and categorizing has been reported (Scheffy 1999, Hugo et al. 1997 and Groenendijk et al. 1997).

Pavement layer fatigue performance characterization reported in this thesis was done with non-destructive seismic wave methods.

The presented literature review of APT illustrated the role that APT fulfills in pavement design and the appropriateness of the research methodology followed for the Mozambican APT project.

After Hugo and Epps (2004), APT results have in essence been applied toward:

- *"Validation and modification of design procedures,*
- *Pavement configuration comparison in terms of performance,*
- *Evaluation of material performance,*
- *Performance prediction of pavements,*
- *Evaluation and improvement of construction practices, and*

Evaluation of maintenance and rehabilitation practices."

2.2 Seismic Pavement Testing

The reader is introduced to non-destructive testing and the fundamentals of seismic pavement testing in this subsection. The reader is further referred to Appendix A that contains excerpts of the literature study presented by Rydèn (2004) in his doctoral thesis: Surface Wave Testing of Pavements and adjusted excerpts of report MBTC – 2032, Development of Testing Protocol and Correlation for Resilient Modulus of Subgrade Soils, conducted by Dennis and Bennett (2005) for the Arkansas State Highway and Transportation Department. This is appended for the purpose of giving the reader more insight into more detailed technical overview of elastic and seismic waves, signal processing and the development of an experimental dispersion curve for seismic pavement testing.

Non-destructive testing (NDT) techniques are used to estimate the resilient moduli of material that constitute pavement layers of a pavement structure without changing the structural composition of the material layer.

NDT testing has several advantages over laboratory testing of materials:

- NDT could be carried out much faster and is less expensive
- A larger volume of material could be evaluated
- Materials could be tested in situ, resulting in better representation of material properties.

In situ testing is beneficial since it evaluates resilient modulus under prevalent environmental conditions and state of stress.

The Falling Weight Deflectometer (FWD) is one of the most popular NDT methods currently used to estimate resilient modulus of pavement layers. The FWD is based on deflection measurements on the pavement surface resulting from a dynamic impact load. This methodology enables the backcalulation of the resilient modulus of each pavement layer. This method produces good estimates of the actual non-linear response of the complete pavement system a relatively large levels of strain (Ullidtz, 1998). However FWD testing have several limitations which do not produce unique results.

Resilient moduli of a material are not a constant property. It is a function of stress and environmental conditions. Thus resilient modulus is considered to be a seasonal variable material property and should be accounted for appropriately during design of pavement systems.

Seismic pavement testing started to gain popularity in determining moduli of layered pavement systems thought the specteral analysis of surface waves technique (SASW). Wave propagation techniques affect tested material in the linear elastic region and provide material properties that are not affected by non-linear properties. Wave propagation techniques offer dynamic stiffness properties representative of very low strain levels (Ryden 2004).

Seismic Pavement Testing

SASW allows the thickness and resilient modulus of each pavement layer of a system to be estimated though using a combination of elastic wave propagation theory and signal processing techniques. The SASW method is based on the dispersive nature of surface waves in a layered medium after Nazarian (1995) from Dennis and Bennett (2005).

Surface waves are stress waves traveling along the surface of a material (pavement surface). The velocity of wave propagation is dependent on the elastic properties of that medium. This principle is used in seismic pavement testing, to estimate stiffness and thickness of the different layers in the pavement structure (Ryden 2004).

To conduct seismic testing two receivers is placed on the medium (pavement surface in this instant). The receivers are connected to a digital signal analyzer. An impact is applied to the pavement surface to generate seismic surface waves. Surface waves (Raleigh waves or R waves) carry the most seismic energy and makes the most dominant arrival making it the easiest to measure. Particle movement caused by passing surface waves are sensed by receivers and transformed into electrical signals. Raleigh wave velocity is calculated using equation 2.1 with ΔX the distance between the receivers and Δt the time of the wave front to travel between the receivers.

$$V = \frac{\Delta X}{\Delta t} \tag{2.1}$$

Subsequently shear wave velocity V_S could be calculated from surface wave velocity V_R and Poisson's ration *v* though equation 2.2.

$$V_S = V_R\,(1.13 - 0.16v) \tag{2.2}$$

Shear modulus G could be calculated from the shear wave speed using

$$G = \rho\, V_s^2 \tag{2.3}$$

Subsequently the Young's modulus E could be determined from the shear modulus G through the Poisson's ratio v of the material using

$$E = 2\,(1+v)\,G \tag{2.4}$$

Both the shear modulus, shear wave velocity and subsequently the elastic modulus are profoundly dependent of the skeleton stiffness (mean effective stress state) of particulate materials.

The objective of seismic non-destructive testing (NDT) of pavements is to estimate the unknown structural properties, stiffness and thickness, of the different pavement layers in a pavement structure. Efficient techniques can map these properties as functions of space and time, providing a valuable tool in pavement design and management (Ryden 2004).

2.3 Cement treated base material

The reader is referred to the following publications for supplementary information pertaining to cement treated materials and the performance thereof under simulated loading conditions in Southern Africa:

- Aspects of the design and behaviour of road structures incorporating lightly cementious layers, PhD Dissertation of Morris de Beer, 1990.
- Improving mechanistic design of cementious materials, Project Report PR 88/027 for South African Roads Board, March 1991.
- A structural design procedure for cement-treated layers in pavements, DSc Dissertation of Eddie Otte 1978.

Permanent deformation behaviour of pavements with cementitious layers is discussed. Most of the behaviour was characterized through extensive studies conducted with the Heavy Vehicle Simulator (HVS). Two basic types of failure mechanisms, associated with cement treated base pavements were identified and discussed in detail. Investigation into the rate of deformation indicated it to be linear. Concepts of life to initiate compression failure and effective fatigue life are introduced.

The work presented in the above referred publications formed the basis for the development of the transfer functions for the SAMPD system. Excerpts of an overview of the SAMPD system by Theyse et al. (1996) are presented in Chapter 5 where a comparison is drawn between the SAMPD system and the findings reported in this thesis.

2.4 Pavement deflection measurements

Since deflection measurement was only used to characterize pavement behaviour and deflection properties and methodology not investigated in full depth the author provides a list of relevant source material to obtain supplementary information on surface deflections:

- Analysis and development of some pavement rehabilitation design methods, PhD Dissertation of Gerrit Jordaan 1988.

- Aspects of deflection basin parameters used in mechanistic rehabilitation design procedures for flexible pavements in South Africa. PhD Dissertation of Emile Horak, 1988.
- A comparative analysis of deflection measurement techniques for roads using the falling weight deflectometer and deflectorgraph. Project Report for M.Ing Thesis. Jürgen Gentz, 2007.

2.5 Closure

The literature overview presented illustrates the appropriateness of the various individual and overall research methodologies followed for the characterization of the sandy CTB material of Mozambique. The different roles that APT and NDT fulfil in general pavement evaluation, design validation and improvements of structural design are also illustrated. Important elements of vehicle-pavement-environmental interaction was also presented and discussed. Material characterization, enhancement of modelling and pavement engineering applications and issues were presented and discussed.

The reader was referred to Appendix A for excerpts of background information on seismic pavement testing. The established surface wave methods and fundamentals of measured parameters are also described. Part 2 of Appendix A is appended with the objective of explaining the technical detail of seismic waves and data processing and analysis.

Readers are referred to relevant source material for supplementary information pertaining to experiences from full-scale testing of cement treated base material in Southern Africa and surface deflection measurements. This chapter is followed by Chapter 3 in which the various research methodologies are set out.

Chapter 3

Research Methodology for Accelerated Pavement Testing

This chapter describes the methodology for characterization of cement stabilized sand base performances and responses developed and utilized by the author. Background information pertaining to CTB performance characterization from the research project is presented in terms of material, pavement design and construction and APT device and test protocols. Methods of data acquisition, processing and presentation are presented subsequently. Figure 3.1a provides an overview of the Mozambique APT project to illustrate the work flow and applicability of the scaled MMLS3 laboratory testing. This chapter also describes the development of pavement response data and analysis thereof as illustrated in Figure 3.1b.

3.1 Elements pertaining to pavement response generation

Details of elements considered and processes followed to develop pavement responses under traffic loading are presented in this subsection. These include material characterization, pavement design, construction as well as APT device and test protocols. Pavement design and construction specifications are based on aspects of the first phase of the project reported by the project team. (Strauss et al. 2005; 2006). This entailed interviews with design consultants, contractors and the roads agency, results of construction experiments carried out by the research team in Mozambique and scaled laboratory MMLS3 testing carried out by the author in Stellenbosch.

3.1.1 Material

Background information regarding various aspects of Mozambican material and the material used in this research study are presented in this subsection.

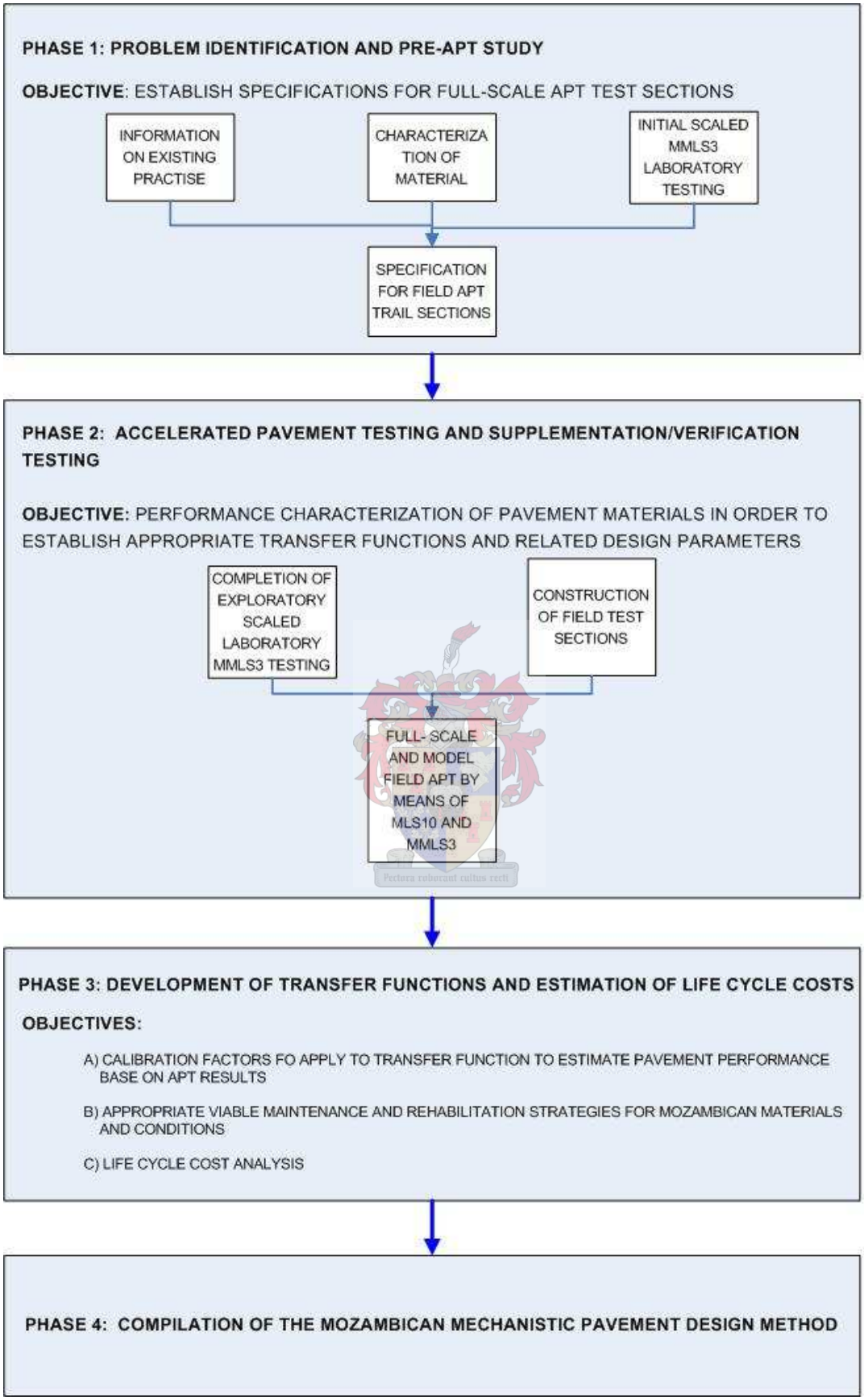

Figure 3.1a: Flowchart overview of total research project

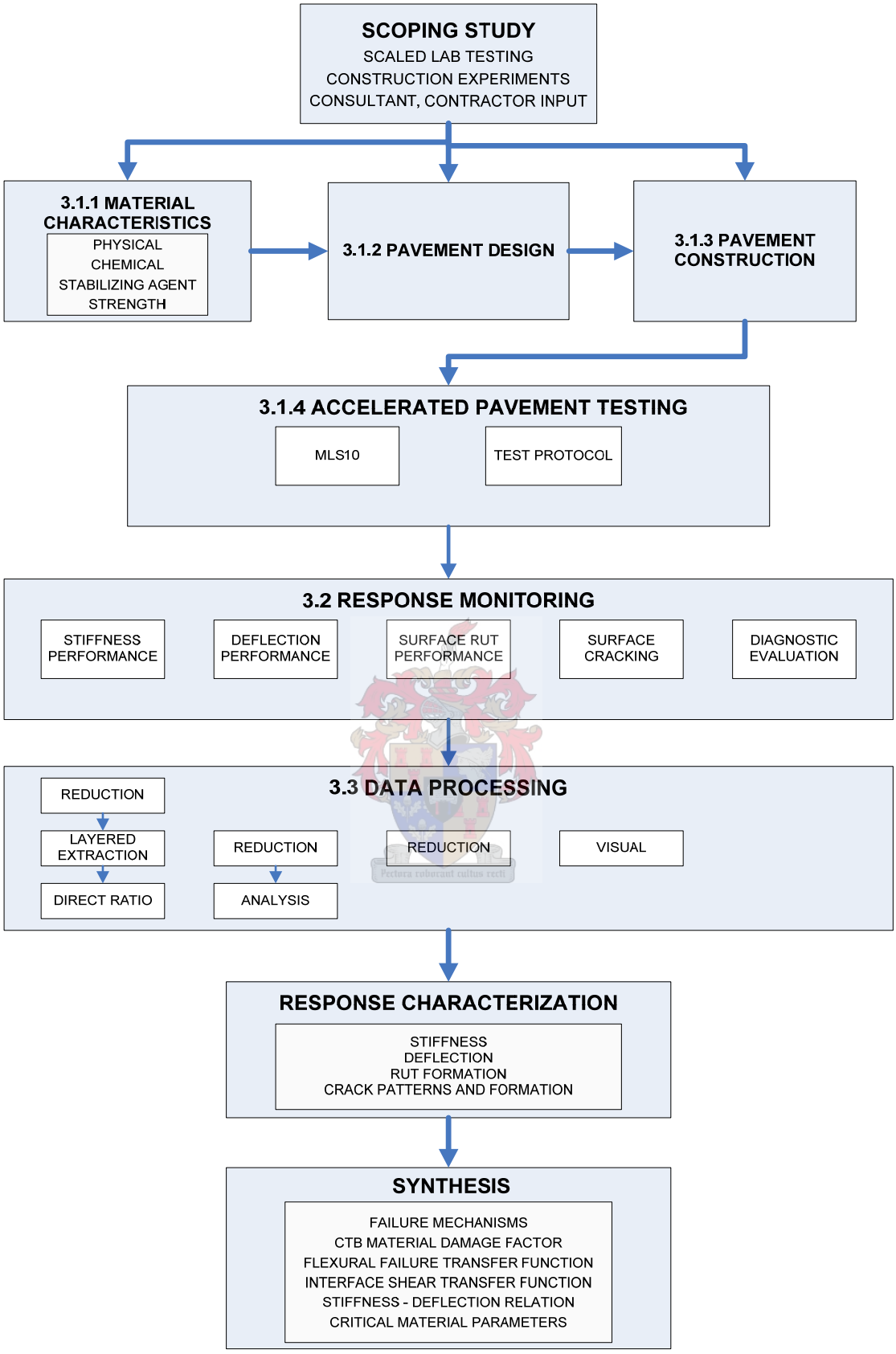

Figure 3.1b: Methodology layout of pavement response generation, monitoring and evaluation

3.1.1.1 Mozambican geology

Mozambique, located in southeast Africa, has a 2,500 km coastline with the Indian Ocean and a wide coastal plain that varies in width from 150 to 600 km. The major part of the country consists of undulating plateaus. Mountainous areas occur along the border with Zimbabwe.

Mozambique's geology is highly varied and consists mainly of Precambrian terrains (ranging from Archaean to Upper Proterozoic rocks), covered predominantly in the south by Phanerozoic cover (ranging from Jurassic through to Tertiary rocks) (Bigioggero et al. 1989).
Soil distribution in Mozambique generally follows the physiographic characteristics. The southern region and the coastal plains have sandy soils. The dominant soils of the coastal dunes and coastal plains of Mozambique are Arenosols, with Gleysols found in secondary occurrence, Fluvisols dominate the extensive floodplains along the Limpopo, Changane and Elephant Rivers (Pinna et al. 1993).

The materials used in this research study are those most commonly used by local consultants and the most abundant material available in the coastal plains of the southern region. These are the reddish and yellowish coloured sands. These two sands were evaluated in terms of physical, chemical and strength chrematistics.

3.1.1.2 Physical Characteristics

Wet and dry sieve as well as hydrometer analysis for the evaluation of particle size distribution were performed on the two sand types, according to Methods A1(a),(b) and A6 (TRH 1 1986) respectively.
Particle size distribution from the wet and dry sieve analysis is illustrated in Figure 3.2 and hydrometer results are set out in Table 3.1.

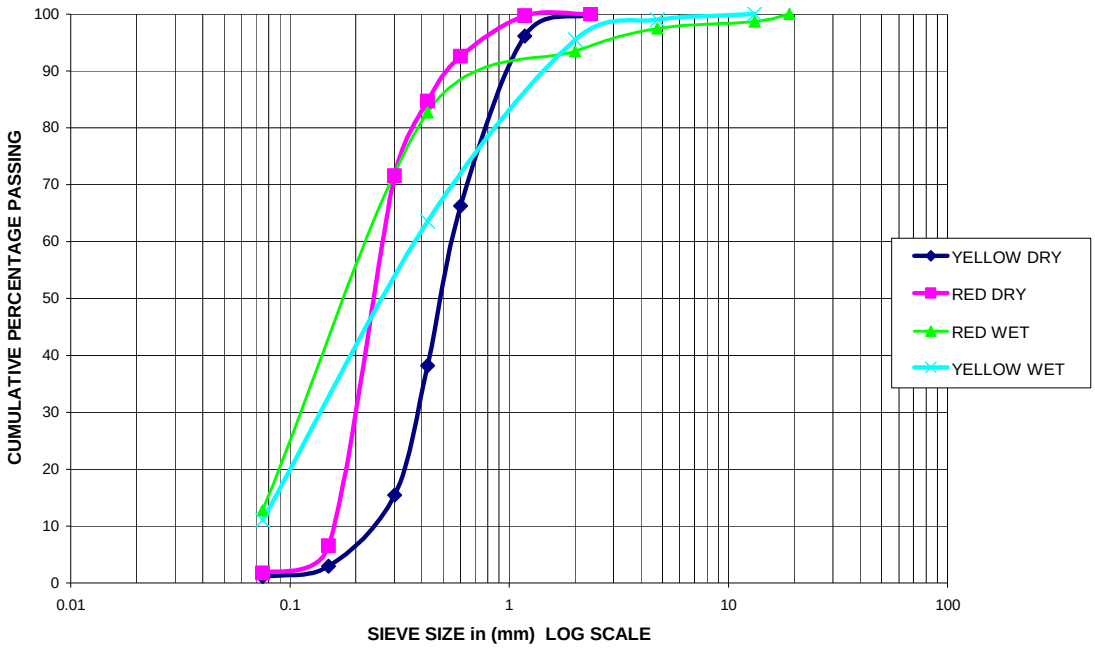

Figure 3.2: Wet and Dry Sieve analysis of Red and Yellow sand types

Table 3.1: Summary of hydrometer test results

FRACTION	FRACTION SIZE	RED	YELLOW
		PERCENTAGE	PERCENTAGE
COARSE SAND	2.0 mm > % > 0.425 mm	15.3	61.8
FINE SAND	0.425 mm > % > 0.05 mm	72.8	32.9
SILT	0.05 mm > % > 0.005 mm	6.8	1.3
CLAY	0.005 mm > %	5.1	4.0
SILT + CLAY	0.05 mm > % > 0.005 mm	11.9	5.3
% PASSING 0.075	0.075 mm > %	14.0	5.3

The hydrometer analysis shows that the silt content of the red sand is five times more than that of the yellow sand (6.8 vs. 1.3). It also indicates that the yellow sand is coarser that the red. Furthermore the percentage red material passing 0.075 mm is three times more than that of the yellow material. Grading modulus for the red and yellow sands is 1.1 and 1.3 respectively.

Maximum Dry Density (MDD) of the red and yellow sand is in the ranges of 1920 to 1950 kg/m^3 and 1820 to 1850 kg/m^3 respectively.

Electron microscope analyses were conducted by means of Energy Dispersive Spectroscopy (EDS) at the Geology Department of University of Stellenbosch to

assist with the evaluation of the particle size and texture characteristics. High resolution imaging yielded the images portrayed in Figure 3.3.

These images indicate that the yellow sand is more single sized and has larger particles than the red sand that has smaller particle size and exhibit some apparent grading. The yellow sand also exhibits a smoother surface texture with less of a surface layer than the red sand which is textured and covered in a surface deposit.

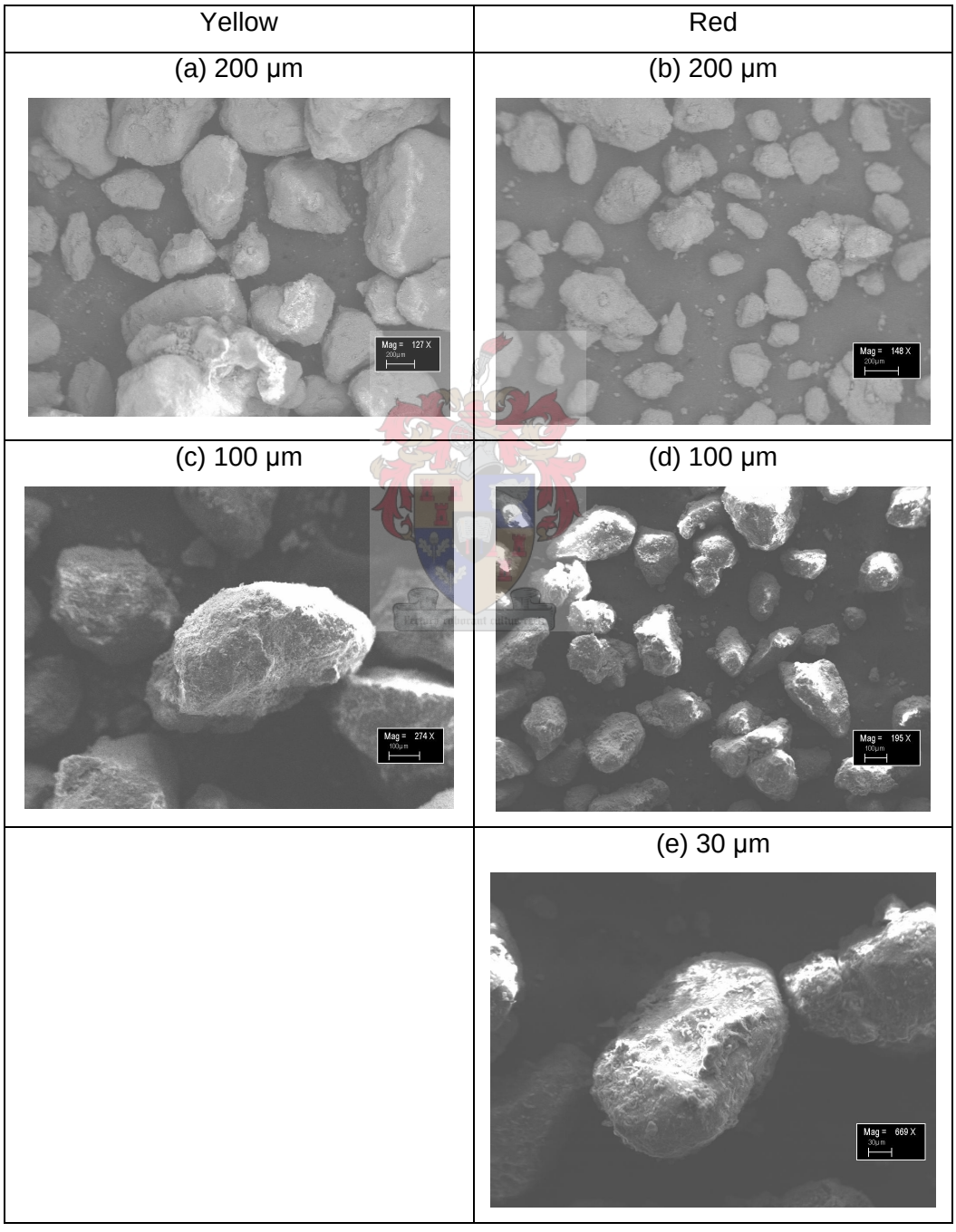

Figure 3.3: Electron microscope photos of Yellow sand vs. Red sand

During construction of scaled pavements prior to the full scale test section construction it was observed that the red sand dried very slowly after being wetted to above optimum moisture content. It retained the moisture for an extended period of time. Soil suction was also high.

This phenomenon indicates the red sand to be water sensitive impacting on constructability of sub base and base layers of the pavement.

3.1.1.3 Chemical Characteristics

A quantitative analysis on the major elements of the sand particles was also conducted by EDS for the two sand types, results are set out in Table 3.2.

Table 3.2: Quantative Analysis of Major Elements in Red and Yellow sands particles

Spectrum	C	Al	Si	K	Ti	Fe	O
YELLOW SAND		14.80	32.23			2.40	50.57
RED SAND	6.82	16.17	18.28	0.35	0.30	3.44	54.64

These results indicate that the yellow sand has a significantly higher percentage of Silica (32 vs. 18). The red sand has a higher percentage of Iron and Aluminuim.

The chemical composition of the surface deposit on the sand particles (the dust on the sand particles) was determined by comparing the grey scales of polished discs of sand and carbon using the backscatter detector during EDS. Typical photo of a prepared specimen is shown in Figure 3.4. Results are set out in Table 3.3.

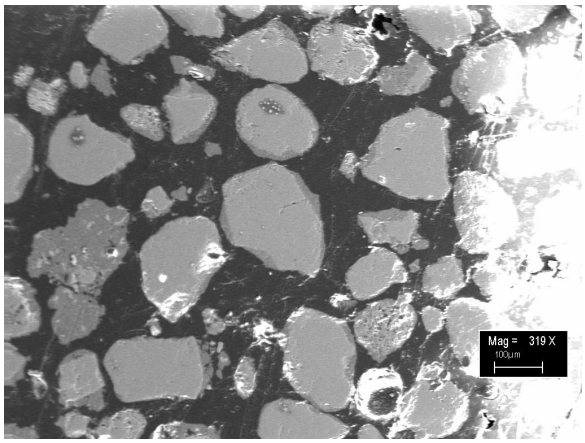

Figure 3.4: Polished red sand disc for determining chemical composition of surface layer using backscatter detector (100µm)

Table 3.3: Chemical composition of surfaces coatings for red and yellow sands

SPECTRUM	Na	Mg	Al	Si	S	Cl	K	Ti	V	Mn	Fe	O
YELLOW SAND	0.143	0.219	4.907	23.87	0	0.028	0.168	4.05	0.016	0.033	10.04	37.4
RED SAND	0	0	7.887	33.63	0.057	0	0.204	0.133	0	0	1.076	45.88

The main difference in the chemical composition of the surface coatings is that the red sand exhibits higher percentages of Silica and Aluminuim than the yellow sand. The yellow sand surface deposit exhibit a higher Iron content than that of the red sand.

From the results of the physical and chemical evaluation the yellow sand can be described as coarse, rounded, single sized sand with high silica particle composition. The red sand is finer sand that has an apparent grading and surface texture and deposit.

3.1.1.4 Stabilizing Agents

Two binder types and compositions were selected for this study, cement and a fifty percent cement-lime blend. This decision was based on past and current practice of stabilizing with cement, as well as exploration of a new binder blend in the cement-lime blend. The cement used was Portland Cement Type II Class 32.5/ A-L produced by Cimentos de Moçambique and conforming to South Africa Burau of Standards (SABS) 6237 / 9174 of 1998. Common hydrated lime, $Ca(OH)_2$, is the lime agent used for stabilization. The reason for inclusion of the cement - lime blend was to evaluate to what extent the delayed strength gain influences final strength and performance under loading. These two binder types were used for the construction of the scaled and full-scale test sections as well as specimen preparation for material strength testing.

3.1.1.5 Strength Characteristics

For a better understanding of the material characteristics that influence the performance of CTB pavements, a variety of experiments were conducted as supplementary tests to determine material tensile, compressive and shear strength.

Tests conducted included the following:

- Indirect Tensile Strength (ITS)
- Unconfined Compression Strength (UCS)
- Shear Split Test

ITS and UCS tests were conducted according to methods A16T and A14 of TRH 1 (1986) respectively. For ITS testing lateral displacement was measured according to the method proposed by Dunaiski et al. (1990). The shear split test was incorporated to assess material shear strength since interface distress between the HMA and CTB occurred in full-scale and scaled pavement sections tested. The shear split test involves vertical splitting along the diameter of a 60 by 100 mm diameter specimen or core at a displacement rate of 50.8 mm per minute while monitoring the load applied. The shear split test method was developed by Lorio (1993, 1997). The testing rig was modified and the methodology adapted for use in the Materials Testing Machine (MTS), the test setup is illustrated in Figure 3.5.

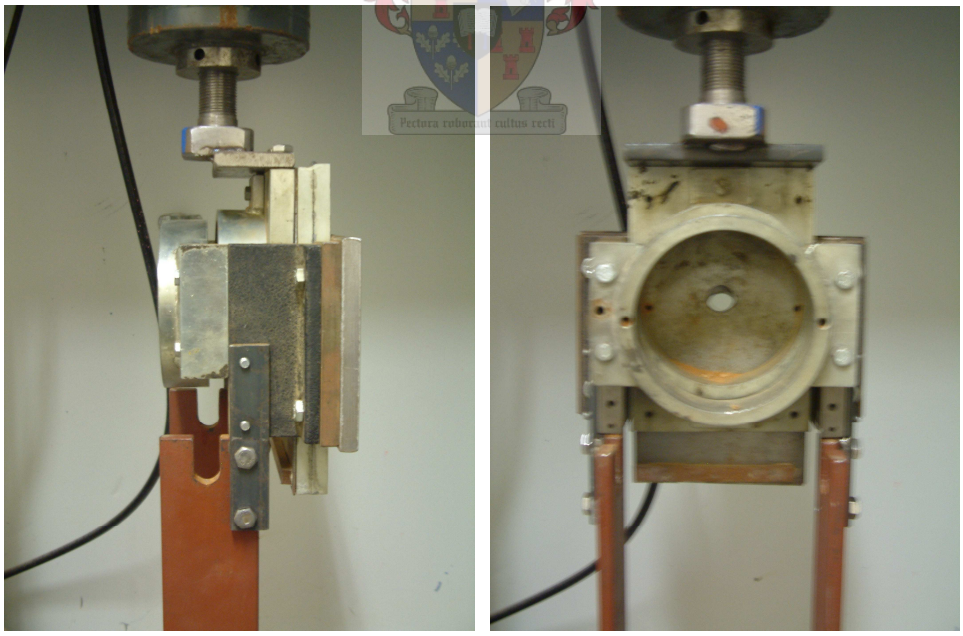

Figure 3.5: Shear split test setup (side and frontal view)

Tests were conducted on laboratory compacted briquettes at ages of seven and twenty eight days. Laboratory specimens were 152.4 mm in diameter and

compacted to 100 % MOD AASHTO. Specimens were cured in sealed plastic bags at room temperature. Cored specimens (100 mm diameter) from the full scale and laboratory scaled test sections were also tested to indicate the one and a half year strength of in-situ pavements constructed and cured according to current construction practice. Strength testing was conducted on the Materials Testing System (MTS) at the University of Stellenbosch. Specimen preparation, testing and analysis was conducted or overseen by the author. Cores taken from the full-scale test sections were transported to the University of Stellenbosch, prepared and tested. Strength test results are presented and discussed in Chapter 4 as the sandy cement treated base material strength parameters are one of the primary elements for the synthesis of pavement response and performance.

3.1.2 Pavement Design

This subsection presents and discusses the designs of the pavement structures and specifications for construction of the full-scale test sections.

The specifications for the test sections that were to be built for APT testing were established from the results of the exploratory scaled laboratory APT performance and research conducted and reported under Phase 1 of the Mozambique contract (Strauss et al. 2005). The APT program planned to use a research matrix that contained sections to evaluate the full spectrum of performance results. Information obtained from existing practice, characterization of materials strengths and initial MMLS3 testing reported in Phase 1 by Strauss et al. (2005) were used to define the sections to be constructed for full scale APT. The pavement structure comprised of insitu sandy sub grade, 150 mm imported red sand sub- base, 150 mm CTB and a surfacing of HMA or double seal. Base material type and the quantity and type of stabilizer used were varied. The pavement structure and base material composition of the different test sections are set out in Table 3.4. Two different methodologies for compaction of the CTB in the fieldwere specified:

Type 1 : Compaction by vibrating pad foot roller for six passes followed by pneumatic tyre rolling for four hours. Compaction had to be completed six hours after mixing of the stabilizing agent has started.

Type 2 : Compaction by vibrating pad foot roller for six passes followed by pneumatic tyre rolling for six passes only. Compaction had to be completed three hours after mixing of the stabilizing agent has started.

Construction Type 1 was conventionally used by contractors to attain the high design base densities prescribed – 97 percent of Modified AASHTO (MAASTHO). This required a relatively long compaction period resulting in the break down of initial cementing action by the heavy construction equipment. This was concluded by the research team and confirmed with PSPA testing (Strauss et al. 2005).

Over compaction and subsequent destruction of the base layer surface occurred with some rollers when the number of passes exceeded a critical level. Construction experiments, conducted in the first project phase and reported by Strauss et al. (2005), indicated that the steel drum roller caused surface shear while the pneumatic tyre roller has a kneading action on the fresh CTB material and smooth surface finish. Accordingly compaction Type 2 described above were prescribed for the construction of the full-scale APT sections.

Table 3.4: Composition of full-scale test sections

SECTION NUMBER	SURFACING	STABILIZING AGENT	SAND TYPE	CONSTRUCTION TYPE
1	S2 Seal	5% CEM II 32.5	Red	1
2	40 mm AC	5% CEM II 32.5	Red	1
3	60 mm AC	5% CEM II 32.5	Red	1
4	40 mm AC	5% CEM II 32.5	Red	2
5	40 mm AC	2.5% CEM II 32.5 + 2.5% LIME	Red	2
6	40 mm AC	3.5% CEM II 32.5 + 3.5% LIME	Yellow	2
7	40 mm AC	7% CEM II 32.5	Yellow	2
8	40 mm AC	7% CEM II 32.5	Red	2
9	S2 Seal	7% CEM II 32.5	Red	2
10	S2 Seal	5.5% SS60	Red	2
11	S2 Seal	1.5% CEM II 32.5 + 4% SS60	Red	2

Further detailed specifications pertaining to CTB construction methodology included the following:

- Sub base for all sections to be compacted to same standard as currently specified for road works. Sub base layers are unstablized sands with moduli in the order of 200 MPa.

- Prewetting of unstabilzed material before addition of stabilizing agent. Moisture content close to optimum.
- Thorough mixing of cement with pug mill mixer set at predetermined depth had to be achieved. Manipulation of material with grader had to be kept to a minimum to reduce mixing time.
- Optimum moisture content had to be maintained during mixing by addition of sufficient water.
- Roller speed was maintained at below 5 km/h in order to achieve complete compaction throughout layer depth.
- CTB layers had to be covered immediately after completion with sand material which had to be kept moist with water for seven days.
- After removal of moist curing sand layer seven days after construction, the section had to be primed immediately.
- The SS60 tack coat was only to be applied prior to the application of the HMA.

HMA design was similar to that used for the overlay construction of the EN1 highway pavement. The mix comprised of 40/50 penetration bitumen with a continuously graded 19 mm aggregate. Optimum binder content was selected on the basis of 7 % voids using Superpave gyratory compaction. The 13 mm chip seal was constructed as a double seal (9 mm/6 mm) using aggregate from the site and 60 percent stable grade emulsion. Both surfacing types comprise of local Mozambican materials based on proven design recipes. Sections were primed with a MC70 primer at an application rate of 0.5 l/m^2. A tack coat of SS60 stable grade emulsion was to be applied at 0.9 l/m^2 prior to HMA construction.

Not all of the tests sections set out in Table 3.4 were tested. The sections and the extent to which they should be tested were optimized within the total number of axles that the research contract allowed.

Emulsion treated bases (Sections 10 and 11) were included since the bituminous binder in the base course was considered to be a sound way of increasing the bond at the interface between the surfacing and the base course. However these sections were not trafficked by the MLS10 being outside the scope of work in terms of total axle loads trafficked. The interface bond of these sections was tested by the MMLS3 in lieu of the MLS10 since sufficient normal and shear stresses could be developed

under the third scale load. Results of these tests are not further presented in this thesis because if falls outside the scope of work which primarily focuses on characterization of cement treated base materials. These tests are touched upon in the paper of De Vos et al. (2006) presented at the Transportation Research Board.

3.1.3 Pavement Construction

This subsection gives an overview of the construction of the APT full-scale test sections. This was to follow current construction methodology but varying compaction of the cement treated base material with respect to roller type and number of passes was applied.

The APT test site is 80 km north of Maputo and 2 km north of the town Manhiça on the national highway EN1. The site for construction was next to the national highway, EN1, under rehabilitation by consulting engineers BKS Global Ltd. and Italian contractor CMC - Tamega Joint Venture. Construction of test sections was executed according to prescribed guidelines on 9 and 10 June 2005. The constructed sections are adjacent to the existing rehabilitated road, highway EN1, and are to be utilized as bus stops after completion of the study. Figure 3.6 depicts the location of the respective test sections. The results of the respective control tests done by the consultant are shown in Table 3.5. It should be noted that rapid curing was performed on specimens for 28 day strength testing. Test sections were cured, primed and tacked as prescribed. Surfacing construction was completed on 27 to 30 June 2005.

The asphalt overlay was constructed by normal HMA techniques and the double seal constructed with a labour intensive chip spreading method which involved conventional emulsion spraying but hand driven and operated chip spreading.

Once these test sections had been completed they were protected from damage by road users during the curing and stiffening of the stabilized layers. Unfortunately the road users took the sections to be convenient stopping areas for pick-ups and more importantly for repairing break-downs such as gearboxes and axles. This left scars on some of the test sections. The selection of appropriate areas for the tests therefore had to take this into account. The sections were in general found to be in an acceptable condition with the commencement of APT.

TABLE 3.5 Summary of Construction Test Results at Manhiça Mozambique

Section No.	1	2	3	4	5	6	7	8	9	10	11
Surfacing	S2 Seal	40mm AC	60mm AC	40mm AC	40mm AC	40mm AC	40mm AC	40mm AC	S2 Seal	S2 Seal	S2 Seal
Stabilized Base Course	5% CEMII 32.5			5% CEMII 32.5	2.5% CEMII 32.5 + 2.5% LIME	3.5% CEMII 32.5 + 3.5% LIME	7% CEMII 32.5	7% CEMII 32.5	7% CEMII 32.5	5.5% SS60	1.5% CEMII 32.5 + 4.0% SS60
Sub base	All Sections 150mm imported red sand										
Sub grade	Insitu sand										
MATERIAL SOURCE	Palmeira LHS - Red			P/LHS -R	P/LHS -R	P/RHS -Y	P/RHS -Y	P/LHS -R	P/LHS -R	P/LHS-R	P/LHS-R
SIEVE ANALYSIS											
19.0mm				100				100		100	
13.2mm				98	100	100		96	100	98	100
4.75mm	100			94	99	98	100	96	99	98	96
2.0mm	94			85	96	95	96	92	98	97	92
0.425mm	81			79	84	83	44	79	92	81	83
0.075mm	7			15	11	16	6	6	19	15	16
CONSTANTS											
GM	1.81			1.21	1.09	1.06	1.54	1.23	0.91	1.07	1.09
PI (%)	NP			NP	NP	NP	NP	NP	NP	NP	NP
LINEAR SHRINKAGE	0.0			0.0	0.0	0.0	0.0	0.0	0.0	0.0	0.0
MOD AASHTO											
MDD (kg/m^3)	1956			2025	2012	1887	2022	2023	1948	2069	1951
OMC (%)	10.4			9.0	9.8	10.8	8.4	9.1	9.7	7.8	9.8
MOULDING MOISTURE(%)	10.4			8.7	9.8	11.3	8.2	9.1	9.8	8	11.8
RELATIVE COMPACTION (% of MDD)	97.6			94.1	94.6	102.1	96.7	94.8	96.8	95.4	101.0
ITS											
ITS (kPa)	280.00			600.00	550.00	620.00	300.00	610.00	490.00	280.00	80.00
Avg. Compaction	100.3			99.6	100.2	99.1	98.7	98.6	99.7	97.8	99.1
UCS											
PROC COMPACTION %	88.8			89.0	89.2	89.3	89.7	88.7	86.8	91.1	89.8
PROC 28 day UCS(MPa)	0.55			1.56	1.22	1.27	1.05	1.05	0.66	0.43	0.74
MOD COMPACTION %	98.8			99.7	100.3	98.2	98.8	98.4	99.5	98.1	99.0
MOD 28 day UCS(MPa)	2.42			2.33	3.94	2.38	1.90	3.81	3.53	1.45	0.84
ITS (kPa) 3 Field cores per section 19 Months											

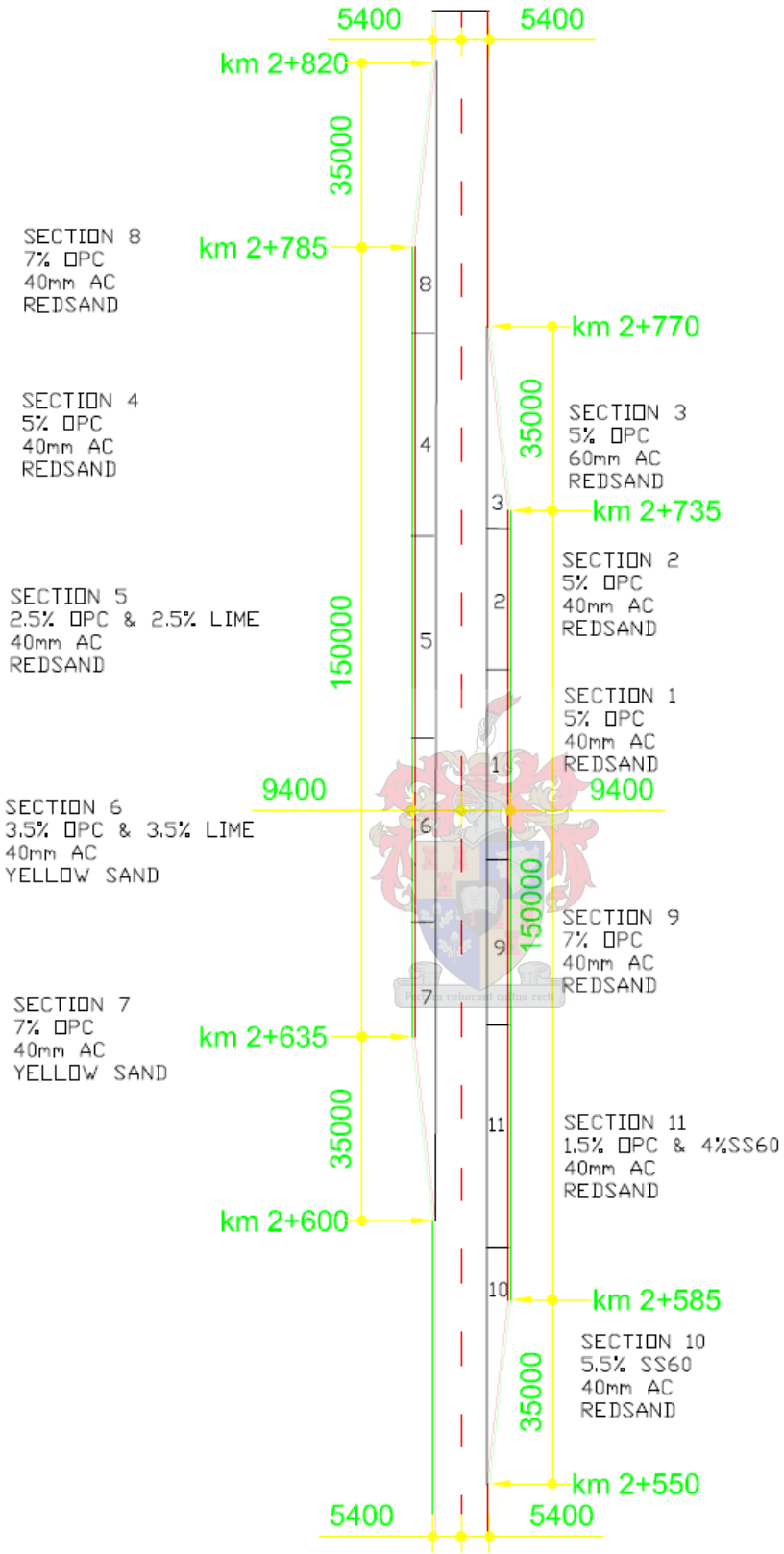

FIGURE 3.6: Layout of test sections constructed adjacent to highway EN1 (dimensions in millimeter)

3.1.4 Accelerated Pavement Testing

The MLS10 and the APT protocol used for sections tested are presented and discussed in this subsection.
The field APT trials were executed to cover the optimum number of test sections. Test selection was based on a progressive review of the findings from completed tests. Accordingly decisions on the number of load applications and degree of distress of the respective test sections were not fixed beforehand. Diagnostic surface evaluation and preliminary seismic testing formed an integral part of test selection.

3.1.4.1 MLS10 APT Device

The MLS10 (Full Scale Mobile Load Simulator) produced by MLS Test Systems Pty Ltd in Stellenbosch, South Africa is based on the third scale load simulator, MMLS3 produced by the same company. A comparison of the MMLS3 and MLS10 APT machine parameters was reported by De Vos et al. (2006). The operating principle of the two devices is very much the same. The machine structure is a space frame approximately 10m long, 3m high and 2.4m wide. The MLS10 has four wheel bogies, each fitted with two 295/65 R22.5 (940mm diameter) or similar tyres. The load on each set of dual wheels is 6 tons (60 kN) at maximum speed. The maximum load can be increased to 70 kN when the speed is reduced. The system is designed to enable the bogies to travel at up to a maximum speed of 7.2 m/s (26 km/hr), when 7 200 axle loads are being applied per hour. Load control is semi-automatic with the load being applied hydraulically.

An electrical drive system consisting of pairs of linear induction motors (LIM) mounted on the side walls at the lower and upper levels of the structure propel the bogie system. Aluminium reaction plates mounted on the chain and the bogies pass in between the LIMs and are driven contactless forward by the electro-magnetic fields developed by the LIMs. Electric power is supplied from the onboard generator.

The operating dead load of the machine, including ballast weights is approximately 27 tons. Lateral movement of the device for simulating wander can be applied. Tyre contact pressures are variable within the guidelines provided by the tyre manufacturer's specification.

Each bogie has 12 sets of guide wheels. Each wheel set consists of two wheels, the inner one being a 250mm diameter flanged steel wheel to apply the load. The outer one is also a 250mm diameter steel wheel linking the bogie chain.

An on-board hydraulic system is used to lift the MLS10 vertically by means of hydraulic cylinders for the purpose of pavement monitoring and diagnostic inspection. Hydraulic jacks on four corners seat the structure on the pavement and can be adjusted in pairs or independently. The same system drives a hydraulic motor for short distance travel of the MLS10. In travel mode the machine is remote controlled by radio and can move forward or reverse and can be steered left or right. All other hydraulic actions are also controlled remotely. Long distance transport of the machine is by low bed trailer by road or rail.

Trafficking can be done in either dry ambient conditions or artificial wetting of the pavement surface.

Technical attributes of the MLS10 are tabulated in Table 3.6. Figures 3.7, 3.8 and 3.9 provide a schematic of the device as well as pictorial views of setup for testing and pavement monitoring respectively.

TABLE 3.6: MLS10 APT machine parameters

	Item		**Standard MLS10**
1	Testing length	m	4
2	Tread path width	mm	610
3	Size of test section	m	5 x 1.6
4	Wheel configuration		Dual
5	No of axles		4
6	Trolley description		Four bogies with hydraulic suspension
7	Wheel load	kN	60 maximum 70
8	Wheel velocity	m/s	7.2 maximum
9	Repetition /h		7200 maximum
10	Tyres		Continental R22.5 295/65
11	Tyre pressure	kPa	800
12	Trafficking conditions		Dry, Wet
13	Lateral wander		Optional, not utilized in Mozambique APT tests

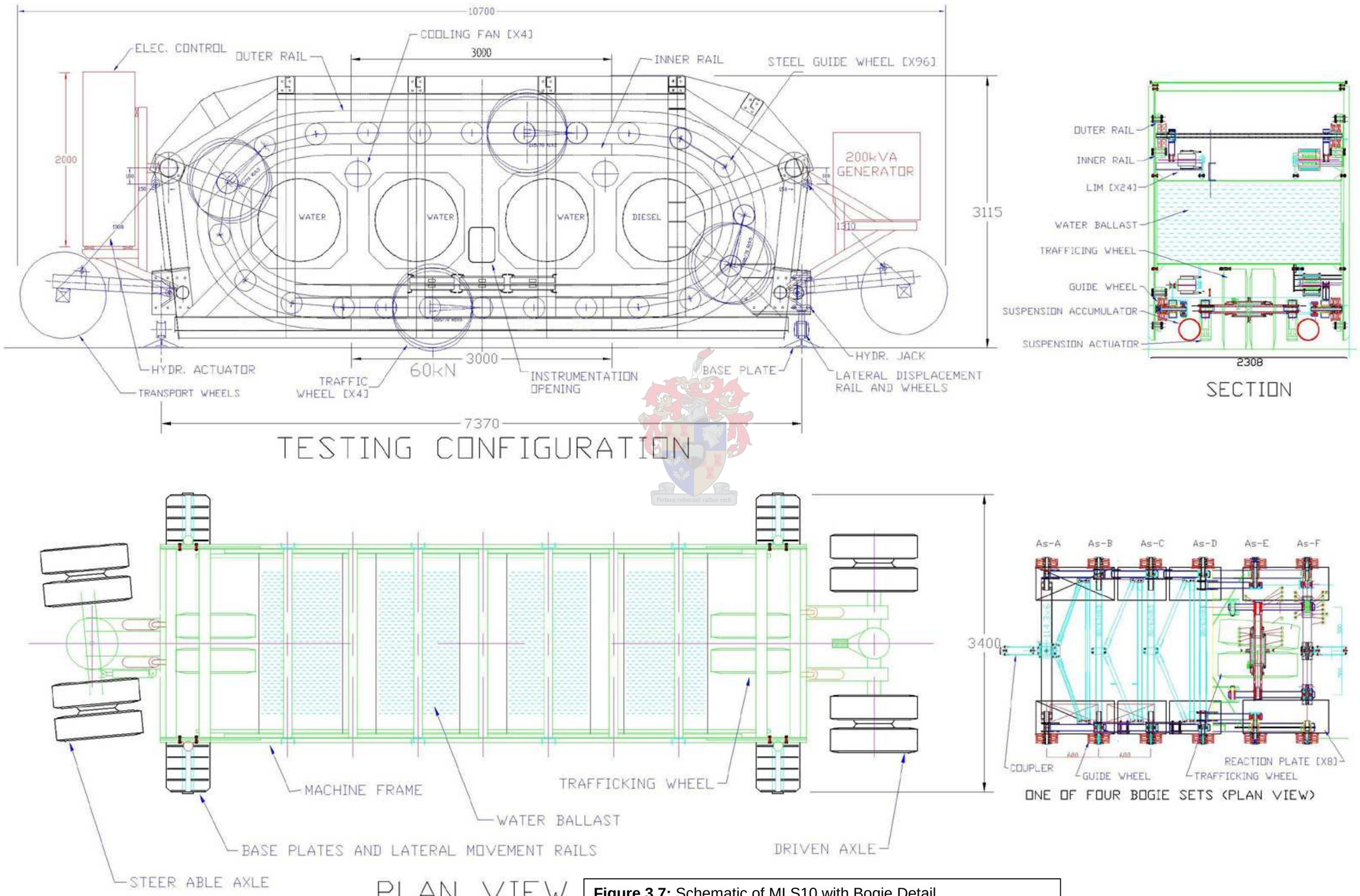

Figure 3.7: Schematic of MLS10 with Bogie Detail

Figure 3.8: View of the MLS10 trafficking on the test site at Manhiça in Mozambique

Figure 3.9: View of the MLS10 lifted in pavement monitoring and visual inspection configuration

3.1.4.2 Accelerated pavement testing protocol

In this subsection the author presents the protocol used for the APT of the full scale test sections. This encompasses trafficking load, tyre pressures, environmental conditioning and pavement response measurements. The environmental conditioning is based on the undergraduate research reported by De Vos (2004) and similar to that used during the scaled laboratory testing.

APT was conducted with full-scale test loads and tyre characteristics as set out in Table 3.6. Environmental conditioning of the full scale tests included cyclic ambient dry and wet pavement surface conditions. Trafficking was alternated between 200 000 ambient dry and 50 000 load cycles with water sprayed onto the pavement surface. Smit et al. (1999) reported that a 1mm layer of water is equivalent to rain falling at a rate of approximately 5 mm per hour. Sheet flow approximately 1 mm thick across the pavement surface was maintained by control of the water spray rate during wet testing. This environmental conditioning protocol is based on the one developed by De Vos (2004) for scaled pavement testing, although the surface temperature of the dry cycle was ambient and not 50 ˚C as proposed. Surface heating for full-scale tests is feasible but was not considered for this program. Averaged pavement temperatures at time of measurement after dry and wet trafficking are set out in Table 3.7.

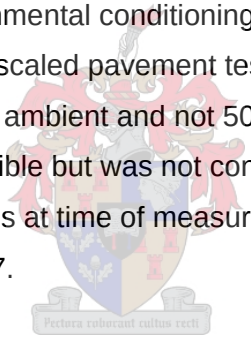

Table 3.7: Average test surface temperatures during full-scale APT study

TEST SECTION	AVE TEMP ˚C	COV*
SECTION 4A	25	13
SECTION 4B	30	21
SECTION 5A	27	17
SECTION 5B	22	15
SECTION 8	30	16
SECTION 7	29	15

*COV = Coefficient of Variance = Standard Deviation / Average x 100

The sequence of testing with the MLS10 was determined with due regard to the findings of the laboratory MMLS3 tests (Strauss et al. 2005) Accordingly, the 5 percent CTB structures, Sections 4 and 5, were selected for the first MLS10 tests. This was to be followed by Sections 8 and 7 where the binder content had been increased to 7 percent. Test loads of 60 kN and 70 kN were selected for the 5 and 7

percent stabilized sections respectively. A 70 kN load test was also conducted on the 5 percent cement stabilized Section 4 for determination of the CTB material damage factor. Canalized loading was applied at all times with no lateral load distribution.

It was decided to limit load applications on each of the respective sections to a level perceived to provide the most information towards the understanding of differences in performance and response. Therefore initial tests were conducted up to a stiffness loss of 50 percent, as monitored by seismic PSPA under 60 kN axle loads. Subsequent tests conducted on the stronger 7 percent stabilized sections were trafficked until ultimate failure to evaluate performance up to a terminal condition.

In order to monitor the pavement response and performance under MLS10 APT a number of tools and special developed procedures were utilized. These include:

1. Measurement of dynamic surface deflections during trafficking by means of a Benkelman Beam (BB)
2. Measurement of seismic stiffness using the Portable Seismic Pavement Analyser (PSPA)
3. Monitoring surface deformation by means of an electronic profilometer
4. Monitoring and recording surface cracking and related distress
5. Diagnostic trenching after completion of traffic loading

The full range of non-destructive monitoring was done before the start of pavement trafficking and intermittedly as traffic loading progressed and pavement response and performance deteriorated. For the lower strength pavements (5 percent CTB) monitoring was done more frequently than the higher strength 7 percent CTB pavements. Higher strength pavements were monitored after every 100 000 load applications during the dry loading cycle and after the 50 000 load applications of the subsequent wet loading cycle.

3.2 Data Acquisition

The following subsections describe in brief the equipment used and recoding procedures followed during intermitted pavement response data acquisition.

3.2.1 Recording Equipment

Seismic Stiffness

Seismic stiffness monitoring was conducted with the Portable Seismic Pavement Analyser (PSPA) device developed by Baker et al. (1995) shown in Figure 3.10. The device consists of two transducers (accelerometers) and a source packaged into a hand-portable system. The source package is also equipped with a transducer. The device is operated from a portable computer, Panasonic Tough book 51, tethered to the unit though a cable that transmits operational commands to the PSPA and returns the measured signals to the computer.

Figure 3.10: Portable Seismic Pavement Analyser

The operating principle of the PSPA is based on generating and detecting stress waves in a medium. The Ultrasonic Surface Wave (USW) interpretation method (Nazarian et al., 1993) is used to determine the modulus of the material. Surface waves (or Rayleigh, R-wave) contain two-thirds of the seismic wave energy. Accordingly, the most dominant arrivals are related to the surface waves making them the easiest to measure. This method utilizes the surface wave energy to determine the variation in surface wave velocity (modulus) with wavelength (depth). The surface wave velocity, V_R, is converted to modulus, E, using:

$$E= 2 [\rho (1.13 – 0.16)V_R]^2 (1 + v) \quad (3.1)$$

Where:

E = modulus (MPa)

V_R = velocity of surface waves (m/s)

ρ = mass density (kg/m^3)

v = Poisson's ratio

The acquired data is converted to a digital signal and the linear spectrum, auto-spectrum (of the output signal), cross-spectrum (between the input and output signal), frequency response function and coherence functions are obtained through frequency domain analysis (Jones, 1962). The phase information is obtained from the cross-power spectrum and the coherence function indicates the extent of background information (Nazarian et al. 1986). The dispersion curve, representing the variation of wave velocity with frequency, is developed from the phase information and the cross-power spectrum. The inversion of the dispersion curve provides the information regarding the layer depth, and the true wave velocities, or the seismic moduli of the layers.

To collect data with the PSPA, the operator initiates the testing sequence through the computer. The high-frequency source is activated seven times. Pre-recording impacts of the source are used to adjust the gains of the amplifiers in a manner that optimizes the dynamic range of the electronics. The outputs of the three transducers from the final three impacts are saved and stacked. Typical voltage outputs of the three accelerometers are shown in Figure 3.11.

An actual variation in modulus with wavelength (a.k.a. dispersion curve) from the time records shown in Figure 3.11 is included in Figure 3.12. For practical reasons, the wavelength is simply relabeled as depth.

The dispersion curve shown in Figure 3.12 is developed from the phase spectra shown at the bottom of the same figure. The phase spectrum, which can be considered as an intermediate step between the time records shown in Figure 3.11 and the dispersion curve shown in Figure 3.12 (Nazarian et al., 1993), is determined by conducting Fourier transform and spectral analysis on the time records from the two sensors. This step makes the determination of the modulus with wavelength much easier. Two phase spectra are shown, one measured from the time records, and the other that represents the best estimation of the phase when the effect of the

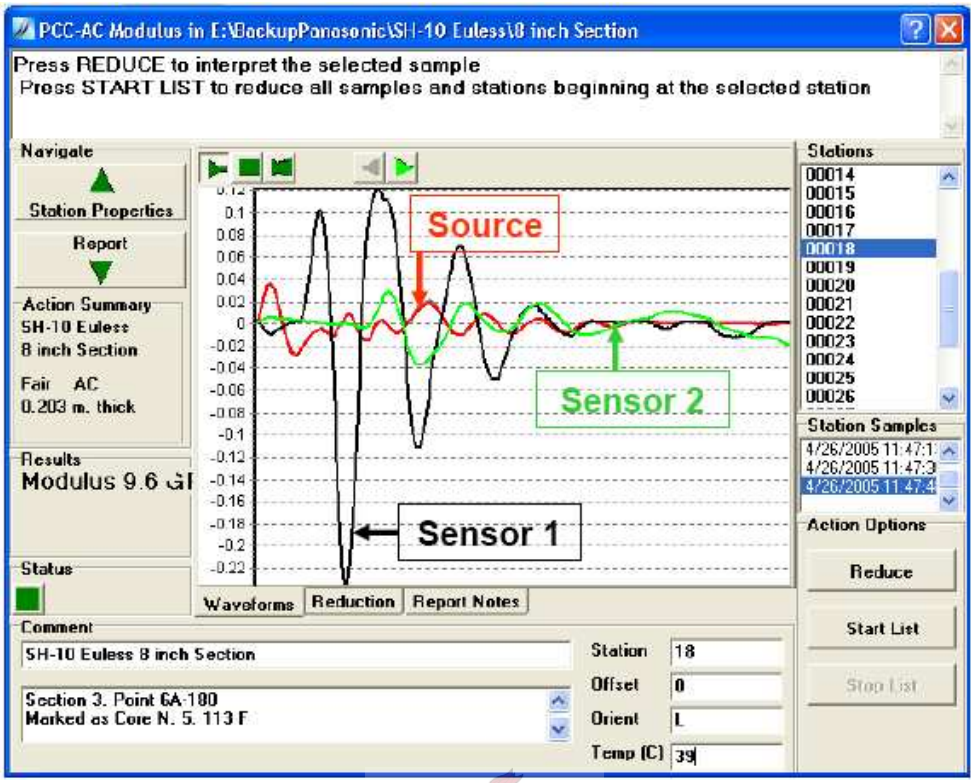

FIGURE 3.11: Typical time records from PSPA and SPA Manager software detail

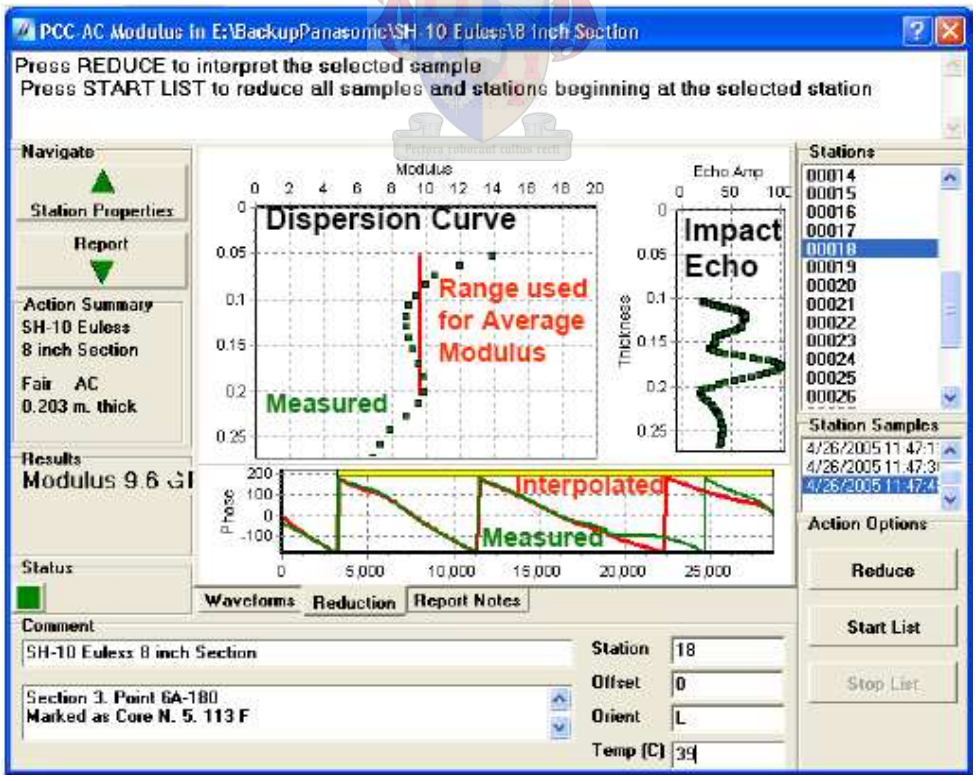

Figure 3.12: Typical dispersion curve obtained from time records in Figure 3.10 and phase spectra detail

body waves are removed. The second one is used to compute the dispersion curve as described above and detailed by Nazarian et al. (1993).

The variability of tests results with PSPA is less than 3 percent without moving the device and around 7 percent when the device is moved in a small area (Celayn and Nazarian, 2006). A study conducted for Texas Department of Transportation (TxDOT) by Nazarian et al. (2004) on the quality management of flexible pavement layers with seismic methods found the comparison between low-strain resilient modulus and seismic modulus for granular base material as shown in Figure 3.13.

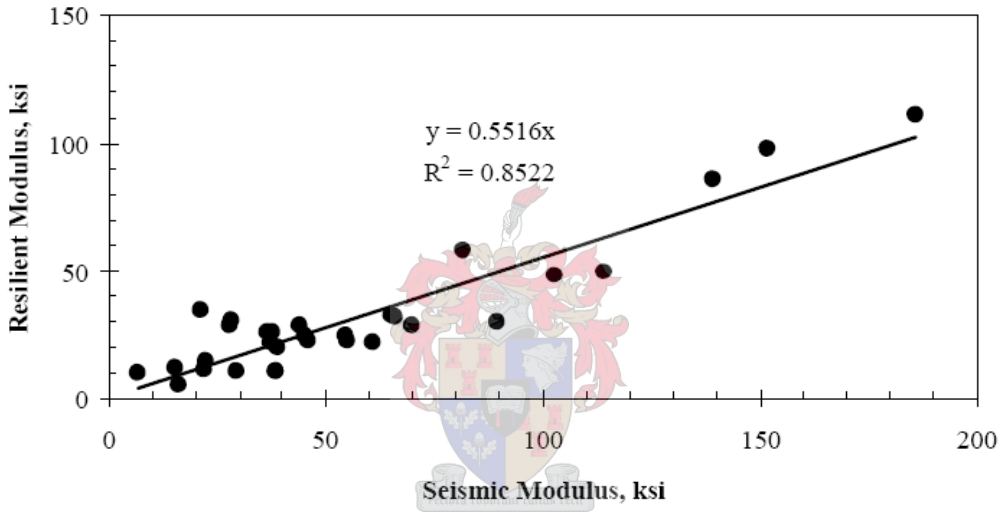

Figure 3.13: Relationship between seismic and low-strain resilient moduli for granular base material (Nazarian et al., 2004)

A comparative study between PSPA and FWD tests were carried out under the same project and reported by Abdallah et al. (2003). It was found that the PSPA and FWD provided complementary results. The repeatability of the PSPA has been evaluated in a number of TxTOD projects, Alexander (1996) demonstrated through a repeatability study that the PSPA tests are highly correlated. Mallick et al. (2005 and 2006) further concluded that that the PSPA moduli collection and prediction method produced reliable data with low variability and good accuracy.

PSPA test results and stiffness performance of test sections are presented as relative dimensionless ratios of the initial untrafficked stiffness and not absolute

stiffness values, this was done to enhance general applicability of the proposed performance models.

Dynamic Surface Deflections

Dynamic surface deflection profiles were monitored intermittently by means of a Modified Benkelman Beam (MBB). The Benkelman Beam, developed by AC Benkelman, was instrumented with a Linear Variable Differential Transducer (LVDT) and displacement measurements were conducted in real time with Vernier Logger Pro 3.4.5 software on the Panasonic Toughbook 51. The MBB was inserted underneath the MLS10 in the center of the wheel path and the four bogies' wheel sets rolled over the beam with the wheels making surface contact on either side. The setup is illustrated in Figure 3.14.

Figure 3.14: View of the modified Benkelman Beam setup under the MLS10

Surface Deformation

Transverse surface rutting was monitored intermittedly by means of the electronic profilometer developed for the MMLS3. A special frame was constructed that enabled the operator to conduct two overlapping measurements at each position to cover the width of the tread.

3.2.2 Recording Procedure

Seismic Stiffness

PSPA measurements were taken at monitoring intervals as indicated. Measurements were taken in two directions, longitudinal and transverse relative to the wheel path. This was done to evaluate the development of pavement failure in two perpendicular directions and relate the decreasing stiffness ratio's with different failure mechanisms once diagnostic investigation are done after traffic completion. Measurements were taken at three positions along the test section. Figure 3.15 depicts the layout of a test section with positions of measurement indicated. At each position five sets of measurements were taken relative to the wheel path. Each set consist of a longitudinal and transverse measurement. These were two reference points outside the wheel path, one measurement in each wheel path and one measurement between wheel paths. During one monitoring session a total of thirty measurements were taken. Measurements were meticulously carried out on the same spot within +/- 2 mm. In the event of poor wave transmission or doubt, measurements were repeated until satisfactory.

Dynamic surface deflection

Dynamic deflection measurements were taken on the same spot namely 900 mm back from the centre of the test section as indicated in Figure 3.15. This allowed for measurement of a complete deflection bowl of 2400 mm as only one MLS10 wheel set are on the pavement at any time. Measurements are taken continuously for a few load cycles before the trafficking is halted for the extraction of the beam. The influence of the deflection bowl on the support of the Benkelman Beam was investigated by evaluating the BB geometric setup, linear elastic deflection bowl analysis with BISAR 3.0 and the measured deflection bowls. It was concluded that the influence of the deflection bowl on the BB support was negligible small.

Surface Deformation

Transverse surface rutting was monitored at the same three positions across the wheel track used for seismic measurements. Relative positions are indicated on the test section layout, Figure 3.15.

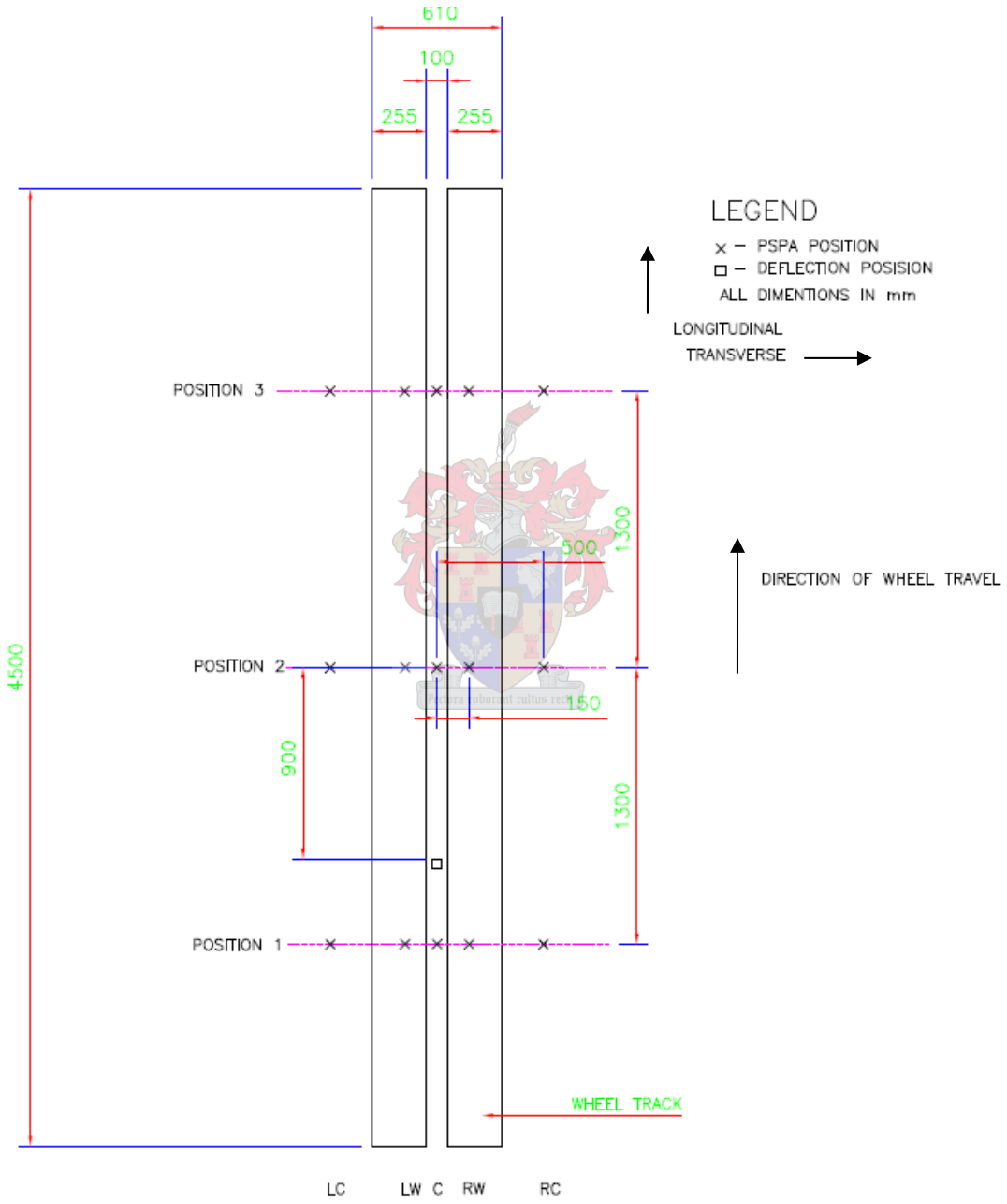

Figure 3.15: MLS10 APT test section layout

3.3 Data Processing

The procedure of data processing and analysis of data from the test devices and recording procedures discussed above are presented in this subsection.

3.3.1 Seismic Stiffness

3.3.1.1 Modulus plots

After seismic measurements, phase frequency plots were reduced over the full frequency range. Subsequently the dispersion curves were recalculated and data points to higher frequency (shallower depth) were added. Figure 3.16 indicate dispersion curves with increase traffic loading to illustrate the relative reduction in the shear wave speeds (seismic modulus) with increased pavement distress. All measurements illustrated in Figure 3.16 were taken on the same location.

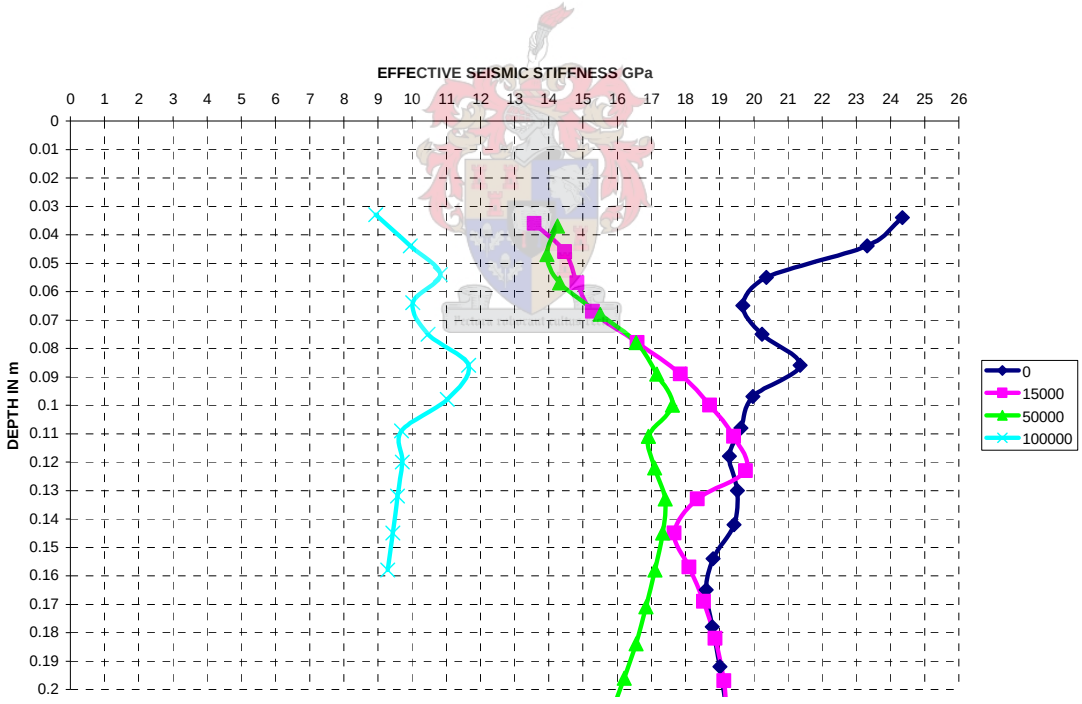

Figure 3.16: Typical seismic stiffness vertical profiles with axle load applications

3.3.1.2 Layered Extraction

From the initial MML3 test findings reported in Phase 1 of the Mozambique project (Strauss et al. 2005) it was found that different mechanisms of failure encountered occurred in certain particular pavement zones. Interface distress in the form of shear

failure between the surfacing and the CTB occurred on the top of the CTB. Horizontal shear planes were found to form in the middle of the CTB layer.

Flexural cracking in the longitudinal and transverse directions initiates at the bottom of the layer and progress with traffic loading to the top. The bottom of the CTB crushes into smaller pieces when pavement life nears its end. Diagnostic trenching after completion of traffic loading confirmed these phenomena. Full-scale CTB blocks extracted from diagnostic trenches and cross-sections of trafficked scaled pavement sections illustrated in Figures 3.17 a to e exhibits similar modes of distress. De Vos et al (2006) reported results that further explore the relation between failure mechanisms found under the respective full and scaled tests. Subsequently wave speed – frequency dispersion curves were analysed accordingly. The CTB layer was partitioned into the thee zones of mechanism occurrence, the Top, Middle and Bottom comprising of the top 25 mm, 50mm and 75 mm of the 150 mm CTB layer.

The dispersion curves were further reduced by averaging of the data points occurring in or on the boundry of each respective zone, Top, Middle and Bottom. After completion of the layered extraction the stiffness condition of each pavement zone is presented by a single averaged number. This was done to evaluate comparative behaviour in the respective zones where the different mechanisms of failure occurred.

This approach adjusted according to the diagnostic findings was also used for analysis of the scaled pavement sections not reported in this thesis. For this application however the pavement was partitioned into two zones only. The reason for this being the inability of the PSPA to determine very shallow (less than 25 mm) stiffness's due to the upper frequency range limitation of 50 kHz.

The stiffness reduction methodology followed is newly developed by the author for the characterization of specific pavement zones based on the structural performance thereof.

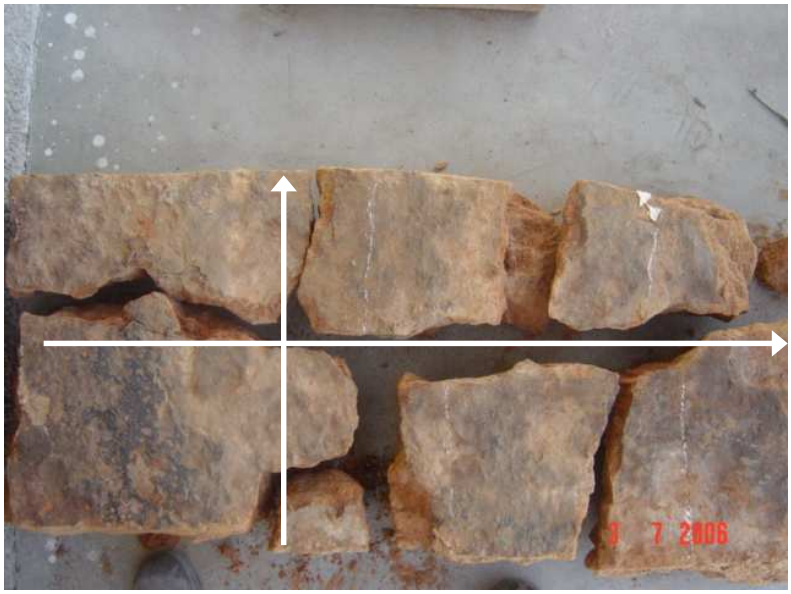

Figure 3.17a: Plan View of the CTB slab extracted from 5 percent cement stabilized full scale test section 4 after 340 00 60 kN load repetitions for diagnostic investigation (550 x 1200 mm length and width as indicated by the white arrows)

Figure 3.17b: Elevation View of the CTB slab extracted from 5 percent cement stabilized full-scale test section 4 after 340 000 load repetitions for diagnostic investigation (160 x 1200 mm height and width as indicated by the white arrows)

Figure 3.17c: View of underside of HMA extracted from full scale test section 4 after 340 000 load repetitions for diagnostic investigation showing marked positions of cracks

Figure 3.17d: Side view of beams taken from scaled 3 percent cement stabilized section after 150 000 2.7 kN load repetitions. Note progressive phases of failure

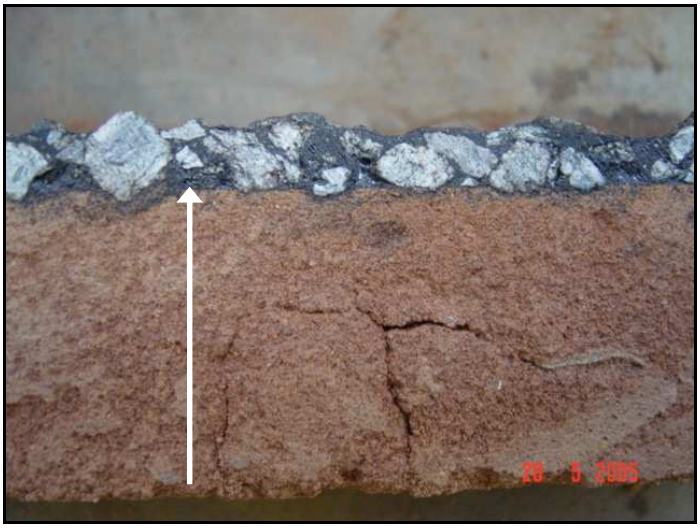

Figure 3.17e Close-up of 3 percent cement base with seal, shear plane on neutral axis of the 3 percent cement stabilized 50 mm scaled pavement clearly visible after 150 000 2.7 kN axle load repetitions

3.3.1.3 Data interpretation

Direct seismic modulus ratios were calculated between initial untrafficked and subsequent measurements taken as traffic accumulated for each zone. This was done at each measurement location in each of the two directions of measurement. Ratios were taken to illustrate the relative extent and nature of structural degradation in terms of material stiffness under trafficking conditions for the three pavement zones. This method is contrary to the methodology of comparing a measured value to a general standard number or index for performance evaluation or pavement characterization, by evaluating individual performance relative to untrafficked initial status.

3.3.2 Dynamic Surface Deflection

Voltage outputs of the installed LVDT on the MBB were reduced to measurements in millimeter of which the maximum surface deflections of each measurement were determined. Initial untrafficked deflection bowls were plotted and indices were determined according to FWD standards for relative comparison. Relative increases in maximum surface deflection with increased loading were determined to evaluate pavement performance in terms of deflection. This was also used for the establishment of a relationship between deflection performance and decreasing base stiffness.

3.3.3 Transverse Surface Rutting

Subsequent measurements were subtracted from the initial untrafficked rutting plot to evaluate development of transverse rut profile formation with traffic loading. Maximum rut depths were determined for the evaluation of the rate of rut formation and rutting trends.

3.4 Data Presentation

In this subsection a pavement damage model reported by Molenaar et al. (1999) based on APT work done at Lintrack is presented to form the bases for stiffness and deflection performance presentation of research reported in this thesis.

Pavement damage occurs as a result of traffic and environmental loading. Molenaar et al. (1999) showed that the phenomenological progression of damage lends itself to modeling using S-shaped curves. Damage, such as asphalt cracking, normally develops slowly during some period of initiation; the rate of damage then accelerates with further loading. Finally, after a certain amount of damage has developed, the rate of progression decreases. This S-shape failure trend may be described using the Weibull distribution, which can be written as

$$F_w(t) = 1 - \exp\left[-\left(\frac{n}{N}\right)^{\beta}\right] \tag{3.2}$$

where

$F_w(t)$ = probability that failure has occurred before time t,

n = number of load repetitions at time t,

N = number of load repetitions at which a defined failure occurs, and

β = curvature parameter.

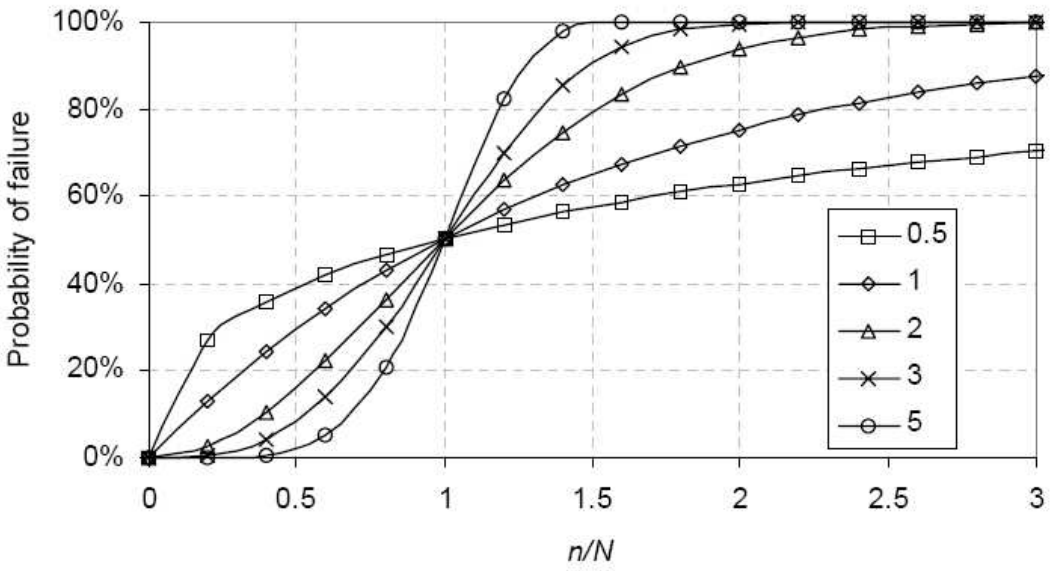

Figure 3.18: Weibull probability of failure distribution for different β–values

Figure 3.18 shows examples of Weibull distributions for various values of β (as shown in the legend), using a non dimensional number of load repetitions scale *n/N*, to represent the relative damage that occurs with loading over time. When the ratio *n/N* is equal to 1, the probability of failure is 50 percent. This may represent a 50 percent loss in stiffness or a 50 percent cracked area. With additional loading the rate of deterioration diminishes progressively. Molenaar et al. (1999) noted that the complete S curve seldom develops fully in practice, because road authorities will not allow pavements to deteriorate to such a great extent. This is in contrast to APT tests that may be continued until total failure occurs.

Initial full scale tests with axle loads of 60 kN (Sections 4A, 5B) were trafficked until a stiffness loss of 50 percent was monitored. Subsequent tests, 4B, 8 and 7 with 70 kN axle loads were conducted until levels as low as 20 percent of initial stiffness were measured. This was done to explore the nature of performance under high levels of damage.

Structural failure for the specific CTB pavement structures evaluated is defined as a 50 percent loss of stiffness in the bottom layer of the CTB. Upon stiffness loss of such extent the surface area was generally cracked 100 percent and pavement surface deflection increased twofold or more than that of initial untrafficked deflection. At this point in the pavement life interface distress was already manifested for the lower strength bases. Due to interface distress the pavements' surfacing rolled dynamically, like a wave, in front of the trafficking wheel load. Upon water ingress

through transverse cracks, fine pavement material washed out. The selection of a 50 percent loss of stiffness for the CTB is in contrast to other failure criterion imposed on CTB that are primarily related to surface deflections. This is justified by the advances made in non-destructive pavement testing that enables base layer performance characterization in terms of continuous stiffness evaluation. Furthermore this methodology followed provides a more direct representation of specific pavement elements that contributes to the overall pavement structure performance. Subsequent enhanced pavement performance modelling based on the continuous measured stiffness performances are a further justification of the approach followed.

Stiffness performance curves for the respective pavement structures under investigation are based on the first of the three measurement positions to exhibit CTB Bottom zone stiffness loss to the extent of 50 percent. The worst performance scenario for a specific test is thus used for pavement performance characterization in terms of stiffness response to traffic loading. Therefore the performance curves present the probability that one third of the pavement has failed structurally.

Surface rut performance was determined from measurements taken in the middle measurement position of the section tested. Surface deflection performance is solely based on the monitoring of the one specific point as indicated. Measurement of only one position with the objective to cover a 2400 mm deflection bowl was feasible with the special constraints of the MBB underneath the MLS10.

3.5 Diagnostic Evaluation

For evaluation and postulation of base performance and mechanisms of failure, pavement sections were trenched after completion of traffic loading. The objective was the extraction of undisturbed base blocks sections (1000 x 500 mm) for the evaluation of crack patterns and the base structure after testing. Figures 3.19 a, b and c depict the diagnostic trenching methodology followed and discussed subsequently. Cutting was done by diamond blade (HMA and CTB) and perforation of the CTB by means of drilling after which material were removed. Because of the severe interface distress the HMA mat came off completely after box cutting by diamond blade. For extraction of undisturbed base blocks the CTB material around the block was first removed up to the sub base level. This was achieved by dual box cutting with an inner and outer rectangle, where the material in between was removed. Utmost care was taken in the extraction of the blocks to prevent the

formation of non-traffic related fractures by shifting the continuously supported blocks by hydraulic jack instead of creating local high shear forces by working with a pick of crowbar.

Figure 3.19a: Removed HMA after dual box cut by diamond blade grinder

Figure 3.19b: CTB block ready for removal all surrounding CTB material

Figure 3.19c: Shifting of CTB block with hydraulic jack to prevent formation of non-traffic related fractures

This chapter presented the successful development of pavement response characterization methodologies. The methodologies for the different methods of pavement response characterization presented in this chapter were executed on the response monitoring data gathered during testing. Subsequent diagnostic trenching was done according to the methods presented. Results and findings of the methodologies followed are presented in Chapter 4.

Chapter 4

Results and Findings of Applied Test Methodologies

This chapter is the presentation of results obtained from the respective monitoring and analysis methodologies presented and discussed in the previous chapter. Six comprehensive MLS10 tests were completed. The general test section pavement structure is illustrated in Figure 4.1. The details pertaining to the load applications of the full-scale sections are shown in Table 4.1. From the test results the performance of the sections was found to be in accordance with expectations

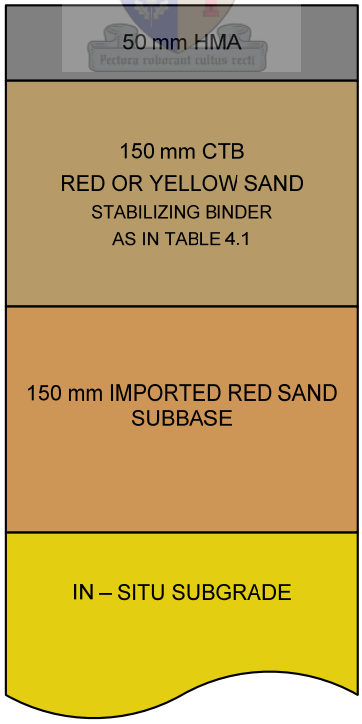

Figure 4.1: General pavement structure and compostion of sections tested

Table 4.1: Summary of MLS10 tests

SECTION	4a	5a	5b	4b	8	7
Stabilizing Binder	5 % CEM	2.5% CEM 2.5% LIME	2.5% CEM 2.5% LIME	5% CEM	7 % CEM	7 % CEM
Sand	RED	RED	RED	RED	RED	YELLOW
Surfacing	HMA	HMA	HMA	HMA	HMA	HMA
Axle load applications X 1000	330	100	1080	150	730	1050
Axle Load kN	60	60	60	70	70	70

Pavement behaviour at different stages during performance phases under trafficking was similar for the tested sections. Transverse and diagonal cracking of the surface started at the same time. After occurrence of HMA and CTB interface de-bonding, pavement surfaces started to roll dynamically in waves under traffic loads with deflections visible to the naked eye. Complete transverse cracks were visible at this phase of pavement life. The pavement performance results were found to be very informative. Results of the full scale tests pertaining to the methodologies discussed in the preceding chapter are presented and discussed.

4.1 Material strength tests

The results obtained from the material strength testing as described in Chapter 3 are set out in Tables 4.2, 4.3 and 4.4. Tests conducted on laboratory prepared and cured specimens at the ages of seven and 28 days are set out in Table 4.2. Results for 100 mm cores taken from the full-scale test sections are shown in Table 4.3. Age at testing of these cores was one and a half years after construction. Cored samples (100 mm) from scaled laboratory test sections were also tested and these results are presented in Table 4.4. The age of specimens was also one and a half years at time of coring. Instrumented ITS testing yielded a Poisson value in the range of 0.18 to 0.21 according to the analysis methodology proposed by Kennedy et al. (1983). The number of tests conducted for each material strength parameter are six, three and three for the ITS and UCS and shear tests respectively.

An interesting phenomenon occurred during ITS testing. In some instances the transverse displacement reached a maximum value before specimen failure and would reduce up to the point of specimen failure. This phenomenon was not further investigated as it falls outside the scope of work.

Table 4.2: Summary of material test results conducted on laboratory prepared specimens

		ITS		ITS		UCS		SHEAR	
SAND TYPE	BINDER	7 DAY		28 DAY		28 DAY		28 DAY	
		kPa	COV*	kPa	COV*	kPa	COV*	kPa	COV*
RED	3 % CEM**	200	8	290	15	1500	23	270	9
RED	5 % CEM**	310	11	540	8	2220	14	540	3
RED	7 % CEM**	350	15	550	16	2500	25	650	11
RED	2.5 % CEM** 2.5 % LIME	130	15	200	13	880	21	400	1
RED	3.5 % CEM** 3.5 % LIME	210	13	450	15	1490	23	470	12
YELLOW	7 % CEM	390	18	870	5	3600	8	690	11

*COV – Coefficient of Variation = Standard Deviation / Average x 100

**CEM – Portland Cement Type II Class 32.5/A-L

Gain in tensile strength from ITS testing is illustrated in Figure 4.2 this would serve as basis for comparison with tensile strengths one and a half years after construction of the field sections.

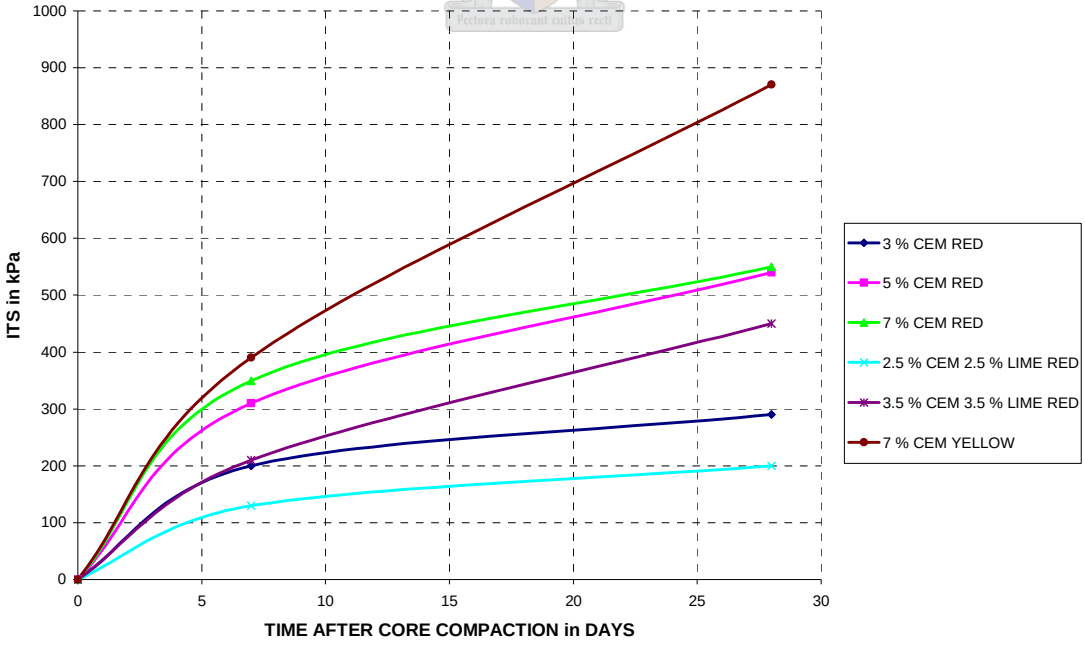

Figure 4.2: Indirect tensile strength growth chart for cemented material tested

From comparison with SAMPD standards (TRH 14, 1985) the CTB material conforms to C2 and C3 material class standards according to ITS and UCS results respectively. It should be kept in mind that this stabilized sand material is compared to predominantly granular stabilized materials and it only conforms to the ITS and UCS requirements of the material and not to the full requirement which states that the unstablized material must be at least a G5 or G6.

Table 4.3: Summary of test results obtained from tested full-scale field test section cores at an age of 1.5 years

SAND TYPE	BINDER	ITS		UCS	SHEAR
		TYPE 2	TYPE 1		
		kPa	kPa	kPa	kPa
RED	3 % CEM	-	-	-	-
RED	5 % CEM	360	600	4880	270
RED	7 % CEM	680	-	5190	360
RED	2.5 % CEM 2.5 % LIME	940	-	4720	-
RED	3.5 % CEM 3.5 % LIME	-	-	-	-
YELLOW	7 % CEM	1100	-	3870	370

Table 4.4: Summary of ITS test results of cores taken from scaled laboratory test sections at an age of 1.5 years

SAND TYPE	BINDER	HMA		SEAL	
		kPa	COV	kPa	COV
RED	3 % CEM	-	-	-	-
RED	5 % CEM	350	10	-	-
RED	7 % CEM	1700	15	1000	17
RED	2.5 % CEM 2.5 % LIME	550	29	-	-
RED	3.5 % CEM 3.5 % LIME	680	10	-	-
YELLOW	7 % CEM	530	2	-	-

Tensile and shear strengths obtained from laboratory compacted specimens and specimens cored from full-scale and scaled test sections do not correlate well. This could possibly be attributed to differences in the mixture quality, compaction and curing methodology and environmental circumstances. The sand material of all the specimens tested was sourced from the same borrowpit. Although the results of the scaled APT test are not presented in this thesis material test results of these sections are to evaluate the relation between the aged full-scale and scaled stabilized base

materials. Field sections were subjected to environmentally induced distress and traffic loading of paving and surface compaction machinery during early life strength gain. Compressive strength results compare favourably by indicating increased compressive capacity with ageing. It would appear that the compressive strength of the field CTB is less susceptible to early age damage caused by heavy loading of the construction equipment than the shear and tensile characteristics. The results further indicate that the retarded initial strength gain of the cement – lime blends relative to the cemented material grew with time to surpass the materials stabilized with cement only.

The above results compare favorably with other reported studies of soil lime subgrade and stabilized sand materials (Melis et al. 1985 and Croney and Croney, 1991) it was therefore considered reasonable to utilize relationships that had been developed in those studies. ITS strengths of pavement materials were studied in-depth at the University of Texas at Austin. One of the outcomes was the relationship between UCS, Modulus of Rupture (M_R) and ITS (Melis et al 1985). It was concluded that M_R was about 50 percent greater than ITS strength. This correlation was then applied to the ITS values measured on the Mozambican sands, with a further correction to allow for ageing after research on stabilized materials reported by Croney and Croney (1991). This reported research is illustrated in Figure 4.3. The results were subsequently used to determine the ratio of tensile stress under loading relative to tensile strength at failure to adjudicate fatigue performance [Figure 13.9 Croney and Croney (1991)]. These working stress strength ratios' are utilized for transfer and fatigue performance curve development presented in Chapter 5.

Results from the material tests were found to be invaluable for the analysis of the performance of the pavement sections. It indicated the material parameters that are susceptible to failure, later confirmed by diagnostic evaluation and linear elastic stress analysis. It further indicated the degree of influence provided a measure of the effect of the CTB construction and environmental conditions on these material parameters.

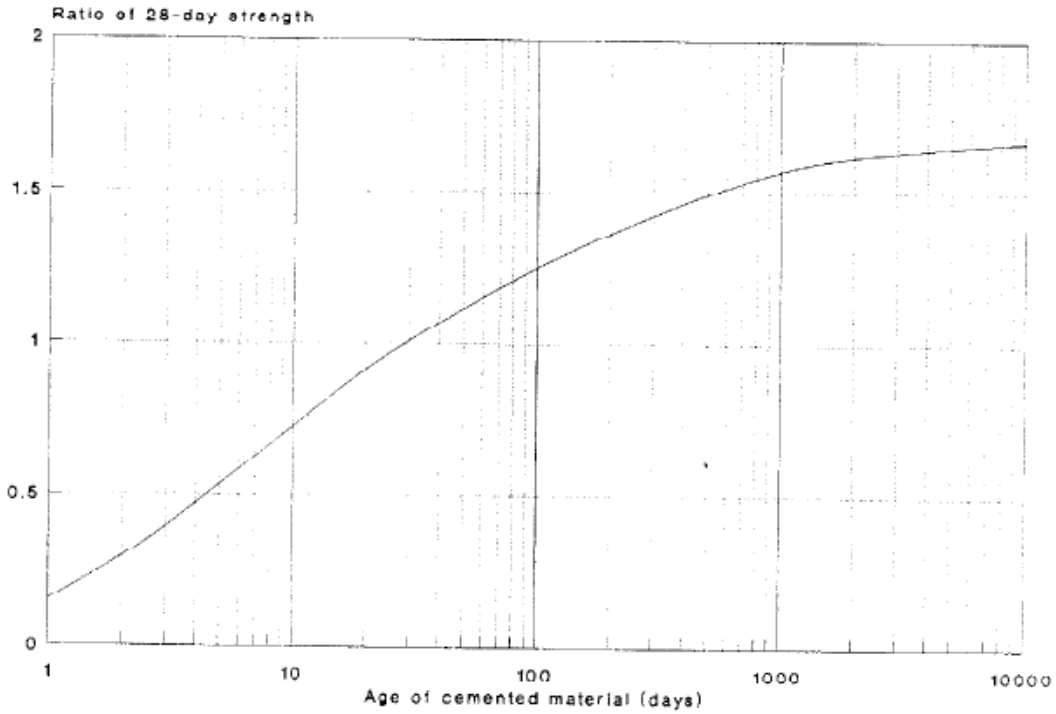

Figure 4.3: Influence of age on compressive strength of cemented materials (Croney and Croney, 1991)

4.2 Deflection performance

This subsection is the presentation and discussion of deflection measurements and performance. Deflection bowl indices measured at the commencement of accelerated pavement testing trafficking for each section are set out in Table 4.5 and illustrated in Figures 4.4a and b. It should be kept in mind that these relate to 60 and 70 kN axle loads, and not 40 kN commonly used for Falling Weight Deflectometer (FWD) measurements. Geometric indices of the defection bowls were determined in accordance with FWD norms for comparative evaluation.

Table 4.5: Initial untrafficked modified Benkelman beam deflection bowls (µm)

Off-set Mm	CTB	0	200	300	450	600	900	1200	1500	1800	Geometric parameters (µm)		
											BLI*	MLI**	LLI***
60kN Axle load													
4a	5% CEM	565	490	450	380	300	160	50	35	30	115	150	140
5a	2.5 % CEM 2.5 % LIME	657	575	500	425	340	180	100	40	20	98	125	165
5b	2.5 % CEM 2.5 % LIME	445	365	325	270	220	160	100	60	30	157	160	160
70kN Axle load													
4b	5% CEM	623	570	525	460	400	235	160	100	60	120	105	60
8c	7 % CEM	520	475	375	325	275	175	120	60	40	145	100	100
7	7 % CEM	360	290	245	213	180	125	80	60	30	115	65	55

* BLI = D0 – D300

** MLI = D300 – D600

*** LLI = D600 – D900

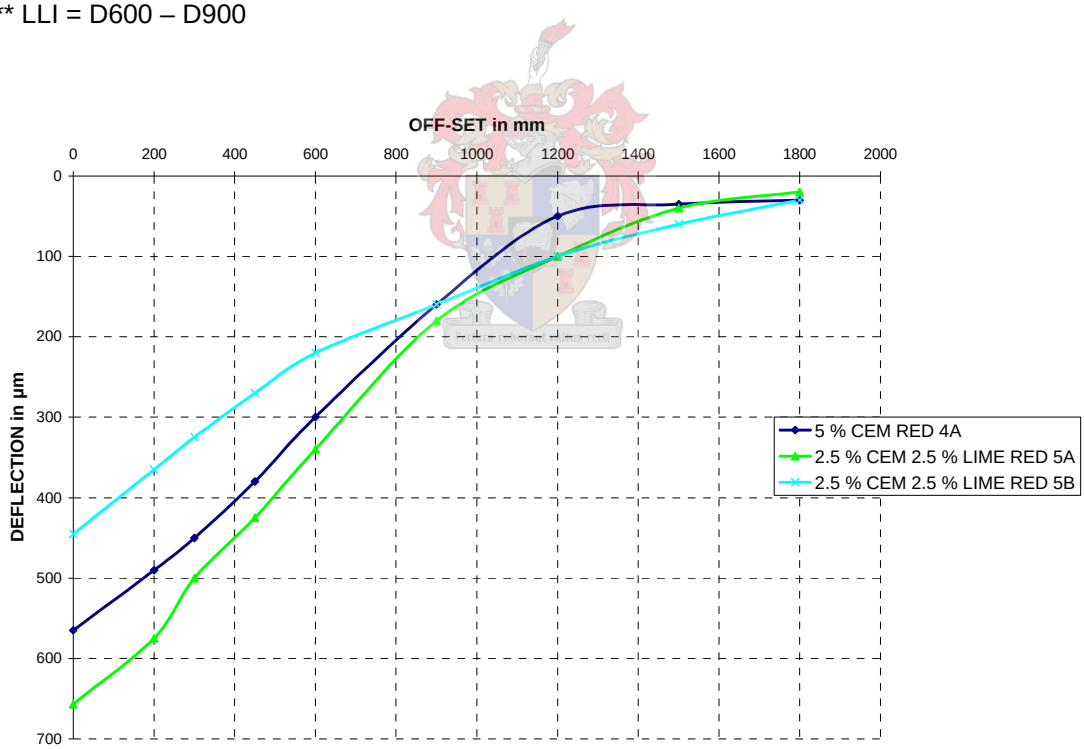

Figure 4.4a: Initial unftrafficked deflection bowls for sections tested with 60 kN axle load

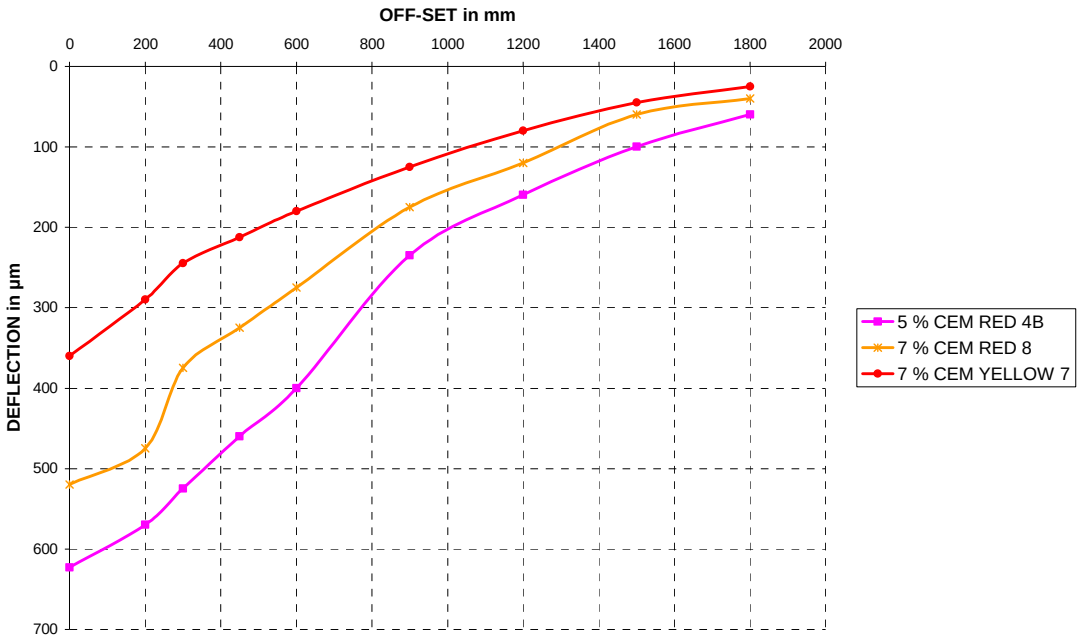

Figure 4.4b: Initial unftrafficked deflection bowls for sections tested with 70 kN axle load

As the pavement suffered distress the deflections progressively increased. This phenomenon is demonstrated by illustrating surface deflection plots of Section 5A in Figure 4.5. This specific section stabilized with a blend of 2.5 percent cement and 2.5 percent lime and trafficked with a 60 kN wheel load exhibited fairly rapid deterioration. Figure 4.6 illustrates maximum surface deflection trends exhibited by full scale sections trafficked. Deflection performance was evaluated by the calculated ratio of the subsequent measurements relative to the initial untrafficked deflection. Table 4.6 summarizes the initial, final and deflections at 50 percent decrease in base stiffness measured for the respective test sections. Relative surface deflection performance of CTB pavements evaluated could be presented by means of a power function.

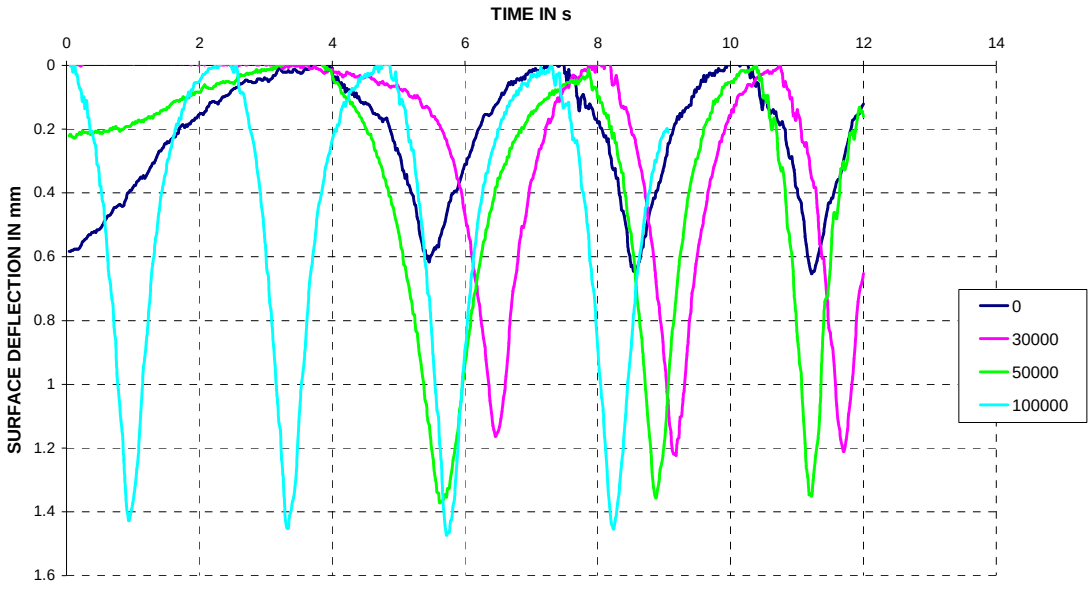

Figure 4.5: Deflection profiles for Section 5A monitored at intervals during axle load trafficking

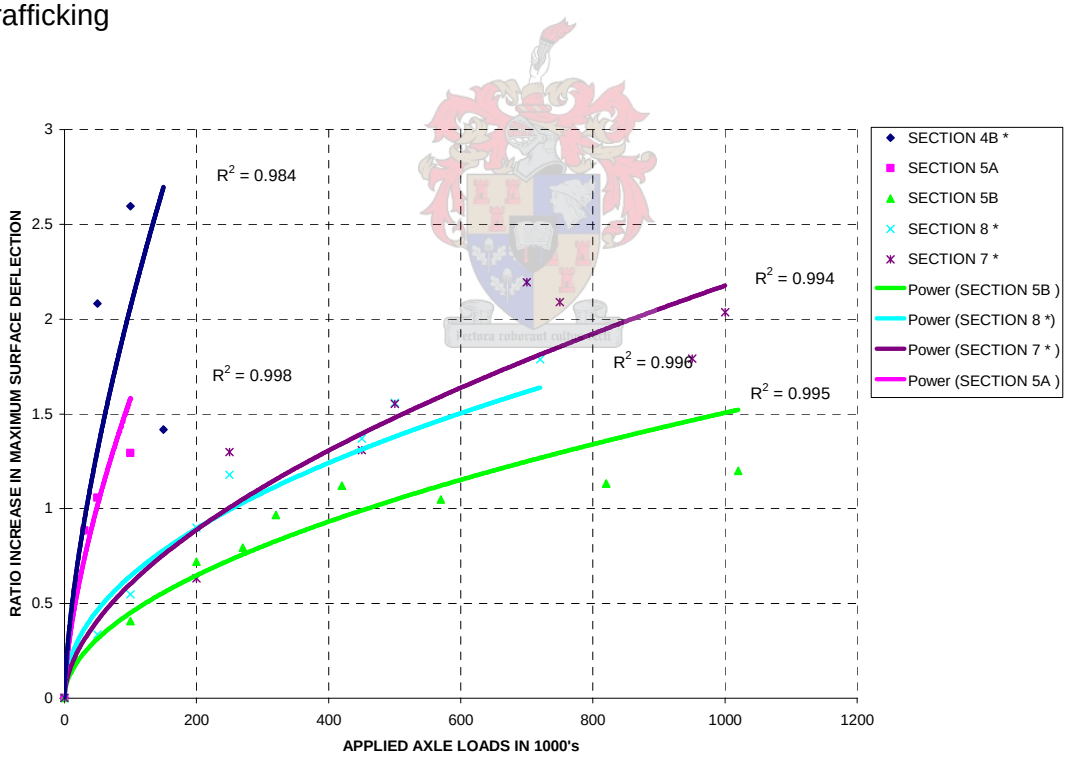

Figure 4.6: Maximum deflection growth trends with axle load applications for respective test sections (Axle load 60 kN and 70 kN indicated with *)

TABLE 4.6: Summary of Deflection Data for Full-Scale Test Sections

SECTION	COMPOSITION	LOAD	INITIAL	0.5 E	FINAL	RATIO	0.5 E AXLE	FINAL AXLE
		kN	µm	µm	µm	Initial to 0.5E	1000's	1000's
4A	5 % CEM RED	60	883	1590	2093	1.80	400*	330
4B	5 % CEM RED	70	637	1963	1540	3.08	50	150
5A	2.5 % CEM 2.5 % LIME RED	60	669	1534	1534	2.29	100	100
5B	2.5 % CEM 2.5 % LIME RED	60	446	970	972	2.18	1000	1080
8	7 % CEM RED	70	521	1135	1453	2.18	250	740
7	7 % CEM YELLOW	70	339	-	-	-	-	1050

To obtain an indication of the pavement fatigue life based on deflection measurement FWD indices the measured high wheel load deflection bowls were transposed to 40 kN deflection bowls by means of mathematical manipulation based on linear elastic analysis done with BISAR 3.0. The objective of this was just to get and indication of the expected fatigue life of the pavement structures under normal traffic axle loading of 40 kN. This was not done to determine the damage factor exponent. It should also be noted that the deflection parameters presented in TRH12 (1986) are based on pavement structures with graded granular and not sandy materials; hence this is used only as an indicator.

The methodology followed was to calculate with BISAR 3.0 the differences between the 70 or 60 kN and 40 kN deflection bowls of the CTB pavement models. These differences were then subtracted from the measured 60 or 70 kN deflection bowls to obtain an artificial 40 kN deflection bowls. The interface layer was bonded during the analysis since it is based on measurements taken at the commencement of APT trafficking. The artificial deflection bowls are based on the real higher load level measurements. FWD deflection bowl indices were calculated for the artificial simulated bowls and compared to the values presented for the different traffic classes in TRH12 (1986). According to the TRH12 (1986) norms the traffic life of the specific pavements are likely to extend well beyond 10 million axles in the event of normal 40 kN axle traffic loading.

The performance of the CTB pavement structure was essentially as would be expected from a rigid structure. Initially the deflection was very small under the wheel load, slowly progressing to a value of between two and three times the initial value. Individual deflection performance graphs for sections tested are presented in Appendix B.

Deflection measurements and characterization of performance was successful. A stiffness – deflection relation for CTB is developed in the following chapter.

4.3 Stiffness performance curves

This section is the exposition of results obtained from the seismic data reduction and analysis methodologies presented in Chapter 3.

Raw PSPA measurement data were analyzed and the findings were as expected; namely a stiffness reduction due to the distress under the trafficking. More importantly was the nature of the change in the stiffness. In general the change in longitudinal stiffness was more than that in the transverse direction. This is to a large extent due to the faster growth in the cracks in the transverse direction than the cracks in the longitudinal direction. Figures 4.7 to 4.12 illustrate the stiffness performance of the respective pavement zones and orientations of the sections tested. Figure 4.9 illustrates the performance of the Bottom zone of CTB at the worst performing position of each tested section in the longitudinal direction. The performance of this zone and in this direction was the worst and accordingly the principle presentation of pavement stiffness performance from seismic measurements. This pavement zone (Bottom – lower 75 mm of the CTB) and orientation suffered the most severe reduction in stiffness. It should also be noted that trends illustrated in Figures 4.7 to 4.12 relate to 60 and 70 kN test results. Similar trends with equivalent 60 kN axle loads were developed after the material damage factor was determined. The full range of performance graphs for equivalent load levels of each pavement zone in both longitudinal and transverse directions are illustrated in Appendix C.

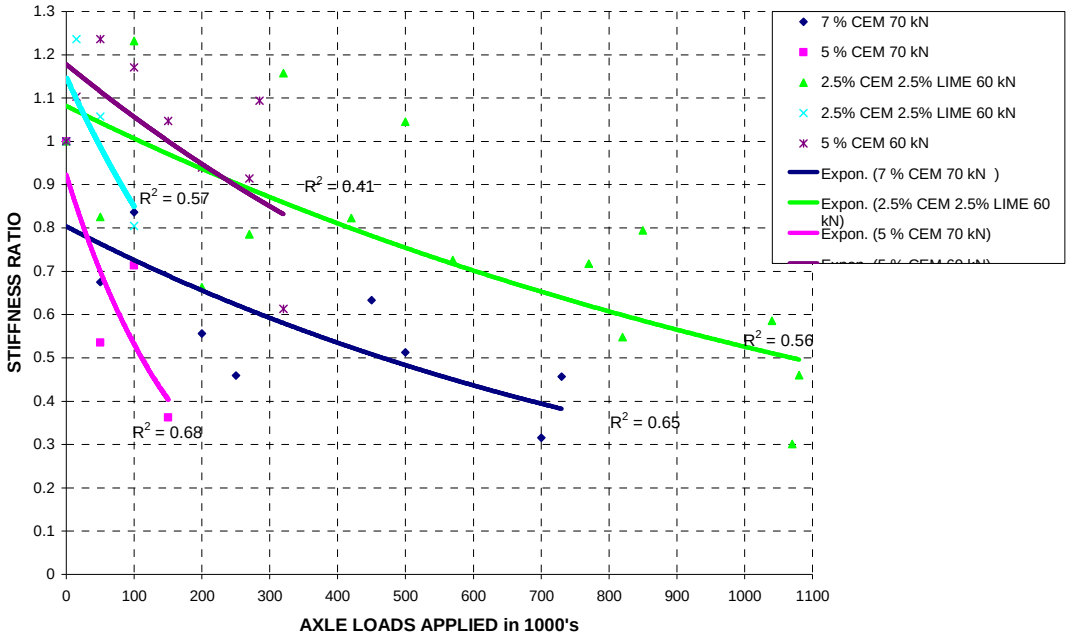

Figure 4.7: Comparative Stiffness Performance Chart for Top of CTB in Longitudinal Direction

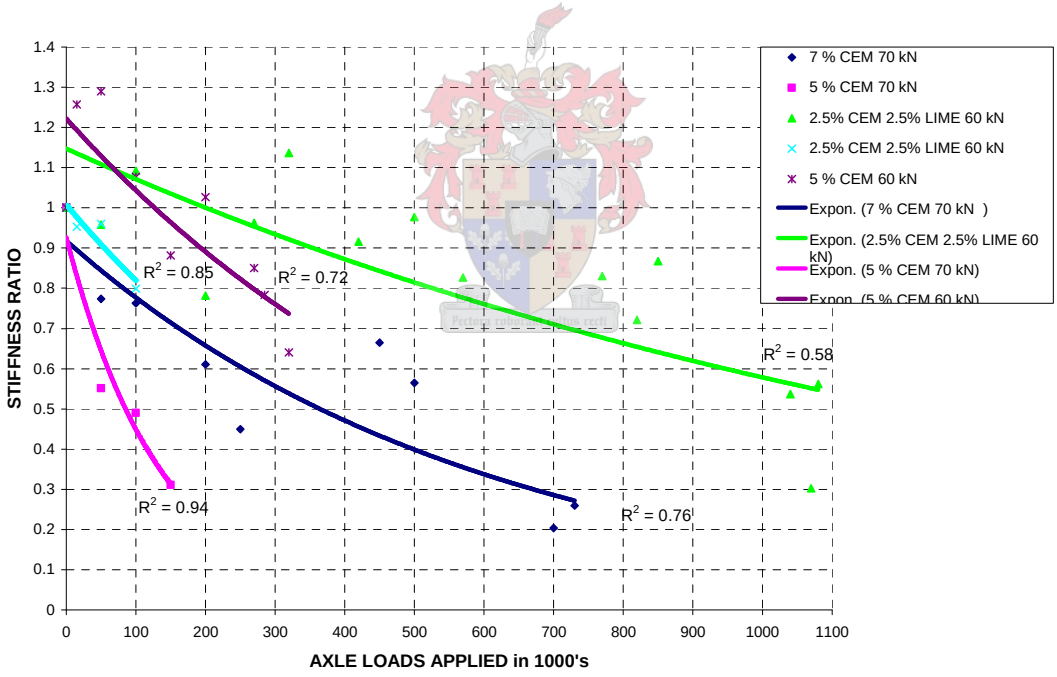

Figure 4.8: Comparative Stiffness Performance Chart for Middle of CTB in Longitudinal Direction

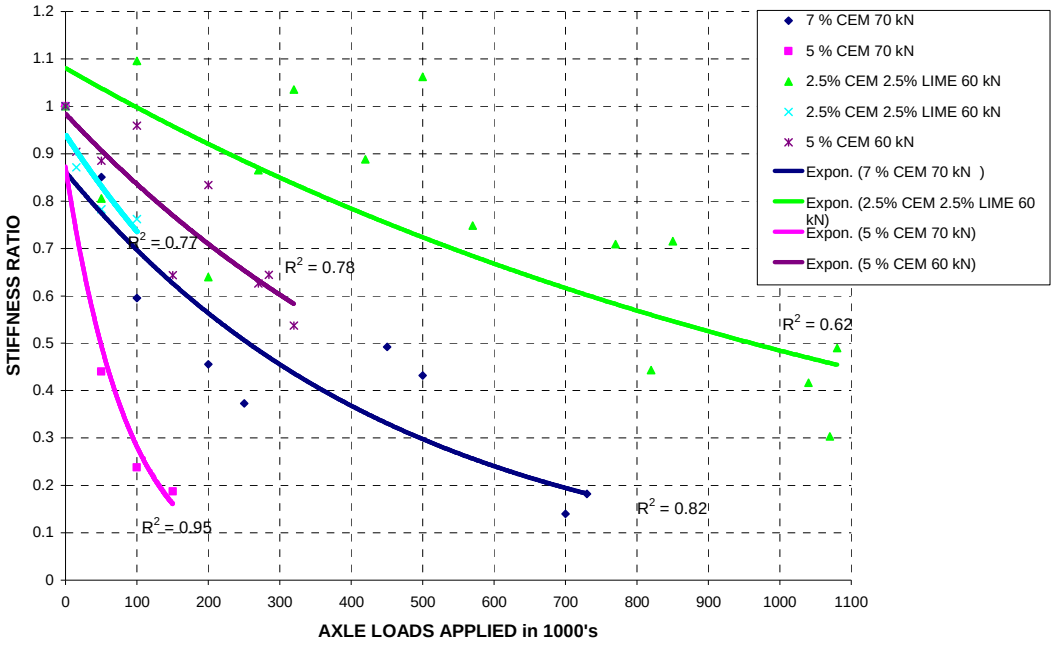

Figure 4.9: Comparative Stiffness Performance Chart for Bottom of CTB in Longitudinal Direction

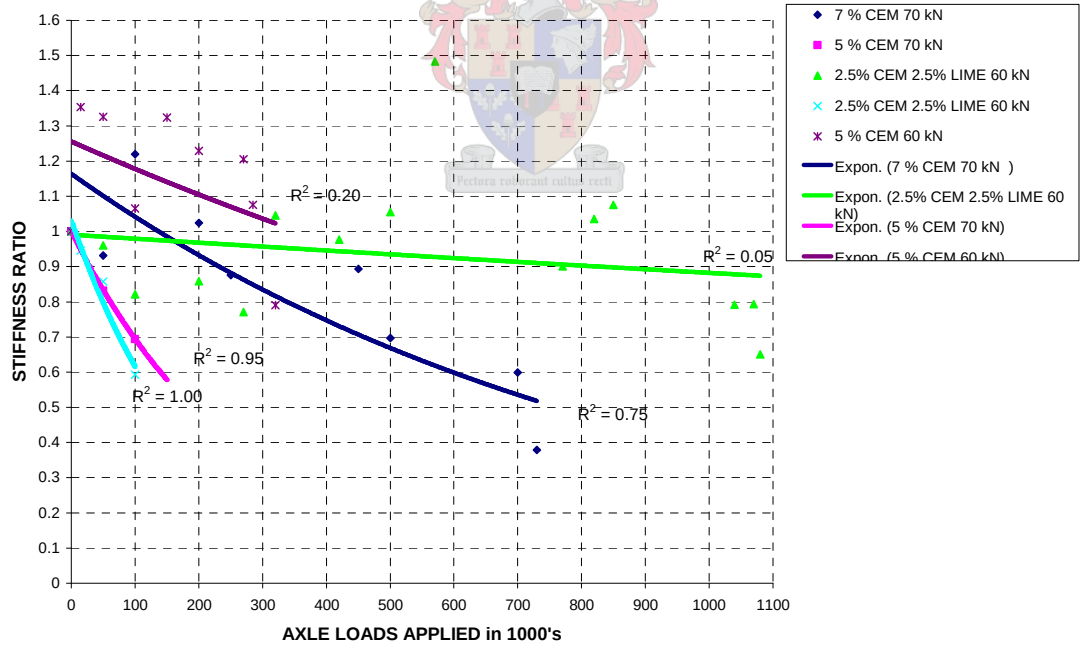

Figure 4.10: Comparative Stiffness Performance Chart for Top of CTB in Transverse Direction

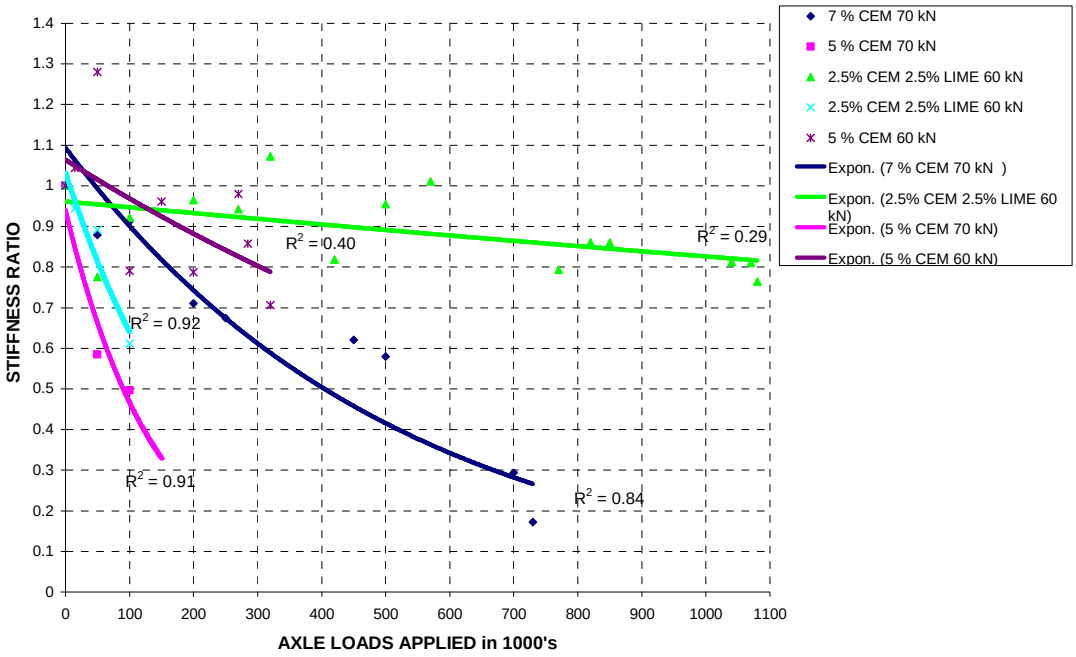

Figure 4.11: Comparative Stiffness Performance Chart for Middle of CTB in Transverse Direction

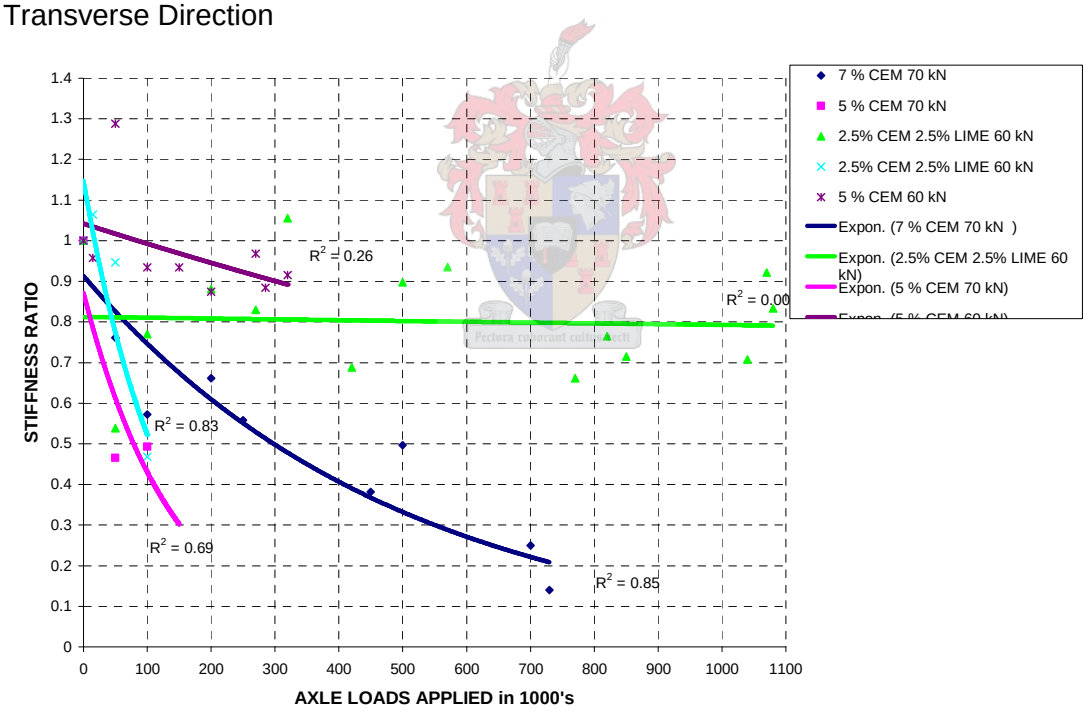

Figure 4.12: Comparative Stiffness Performance Chart for Bottom of CTB in Transverse Direction

These performance graphs served as one of the primary inputs in the development of the CTB transfer and fatigue performance charts. It also served as the point of

reference for the evaluation of the material damage factor. Both deductions are presented in Chapter 5.

These continuous stiffness performance trends for the respective pavement zones will subsequently be used as the basis to model pavement stiffness behavior in a pavement design software program.

4.4 Surface rut formation

Surface rut formation monitored intermittently during traffic loading by the electronic profilometer is presented in this subsection.
Typical progressive increase in transverse rut formation under traffic loading is illustrated in Figure 4.13. This is to illustrate transverse surface rut formation with increased traffic loading. Figure 4.14 illustrates the corresponding cumulative rut formation. Table 4.7 provides a summary of the final rut depths for sections tested. Graphs illustrating individual transverse rut profiles and cumulative rut performance are set out in Appendix D. In contrast to HMA pavements, the increase in rutting is more gradual as can be seen from the results, where HMA generally exhibits significant initial early life rutting and consolidate with further increased load application.

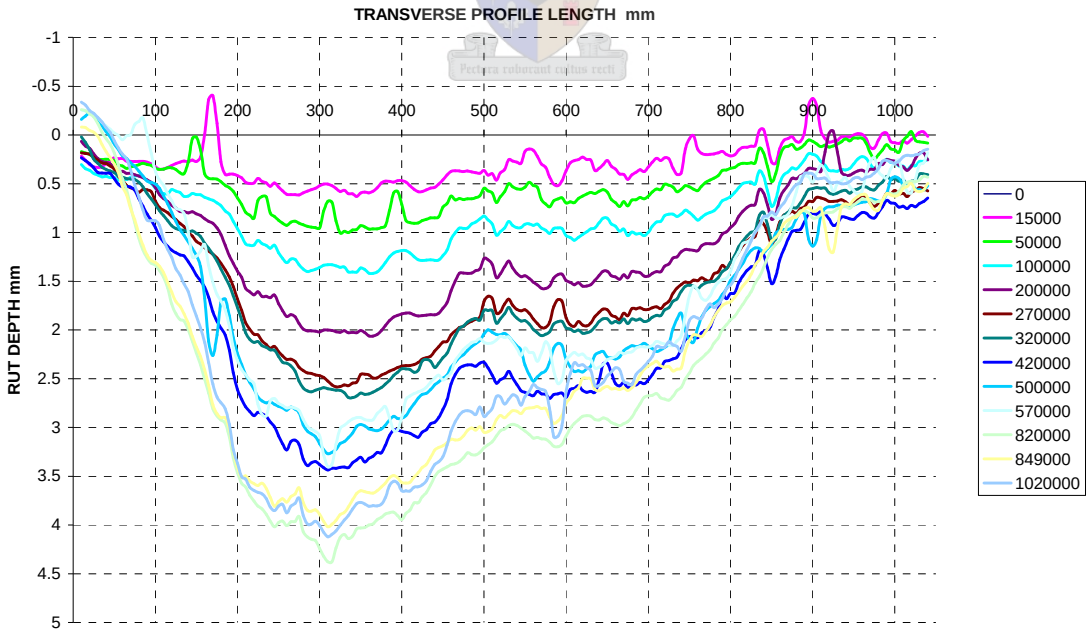

Figure 4.13: Transverse surface rut profiles with load applications for Section 5

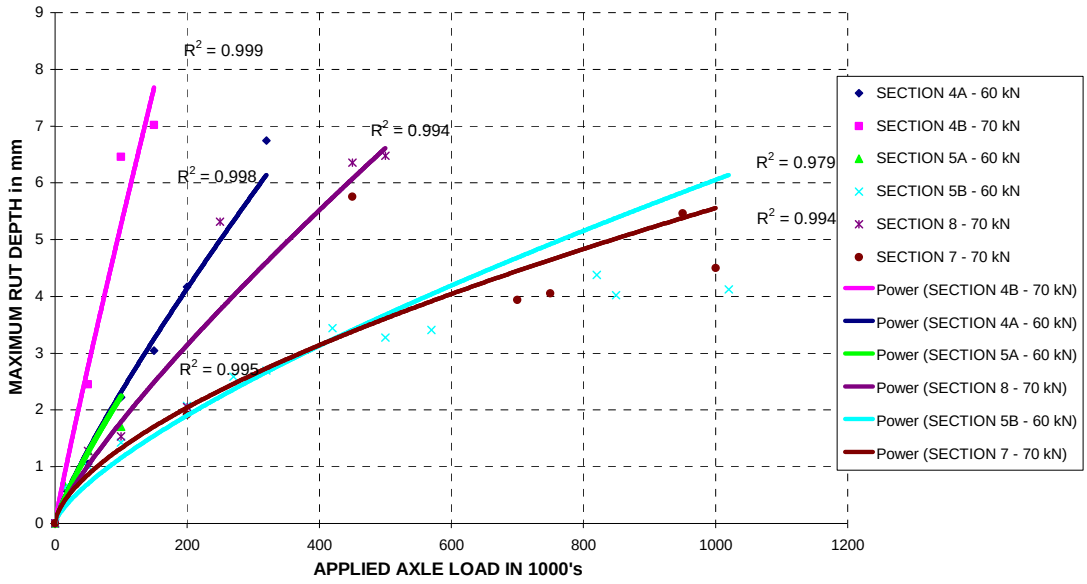

Figure 4.14: Cumulative maximum rut depth for sections tested

Table 4.7: Summary of rut depths at termination of testing for respective test sections

SECTION	COMPOSITION	AXLE LOAD	MAX RUT DEPTH	
			LEFT WHEEL	RIGHT WHEEL
		kN	mm	mm
4A	5 % CEM RED	60	6.74	6.05
4B	5 % CEM RED	70	7.02	7.16
5A	2.5 % CEM 2.5 % LIME RED	60	1.70	1.69
5B	2.5 % CEM 2.5 % LIME RED	60	4.12	3.10
8	7 % CEM RED	70	6.47	6.11
7	7 % CEM YELLOW	70	4.48	4.50

From diagnostic evaluation it appeared that no sub base rutting took place. Rutting that formed was the result of minimal asphalt deformation, interface distress, fracturing of the CTB as well as the removal of the subsequent loose material being pumped out through the surface cracks.

4.5 Surface crack formation

Cracking was monitored intermittently by visual inspection. Growth was recorded and evaluated by comparison of photographs taken at the various trafficking intervals. Typical isometric views to illustrate crack growth phenomenon of Section 4A are shown in Figure 4.15. Note pumping and longitudinal cracks in the left wheel track at

320 000 load applications. Full ranges of surface cracking and deformation images for each section tested are presented in Appendices E to J.

(a)Transverse shear crack initiation at 270 000 60 kN load applications - Section 4

(b)Transverse propagation of shear cracks at 285 000 60 kN load applications - Section 4

Figure 4.15: Isometric views of cracked surface at different stages of traffic loading

(c) Continuous transverse cracks and longitudinal crack formation after 320 000 60 kN load applications - Section 4

(d) Plan view of cracking pattern after 1 million 70 kN load applications on Section 7

Figure 4.15: Isometric views of cracked surface at different stages of traffic loading

(e) Overview of Section 7 after 1 million 70 kN load applications

Figure 4.15: Isometric views of cracked surface at different stages of traffic loading

Cracks diagonal to and on the outer edges of the wheel track and transverse cracks in between the wheels were first to appear. Diagonal crack formation is the result of the longitudinal in-plane shoving of the HMA resulting from in-plane horizontal shear forces and subsequent interface distress between the HMA and CTB. With increased traffic loading these cracks propagate across the wheel track in a direction perpendicular thereof, connecting with the transverse cracks formed in-between the wheels. This resulted in a complete transverse surface crack. Longitudinal cracks would start to form under the tyres interconnecting with the transverse cracks to form a crocodile cracking pattern.

4.6 Diagnostic evaluation

The trafficked pavements were diagnostically investigated by trenching and excavation across the wheel path at different positions as described in section 3.5. Findings were photographically recorded and presented in Appendices E to J for each pavement section tested. Primary findings are discussed.

Interface distress

Interface shear between the HMA and CTB layers took place under loading. The shear plane generally formed under the prime impregnated CTB surface. In-plane longitudinal displacement of the HMA was also recorded. Shear marks and

smoothed shear surfaces was observed on both the HMA and CTB contact planes. This could not be ascribed to the crushing of a biscuit layer as will be analytically presented in Chapter 5.

Flexural cracking

Longitudinal and transverse flexural cracks were observed. The pavement structure was fractured when the stiffness had reduced by 50 percent. It was also apparent that the fractured CTB blocks had experienced horizontal shoving of the HMA as trafficking progressed. From the test conducted on Sections 8 and 7 it was evident that the structure was more fractured when the stiffness ratio had significantly dropped to below 0.5 e.g. 0.2 – 0.3. With increased traffic loading the fracturing of the CTB progressively increased, reducing the particle size to smaller fractions. From the sections tested up to terminal pavement condition it was found that the fractioned particle size was smaller at the bottom than at the top.

In-plane horizontal shear

Horizontal shear planes were found about one third from the top of the CTB. In the lower cement stabilized bases trafficked up to a stiffness loss of 50 percent, these shear planes were found to connect the bottom up longitudinal cracks at this depth. In the bases trafficked to a more severe state of distress it was found that the shear plane had propagated laterally in the CTB structure, not only connecting the longitudinal cracks where the pavement structure moves into compression.

Section 8 was trafficked to a stiffness ratio as low as 0.2 when the pavement had deteriorated dramatically. Deep rutting occurred and severe pumping took place. The particle fractionation and loss of material through pumping led to the deep rutting as well as shear failure of the asphalt on the edges of the wheel track.

It is important to note that two types of distress could develop simultaneously on the same pavement section. At the far end of the section the distress was in the form of the three types discussed above. In contrast, at the start of the section the CTB had not shattered, but the HMA had deformed due to shoving of the asphalt material longitudinally as well as transverse shear adjacent to the wheel. This is believed not to be a MLS10 feature, this will be discussed in Chapter 5.

In all cases the distress in the bottom of the CTB was similar in relation to the relative reduction in stiffness in both extent and orientation. It is of course important to remember that trafficking had been done without lateral wander. This would influence the performance of the structure. No tests were done to investigate this phenomenon, but it is postulated that for the same level of distress, an increase in the number of load axles would result. This has been reported with APT on HMA. Therefore the current proposals for limit conditions are considered to be conservative. It is proposed that a factor relating to the transverse wheel load distribution be used to account for this possible increase in traffic loading capacity.

The general fatigue-strain probabilistic distributions of HMA for pavement fatigue life with lateral traffic distribution do not apply to the cement treated materials. The model was developed based on HMA performance. This entailed a material with elasto-plastic response, time dependency and strain path history characteristics. The cement treated material is assumed to behave elastically and performance is not dependent on stress history and loading time but on structural integrity of the material. Lateral wander of traffic loading could be conservatively incorporated by a shift factor on the fatigue curve relating channelized trafficking to transversely distributed traffic (Molenaar, personal communication, February 9, 2007).

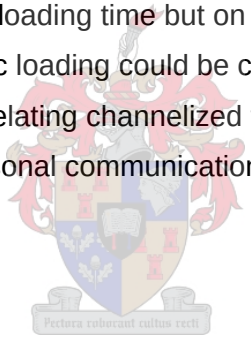

4.7 Closure

The presented collective results of stiffness and deflection performance, material strength tests, crack and diagnostic evaluation will be synthesized and relations determined for the development of interim transfer functions and material response models in Chapter 5.

Chapter 5

Synthesis

In this chapter the author synthesizes the results obtained from response measurements for better understanding and characterization of CTB material behaviour under repeated loading. The synthesis is based on the research results reported in this thesis as well as inputs reported under the Mozambican project where stated. The synthesis is primarily formulated on correlations and interpretation of the pavement response characterization conducted by the author. The reported synthesis will form an integral part of the synthesis of the Mozambican project since the objectives of the research presented in the thesis correspond to the objectives of Phases 1 and 2 of the project.

The APT program yielded a significant amount of invaluable findings. From diagnostic trenching different mechanisms of failure were identified. The material damage factor for cement stabilized sand bases was determined from different load tests conducted on the 5 percent cement stabilized sections. Synthesis of the results presented in Chapter 5 resulted in the development of a transfer function for pavement performance in terms of traffic induced stresses and number of axle repetitions to failure for the two failure mechanisms presented, flexural cracking and HMA - CTB interface shear. Interface shear failure was correlated to shear stress strength ratios under traffic loading. Simultaneous evaluation of deflection and stiffness performance with increased traffic loading yielded a model for determining a parameter for pavement management and gauging the extent of distress in terms of stiffness loss at any point of pavement life. Curvature parameters (β) for the general pavement damage model described by a Weibull distribution (Molenaar et al. 1999) could be approximated from the stiffness performance graphs for different quantities of stabilizing agent.

5.1 Mechanisms of failure

Manifestation of distress followed a pattern that had been identified in an earlier MMLS3 laboratory study on scaled pavements (Strauss et al. 2005, 2006; De Vos et al. 2006). Distress development in the high-strength cemented bases appears to differ from normal distress development in full depth AC pavements (Hugo et al, 2004) (Sugjoon & Richard 2004). The postulated failure mechanisms are based on the following primary inputs:

- Diagnostic trenching
- Stiffness performance of test sections in terms of pavement zone and orientation
- Surface crack patterns
- Material test results
- Surface rutting
- Linear elastic pavement analysis

5.1.1 HMA - CTB interface shear failure

HMA – CTB interface distress under the asphalt was evident. Asphalt surfacing exhibited in-plane horizontal longitudinal displacement. This is manifested in the development of diagonal shear fractures (cracking) on the sides of the wheel path. This phenomenon is clearly related to shear bond between asphalt surfacing and CTB. Continued traffic loading leads to pulverizing and distress aggravates when water ingress occurs during load trafficking. Pulverized material migrates through cracks by means of pumping action. Initial surface rutting relates to removed pulverized interface material. Diagnostic trenching exhibited clear evidence of the postulated nature of distress (see Figure 5.1), from evaluation of diagnostic picture sequences of sections tested presented in Appendices E to J. In the later stages of pavement life the HMA shears off completely and the whole pavement experience a dynamic bow wave under trafficking loads. The bow wave was to such an extent that it was visible to the naked eye.

(a) Underside of HMA

(b) Top of CTB

Figure 5.1: Pictorial view of HMA-CTB interface distress surfaces, Section 8 (note longitudinal shear markings)

Commencement of interface shear distress and rate of deterioration is a function of the traffic induced stress and shear strength of the material. Development of performance and fatigue functions based on above mentioned characteristics of this phenomenon are discussed in subsection 5.4.

5.1.2 Longitudinal en transverse flexural cracking

Bottom-up transverse and longitudinal flexural cracking of the pavement is the primary mechanism of CTB structural failure. This is concluded from evaluation of the layered stiffness performances where the stiffness reductions in the longitudinal are greater than that in the transverse direction. This is illustrated in Figure 4.5 and

corresponding figures in Appendix C. Reductions in stiffness ratios were found to be greatest in the Bottom pavement zone for all pavements. Subsequently transverse cracking from bottom to the surface starts earlier in pavement life and progresses more quickly than longitudinal cracking under the wheel track. This is also manifested by translation of the CTB crack pattern through the HMA to the surface, where transverse cracks appear and propagate before cracks in the longitudinal direction. Figure 5.2a and b depict the pavement blocks extracted from section 4B exhibiting above mentioned phenomena, these blocks were not extracted from the worst performing part of this section. Diagnostic trenching further supports the hypothesis by indicating that transverse crack formation happened before that in the longitudinal direction. The Section 4A pavement block illustrated in Appendix E indicated this through the uninterrupted transverse crack while the propagation of the longitudinal crack is interrupted by die transverse crack. This phenomenon was also observed during field inspection of old sections, 30 years, of highway EN1, where such cracks had migrated to the pavement surface.

(a) Side view – note two longitudinal cracks and in-plane shear crack (direction of traffic indicated with arrow)

(b) Plan view (direction of traffic indicated with arrow)

Figure 5.2: Plan and side views of CTB block extracted from 5 percent cement stabilized Section 4B after 150 000 70 kN load applications

From the diagnostic trenching it is apparent that longitudinal crack propagation start through two longitudinal cracks that form under the dual wheel track. Initial transverse cracks are more closely spaced and distance between them is a function of material strength. Development of performance and fatigue functions based on above mentioned characteristics of this phenomenon are discussed in subsection 5.3.

5.1.3 Shear plane formation in the CTB

A secondary CTB structural mechanism of failure is the occurrence of a horizontal shear plane in the CTB. This plane was generally found to occur in the middle of the combined HMA CTB structure (100 mm from the top) this position is also one third of the CTB thickness from the top thereof (50 mm). This plane links the two longitudinal cracks and forms a 'shear box'. As shown in Figures 3.15b, e, 5.2a and 5.4a and c. The similar mechanism has been reported under scaled laboratory testing of this material (de Vos et al. 2006; Strauss et al. 2005, 2006).

A linear elastic shear stress analysis was done with Bisar 3.0 to investigate this phenomenon. Two pavement models were analyzed for the evaluation of the shear stress distribution in the pavement before and after interface distress, were

conducted. The pavement structure representing the pavement before interface distress had a full friction interface between the HMA and CTB. The second pavement model had a 10 mm layer in between the HMA and CTB with the same attributes than the sub base, this was done to simulate the sheared and pulverized interface. Shear stress pavement profiles for the 'Bonded' and 'Unbounded' scenarios are illustrated in Figure 5.3.

The plots illustrate that maximum shear stress is initially at the HMA CTB interface, after failure thereof the maximum shear stress in found in the middle of the combined pavement structure, 100 to 125 mm from the top, hence formation of the horizontal in-plane shear crack. The working stress to strength ratios for both the interface and shear plane mechanisms are set out in Table 5.1. This is to illustrate at what level of stress relative to material strength the CTB material is subjected to. Values greater than one indicates that the induced stress is greater than the material strength for that load – pavement composition scenario. Interface failure will start with the commencement of traffic loading in those scenarios.

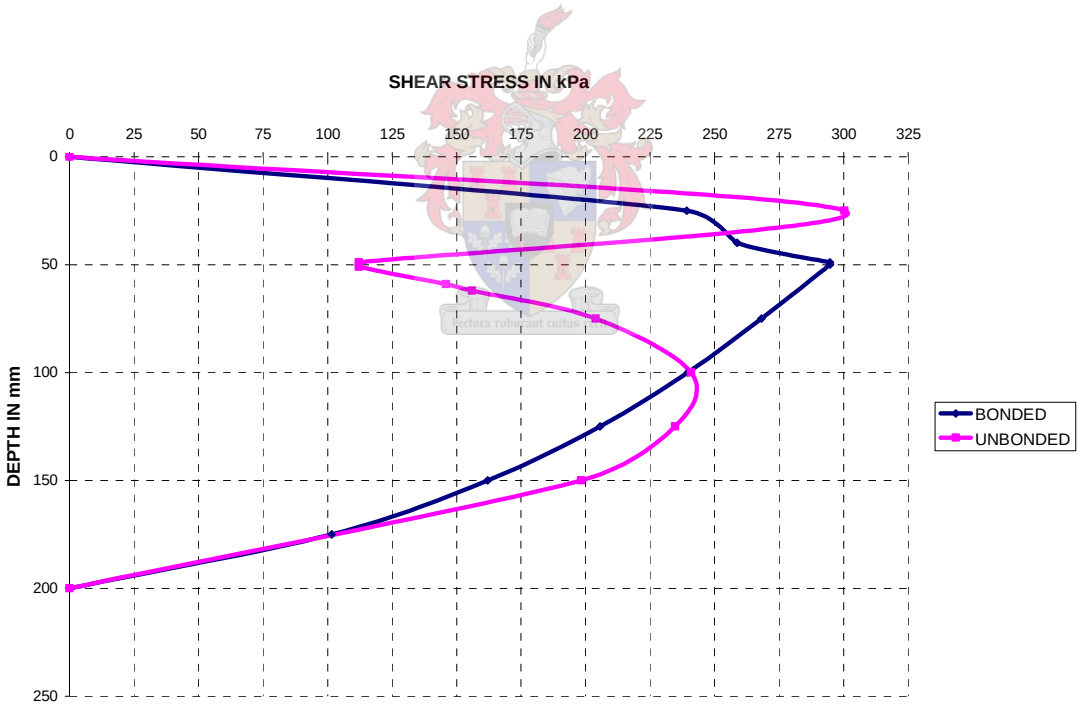

Figure 5.3: Shear stress plots for 5 percent CTB under 60 kN axle load

(a) Front view - note horizontal shear plane and longitudinal cracks

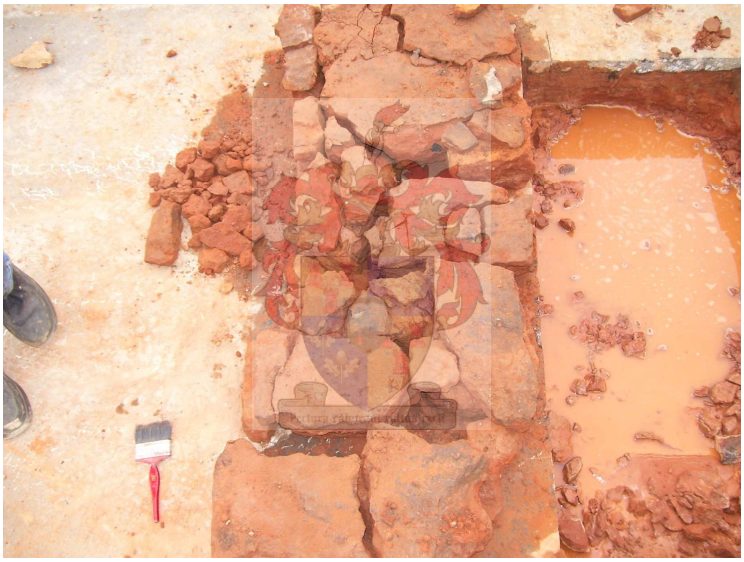

(b) Plan view – note transverse crack

(c) Rear view – note horizontal shear plane

Figure 5.4: Front, plan and rear views of fractured CTB extracted from Section 4B

Table 5.1: Stress to strength ratios for the interface and shear plane failure mechanisms

CONDITION	HMA - CTB INTERFACE MECHANISM	CTB MID LAYER SHEAR PLANE MECHANISM
5% / 60 kN	1.09	0.90
5% / 70 kN	1.12	0.97
7% / 70 kN	0.82	0.75

From the illustrated shear stress plots and ratios presented, it could be concluded that the in face distress occurs first followed by the shear plane formation. The high stress to strength ratios for the 5 percent sections further indicate why the interface distress initiates much earlier relative to the gradual stiffness loss at the bottom part of the base. A comparison between the 5 and 7 percent cement treated sections' ratios indicate why the shear crack formation for the higher cemented sections start later in the pavement life (after 50 percent base stiffness loss).

Trenching of trafficked sections, 4A and 5B which both exhibited a stiffness loss of 50 percent in the bottom zone of the CTB, produced all three of the above mentioned mechanisms. It was found that the CTB of these sections consist of cracked big blocks (+- 400 x 400 mm) under the loose HMA mat (Appendices E and J). At this stage in pavement life the dynamic surface rolling occurred under traffic. The surface deflection generally doubled. Diagnostic evaluation of Sections 4B, 8 and 7, that were tested with higher loads and up to stiffness values as low as 30 to 20 percent of

the initial, showed that these CTB blocks were fractionized further into much smaller particles (Appendices D, I and J). At this stage of pavement life. severe lateral asphalt movement has taken place resulting in wide transverse and diagonal cracks (1 – 2 mm). Fine crushed material was pumped out; this resulted in vertical shear of asphalt as there was less supporting base material left beneath the wheel tracks. Subsequent significant increases in rutting were also observed under these conditions. Maximum surface deflections of 2.8 to 4 times that of the initial untrafficked deflections were measured. Relative increases in the deflection ratios are smaller from 50 to 80 percent stiffness loss as the pavement loses structural integrity and ability to respond elastically under loading. Figure 5.5 illustrates this phenomenon. Excavated CTB fractions for diagnostic investigation from Section 8 trafficked to terminal failure, 70 to 80 percent stiffness losses, were found to be smaller in size at the bottom than the pieces from the top of the CTB, Appendix K. This phenomenon is also indicted by the respective modulus plots of the various pavement zones for the sections in question, where the bottom zone experienced greater decreases in stiffness with loading that the top.

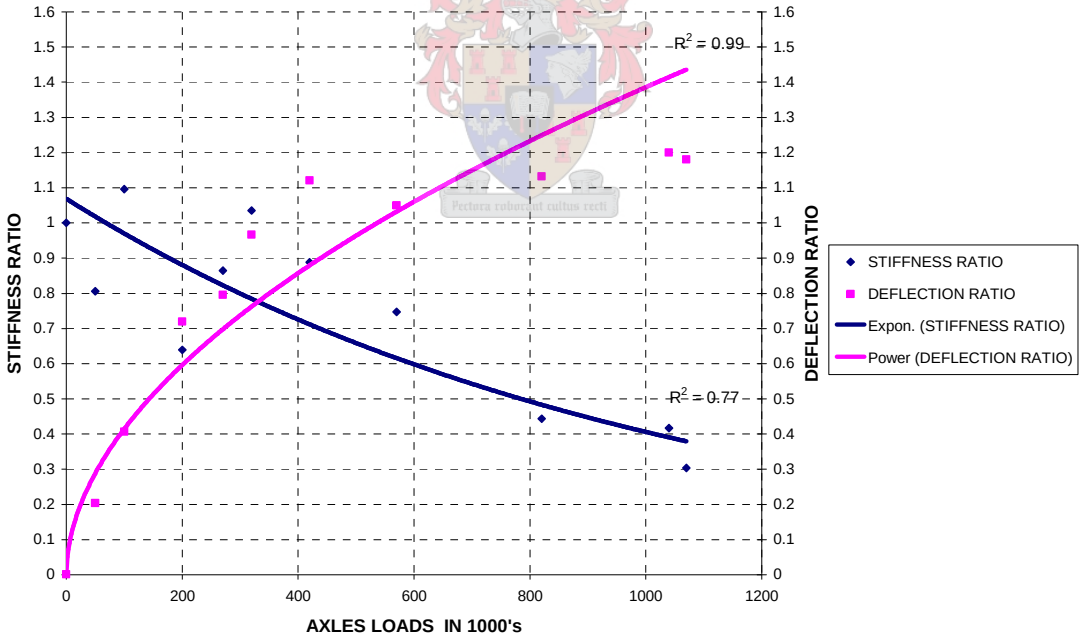

Figure 5.5: Stiffness – Deflection performance of 2.5 % cement and 2.5 % lime stabilized red base material under 60 kN axle loading

The different distress modes causing the disintegration of the pavement structure were found to occur in different sequences depending on the structure of the pavement and the strength of the materials. For the higher strength cemented bases

the interface distress occurred later in pavement life relative to the base stiffness loss than the lower strength cement treated bases. This is ascribed to the stress strength ratio under traffic loading at the pavement interface. The distress mechanisms identified in the pavement system during the study were excellent replicas of those found in similar pavement structures in the region. The proposed failure mechanisms will provide the basis for better modeling the performance of the CTB pavement structures appropriate for use in the region.

5.2 Material damage exponent

The damage exponent (n) for the sandy cemented materials were determined from test results obtained by conducting two full scale tests on the same pavement 5 percent cement stabilized section with axle loads of 60 and 70 kN. From the stiffness performance graphs of the two tests, 4A and 4B, traffic loads applied to induce a 50 percent loss in CTB stiffness were obtained. These values are 380 000 and 50 000 for the 60 kN and 70 kN load tests respectively. This yielded an average material damage exponent n of 12.5 according to equation 5.1. In both these tests the distress in terms of internal fracturing was similar. Surface distress was also similar with delamination occurring before stiffness has reduced by 50 percent. Determination of this material damage exponent is based on one set of tests on a single pavement structure. This exponent is applicable to thin sandy cement stabilized pavements with a structure as illustrated in Figure 5.1.

$$\left(\frac{70kN}{60kN}\right)^{n} = \left(\frac{380000}{50000}\right) \tag{5.1}$$

Jameson et al. (1992) reported pavement damage exponents in the range of 8 to 12 for cement treated crushed rock base material, based on the Mulgrave Trails conducted with the Accelerated Loading Facility (ALF) from 1989 to 1991. A value of 12 was subsequently accepted as the appropriate damage exponent for cement treated base material in Australia.

5.3 Development of flexural fatigue transfer function

Transfer functions were developed based on the following three primary elements:

- CTB stiffness performance relative to trafficked loads
- Indirect tensile strength (ITS) of the CTB
- Traffic induced tensile stress in the pavement

Results of the 60 and 70 KN trafficking tests on Section 4, 5 % cement stabilized red sand, were used to establish the transfer function. The pavements were constructed in June 2005 and tested slightly more than one year later.

ITS values were transferred to M_R strengths by using the results reported by Melis et al (1985). This was done to transpose the base material tensile strength to a bending strength. BISAR 3.0 analysis was then done to determine the initial stress at the bottom of the CTB layer.

Procedure:

1. Initial tensile stress at the bottom of the CTB was determined for 60 and 70 kN dual wheel loads respectively, using BISAR 3.0. These were graphically plotted relative to their respective number of load applications at a stiffness ratio of 0.5. This is shown in Figure 5.6. The graph was extrapolated to include the stress under a 50 and 40 kN wheel loads. This represents the transfer function after one year curing of the CTB.
2. A fatigue curve, Figure 5.7, in terms of ratio of applied stress to strength vs. load repetitions was established. This was based on material strengths from ITS testing, calculated traffic induced pavement stress from BISAR 3.0 and axle repetitions to failure. This curve compares well with results reported by Croney and Croney (1991) for cement stabilized materials, albeit slightly lower.
3. Early life performance (28 days) of the CTB was then modeled by using early life strength and stiffness values. The load stress was found to be at a high percentage of the strength. This effect reduces the number of stress applications to failure. From the established fatigue curve, Figure 5.7, it was determined that pavement life would be reduced by one and a half

orders of magnitude, hence the green line for 28 day performance in Figure 5.6.

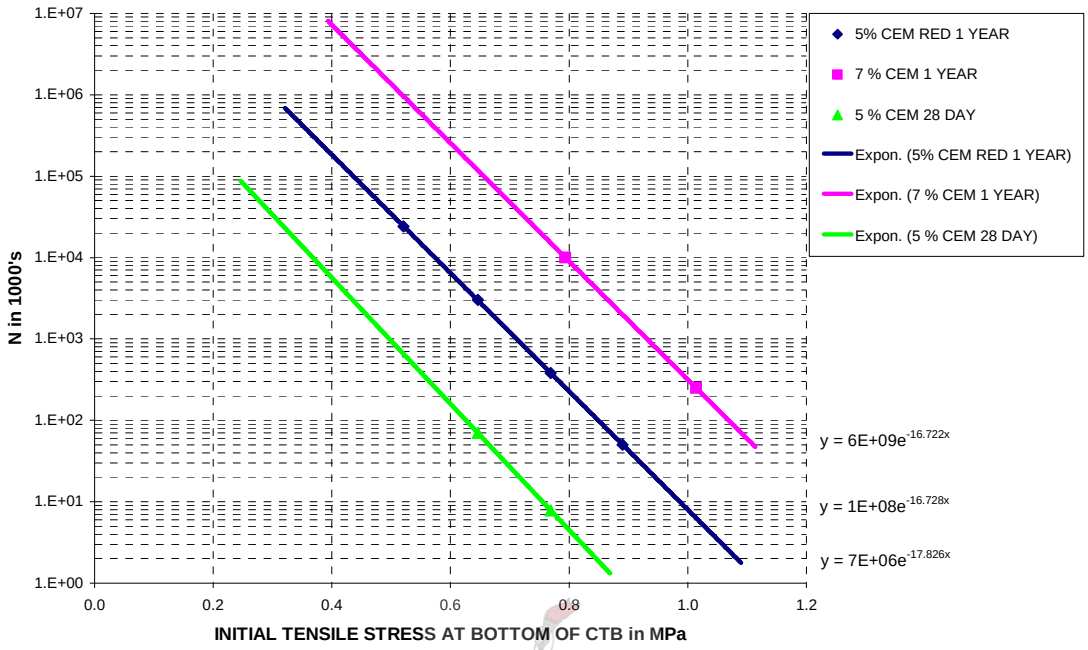

Figure 5.6: Relationship between traffic induced stress and wheel loads trafficked for flexural fatigue

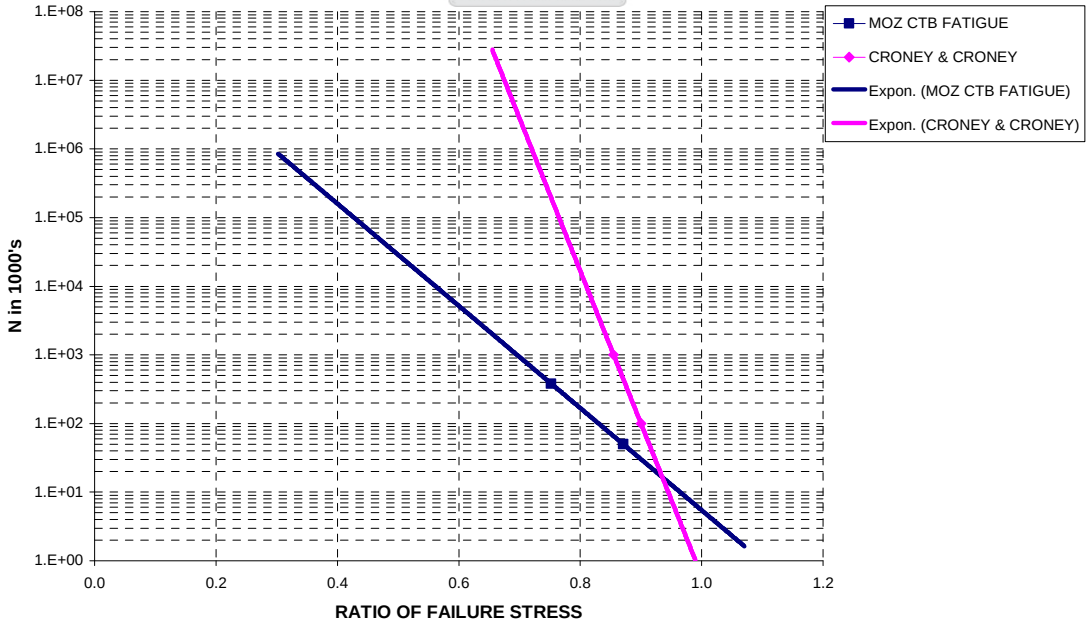

Figure 5.7: Flexural fatigue of 5 percent cement stabilized sand

Results of the test conducted on Section 8, 7 percent cement stabilized red sand base, were analyzed and plotted on the same graph. The data point is above the 5 percent performance graph as expected. Since no 60 kN testing was conducted it was assumed that the graph would be parallel to the 5 percent graph and the line was extrapolated accordingly.

It is proposed that this transfer function be used as the basis for evaluating designs with varying base thickness. This illustrates the importance of the effect that a longer curing time has on flexural fatigue pavement performance.

5.4 Development of interface shear performance and fatigue functions

The development of the transfer function for interface the shear failure mechanism as discussed under mechanisms of failure is based on the following primary elements:

- Shear strength characteristics of cement treated materials
- Traffic induced shear stresses at interface of HMA and CTB (pavement depth 50 mm)
- Commencement of HMA shear cracking under traffic loading

Shear stress analysis by BISAR 3.0 indicated that principle shear stresses develop perpendicular to and on the perimeter of the wheel footprint. Under dual wheel load configuration transverse shear is 3 percent higher than in the longitudinal direction. Analysis was done with the assumption of a circular footprint in lieu of an oval, hence the similarity in longitudinal and transverse directions. Results obtained correlate favourably with work reported by de Beer et al. (2002). Table 5.2 summarizes shear stresses computed and results from measurements as reported by de Beer. Measurements by de Beer were conducted under a single wheel on a thin asphalt pavement.

Shear stress under load and trafficked axles at the moment of shear crack initiation obtained from visual inspection for sections tested are plotted in Figure 5.8. This includes 5 and 7 percent stabilized Sections 4A, 4B, 8 and 7. Surface crack manifestation is illustrated in Appendices E, F, I and J for the respective test sections.

TABLE 5.2: Results from pavement shear stress analysis and reported by de Beer et al. (2002)

SECTION	STABILIZER	SAND TYPE	TYRE PRESSURE	AXLE LOAD	SHEAR STRESS	
					LONGITUDINAL	TRANS-VERSE
			kPa	kN	MPa	MPa
4A	5 % CEM	RED	800	60	0.305	0.315
4B	5 % CEM	RED	800	70	0.315	0.327
8	7 % CEM	RED	800	70	0.307	0.319
7	7 % CEM	YELLOW	800	70	0.307	0.319
DE BEER	THIN HMA	-	-	35*	0.319	0.209

* Wheel load – Single wheel configuration

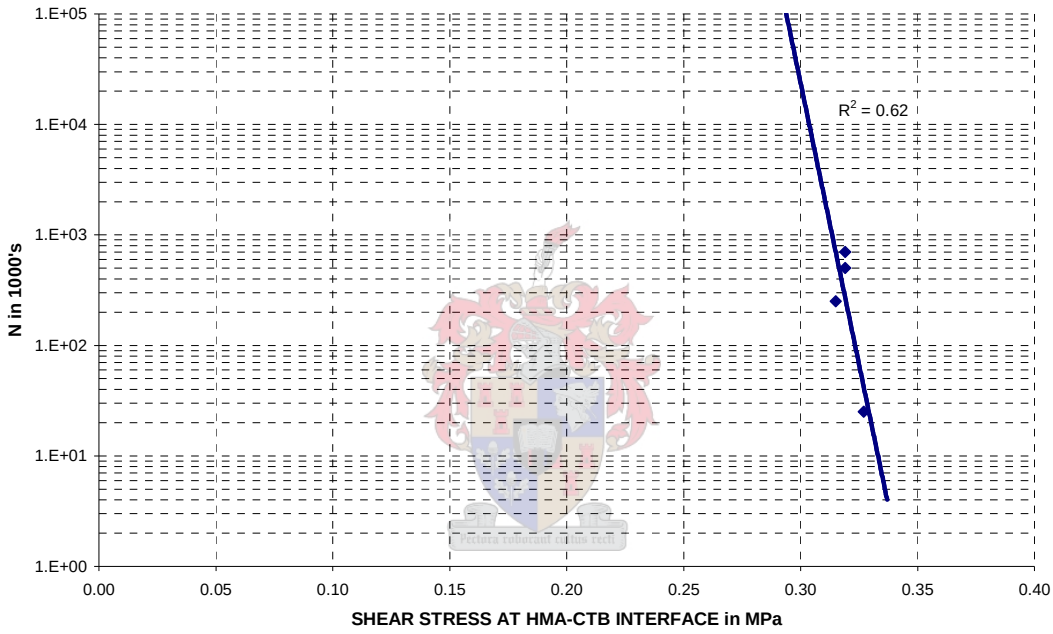

FIGURE 5.8: Shear interface failure performance curve for sand cement stabilized bases

The shear stress CTB fatigue curves for 5 and 7 percent stabilized materials, plotted in Figure 5.9, was developed by relating traffic induced shear stress to strengths obtained from shear testing of test section specimens to trafficked load at crack initiation. Development of this relationship is based on results obtained from Sections 4A, 4B, 8 and 7, hence in-situ strength data after one and half years. The curve for flexural fatigue is also included in Figure 5.9, to illustrate the relative trends.

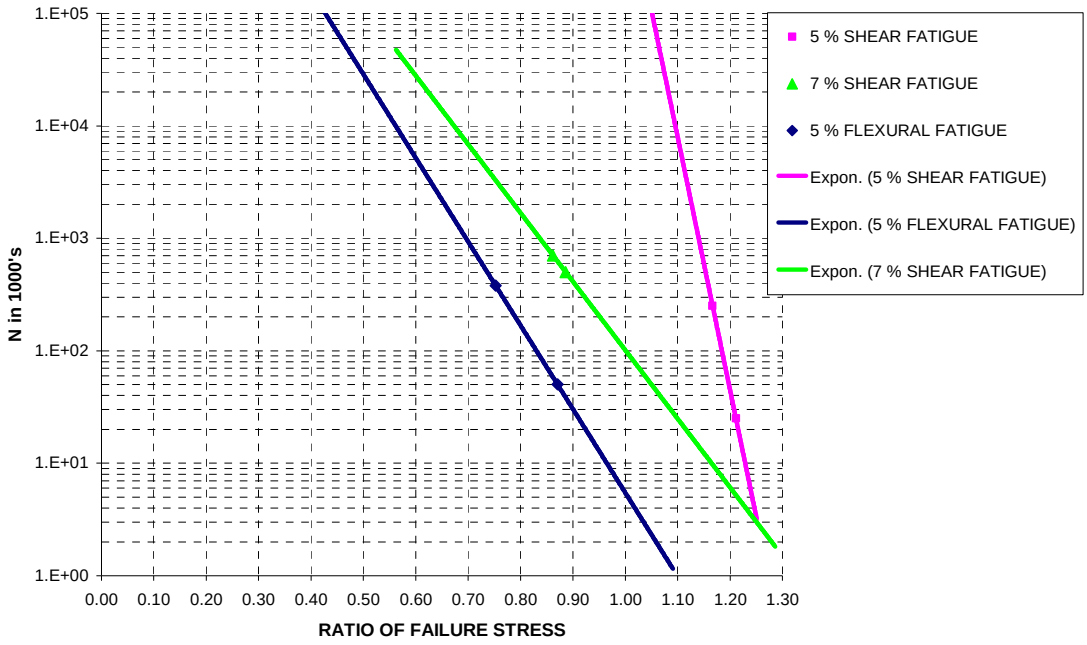

FIGURE 5.9: Interface shear fatigue curves for cement stabilized sand bases

The significance of these curves is in the illustration of the shear failure susceptibility at early age of the CTB, the 5 percent material in particular. The slope of the curves indicates the magnitude of the rightward shift of the performance curve, Figure 5.8, in the case of early age trafficking. Stress to strength ratios would be significantly higher for the 5 percent stabilized material.

Note that this transfer function and fatigue curves for flexural and interface failures were developed according to performance under channelized traffic loading. Lateral wander during loading would result in longer pavement life before distress initiation and terminal fatigue. Conducting of full-scale tests with lateral wander was not possible in the scope of the study.

An analytical solution is proposed for this limitation. Two methodologies could be followed:

- Since the CTB material performance is susceptible to a critical tensile stress situation at the bottom of the CTB layer. It is suggested that the design engineer perform linear elastic analyses at the different transverse positions across the pavement, where axle loading would occur. During this analysis the traffic induced tensile stress at the pavement location with the highest

load frequency should be evaluated relative to the material critical tensile stress. A pro rata ratio of load distribution that induces this critical stress at the position of highest passing frequency relative to the total load distribution could be determined. This should act as an indication of the magnitude of the lateral shift factor for the fatigue transfer function.

- A Miner's Law approach could also be followed on the above mentioned methodology as well as the full spectrum of axle loads.

5.5 Stiffness deflection relation

Concurrent evaluation of the CTB stiffness and deflection responses of the respective tests and test conditions yielded the relations illustrated in Figure 5.10. Where deflection performance as ratio relative to initial deflection at the commencement of APT are plotted against corresponding stiffness performance ratios. Graphs depicting stiffness and deflection performance during trafficking for each section tested are illustrated together with a graph similar to Figure 5.10 but with deflection in millimeter in Appendix K.

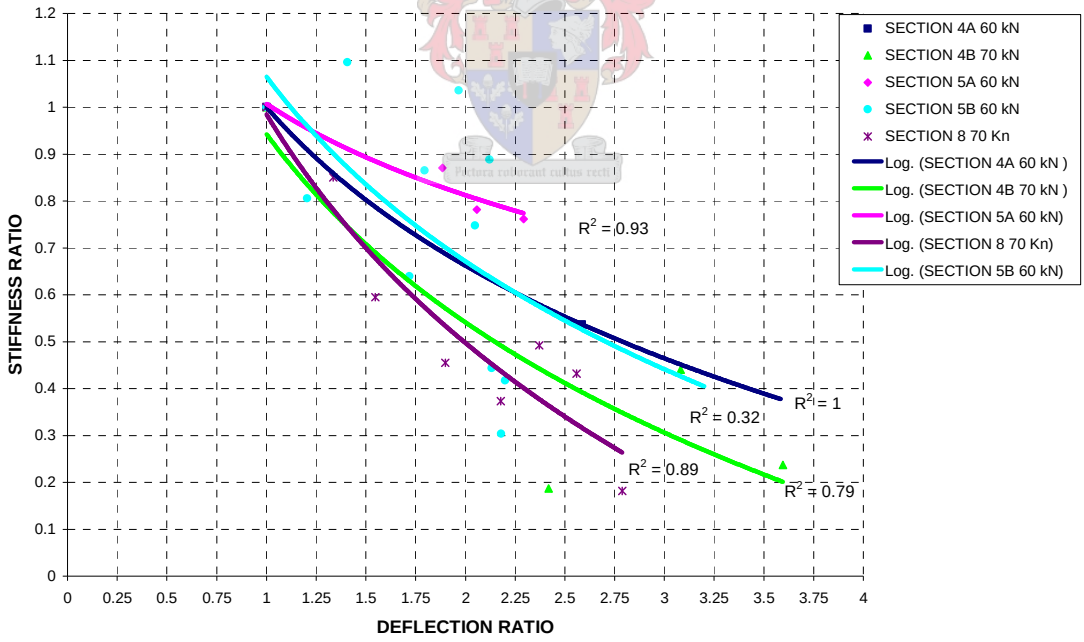

Figure 5.10: Stiffness - Deflection relations for cement treated base materials tested

From Figure 5.10 it is apparent that maximum surface deflections are 2 to 2.75 times the initial maximum surface deflection when CTB stiffness has lowered to half of the initial.

Stiffness - Deflection trends for CTB for the different binder and load characteristics tested are illustrated in Figure 5.11. It should be noted that the 5 % CTB 60 kN trend line represent three different full-scale tests, hence the poor regression fit. This figure could be used as a transfer function for determination of stiffness condition of a pavement section from measured deflection given that the initial untrafficked deflection is known. It is also applicable for the termination of remaining pavement life, based on the fatigue transfer functions presented.

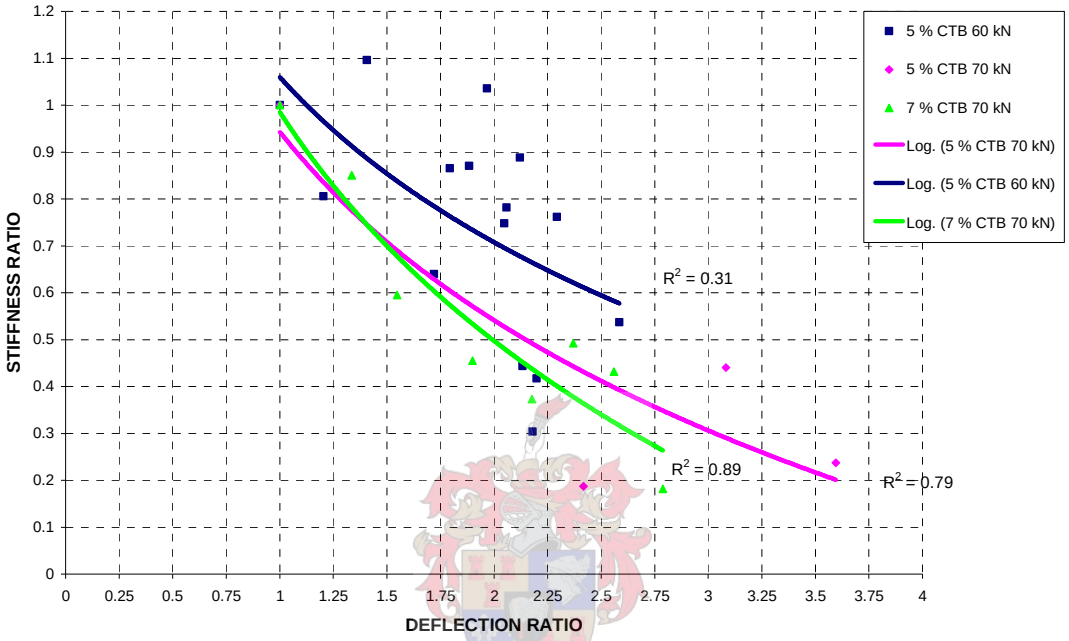

Figure 5.11: Stiffness deflection trends for percentage binder and corresponding axle load

Relationships between tensile strain in the base and Surface Curvature Index (SCI) have been reported (Molenaar et al, DATE). This was developed for bound asphalt bases and is the basis of the TRL overlay design method. The author moved away from the strain based fatigue and performance models based on the reasons presented earlier. The tensile stress and SCI relations for thin sandy cement stabilized base pavements could be further investigated and compared to the TRL overlay design method. It is expected however that similar relations as the ones presented above will be found.

5.6 Comparison of findings to the SAMPD

This subsection presents a comparison between the South African Mechanistic Pavement Design and proposed Mozambican approaches.

For pavement life predictions of the two systems the failure mode for cemented materials is linked to critical parameters calculated at specific positions in the pavement structure under loading. Transfer functions provide the relationship between the value of the critical parameter and the number of load applications that can be sustained at that value of the critical parameter, before the particular material type will fail in a specific mode of failure.

According to an overview of the South African Mechanistic Pavement Design Analysis method reported by Theyse et al. (1996) the SAMPD of cemented materials is as follows:

> *"Cemented material exhibits two failure modes, effective fatigue and crushing of the top part of the CTB (de Beer 1988). The critical parameters for cemented material is the maximum tensile strain ε (εμ) , at the bottom or in the layer controlling the effective fatigue life and the vertical compressive stress σ_v (kPa), on top of the cemented layer controlling crushing life. Transfer functions are provided for two crushing conditions, namely crush initiation with roughly 2 mm deformation on top of the layer and advanced crushing with 10 mm deformation and extensive breakdown of the cemented material.*
>
> *The effective fatigue transfer functions for cemented materials are presented as functions of tensile strain* (ε) *to a tensile strain-at-break* ($\varepsilon_{B)}$ *ratio* ($\varepsilon / \varepsilon_B$) *for different service levels. Transfer functions do not allow for different layer thicknesses. A shift factor was therefore introduced to allow thicker layers to have an extended effective fatigue life compared to thinner layers subjected to the same strain.*
>
> *Transfer functions were also developed for crush initiation and advanced crushing of cemented material. These functions relate the vertical compressive stress to UCS ratio with numbers of load applications for different levels of service. Critical material parameters are strain-at-break,* ε_B (με), *and Unconfined Compressive Strength UCS (kPa).*

Structural behavior of a cemented layer in a pavement structure is in three phases. During the pre-cracked phase the elastic modulus of the layer will be in the order of 3000 to 4000 MPa and the layer will act as a slab with the slab dimensions a few times larger than the layer thickness. This E-value reduces rapidly to values in the order of 1500 to 2000 MPa at the onset of the effective fatigue life phase during which the layer is broken down from large blocks with dimensions of approximately 1 to 5 times the layer thickness, to particles smaller than the thickness of the layer. During the equivalent granular phase the elastic modulus is in the order of 200 to 300 MPa and the cemented material acts typically like a granular layer. Figure 5.12 illustrates the long-term behavior of a lightly cemented layer in a pavement structure. Different conditions of crush initiation and advanced crushing are illustrated according to the long-term behavior model in Figure 5.13."

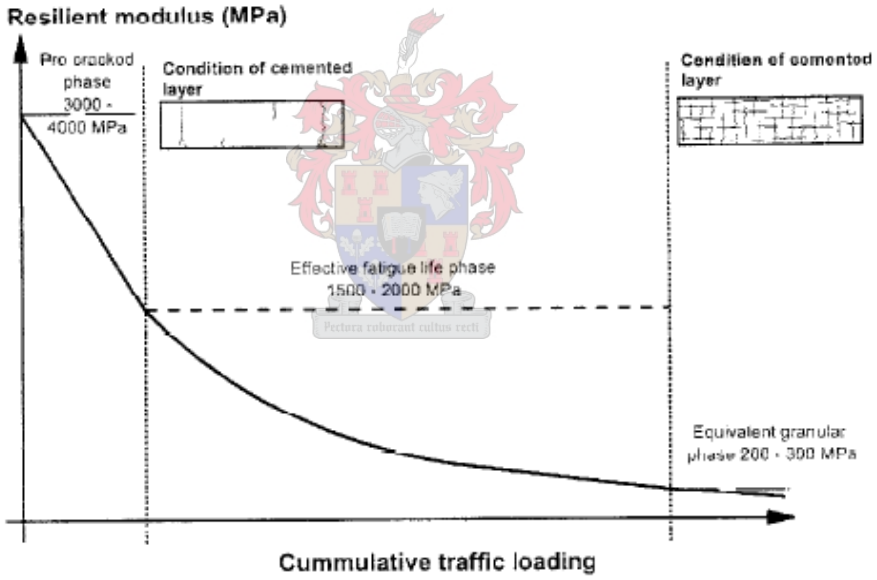

Figure 5.12: Long-term behavior of lightly cemented material

"Although these changes in behavior of the cemented material will gradually occur with time, they are modeled as stepwise phases in the life of the cemented material. The modulus of a cemented material is modeled as a constant value for the duration of a particular phase with as sudden change at the end of each phase. The effective fatigue life phase and the equivalent granular phase of cemented material is used to calculate the layer life for the cemented layer. The pre-cracked phase is considered to be very short in relation to the other phases and is therefore not included in predicting the

layer life for the cemented material. The stresses and strains calculated during one phase are not valid during the following phase. A structural analysis is therefore done for each phase with the applicable reduced modulus for the cemented layer. The stresses and strains calculated for each phase will yield a predicted layer life during each phase."

Comparison between the synthesis of the Mozambican pavement responses and SAMPD are made with regard to the following aspects:

- Failure mechanisms;
- Critical material characteristics;
- Transfer functions;
- Pavement modeling.

The SAMPD are based on two failure mechanisms effective fatigue and the crushing of the top of the CTB whereas the proposed Mozambican approach is based on three failure mechanisms flexural fatigue, interface distress and horizontal shear formation.

The critical design parameters are compressive stress σ_v (kPa) at the top of the CTB and maximum tensile strain ε (με), at the bottom for the SAMPD. Design parameters for the Mozambican approach are the shear stress T_H (kPa), at the HMA - CTB interface, in the middle of the combined bounded structure and the tensile stress σ_T (kPa), in the longitudinal direction at the bottom of the CTB.

The subsequent material test parameters for the two approaches are strain-at-break, ε_B (με), and UCS (kPa), for the SAMPD and tensile and shear strengths, σ_T T_H (kPa), from ITS and shear testing for the proposed Mozambican approach.

Ratios of calculated stresses and strains to material parameters of general material classes are used for determination of the number of load applications to failure for the SAMPD method. It should also be noted that a Poisson's ratio 0.35 is used for cemented material in the SAMPD whereas a ratio of 0.18, obtained from the instrumented ITS testing presented in Chapter 4, is proposed for the Mozambican approach. For the Mozambican approach calculated stresses are used for determination of load applications to failure. Layer thickness manipulation is more easily accommodated in the Mozambican approach.

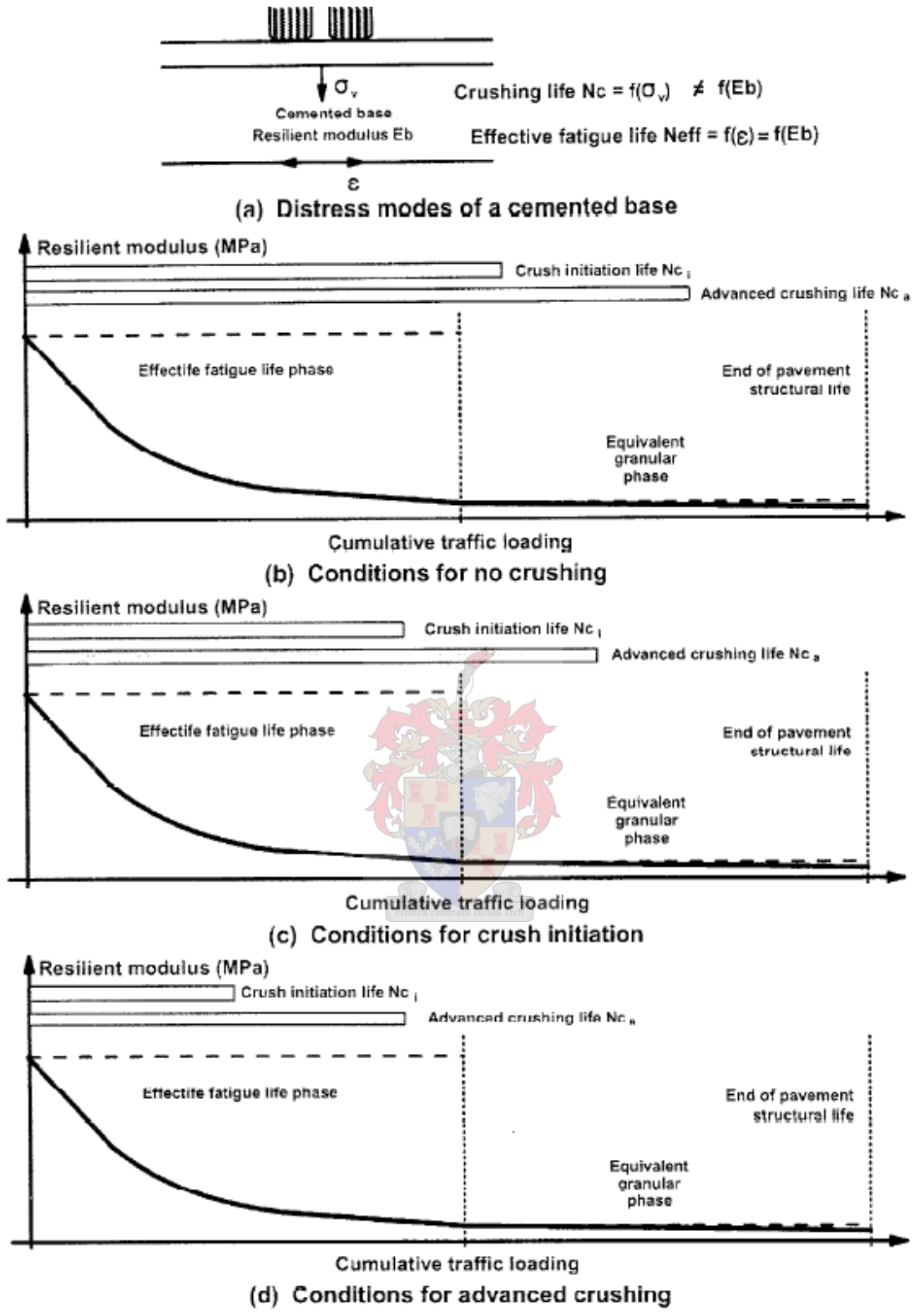

Figure 5.13: Crush initiation and advanced crushing for lightly cemented layers

For the proposed Mozambican approach simultaneous analysis of the failure mechanisms allows optimization of the design whereas in the SAMPD calculation of the ultimate layer life is an iterative process.

For the SAMPD pavement behaviour is modeled through the stepwise phases as described above. Whereas continuous stiffness reduction modelling for the occurrence of the different pavement phenomena in the different performance zones could be done in the Mozambican approach. This would be based on the stiffness performance characterization presented.

The primary difference between the two approaches is the single sized sand and predominantly graded angular granular CTB materials as well as the different pavement structures. These differences produce different failure mechanisms and subsequently critical material and pavement parameters. The two approaches further differ in the continuity of stiffness characterization in modeling and determination of ultimate pavement life.

5.7 Discussion of Synthesis

The general perception in Mozambique is that incorrect construction methodology and curing of CTB layers are the main contributing factors responsible for premature pavement failure due to base delamination after completion of recent construction contracts. Current design is stabilization with 5 to 6 percent cement, construction and curing as prescribed under Type 2 methodology for test section construction. However premature failure of the interface generally occurs after the second rain season following construction completion and opening to traffic (cases reported during post award workshop with ANE personnel). The synthesis of the results reported in this study will assist the design engineer to evaluate this problem from a new perspective.

The performance and fatigue curves developed for the two principle mechanisms of failure must act as tools for evaluation of pavement stress, strain and fatigue performance and optimization of design.

It is very important to appreciate the lower cement, 5 percent, stabilized base is susceptible to shear failure under heavy traffic loading (120 to 140 kN full axles) in early and later life. This has to be addressed in design. This could be achieved

through thicker HMA, higher shear strength materials, better curing techniques and an enhanced layer interface. Current technique of asphalt surfacing within two weeks of base construction and compaction with vibrating steel drum and 22 t pneumatic wheel roller damages the early life base material shear strength capacity by exceeding material shear strength, resulting in poor performance.

Flexural fatigue is the most critical failure mechanism that defines pavement life. Flexural performance could also be optimized according to the proposed performance functions, with regards to material strength at commencement of trafficking (adequate curing time for strength development); layer thickness and optimum binder content for anticipated load levels. The pavement material damage exponent of 12.5 indicates the high damage susceptibility of heavy axle loads.

The flow diagrams illustrated in Figures 5.13 and 5.14 represent proposed design methodologies applying the failure mechanisms and proposed fatigue curves presented in this study.

Another factor that should be kept in mind during evaluation of the transfer functions is that development thereof is based on pavement response data obtained from channalized traffic loading. Real life pavement performance and fatigue would be greater than that predicted by the performance and fatigue curves by a factor relating channelized and lateral wandered loading performance.

The deflection stiffness relationship presented would be a useful benchmark for pavement management. Cement treated base condition could also be assessed at any point in time of pavement life if initial untrafficked deflection is known.

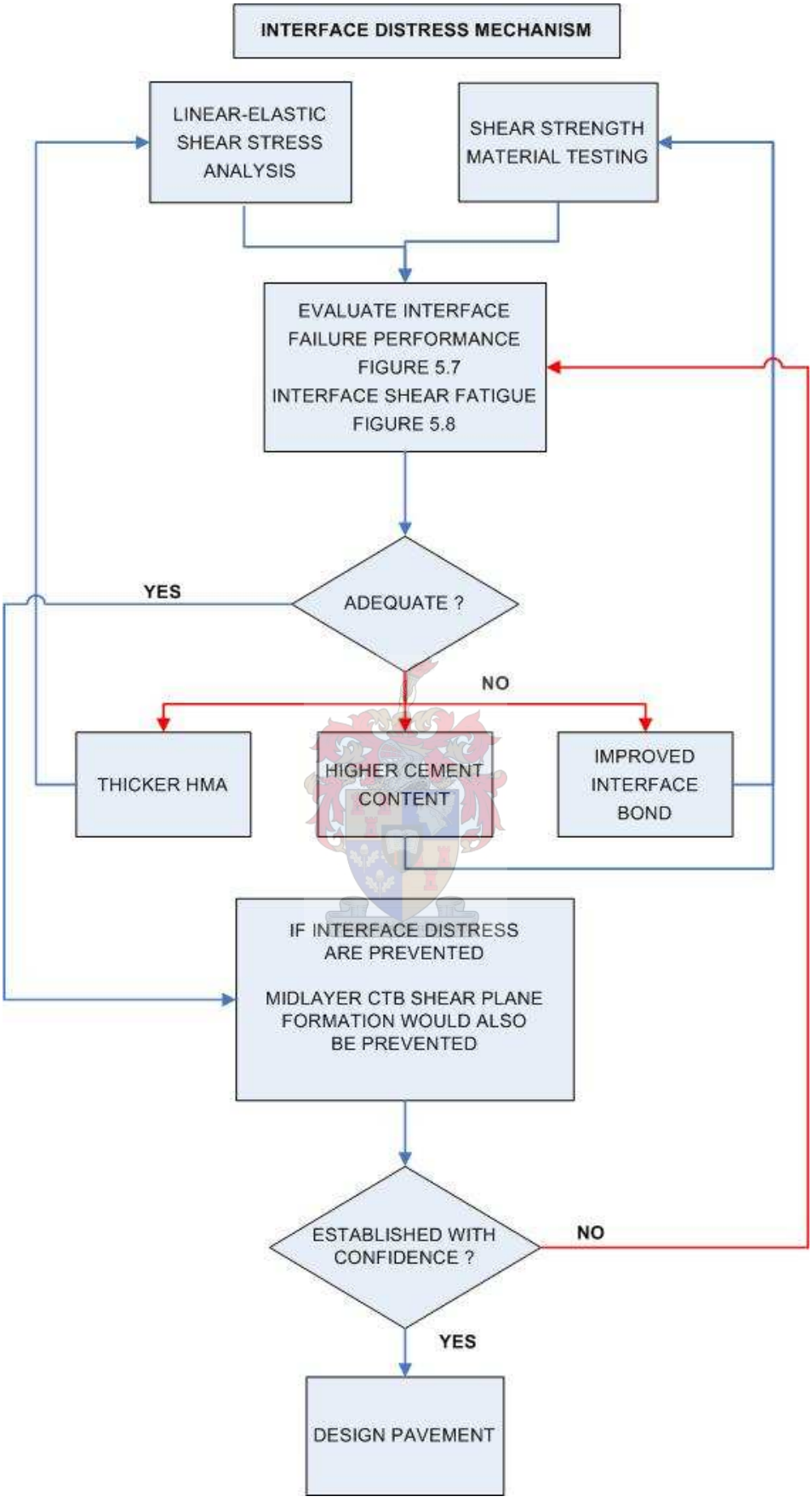

Figure 5.13: Design flow diagram for interface distress mechanism

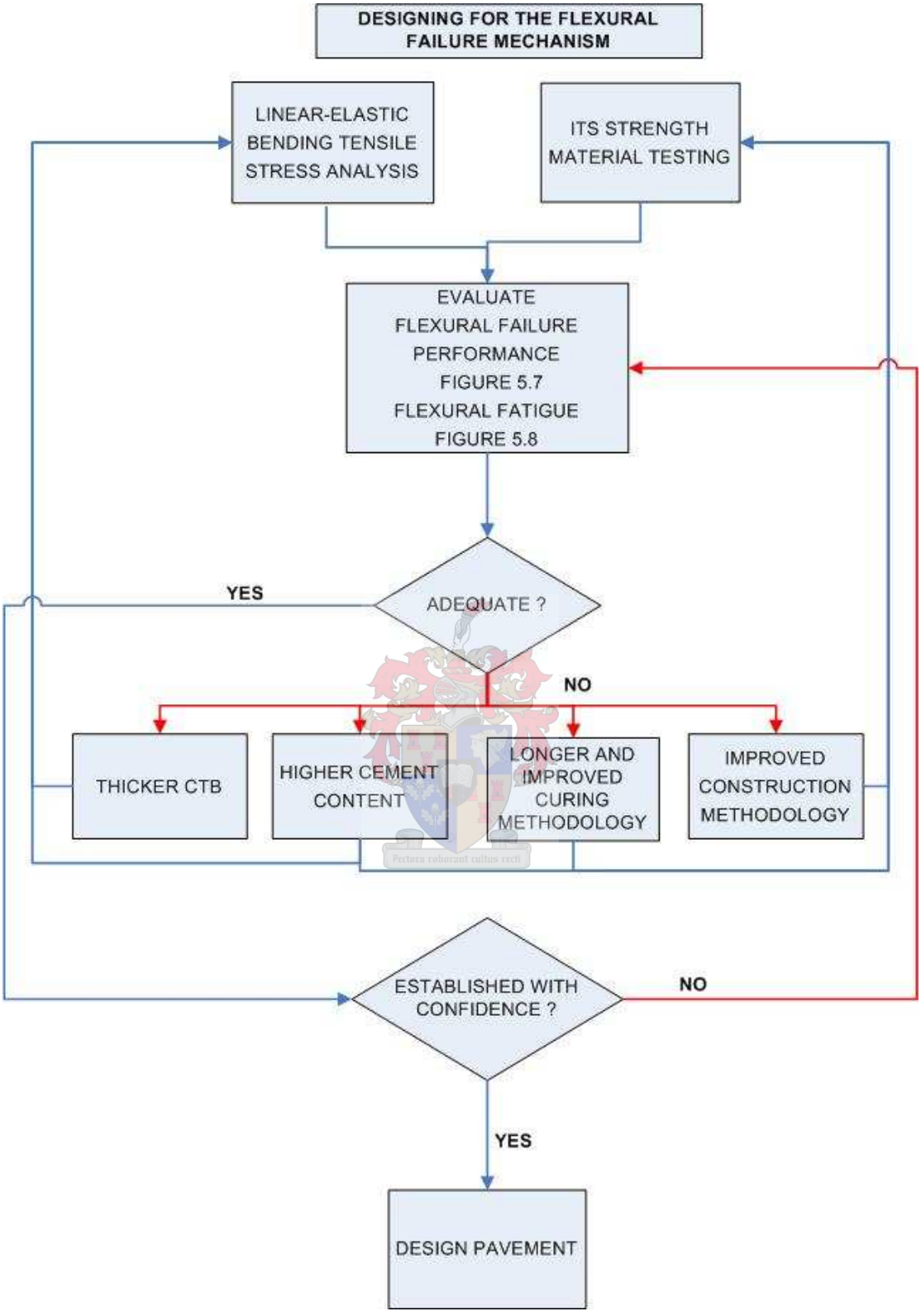

Figure 5.14: Design flow diagram for flexural fatigue failure mechanism

CHAPTER 5

From the stiffness performance of the tested sections the β -parameter (curvature parameter) of the pavement damage model of Molenaar (1999) presented in Chapter 4 could be approximated for these pavement structures and loading conditions. Beta would be 0.5 and 1 for the 60 and 70 kN loads on 5 percent stabilized material respectively. For 7 percent material under 70 kN loading the curvature parameter is 1.

The synthesis of results presented in this Chapter is presented as the basis for development of the Mozambican Mechanistic Pavement Design Method (MMPDM).

Conclusions drawn from the results presented and synthesized as well as recommendations based thereon for future research in these fields are presented in the following chapter.

Chapter 6

Conclusions, Recommendations for future research and Closure

This chapter is the culmination of the research study in conclusion of the presented work and makes recommendations for future research in this field.

6.1 Conclusions

The thesis study and objectives are briefly revisited before conclusions are drawn.

The research study comprised of the pavement performance characterization and subsequent synthesis of findings from six full-scale accelerated pavement tests conducted on test sections of cement stabilized sand bases with a thin asphalt overlay in Mozambique. The accelerated pavement testing entailed the application of 1.51 million 60 kN and 1.93 million 70 kN axle loads on the above mentioned pavement structures. Preliminary pavement fatigue performance curves were developed for the specific failure mechanisms encountered based on the synthesis of material test results, pavement response performances, linear elastic analysis and diagnostic evaluation.

The initial objective of this research study was to characterize the performance of Mozambican cement stabilized sand bases under loading through accelerated pavement testing in terms of:

- stiffness performance;
- surface deflection under loading;
- pavement failure mechanisms manifested during traffic loading.

The ultimate objective was the subsequent development of general performance trends pertaining to specific failure mechanisms and pavement responses derived from synthesis of the above mentioned pavement performance and responses.

The APT program yielded a significant amount of invaluable findings which will provide the basis for development of the Mozambican Mechanistic Pavement Design Method (MMPDM). Pavement load response characterization under repeated loading regarding stiffness performance and surface deflection were successful and informative. Based on the results and findings presented and synthesized the following conclusions are drawn:

1. The methodology developed for extraction and reduction of seismic measurements is unique in stiffness performance characterization of the different pavement zones in which the failure mechanisms take place.

2. Sandy cement treated base pavement failure mechanisms consist of three phenomena:

   - HMA – CTB interface shear;
   - longitudinal and transverse bottom up flexural cracking and
   - horizontal shear plane formation in the CTB layer.

   Sequence of manifestation and severity of the described mechanisms depend on pavement structure, load level and material strength parameters.

3. Seismic wave propagation monitoring can be used to evaluate stiffness changes under APT.

4. It is further concluded that the tensile and shear strength of the CTB material are the critical material parameters for pavement performance and the primary parameters for material evaluation during pavement design. It was found that the CTB compressive strength was sufficient to withstand failure through the crushing mechanism.

5. From the developed transfer functions the highly sensitive nature of the sandy cement treated base material to a change in working stress was found. As a result of this the sandy cement treated pavement structure was found susceptible to early distress due to high loads under construction and early traffic

6. Thin sandy cement treated base material's susceptibility to overloading is ratified by the material damage exponent of 12.5 and resulting load equivalency. Thin sandy cement treated base pavements are more susceptible to overloading compared to inverted, commonly found in South Africa, or thick asphalt pavement structures

7. From comparison between the proposed Mozambican method and the SAMPD it was found that one of the fundamental differences between the two approaches is the single sized sand and predominantly graded angular granular materials used for the CTB layers in Mozambique and South Africa respectively. The other fundamental difference is the pavement structure compositions of the two methods. It is postulated that these two differences are the principle cause of different mechanisms of failure that occur. These differences produced different failure mechanisms and subsequently critical pavement and material parameters. SAMPD evaluates CTB's in terms of crushing and effective fatigue, MMPD in terms of the three failure criteria presented. These two approaches further differ in the continuity of stiffness characterization in modeling and determination of ultimate pavement life.

8. Application of APT as a research tool in the quest for developing guidelines for a Mechanistic-empirical pavement design method for cement stabilized coastal sand bases in Mozambique proved to be both effective and efficient.

It is therefore concluded that the proposed failure mechanisms, performance and fatigue curves developed for occurrence thereof, stiffness and deflection performance graphs, material damage exponent and subsequent performance relations are invaluable to the design engineer for evaluation and optimization of design. Hence it is concluded that this research study was successful in the proposed objective of characterizing the performance of cement treated base material of Mozambique under accelerated pavement testing.

Results reported here should serve to support the preservation, maintenance and upgrading efforts that are underway in Mozambique, and form the basis for development of the MMPDM.

The synthesis of the sandy cement treated base material performance characterization is generally applicable for the enhanced understanding of pavement behavior in Southern African areas or countries with similar conditions e.g. Caprivi, Angola and the Beria red sands found in Natal.

6.2 Recommendations for future research

The following recommendations for future research are made based on the experience obtained, results, findings and synthesis thereof reported in this study:

1. Development of a software tool using Fast Fourier Transforms or Neural Network Algorithms with PSPA generated data as input for extraction of absolute layer stiffness values for the layered pavement systems of Southern Africa.

2. A scoping study to determine the seismic stiffness properties and parameters for standard materials used for road construction in Southern Africa. This would enable rapid in-situ pavement evaluation by means of NDT for pavement management.

3. A correlation study between FWD and PSPA determined stiffness's for layered pavement structures of Southern Africa. From comparative evaluation of results more efficient pavement performance evaluation methodologies could be developed for pavement condition surveys.

4. It is recommended for future MLS10 testing that initial untrafficked deflection measurements are monitored at different wheel loads of 40, 50, 60 and 70 kN for the four bogies. Back-calculation of the 40 kN wheel load deflection bowl would enable comparison to FWD stiffness's and indices. Back-calculation methodology could be evaluated by comparison of the moduli calculated for the different loads.

5. Subsequent measurements at different axle loads could serve to evaluate extent of different pavement life times under different axle loading conditions by analyzing the growth in deflection ratios.

6. The MLS10 is ideal for investigation of surface deflection performance with increased loading speeds to evaluate various pavement structures' (e.g. deep asphalt or CTB) response dependencies on speed.

7. Investigation and evaluation of the tensile stress and SCI relationship with trafficking, to complement the proposed stiffness – maximum surface deflection relationship and to compare to TRL overlay design method.

8. Continuous deflection measurement under loading would produce smoother and more precise structural performance models. It could also be used for the evaluation of the effect that different environmental conditions have on pavement performance under load trafficking.

9. Continuous seismic measurement under traffic loading is another viable option to be considered. This would provide the same benefit as above mentioned continuous deflection measurements and pave the way for an Intelligent Accelerated Pavement Testing System (IAPTS).

10. Pavement strength and or stiffness should be characterized during the early life environment to evaluate the effect that different construction methodologies (CTB and HMA) as well as time of surface construction and opening to traffic has on the material characteristics. This should be done by strength testing of cores extracted and repetitive seismic testing, with PSPA and the cross-hole methodology.

11. An investigation into the relation between channelized and lateral wander loading of the CTB pavement structure with regard to stiffness performance, deflection, surface crack formation and failure mechanisms. The suggested analytical proposals should be investigated and evaluated. A scoping study could be conducted with the MMLS3 on a scaled pavement section.

12. Detailed studies of traffic volumes and axle load information for Mozambican highways would further benefit pavement design.

13. Validation of the proposed transfer and performance functions in terms of lateral load distribution, equivalent standard loads and more sensitive in-situ pavement strength evaluation.

Successful implementation of synthesis and recommendations would lead to a total pavement engineering system if appropriately applied.

6.3 Closure

The research that was reported in this thesis was done as an integral part of project, 206/CON/ES/DEN/2003 for the ANE. The funding was sponsored by the World Bank. The opinions expressed by the author in the thesis do not necessarily reflect those of the research team or these organizations.

The success of research completed will be measured by the impact it has on the total pavement engineering system of Mozambique and subsequent pavement performance and socio-economic benefits thereof.

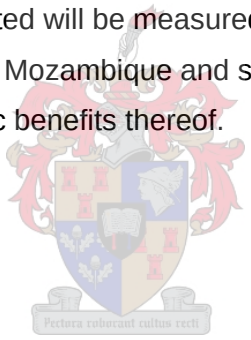

References

Baker, M R, Crain, K., and Nazarian, S 1995. *Determination of Pavement Thickness with a New Ultrasonic Device.* Research Report 1966-1, Center for Highway Materials Research, The University of Texas at El Paso, Texas.

Bhairo, P D, Miradi A, Groenendijk J, Molenaar A A A and Van Dommelen A E, 1998. Levensduur Evaluatie van LINTRACK Proefvak Va (Fatigue Life Evaluation of LINTRACK test section Va), Proceedings Wegbouwkundige Werkdagen, Part II, CROW, Ede, NL, pp. 155–166.

Bigioggero B, Cadoppi P, Costa M, Omenetto P and R Sacchi 1989. *Late Proterozoic granites of Zambezia (Mozambique)*; IGCP 255 Newsletter, Bull 2:5-7.

Celaya, M, Nazarian, S 2006. *Seismic Testing to Determine Quality of Hot-Mix Asphalt*, CD-Rom Proceedings 85th Annual Transportation Research Board Meeting, Washington, D.C.

Committee of State Road Authorities 1986. *Standard methods of testing road construction materials*; TRH1, Pretoria, CSIR.

Committee of Land Transport Officials 1997. *Flexible pavement rehabilitation investigation and design*; Draft TRH12, Pretoria, COLTO.

Committee of State Road Authorities1986. *Cementitious stabilizers in road construction*; TRH13, Pretoria, CSIR.

Committee of State Road Authorities 1985. *Standards for road construction materials*; TRH 14 , Pretoria, CSIR.

Croney, D and Croney, P 1991. *The Design and Performance of Road Pavements*; McGraw-Hill International Series in Civil Engineering, 2nd Edition.

De Beer, M 1991. *Improving mechanistic design of cementitious materials*; Project report PR 88/027, South African Roads Board, Pretoria.

De Beer, M 1988. Aspects of the Design and Behaviour of Road Structures Incorporating Lightly Cementituous Layers. PhD Thesis, Department of Civil Engineering, Faculty of Engineering, University of Pretoria, Pretoria.

de Vos, E R, Hugo, F, Strauss, P J, Prozzi, J A, Fults, K W, Tayob, H 2007. *Comparitive Scaled MMLS3 Tests vs. Full-Scale MLS10 Tests in Mozambique*; CD-Rom Proceedings, 86th Annual Transportation Research Board Meeting; Washington D.C.

de Vos, E R 2004. *Development of a Accelerated Laboratory Testing Protocol for Cement Stabilized Base Layers using the Third Scale Model Mobile Load Simulator*; B.Ing Thesis, University of Stellenbosch, November

Dennis, N D Jr and Bennett, K, 2005. Development of Testing Protocol and Correlations for Resilient Modulus fo Subgrade Soils, Research Report MBTC – 2023, Arakansas State Highway and Transportation Department, Little Rock, Arkansas.

Dunaiski, P E, Hugo, F, 1990. *A proposed method for measuring the lateral displacement during indirect tensile tests of asphalt briquettes using Linear Variable Differential Transducers;* Proceedings Fourth International RILEM Symposium; October.

Groenendijk, J, Miradi A, Molenaar, A A A, Vogelzang, C H, Dohmen, L J M, Maagdenberg, A M, and De Beer, M, 1997. *Pavement Performance Modeling Using LINTRACK*; Proceedings of the 8th International Conference on Asphalt Pavements, Seattle, Washington, August 10–14, Vol. II, pp. 1505–1526.

Hugo, F, McCullough, B F, Van der Walt, B, 1991. *Full-Scale Accelerated Pavement Testing for the Texas State Department of Highways and Public Transportation*. *Transportation Research Record 1293*, Transportation Research Board Meeting, National Research Council, Washington, D.C.

Hugo, F, 1997. *The Development and Application of the Texas Mobile Load Simulator as an Accelerated Pavement Testing* Tool, Thesis–D.Eng., University of Stellenbosch, Bellville, South Africa.

Hugo, F, Epps, AL, 2004. *NCHRP Synthesis 325: Significant Findings form Full-Scale Accelerated Pavement Testing*, Transportation Research Board, National Research Council, Washington, D.C.

Hugo, F, Smit, A d F, Poolman, P, Powell, B, Bacchi, C 2004. *Distress of hot mix asphalt on the NCAT test track due to accelerated wet trafficking with the MMLS3*, CD-ROM Proceedings Second International APT Conference, Minneapolis, USA.

Jameson, G W, Sharp, K G, Yeo, R, 1992. *Cement-treated Crushed Rock Pavement Fatigue under Accelerated Loading: The Mulgrave (Victoria) ALF Trail, 1989/1991*; Research Report ARR 229, Australian Road Research Board, July.

Jones, R 1962. *Surface Wave Technique for Measuring the Elastic Properties and Thickness of Roads: Theoretical Development;* British Journal of Applied Physics, Vol. 13.

Jooste, F J, Kekwick, S V, Sadzik, E S, and Rohde, G T, 1997. *Comparison of Accelerated Pavement Test Results with Long-Term Pavement Behaviour and Performance*. 8th International Conference on Asphalt Pavements, Seattle, Washington , August 10–14.

Kennedy, T and Anagnos, J 1983. *Procedures for the Static and Repeated-Load Indirect Tensile Test*; Research Report 183-14, Center for Transportation Research, The University of Texas at Austin, August.

Lee, S and Kim, R, 2004. *Development of Fatigue Cracking Test Protocol and Life Prediction Methodology Using MMLS3 Proceedings;* Fifth International RILEM Conference on Cracking, Limoges, France, May.

Lorio, R, 1994. *The Asphalt Shear Box Test*, B.Eng Thesis, University of Stellenbosch, Stellenbosch.

Lorio, R, 1994. *An investigation into and validation of the shear strength of asphalt mixes as a performance related material property with regard to pavement rutting*, M.Sc Thesis, University of Stellenbosch, Stellenbosch.

Molenaar, A A A, Houben, L J M, Visser, A F H M, Vogelzang, C H, Van Dommelen, A E, and Maagdenberg, A C, 2001. *Full-Scale Testing and Modeling of Permanent Deformation in Asphalt Pavements*, 2nd International Symposium on Maintenance and Rehabilitation of Pavements and Technological Control, Auburn, July 29–August 1.

Melis, L M, Meyer, A H and Fowler, D W 1985. *An Evaluation of Tensile Strength Testing*; Research Report 432-1F, Centre for Transportation Research, The University of Texas at Austin, November.

Metcalf, J B, 1996. *NCHRP Synthesis of Highway Practice 235: Application of Full-Scale Accelerated Pavement Testing*, Transportation Research Board, National Research Council, Washington, D.C.

Nazarian, S, Baker, M R, and Crain, K 1993. *Fabrication and Testing of a Seismic Pavement Analyzer; SHRP Report H-375*. SHRP, National Research Council, Washington, D.C.

Nazarian, S, Baker, M, and Crain, K, 1997. *Assessing Quality of Concrete with Wave Propagation Techniques ;* Materials Journal, American Concrete Institute, Farmington Hills, MI, Vol. 94, No. 4.

Nazarian, S, and Yuan, D, 2003. *Comprehensive Mechanistic-based Quality Control of Flexible Pavements with NDT Methods*; European Civil Engineering Nondestructive testing Conference, Berlin.

Nazarian, S, and Stokoe II, K H, 1986. *Use of Surface Waves in Pavement Evaluation;* Transportation Research Record, No. 1070, TRB, National Research Council, Washington, D.C.

Pinna, P, Jourde, G, Calvez, J Y, Mroz, J P and Marques, J M,1993. *The Mozambique Belt in northern Mozambique: Neoproterozoic (110-850 Ma) crustal growth and tectogenesis, and superimposed;* Pan-Africa (800-550 Ma) tectonism. Precambr.

Ryden, N, 2004. Surface wave testing of pavement structures, PhD dissertation, University of Lund, Sweden.

Scheffy, C, Coetzee, N and Diaz, E, 1999. *Asphalt Concrete Fatigue Crack Monitoring and Analysis Using Digital Image Analysis Techniques* (CD-ROM), Proceedings of the First International Conference on Accelerated Pavement Testing, Reno, Nev., October 18–20.

Smit, A de F, Hugo F, and Epps A 1999. *Report on the First Jacksboro MMLS Tests*, Report Number 1814-2, Centre for Transportation Research at the University of Texas at Austin.

Shell International Oil Products BV 1998. *Bisar 3.0 (computer programme)*,

Strauss, P J, Hugo, F, Slavik, M, de Vos, E R, Prozzi, J A, Fults, K, Smit, A de F, 2005. *Final Phase 1 Report*; ANE; Mozambique

Strauss, P J, Hugo, F, Slavik, M, de Vos, E R, Prozzi, J A, Fults, K, Smit, A de F, 2006. *First Draft Phase 2 Final Report*; ANE; Mozambique

Theyse, H L, de Beer, M, Rust, F C 1996. *Overview of the South African Mechanistic Pavement Design Analysis Method*. CD-Rom Proceedings 75th Annual Transportation Research Board Meeting, Washington, D.C.

Walubita, LF, Hugo F, and Epps A E, 2000. *Performance of Rehabilitated Lightweight Aggregate Asphalt Concrete Pavements Under Wet and Heated Model Mobile Load Simulator Trafficking: A Comparative Study with the TxMLS*, Report Number 1814-3, Center for Transportation Research at the University of Texas at Austin

Vuong, BT, Sharp, KG, Baran, EJ, Johnson-Clarke, JR, and Reeves, IN, 1996. *Performance of Unbound and Stabilized Pavement Materials Under Accelerated Loading: Summary of Report of Beerburrum II ALF Trial*, Report ARR 286, Australian Road Research Board, Vermont South, Victoria, Australia.

Yoder, E J, Witczak, M W, 1975. *Principles of pavement design*. John Wiley & Sons, Inc. Toronto. Pages 73 – 75.

Appendix A

Accelerated and Seismic Pavement Testing

In this appendix literary extractions and overviews of accelerated and seismic pavement testing are provided. It consists of three parts. The first part covers accelerated pavement testing and consists of interpreted extractions from NCHRP Synthesis 325: Significant Findings from Full-Scale Accelerated Pavement Testing (Hugo and Epps, 2004).

Part 2 is fully based on the literature study presented by Rydèn (2004) in his doctoral thesis: Surface Wave Testing of Pavements. The presented work is directly quoted from the above mentioned source since it gives an excellent overview of the work conducted in the seismic pavement testing domain and is directly relevant to the seismic testing methodology used in this research study. The section presented here gives a short background on non-destructive testing with focus on base and subgrade materials followed by a literature overview of seismic pavement testing.

This section is followed by Part 3 which gives a more detailed technical overview of elastic and seismic waves, signal processing and the development of an experimental dispersion curve for seismic pavement testing. Part 3 consists of adjusted excerpts of report MBTC – 2032, Development of Testing Protocol and Correlation for Resilient Modulus of Subgrade Soils, conducted by Dennis and Bennett (2005) for the Arkansas State Highway and Transportation Department.

A1 Accelerated Pavement Testing

In this subsection extractions of NCHRP Synthesis 325: Significant Findings from Full-Scale Accelerated Pavement Testing (Hugo and Epps, 2004) are presented to illustrate the significant findings and philosophy of full-scale APT as well as all the elements that has to be taken into account during the testing and evaluation of the results. This specific document was used as only source

since it gave such a comprehensive interpreted overview of all the important elements and findings of full-scale APT up to date.

> *"Accelerated pavement testing is defined as the controlled application of wheel loading to pavement structures for the purpose of simulating the effects of long-term in-service loading conditions in a compressed time period. APT is a facet of pavement engineering and generates knowledge over a wide spectrum. Figure A.1 places APT programs in context to the broad basis of pavement engineering*."

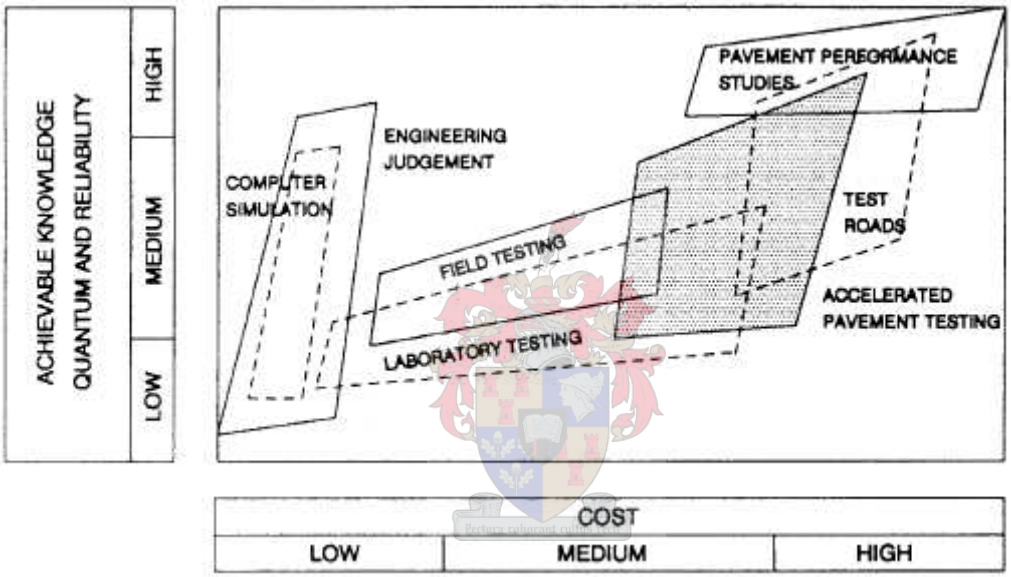

Figure A.1: Interrelationship between pavement engineering facets that collectively and individually contribute to knowledge (Hugo et al. 1991)

> *"APT is an activity that can stand alone and provide some insight into the performance of a pavement. However, to gain full benefit, APT programs must be supplemented with laboratory testing programs. The extent of this varies in scope, depending on the nature of the respective APT programs. In addition, environmental conditions prevalent during APT are of paramount importance, because the behaviour of the materials that are being tested may be significantly influenced by the conditions prevailing during the tests."*

> *"A wide variety of APT programs are operational in the world today most of these tests are being conducted at fixed sites. The scope of APT studies is large and will be discussed under the following topics that relate to elements of the pavement system:*
>
> *• Evaluation, Validation, and Improvement of Structural Designs;*
> *• Vehicle–Pavement–Environment Interaction;*
> *• Evaluation of Materials and Tests;*
> *• Enhancement of Modelling in Pavement Engineering;*
> *• Pavement Engineering Applications and Issues."*

Although the objective of this subsection is to provide the reader with an overview of all the important elements of APT, the focus is primarily on the elements affecting CTB performance under traffic loading. Elements that have a primary effect on asphalt performance will be mentioned but not discussed in detail.

A1.1 Evaluation, Validation, and Improvement of Structural Designs

> *"APT research is used to enhance structural design of pavements. In structural design, the stiffness and thickness of the pavement layers are selected to ensure an adequate support structure such that the bearing capacity of the underlying subgrade is not exceeded. Structural design form the core of pavement engineering, but design could not be considered in isolation because of the strong interaction with other fields of pavement engineering, such as materials and vehicle–pavement–environment interaction. Changes that take place over time, particularly in the case of materials and changes in vehicle configuration should also be taken into account."*

Applications of accelerated pavement testing to asphalt pavement designs

"In South Africa, APT testing has been used to validate the performance of well-balanced, deep pavement structures. These pavements are constructed with materials such that there is a gradual decrease in stiffness with depth in relation to the bearing capacity of the respective layers. APT testing has demonstrated that poorly balanced, shallow pavements, where most of the stiffness of the structure is concentrated at the top of the pavement, are normally load sensitive. These types of pavements may appear to have adequate bearing capacity but deteriorate rapidly under overloaded conditions. The results obtained from the Mozambican APT study and presented in this thesis support these findings. However, they warn against increasing the test wheel load to levels far above those of the standard design load. This may induce failure mechanisms that will never manifest under normal traffic loading conditions, especially in the case of bound layers.

The South African Heavy Vehicle Simulator (SA–HVS) testing program has been instrumental in the development of the South African Mechanistic Design Method for Pavements (Theyse et al. 1996). It is an example of how APT can benefit pavement engineering overall. They discuss how HVS test results were used to develop transfer functions for the mechanistic–empirical modelling of the permanent deformation of unbound pavement layers in pavements with asphalt and granular base layers as well as granular and stabilized subbase layers. This method was applied to establish standard pavement structures for use in different climatic regions of South Africa and different levels of design traffic. These standard pavement structures are catalogued in manuals for implementation by the road industry and have, over the years, been validated and refined in the field using HVS testing. The significant amount of data collected during HVS testing of numerous types of pavement structures has allowed confidence limits to be established to assess the reliability of design methodologies (Structural Design of Interurban and Rural Road Pavements 1980, 1985, 1996)."

Similarly the MLS10 was used for characterization of the CTB pavements of Mozambique, findings from the research study reported in this thesis will be used for the development of CTB performance and transfer functions for the Mozambique Mechanistic Pavement Design Method. A comparison between the findings from the research study reported in this thesis and the SAMPD method are presented in Chapter 5.

Applications of accelerated pavement testing to composite structures

> *"HVS testing has been instrumental in validating the effectiveness of inverted pavement structures, which are now used extensively throughout South Africa. These structures incorporate stabilized or lightly cemented (<4%) subbase layers that provide support to granular or asphaltic base layers. The stiffness of these stabilized subbase layers, while intact, are higher than that of the base layers. This allows adequate compaction of the base layer, and in the case of asphaltic base layers, reduces the development of horizontal tensile strains beneath the layer, hence extending the fatigue performance of the pavement structure. In the case of high-quality granular bases (these are generally bases comprising crusched stone eg G1, G2 ect. TRH 4 (1985)), the stiff subbase layer confines the base, and this "sandwich" effect has been shown to significantly increase the shear strength of high-quality granular bases. The influence of climate as well as traffic level is accounted for in the structural design of pavements."*

Summary

> *"For composite structures, the effectiveness of inverted structures has been illustrated. APT has contributed to advances in the field of stabilization of marginal materials to strengthen pavements and the use of geofabrics for reinforcement.*
>
> *APT has also been instrumental in validating and refining agency structural design guidelines.*

In addition, improvements in structural design have been brought about by the insight gained on the effect of a number of factors on pavement performance, including:

- *The influence of water on performance and related failure mechanisms,*
- *The importance of bond between layers and the quantification of the effect, and*
- *The interaction between structural composition and material characteristics."*

A1.2 Vehicle–Pavement–Environment Interaction

The structural configuration of the pavement system is normally fixed by design or policy, including the materials that are to be used. The structural system is then subjected to the impact of traffic loading under the prevailing environmental conditions that affect its performance. The response and performance of the pavement system is therefore subject to an array of influential factors that have variable levels of control and are time dependent to a greater or lesser degree. The following elements need to be considered:

- Trafficking comprising
  - Wheel loads that can be single axle or multiple axle,
  - Wheel load(s) that can be static or dynamic,
  - Wheel loads that wander laterally,
  - Suspension systems,
  - Tyre pressure/contact stress,
  - Tyre type, and
  - Speed;
- Environmental impact of
  - Wind and radiation,
  - Temperature, and
  - Water in a variety of forms.
- Pavement materials.

Pavement performance are dependent of the interaction of these factors. It should be noted that pavement structures with a shallow CTB, as used in Mozambique, respond differently to these elements than a pavement with an asphalt or composite pavement design.

Trafficking

> *"APT programs use conventional trucks and a variety of vehicles for simulating conventional trafficking of pavements. Wheel loads is applied at selected static levels that varies according to the needs of the experiment. Tyre pressures are being varied to accommodate conventional and extraordinary tyre pressures to explore the impact of this variable."*

The focus will be on the aspects of APT trafficking that affect pavement performance.

Wheel load intensity and load equivalency

> *"Wheel load intensity has the most profound effect on pavement performance and it is to a large extend an uncontrolled variable in real traffic. It has been reported that the relationship of load with performance was neither constant nor linear. The fourth power law was found to be exponential and highly dependent on the thickness and configuration of layers. It is also a function of the axle suspension type and degree of pavement surface smoothness. Results from various APT studies indicate that load equivalency is a function of pavement configuration, material characteristics, subgrade strength, climatic conditions and type of testing."*

Determination of a material damage factor for the CTB materials of Mozambique are presented in this thesis.

Suspension/Dynamic load

The fourth power law of load equivalence was derived from experiments in which the applied wheel forces were dynamic. (AASHO 1961). Load equivalency for the Mozambican CTB material is also determined under dynamic loading conditions.

Unidirectional/Bidirectional loading

"Contradictory findings have been reported on effects of unidirectional versus bidirectional trafficking. Tests in the United Kingdom reported that bidirectional trafficking is more severe in terms of relative performance. Finnish researchers found no difference in performance (Huhtala et al 2000). Theoretical analyses have indicated that a difference in performance should be expected because of residual stresses (Yandell and Behzadi 1999)."

Cement treated base material is less susceptible to the effect of bidirectional loading since it is assumed to initially behave elastically before the onset of cracking and does not exhibit residual stress material behaviour. The MLS10 full-scale test device used for the Mozambican APT study could only load the pavement in a unidirectional load application configuration.

Lateral wander during traffic loading

"Lateral wander has an important influence on the performance of pavements. Most APT devices have the capability to apply lateral wander, but in the interest of increased rates of load application on the centre of the wheel path it is often not applied. Such an approach needs to consider the affects it has on the relationship between distress and load applications at transverse positions relative to the wheel path."

Concentrated wheel loading was applied during the Mozambican APT studies for the above mentioned reason. Performance curves developed in this study will have to be adjusted with a shift factor to provide for the effect of lateral wander during normal traffic loading.

Tyre Characteristics and related contact stresses

"It has become clear that the tyre-pavement interface has a major impact on the performance of upper layer(s), especially for flexible pavements. De Beer et al. (1997) and Bab (1999) reported on research conducted contact stresses under tires. De Beer concluded that the contact pressure is not uniform over the contact surface. Blab (1999) found that tire inflation pressure, load, and tire type are the dominant factors affecting vehicle-pavement contact stresses. Increase in tire pressure affects rutting in APT. Both Gramsammer et al. (1999) and Hugo (2000) found the increase in rutting of the asphalt layers to be proportional to the increase in tire pressure."

Trafficking speed

The effect of trafficking speed has not received as much attention as other pavement interaction factors.

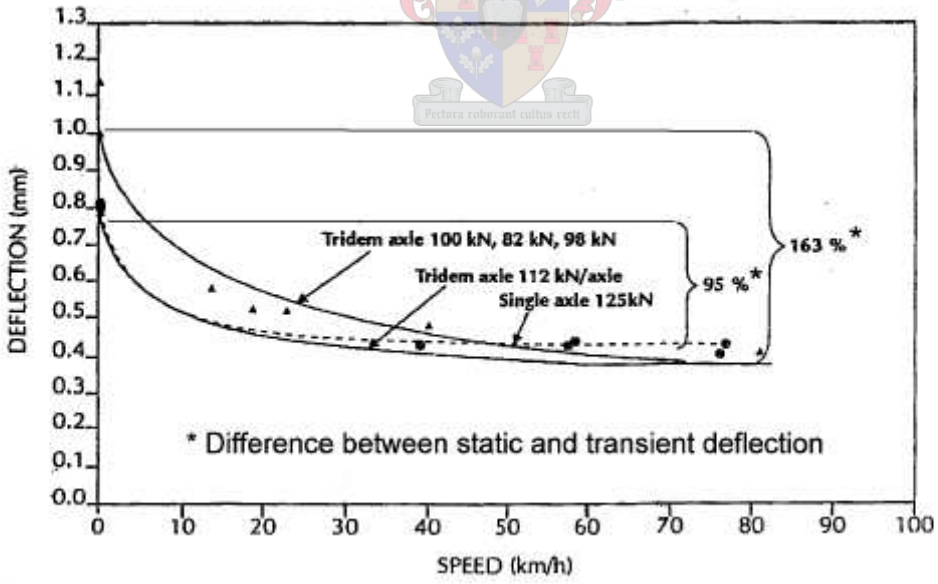

Figure A.2: Effect of speed on pavement deflection (Lourens 1995)

"Lourens (1995) measured both static and dynamic deflections under wheel loads on in-service highways to relate these to deflections measured under the HVS as show in Figure A.2.

Because of the relationship between elastic and plastic strain this would lead to a similar reduction in deformation of the asphalt. Because CTB material is assumed to behave elastically, the performance thereof is more susceptible as HMA is to trafficking speed, where higher deflections on CTB would be more detrimental to performance. Speed of loading has to be carefully considered in judging results from APT trafficking, especially when a substantial layer of asphalt is present in the structure.

Load composition and configuration

Wolff (1992) found that the application of different load sequences on the pavement structure affected the performance. It appeared that the stress path influenced the final performance.

Environmental impact

Environmental impact is essentially caused by physical and chemical action related to temperature, water, wind and solar radiation. The impact of temperature and water on pavement structures has been investigated in a number of APT tests consisting of a wide variety of pavement structures and materials. Wind and solar radiation have not been featured to any extent in APT studies.

Impact of temperature on performance

Performance of pavements is affected by the full temperature range that occurs during its life cycle."

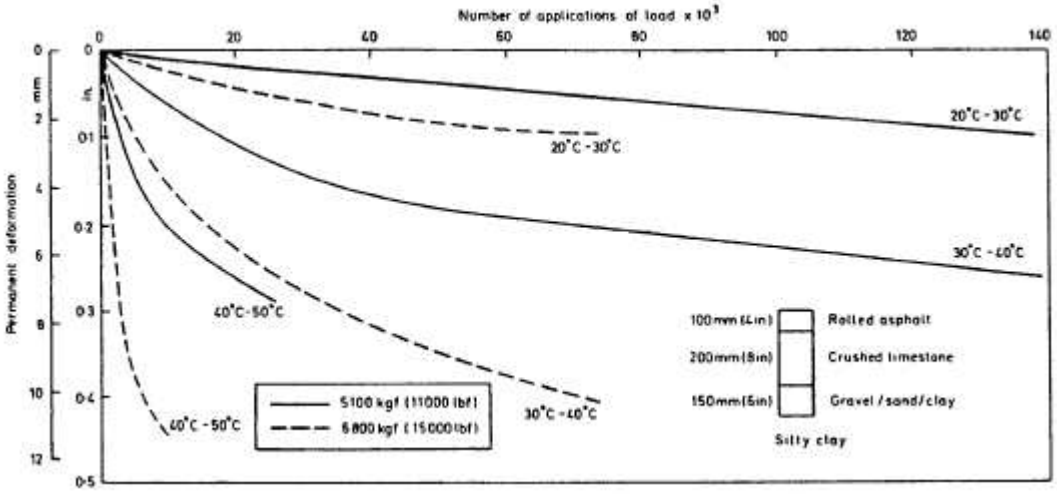

Figure A.3: Effects of wheel load and temperature on permanent deformation

"Corté et al. (1997) discussed in detail the effect of temperature on rutting. They reported that there is a threshold temperature above which asphalts show susceptibility to rutting. This threshold value appears to be close to the Ring and Ball softening point temperature of the binder. For this reason the thermal history of a pavement plays an important role in the development of rutting and related performance. Lister reported this in 1972 (Lister 1972 and Metcalf 1996) in one of the very early APT studies in the United Kingdom (see Figure A.3). From this figure, the dramatic effect of a 10℃ or 20℃ change in temperature on d eformation can be seen".

CTB performance under traffic loading is contrarily not susceptible to temperature.

Impact of water on performance

"The effect of water ingress into a structure is dramatic. The exclusion of environmental factors such as moisture greatly increases pavement life when compared to the expected design life. Differentiation between the effect of surface infiltration of

water and subsurface ingress of water is made. A major non-traffic-related effect that water has is chemical distress, which is primarily the result of chemical disintegration of material(s) or deterioration of layers."

Infiltration of Surface Water

"Infiltration of surface water affects pavement performance when it gains access to the pavement structure. During trafficking pore water pressures develop, causing loss of shear strength and even disintegration, depending on the nature and quality of the pavement materials.

Walker (1985) discussed the impact of moisture on pavement performance and used data obtained from various HVS tests on South African field pavements to show how the effect differs depending on the type of pavement and the degree of saturation. Related findings indicated that the impact of water during trafficking on the remaining life and performance can be significant."

Surface and subsurface water

"Vuong et al. (1996) reported on 34 experiments applying 3 million light load cycles to 10 pavement types and concluded that the effect of heavy rain in a concentrated short time period needs to be considered in the adjudication of performance. Granular materials that are sensitive to moisture do not dry back quickly and the prevention of ingress of water and the possible increase in moisture content within the material is critical. It was concluded from an environmental damage exponent that environmental effects could be more significant than loading effects."

It was reported from tests done on highways in China by Meng et al. (1999) that rainfall is one of the major environmental factors that can accelerate pavement deterioration. Their research program concentrated on the performance of five alternatives of new-design stabilized base pavements

under the accelerated loading. The objectives of this research are to investigate:

(1) the rutting of stabilized base asphalt pavements;
(2) the bearing capacity of pavements of this type;
(3) the pavement failure process and
(4) the effects of rainfall on the life of stabilized pavement.

It was found that the rutting of the stabilized base asphalt pavements was due to the asphalt surface layer and the erosion at the interface and asphalt and base layers. Heavy loading accelerates the development of rutting significantly. Stabilized base pavement fail from surface layer and not from the fatigue cracking of stabilized bases.
They commented that damage was primarily the result of pumping and erosion at the underside of the asphalt layer.

"Figure A.4 shows the impact of water on deformation performance schematically as pointed out by Rust et al. (1997) after extensive studies have been undertaken to explore the impact of water on the performance of the pavement.

Under freeze-thaw conditions, the effect of water is greatly increased because of the development of pore water pressures."

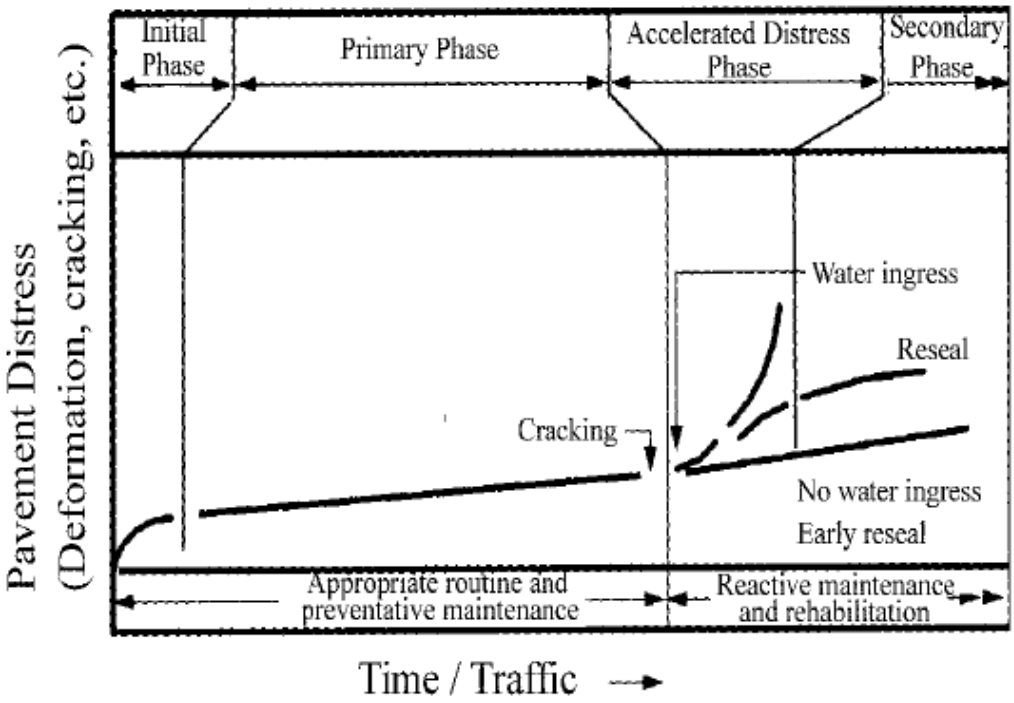

Figure A.4: Impact of water ingress on pavement performance (Rust et al. 1997)

Artificial wetting of the pavement structure

"Innovative ways have been used to simulate the ingress of water into the pavement structure to study the effect of water and/or moisture. These include trafficking with water on the surface (Walubita et al. 2000). In the SA–HVS program the researchers spray water onto the surface to apply wet trafficking. In addition, they inject water through drilled pipes into one or more of the pavement layers under 1 to 2 m positive static pressure (Maree et al. 1982; Rust et al. 1997)."

Mozambican full-scale test sections were also conditioned environmentally by artificial wetting by spraying water onto the surface during traffic loading to simulate real life environmental conditions. Ingress of surface water through shear cracks in the asphalt accelerated pavement deterioration.

Closure

The studies cited show the importance of properly incorporating of vehicle–pavement–environment interaction for better APT result analysis. Several knowledge gaps do exist, particularly in terms of the impact of the environment on pavement performance.

A1.3 Material characterization

"Most APT programs use both field and laboratory material characterization to assess pavement response and performance under full-scale APT loading. Performance monitoring at the APT test section generally involves measurement of transverse and longitudinal profiles, deflection and deformation at the surface or with depth in response to a moving load or falling weight, in situ density, environmental conditions including moisture and temperature with depth, visual surface distress, and in situ stresses and strains. Other field characterization used in some APT programs included Spectral Analysis of Surface Waves (SASW) to determine stiffnesses (elastic moduli) and detect damage prior to visual distress identification (Lee et al. 1997), in situ permeability testing, trenching after failure, and measurement of the relative shear resistance of unbound materials.
In some research programs a scaled APT device was used on a section adjacent to the section tested by the full-scale device to aid in evaluating the effects of different environmental conditions including moisture and elevated temperatures. In the case of the Mozambican APT project scaled testing was conducted to narrow down the scope to testing for full-scale tests still to be conducted.

Laboratory characterization varies widely from program to program depending on the goals, experience, and available equipment. Stiffness measured by resilient modulus and density of field cores and each layered material are determined as part of most APT tests. Triaxial testing of unbound materials through the use of standard or modified equipment is common. Permeability tests on these materials in the laboratory have also been completed. Material strength test was conducted on the CTB material under investigation of the Mozambique APT study.

Testing was limited to characterization of CTB material properties with no test conducted on the HMA. Laboratory measurements are analyzed to determine pavement performance in terms of primary forms of load related distress. The possible effects of environmental conditions can be assessed through the use of laboratory characterization and modelling or analysis.

Surface

To date the majority of APT tests have been conducted using AC or a bituminous chip seal as the surface pavement layer. For many of the AC surfaces, modified binders were included and exhibited enhanced performance in terms of resistance to rutting and/or fatigue cracking

Base/Subbase

Numerous APT tests have been conducted to examine the performance of unbound and stabilized granular materials used as base or subbase pavement layers. These studies are particularly prevalent in international APT programs because of the role and importance of these layers in many low-volume road networks. On these networks, thin AC layers or chip seals are usually only providing a surface that waterproofs the underlying base and/or subbases.

The first APT test in the Australian Accelerated Loading Facility (ALF) program investigated the performance of unbound and stabilized base materials beneath a thin surface seal (Kadar and Walter 1989). The use of base materials stabilized with slag in place of high-quality crushed rock was validated under full-scale loading when adequate support from the subgrade and protection from a surface layer are provided.

The third ALF test demonstrated that deterioration of a cement-treated crushed rock (CTCR) base could be duplicated under ALF loading (Kadar et al. 1989; Sharp et al. 1999a). This material

failed by debonding at the interfaces of the multiple lifts placed during construction and by erosion of the bottom of the top layer. It should be noted that interface bond disintegration was also encountered in the Mozambique APT study. The CAPTIF program also investigated the effect of aggregate size and shape in unbound base layers beneath open-graded AC surface layers (Pidwerbesky 1995a). There were also differences in the performance of base materials with the same gradation. Possible reasons for this could be differences in compacted density and the percentage of angular particles in the mix. The higher density appeared to outweigh the effect of the percentage of angular particles, because the former materials had less deformation. As part of the CAPTIF program in New Zealand the performance of lime-stabilized subbase materials was compared with that of unbound crushed aggregate materials in nominally identical pavement structures (Pidwerbesky 1995a). Laboratory testing was used to determine optimum stabilizer content, and the stabilized materials outperformed the unbound materials in terms of deflection and deformation measured at the surface under full-scale loading. Increasing the thickness of the stabilized subbase layer also substantially improved performance. Stiffness values measured in the laboratory and those determined based on deflections measured in the field did not agree because of compaction problems on a weak subgrade.

The SA–HVS program has traditionally tested in-service pavements; therefore, evaluation of rehabilitation techniques is common. In terms of materials evaluation, this program examined the performance of labour-intensively constructed bases under full scale loading and in static and dynamic trail tests (Theyse 1999). Emulsion-treated natural gravel, water bound and composite macadam's, and an untreated and emulsion-treated ash waste material were compared to a machine-constructed, crushed-stone base. Each base material was supported by a cement-treated sandstone base and either imported sandstone or ferricrete. The crushed-stone base exhibited the best performance under full-scale loading in terms of rate of permanent deformation and

bearing capacity (defined as the number of load repetitions to a specific level of permanent deformation). The best labour-intensively constructed base material was the emulsion-treated natural gravel. Waterbound macadams were also recommended for heavier traffic loads on light pavements, although the ash waste material with adequate compaction is appropriate for lower traffic loads.

The SA–HVS program has also used APT tests in the development of guidelines for the use of new base materials, specifically large aggregate mixes for bases (LAMBs) and granular emulsion mixes (GEMs) (De Beer and Grobler 1993). LAMBs were tested under full-scale loading to validate an extensive laboratory testing program that demonstrated adequate performance of these materials in heavy-duty pavements. Dynamic creep modulus was also correlated with deformation under full-scale loading.

Other base materials evaluated in the CSIR program in South Africa included roller-compacted concrete, slag, recycled AC, and emulsion-treated recycled granular material (Horak et al. 1992; Rust et al. 1997). Design and usage guidelines for all of these materials were developed based on their performance under full-scale loading. For example, in rehabilitating untreated or cement-treated bases, the addition of cement and lime to emulsion-treatment improves strength and durability. This type of base material exhibited decreased fatigue performance when compared with AC, but resistance to fatigue was greater than for cement-treated bases (Horak and Rust 1992). Guidelines for the stabilization of marginal natural aggregate materials were also developed based on APT test results. High quality granular materials were also tested under full-scale loading to verify their use in heavy-duty pavements.

The LA ALF program also investigated base and subbase materials with AC surface layers (Metcalf et al. 1999). Crushed-stone and stabilized soil–cement materials were combined in nine different base/subbase structures and evaluated in terms of

performance under full-scale loading. When the stabilized soil cement was used as a base layer, the AC surface layer cracked as a result of reflection shrinkage cracks and top-down cracks. All stabilized base structures failed because of softening and erosion of these materials and subsequent loss of support. The researchers noted that the source material for the soil–cement was silty and prone to erosion. The modes of distress were probably related to the nature of the material.

The CEDEX program conducted a third set of APT tests in Spain to examine the performance of base and subbase materials beneath AC surface layers in terms of load related distress (Romero et al. 1992; Ruiz and Romero 1999). Granular and soil–cement base materials were compared with a third combination of a gravel–cement base with a soil–cement subbase. Two different subgrade materials were also used. Results under full-scale loading indicated that the cement-treated materials provided improved resistance to rutting and exhibited no cracking as compared with the unbound granular material.

Subgrade

Relatively few APT tests have been conducted specifically to evaluate subgrade materials.

Conclusion

The primary objective of many full-scale APT programs is to evaluate pavement material response and performance. That is why APT was considered for the evaluation of long term performance of the Mozambican CTB structures. APT programs have produced significant findings that allow for validation of existing materials and implementation of new and innovative materials. APT testing programs allow for performance-based evaluation of these materials, which is often related to material characterization programs and testing in the laboratory. It is of great importance to consider differences between APT and

laboratory characterization in terms of loading and environmental conditions, measurement and analysis techniques, as well as failure definitions."

The sandy materials used in this research study are those most commonly used by local consultants and the most abundant material available in the coastal plains of the southern region of Mozambique. These are the reddish and yellowish coloured sands. Mentioned sands were fine in particle size, rounded to semi-rounded in texture and have a single sized particle distribution. These sands were used for rehabilitation of the national road by the contractor and consultant that facilitated the construction of the full-scale test sections on the same road section. The base material used in this study is contrarary to other APT studies that involved predominatly resonably graded angular granular materials.

A1.4 Enhancement of Modelling in Pavement Engineering

"Pavement performance is a measure of the extent to which a pavement fulfils its principal objective. Performance models are tools to predict performance; they may ultimately be used in pavement management systems, in the structural design of pavements, and in the development of performance-related specifications. Jooste et al. (1997) reported that APT provides a window on pavement performance, which can possibly be used to predict how the pavement will perform under real traffic.

Modelling pavement damage

One of the major shortcomings of modelling pavement performance using the mathematical models is that the models may have limited applicability and may only be valid for the conditions and sites for which they were established. For this reason, Molenaar et al. (1999) suggested that generalized models be obtained by making them dimensionless. This suggestion was

also followed with the presentation of the research results in this thesis. This is done by relating the damage as a relative ratio to the cause of damage, also represented as a relative ratio, in the following from: Molenaar et al. (1999) pointed out that the use of such power models is problematic in cases of damage types for which the exponent β is larger than 1. They reported that such power models do not allow pavement condition predictions to be made in cases where maintenance is already overdue; that is, in cases where the condition is beyond the terminal condition.

Modelling of accelerated pavement testing subgrade rutting performance

The SAMPD method has been used in South Africa for a number of years (Theyse et al. 1996). This is a mechanistic– empirical design method that includes fatigue transfer functions for asphalt surfacing, asphalt base, and lightly cemented layers, as well as permanent deformation transfer functions for unbound structural layers and the roadbed. All of these were developed through the SA–HVS program. The method is based on a critical layer approach whereby the shortest layer life of the individual pavement layers determines the pavement life. This approach may be suited to the fatigue failure of bound layers, but does not allow for each of the pavement layers to contribute to the total surface rut. Current research is therefore aimed at developing permanent deformation models for individual pavement layers, to enable the designer to predict each layer's contribution to the total permanent deformation of the pavement system.

Accelerated pavement testing modelling of base fatigue and cracking performance

Fatigue of APT test sections may be quantified by monitoring the deterioration of pavement stiffness with trafficking. Non-destructive tests such as FWD allow the performance of the pavement structure to be expressed in terms of surface deflection. As the structure weakens, the deflection on the surface increases.

Seismic tests such as SASW allow the stiffness of the upper layers of the pavement to be monitored. If cracking is apparent, this can be mapped and related to fatigue performance.

Because of the limited extent of APT testing done on pavements with cement treated bases it is understandable that related modelling of APT performance is also limited. Development of pavement performance transfer functions are presented for the scenario of elasto-plastic behaviour of unbound materials reported by Wolff (1992).

A unique application of HVS data is the work done by Wolff (1992). He used the South African HVS data to develop a mechanistic model for use in a design model for granular pavement materials. His aim was to simulate the actual behavior of granular materials under APT. In this analysis, he assumed the material to be in a stress state well below the yield stress condition, which is the situation in a functional pavement. The basis for Wolff's model is the relationship between stress (S) and the related load repetitions (N) to a defined failure condition. He developed a family of S-N curves for use as transfer functions for rutting in granular materials.

For the development of the transfer function, failure had to be defined as a specific terminal permanent strain value corresponding to a selected layer thickness and terminal rut depth. He developed a series of S-N curves for different materials. This required the determination of the stress induced in a layer by the wheel load under HVS trafficking, in accordance with the measured material parameters. By using different load levels he was able to generate a family of performance curves using HVS data. He opted to use theta, the octahedral normal stress, as the invariant for his sum of the principal stresses (bulk stress) on the vertical axis and the load repetitions on the horizontal axis. He then used Miner's hypothesis to determine the cumulative strain as a result of different wheel loads trafficking the pavement. A cumulative value less than unity is acceptable,

whereas failure is considered to occurred when the value exceeds unity. In the design process, the sum of the permanent strains in each of the pavement layers must not exceed the appropriate design standard. Naturally, deformation in the bound layers has to be added to the value developed in the unbound materials. The method was very successfully applied to low-volume road pavements where the unbound material dominates the structure. Using this method in an iterative manner, he was able to accumulate the permanent strain in predefined pavement layers and relate this to the total deformation of the layer. The latter is a value selected in accordance with design guidelines.

The basis of his model is S–N curves (with N being the number of load reversals that will cause structural failure at peak stress S) that were used as transfer functions for rutting. The S–N curves were developed by Wöhler, and they are used in the mechanical engineering field (Wolff 1992). For the development of the transfer function, failure had to be defined as a specific terminal permanent strain value. Wolff developed a series of S–N curves that could be used to determine cumulative permanent strain. This required the determination of the stress induced in a layer by a wheel load in accordance with the material parameters that he determined from HVS testing. This yielded a point on the S–N curve where the vertical axis represents invariant stresses and the horizontal axis shows the load repetitions. Wolff opted to use theta, the octahedral normal stress for his model. By using HVS data for a variety of materials, he was able to develop a series of S–N curves that could be used to determine cumulative permanent strain. He then used Miner's hypothesis to determine the cumulative strain as a result of different wheel loads trafficking the pavement. A value smaller than unity is then taken to be acceptable, whereas failure is considered to occur as soon as it exceeds unity. In the design process, the sum of the permanent strains in each of the pavement layers must not exceed the appropriate design standard. Naturally, deformation in the bound layers has to be added to the value developed in the unbound materials. The method was very successfully applied to low-

volume road pavements, where unbound material dominates the structure."

Summary

It was apparent that an immediate benefit of APT is that pavement performance may be modelled directly. This is possible because many of the factors influencing performance can be controlled, including:

- Wheel loads (magnitude, wandering, rest period est.),
- Tire pressures,
- Pavement structures (compaction, layer thickness, drainage, etc.),
- Pavement materials (gradations, binder contents, ect.),
- Pavement temperatures (only when tests are performed within environmental chambers), and
- Subgrade moisture conditions (When tests are done in test pits or between seasonal variations).
-

A wide range of models have been developed as part of APT research including:

- Pavement damage
- Subgrade rutting performance
- Asphalt rutting performance
- Asphalt cracking and fatigue performance
- Elasto-plastic behaviour of unbound materials; and
- concrete performance

"There are limitations to APT modelling of pavement performance. APT cannot directly account for time-related factors that influence distress. These are primarily limited to environmental influences, although traffic-related influences must also be taken into account. Furthermore it is not always possible to relate APT performance to the performance of in service pavements under conventional traffic. Real-time trafficked pavements are subject to maintenance before pavement failure. Perhaps the most significant shortcoming of APT modelling is the lack of applicability of models based on one site to other sites. It has necessitated the

normalization of data to reference parameters and motivated development of models based on probabilistic approaches."

A1.5 Pavement Engineering Applications and Issues

"Relationship of accelerated pavement testing to in-service pavements with conventional trafficking

The first question that needs to be asked is: Why is there a difference between APT and conventional trafficking? According to Metcalf (1996) there are essentially two reasons.

• Environmental effects, especially long-term aging, are difficult to capture in APT. (The combined effect of environment and time difference is not simulated.)
• A full spectrum of in-service wheel loads are not applied in APT.

In reality, all APT tests have to consider these two factors when developing methodologies for using APT results optimally. Therefore, conventional in-service highways and/or formal LTPP studies feature both in such development. This is an important aspect of APT. Very little has been reported on this issue. However, the approach of some well-advanced APT programs provided valuable input.

South African Approach

The South African approach does not have conversion factors between APT structural pavement behaviour and real life structural pavement performance. However, this is not believed to be crucial to the success of the process (De Beer et al. 2001). They consider the number of variables that affect the real life performance and life expectancy of a road to be so high that they state:

It is extremely difficult to directly relate real-life to APT unless you have a huge APT database where you have varied (and tested) all

these impacting factors. The approach on the implementation side is therefore rather an "adaptive management process" than a "predictive control process." Real-life dictates and we have to manage our activities (maintenance and rehabilitation) to ensure we get the performance that we want from the road.

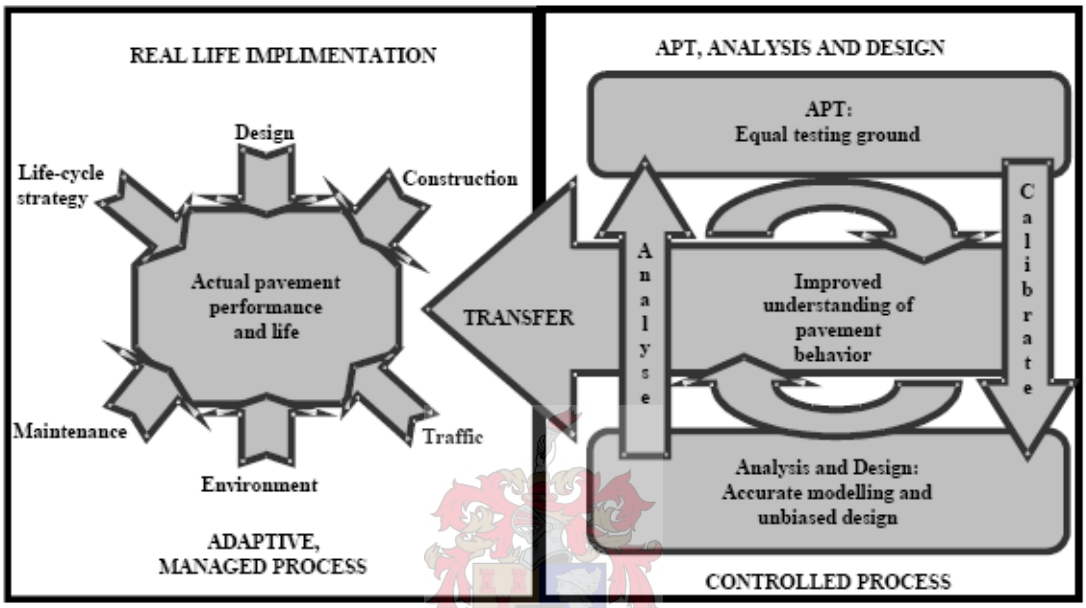

Figure A.5: *Schematic outline depicting the interaction between SA–HVS APT results and real-life Implementation and pavement performance (De Beer et al. 2001).*

The South African process is shown in Figure A.5. In essence, there is no attempt to convert APT-initiated pavement structural behaviour to real field pavement performance. The approach is to study pavement response and performance in great detail by means of APT and then develop practical pavement designs by applying the knowledge gained. The South African mechanistic–empirical pavement designs are calibrated from time to time in collaboration with pavement engineering consultants and the road authorities. This approach is underpinned by the work that was done during the early phases of the SA–HVS program. In 1984, Freeme summed up the approach as follows:

- *Primary indicators of performance such as rutting and cracking were monitored. In the same vein, secondary indicators, which are responses in terms of deflection with depth, and in situ strength and strain, were monitored. With this process, changes in secondary indicators were linked to primary indicators and used to calibrate mechanistic models of pavement structures. Confidence was built when measured deflection profiles matched calculated deflections.*
- *There has been reasonable correlation between HVS performance and actual in-service pavement performance. This has enabled general performance of pavement structures to be clearly illustrated and understood. In turn, this has improved understanding of factors that influence performance of pavement structures. This knowledge has enabled performance of rehabilitation strategies to be predicted. From the foregoing discussion, it is apparent that APT findings are transformed in various ways to enable the results to be used by the different APT users for their specific purposes. This process is not without constraints.*

Failure criteria

It is the basis for defining benchmarks to ensure comparable APT performance relative to real pavement performance under conventional traffic. Several factors have to be taken into account, such as the limited size of test sections, the difference in the nature of trafficking, the difference in time scale including the effect of aging, the limited number of experiments, and the limited ability to determine the integrity of the pavement non-destructively. Two forms of load-related distress are generally considered, rutting and fatigue cracking. Only fatigue cracking will be discussed.

Fatigue and cracking

Fatigue is a more complicated form of distress because it relates to cracking and stiffness loss. In general, it is accepted that failure has occurred once the in situ stiffness has dropped to a level of 50% of the original untrafficked pavement (Bhairo 1998a). Various methods of monitoring the stiffness loss have been reported (Lee et al. 1997; Bhairo 1998a; Harvey et al. 2000). With full-scale APT it is necessary to monitor the cracking as it develops.

In essence, APT results have been applied toward

- *Validation and modification of design procedures,*
- *Pavement configuration comparison in terms of performance,*
- *Evaluation of material performance,*
- *Performance prediction of pavements,*
- *Evaluation and improvement of construction practices, and*
- *Evaluation of maintenance and rehabilitation practices."*

The presented literature review of APT illustrated the role that APT fulfill in pavement design, the appropriateness of the research methodology followed for the Mozambican APT project as well as the status of the APT research field at the moment.

References

AASHTO Guide for Design of Pavement Structures, 1993American Association of State Highway and Transportation Officials, Washington, D.C.

Bhairo, P.D., J. Groenendijk, A.A.A. Molenaar, A.E. Van Dommelen, A. Miradi, and C.H. Vogelzang, 1998, "Pavement Performance Modeling Using APT," *Proceedings of the 5th International Conference BCRA*, Vol. 2, Norwegian University of Science and Technology, Trondheim

Blab, R., 1999 “Introducing Improved Loading Assumptions into Analytical Pavement Models Based on Measured Contact Stresses of Tires” (CD-ROM), *Proceedings of the First International Conference on Accelerated Pavement Testing*, Reno, Nev., Oct. 18–20

Corté, J.-F., Y. Brosseaud, J.-P. Kerzreho, and A. Spernol, 1997, “Study of Rutting of Wearing Courses on the LCPC Test Track,” *Proceedings of the 8th International Conference on Asphalt Pavements*, Seattle, Wash., Aug. 10–14, 1997.

De Beer, M., C. Fisher, and F.J. Jooste, 1997, “Determination of Pneumatic Tyre/Pavement Interface Contact Stresses Under Moving Loads and Some Effects on Pavements with Thin Asphalt Surfacing Layers,” *Proceedings of the 8th International Conference on Asphalt Pavements*, Seattle, Wash., Aug. 10–14.

De Beer, M. and J.E. Grobler, 1993, *ETBs: Heavy Vehicle Simulator (HVS) Evaluation of the Heilbron Sections*, Output Report ETB/HVS, Southern African Bitumen and Tar Association, Roggebaai, South Africa.

Epps, A., T. Ahmed, D.C. Little, and M. Mikhail, 2001, “Performance Assessment with the MMLS3 at WesTrack,” *Journal of the Association of Asphalt Paving Technologists*, Vol. 70

Epps, A., T. Ahmed, D.C. Little, and M. Mikhail, 2001, “Performance Assessment with the MMLS3 at WesTrack,” *Journal of the Association of Asphalt Paving Technologists*, Vol. 70

Gramsammer, J.-C., J.-P. Kerzreho, and H. Odéon, 1999, “The LCPC’s APT Facility” (CD-ROM), *Proceedings of the First International Conference on Accelerated Pavement Testing*, Reno, Nev., Oct. 18–20

Harvey, J.T., J. Roesler, N.F. Coetzee, and C.L. Monismith, 2000, *Caltrans Accelerated Pavement Test (CAL/APT): Program Summary Report: Six-Year Period: 1994–2000,* Report FHWA/CA/RM-2000/15, Prepared for the California Department of Transportation, Pavement Research Center, CAL/APT Program, Institute of Transportation Studies, University of California, Berkeley, June

Horak, E., E.G. Kleyn, J.A. du Plessis, E.M. de Villiers, and A.L. Thompson, 1992, "The Impact and Management of the Heavy Vehicle Simulator (HVS) Fleet in South Africa," *Proceedings of the 7th International Conference on Asphalt Pavements*, *Vol. 2: Performance,* Nottingham, United Kingdom, Aug. 1992.

Horak, E. and F.C. Rust, 1992, "The Performance and Behaviour of Bitumen Emulsion Treated Road Bases in South Africa," *Proceedings of the 7th International Conference on Asphalt Pavements, Vol. 2: Performance,* Nottingham, United Kingdom, August.

Hugo, F., B.F. McCullough, and B. Van der Walt, 1991, "Full-Scale Accelerated Pavement Testing for the Texas State Department of Highways and Public Transportation, "*Transportation Research Record 1293*, Transportation Research Board, National Research Council, Washington, D.C.

Hugo, F., 2000, *Rutting Performance of Dustrol Rehabilitation Under TxMLS Trafficking with Increased Tire Pressure,* Report Number 1814-4, Center for Transportation Research at the University of Texas at Austin.

Hugo, F., Epps, A.L., 2004, *NCHRP Synthesis 325: Significant Findings form Full-Scale Accelerated Pavement Testing*, Transportation Research Board, National Research Council, Washington, D.C.

Huhtala, M. and J. Pihlajamaki, 2000, *The Activity of the First Period in Finland: 1997–1999*, Finnra Reports 21/2000, The Finnish National Road Association, Helsinki.

Jooste, F.J., S.V. Kekwick, E.S. Sadzik, and G.T. Rohde, 1997, "Comparison of Accelerated Pavement Test Results with Long-Term Pavement Behaviour and Performance," *8th International Conference on Asphalt Pavements*, Seattle, Wash., Aug. 10–14

Kadar, P. and P.D. Walter, 1989, *The Performance of Slag Roadbases Under Accelerated Trafficking: Results and Findings of the Prospect ALF Trial*, Research Report ARR 170, Australian Road Research Board, Vermont South, Victoria

Kadar, P., E. Baran, and R.G. Gordon, 1989, *The Performance of CTB Pavements Under Accelerated Loading: The Beerburrum (Queensland) ALF Trial, 1986/87*, Research Report ARR 158, Australian Road Research Board, Vermont South, Victoria, Australia

Kenis, W. and W. Wang, 1999, "Pavement Variability and Reliability" (CD-ROM), *Proceedings of the First International Conference on Accelerated Pavement Testing*, Reno, Nev., Oct. 18–20

Lee, N.-K.J., F. Hugo, and K.H. Stokoe, 1997, "Detection and Monitoring of Cracks in Asphalt Pavement Under Texas Mobile Load Simulator Testing," *Transportation Research Record 1570*, Transportation Research Board, National Research Council, Washington, D.C., Aug.

Lister, N.W., "The Transient and Long-Term Performance of Pavements in Relation to Temperature, 1972, " *Proceedings of the Third International Conference on the Structural Design of Asphalt Pavements*, Vol. 1

Lourens, J.P., 1995, *Towards Improved Understanding of Surfacing,Base, and Tyre Interaction for Low-Cost Pavement Design*, South African Department of Transport, Chief Directorate Roads, Report No. RR 93/559, Pretoria, South Africa

Maree, J.H., C.R. Freeme, and E.G. Kleyn, 1982, "Heavy Vehicle Simulator Testing in South Africa," *International Colloquium Full-Scale Pavement*, Institute fur Strassen-, Eisenbahn- und Felsbau an der Eidgenossischen Hochschule, Zurich, Switzerland

Meng, S., H. Liufu, W. Daoxin, S. Jinan, and L. Yongqi, 1999, "The Performance of Stabilized Base Pavements Under Accelerated Loading" (CD-ROM), *Proceedings of the First International Conference on Accelerated Pavement Testing*, Reno, Nev., Oct. 18–20

Metcalf, J.B., 1996, *NCHRP Synthesis of Highway Practice 235: Application of Full-Scale Accelerated Pavement Testing*, Transportation Research Board, National Research Council, Washington, D.C.

Metcalf, J.B., S.A. Romanoschi, Y. Li, and M. Rasoulian, 1999, "The First Full-Scale Accelerated Pavement Test in Louisiana: Development and Findings" (CD-ROM), *Proceedings of the First International Conference on Accelerated Pavement Testing*, Reno, Nev., Oct. 18–20

Pidwerbesky, B.D., B.D. Steven, and J. De Pont, 1997, "Dynamic Loading Effects on Flexible Pavement Performance," *Proceedings of the 8th International Conference on Asphalt Pavements*, Seattle, Wash., Aug. 10–14

Pidwerbesky, B.D., 1995, "Accelerated Dynamic Loading of Flexible Pavements at the Canterbury Accelerated Pavement Testing Indoor Facility (CAPTIF)," *Transportation Research Record 1482*, Transportation Research Board, National Research Council, Washington, D.C.

Romero, R., A. Ruiz, and J. Perez, "First Test on the CEDEX Test Track," *Transportation Research Record 1354*, Transportation Research Board, National Research Council, Washington, D.C., 1992, pp. 65–73.

Ruiz, A.R. and R.A. Romero, 1999, "The Cedex Full-Scale Test Track: Accelerated Pavement Testing" (CD-ROM), *Proceedings of the First International Conference on Accelerated Pavement Testing*, Reno, Nev., Oct. 18–20

Rust, F.C., S.V. Kekwick, E.G. Kleyn, and E.S. Sadzick,1997, "The Impact of the Heavy Vehicle Simulator (HVS) Test Programme on Road Pavement Technology and Management," *Proceedings of the 8th International Conference on Asphalt Pavements,* Seattle, Wash., Aug. 10–14

Sharp, K.G., J.R. Johnson-Clarke, and D.W. Fossey, 1999, “A Review of the Australian ALF Program” (CD-ROM), *Proceedings of the First International Conference on Accelerated Pavement Testing*, Reno, Nev., Oct. 18–20

Structural Design of InterUrban and Rural Road Pavements, 1980, TRH4, Committee of State Road Authorities, Department of Transport, Pretoria, South Africa.

Structural Design of InterUrban and Rural Road Pavements, 1986, TRH4, Committee of State Road Authorities, Department of Transport, Pretoria, South Africa.

*Structural Design of InterUrban and Rural Road Pavements,*TRH4, 1996, Committee of State Road Authorities, Department of Transport, Pretoria, South Africa.

Sweatman, P.F., *A Study of Dynamic Wheel Forces in Axle Group Suspensions of Heavy Vehicles*, ARRB Special Report No. 27, Australian Road Research Board, Melbourne, Australia, 1983.

Theyse, H.L., M. De Beer, and F.C. Rust, 1996, “Overview of South African Mechanistic Pavement Design Method,” *Transportation Research Record 1539*, Transportation Research Board, National Research Council, Washington, D.C.

Theyse, H.L., 1999, “Accelerated Pavement and Laboratory Testing of Materials Suited to Labour-Intensive Road Construction” (CD-ROM), *Proceedings of the First International Conference on Accelerated Pavement Testing*, Reno, Nev., Oct. 18–20

Vuong, B.T., K.G. Sharp, E.J. Baran, J.R. Johnson-Clarke, and I.N. Reeves,1996, *Performance of Unbound and Stabilized Pavement Materials Under Accelerated Loading:Summary of Report of Beerburrum II ALF Trial*, Report ARR 286, Australian Road Research Board, Vermont South, Victoria, Australia.

Walker, R.N., 1985, “The South African Heavy Vehicle Simulator, Accelerated Testing of Pavements Session,” *Proceedings of the Annual Transportation Convention*, Pretoria, South Africa, July 29–Aug. 2

Walubita, L.F., F. Hugo, and A. Epps, 2000, *Performance of Rehabilitated Lightweight Aggregate Asphalt Concrete Pavements Under Wet and Heated Model Mobile Load Simulator Trafficking: A Comparative Study with the TxMLS*, Report Number 1814-3, Center for Transportation Research at the University of Texas at Austin

White, T.D., J. Hua, and K. Galal, 1999, “Analysis of Accelerated Pavement Tests” (CD-ROM), *Proceedings of the First International Conference on Accelerated Pavement Testing*, Reno, Nev., Oct. 18–20

Wolff, H., 1992, *The Elasto-Plastic Behaviour of Granular Pavement Layers in South Africa*, Ph.D. dissertation, Department of Civil Engineering, University of Pretoria, South Africa.

Yandell, W.O. and G. Behzadi, 1999, “Rutting Prediction of Twelve Accelerated Loading Facility (ALF) Trials” (CD-ROM), *Proceedings of the First International Conference on Accelerated Pavement Testing*, Reno, Nev., Oct. 18–20.

PART 2

Excerpts from report MBTC – 2032 Development of Testing Protocol and Correlations for Resilient Modulus of Subgrade Soils

This part of the literature review contains extracts from the literature study presented by Rydèn (2004) in his doctoral thesis: Surface Wave Testing of Pavements. The presented work is directly quoted from the above mentioned source since it gives an excellent overview of the work conducted in the seismic pavement testing domain and is directly relevant to the seismic testing methodology used in this research study. The section presented here gives a short background on non-destructive testing with focus on base and subgrade materials followed by a literature overview of seismic pavement testing.

A2.1 Background

"Surface waves are stress waves travelling along the free surface of a material. Most of the energy in these waves is confined to the close vicinity of the surface, similar to waves propagating on the surface of water. The velocity of wave propagation is dependent on the elastic properties of the affected medium. This principle is used in seismic pavement testing, to estimate the stiffness and thickness of the different layers in a pavement structure. With an efficient NDT technique structural properties can be mapped as a function of time and space providing a valuable tool in pavement design and management.

Today pavement design is progressively moving from empirical to analytical methods. Analytical methods are the standard engineering procedure for design and analysis of most civil engineering constructions. Theoretical stresses and displacements are calculated from material properties and analyzed in order to predict the final performance of a construction. To successfully implement any analytical pavement design procedure it is essential to develop tools that can measure material properties at each depth in the field, in-situ. With such

tools pavement material properties can be verified in the field and compared to the required material properties. The most important material properties are those related to the stiffness of the materials, for example Young's modulus (E modulus). A higher E-modulus value results in less deformation (strain) for a given load (Stress). Consequently there is a need to develop improved NDT techniques for pavement applications. A successful and efficient NDT device for pavements can save money spent n the pavement design and maintenance.

The most widespread NDT method for pavements is the Falling Weight Deflectometer FWD) (Huang, 1993). The FWD test is based on deflection measurements at the surface resulting from a given dynamic load. This method provides a good estimate of the actual on-linear response of the complete pavement construction at relatively large strain levels (Ullidtz, 1998). Unfortunately, the E-modulus is a complicated function of both stress and strain level under this load situation, and it is therefore difficult to obtain fundamental material properties from this type of test. Wave propagation methods affect the materials in their linear elastic region and provide material properties that are not affected by non-linear properties. For example, the E-modulus of different materials in different pavement constructions can be compared under the exact same loading condition by using wave propagation based methods. The main result from both deflection and wave propagation methods is a stiffness modulus as a function of depth profile, see Figure A.5.

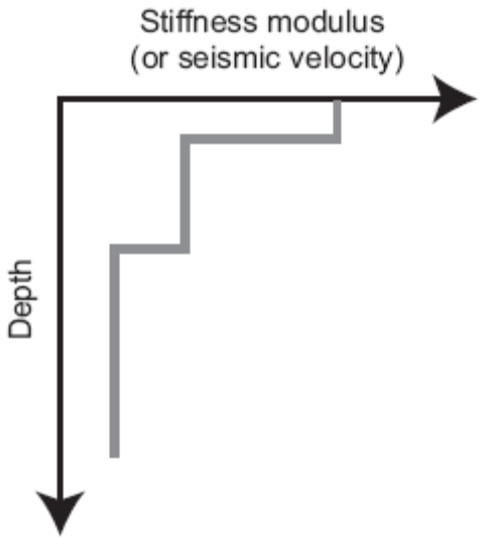

Figure A.5: *The final result from surface wave or deflection based testing of pavements is a stiffness modulus profile of the test section (Rydèn 2004)*

Both base and subgrade materials show a complex behaviour, i.e. stress-dependency and non-linear stress-strain relationship (Larsson, 1994). The long-term response of the base and the upper part of the subgrade is shown as permanent (plastic) deformation, i.e., rutting at the pavement surface. Predicting this long-term response of pavement materials from physical material parameters is a challenging task and has been the objective of many recent studies, for example (Niekerk et al., 1998) and (Hornych et al., 1998). Generally both granular and cohesive soils show a similar behaviour in terms of stiffness properties.

Wave propagation methods offer dynamic stiffness properties representative for very low strain levels. The most important soil stiffness parameter at low strain levels is the shear modulus (G) (Bodare, 1997; Massarsch, 1999). The shear modulus can be calculated from the shear wave velocity (V_S) by using equation A.1 where ρ is the bulk density of the material.

$$G = \rho V_S^2 \qquad (A.1)$$

Both the shear modulus and the shear wave velocity are profoundly dependent on the skeleton stiffness (mean effective state of stress) of particulate materials. The general stress and strain dependency of the shear modulus is illustrated in Figure A.6. The maximum or initial G-modulus is often termed Gmax or G0. Tawfiq et al., (2000) proposed to combine seismic and deflection based tests to obtain the curvilinear modulus relation of the base material in pavements, Figure A.2.

Young's modulus E can be determined from the G modulus and Poisson's ratio (v) by using

$$E = 2G(1+v) \qquad (A.2)$$

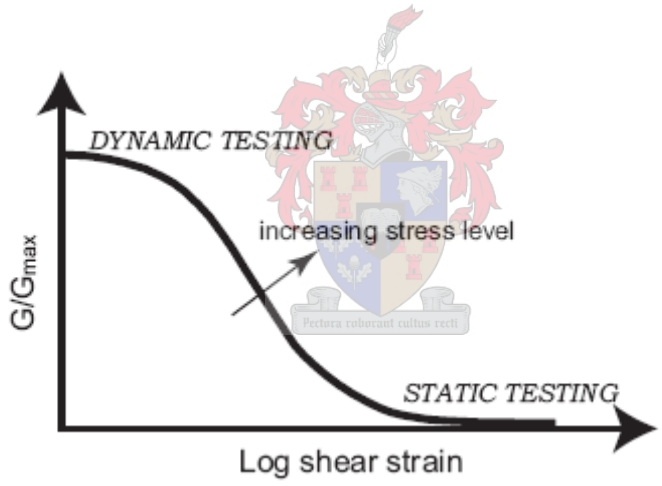

Figure A.7: *Schematic illustration showing shear modulus stress and strain dependency (Rydèn 2004)*

Generally the E-modulus follows the same behaviour as the G-modulus shown in Figure A.7. Many studies have resulted in material models (constitutive laws), which consider that the modulus is dependent on both stress and strain level, for example (Jamiolkowski et al., 1991; Ishibashi and Zhang, 1993; Ekdahl, 1997; Ekdahl et al., 2004).

When the E- or G-modulus is determined from field or laboratory tests it is important to relate the measured value to the specific strain and stress level. Different methods usually affect the material in different ways and therefore absolute values from different tests cannot be compared without taking the non-linear stress and strain behaviour into account.

A2.2 Seismic pavement testing, a literature review

The main objective with seismic non-destructive testing (NDT) of pavements is to estimate the unknown structural properties (thickness and stiffness) of the different layers in a pavement structure. With an efficient NDT technique these properties can be mapped as a function of time and space, providing a valuable tool in pavement design and management. Methods based on surface wave propagation hold the potential to provide this information.

Surface wave methods are based on the dispersive nature of surface waves in a layered medium. The basic approach can be divided into two steps, (1) measure an experimental dispersion curve on the pavement surface, and (2) estimate a layer model by matching the measured dispersion curve with a theoretical dispersion curve from a known layer model (inversion). The first step is the most critical part of any surface wave method. Therefore the following review of surface wave testing of pavements is focused on the measured dispersion curve. The second step where a theoretical dispersion curve is iteratively matched with the experimental dispersion curve is only briefly covered. More information about inversion of surface wave dispersion curves can be found elsewhere (Yuan and Nazarian, 1993; Williams and Gucunski, 1995; Tokimatsu, 1997; Xia et al. 1999; 2000b; Beaty et al., 2002).

The dispersion curve shows the phase velocity (Vph) as a function of frequency (f). The main objective with surface wave measurements is therefore to measure phase velocities at known frequencies along the pavement surface. Before the established surface wave methods are described, some fundamentals of the measured parameters are given. Here we assume that a single mode of harmonic plane wave propagation

in the x direction can be described with F (F = Aeiφ = Aei(k1x1 −ωt)). The amplitude (A) is here included for completeness and it is unity in this example. An example is given of a single frequency component, f=100 Hz (ω=2πf), with a phase velocity Vph=200 m/s (k=ω/Vph). Figure A.8 shows a three-dimensional (3-D) image of the real component of the wavefield F in space (x1), time (t), and amplitude (A). The periodicity is given by the wave number (k1) and angular frequency (ω). The value of F is complex and can be defined with amplitude and phase (φ) as shown in the two 2-D time and space projections in Figure A.8. The phase of one cycle is defined from -π to π and therefore the phase plots wraps around after each period (P) or wavelength (λ). Since we are only interested in the phase velocity along the x1 direction it is the phase values in this dimension that need to be measured. By measuring the phase difference (Δφ) over a known distance (Δx) at a certain frequency, the phase velocity can be calculated as

$$V_{ph} = \frac{\omega \Delta x}{\Delta \phi} \tag{A.3}$$

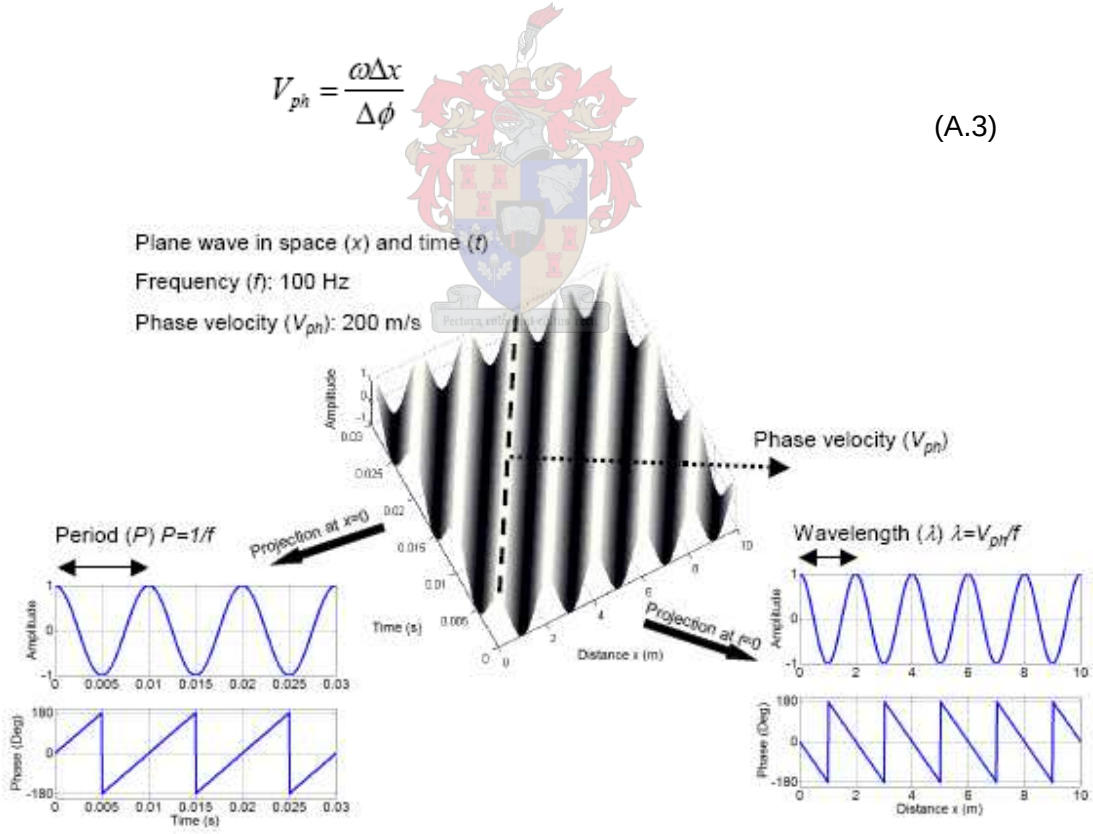

Figure A.8: A plane wave in space and time. The phase velocity vector is indicated with an arrow.

A1.3 The steady state vibration method

"The steady state vibration technique, also called the Continous Surface Wave (CSW) method, was the first attempt to map stiffness of the surface layers by measuring surface wave dispersion. The method was developed in the 1950s and 1960s (Van der Poel, 1951; Jones, 1955; 1962). Sezawa (1938a; 1938b) and Pickett (1945) made the theoretical derivation that showed the possibility to map dispersion of surface waves where the stiffness decreases as a function of depth, i.e. pavement profile. However, at this point there were some speculations regarding the nature of surface wave propagation in this type of layered system (Press and Dobrin, 1956). Jones (1962) was first to acknowledge that phase velocities greater than the shear wave velocity of the subgrade represent leaky waves and must be calculated with a complex wave number. The work by Jones (1962) was refined by Vidale (1964) who studied theoretical dispersion curves from pavement systems in the complex wave number domain. However, without modern computers these studies became limited. Martincek (1994) concluded that even with modern computers it is very difficult to calculate dispersion curves from pavement systems in the complex wave number domain.

The early steady state measuerements on pavement systems were presented by Van der Poel (1951), Heukelom and Foster (1960), Jones (1955; 1958; 1962), and Vidale (1964). In the steady state method, a vibrator is used as a seismic source and one geophone is used as receiver. The geophone is moved progressively away from the vibrator to map wavelengths on the surface with the specified frequency. Originally only successive amplitude maximums as related to the source signal were measured as a function of offset (distance) from the source (Van der Poel, 1951). The length between two maximums corresponds to one wavelength (λ), see Figure A.8. This procedure is repeated for different frequencies and Equation A.4 is then used to calculate the phase velocity at different frequencies to obtain the complete dispersion curve.

$$V\ f\ ph = \lambda \qquad (A.4)$$

In a further development of the method the absolute phase angle was measured at smaller increments from the source for more detailed measurements (Martincek, 1994).
Figure A.9 shows the result from early steady state measurements by Heukelum and Foster (1960). In Figure A.9, the measured dispersion curve is divided into three portions which are interpreted to correspond to each layer in the pavement structure. In this example the depth to each layer in the pavement construction has been correlated to the wavelength divided by two. This simplified evaluation technique was used in the early experiments but was later concluded to be a too crude approximation (Jones, 1962; Vidale 1964).

"In the early 1980s, the steady state method was improved because of the progress in computer power at that time (Gordon, 1997), and is thereafter mostly referred to as the CSW method. Data acquisition could be performed digitally with several receivers and the measuring process became much faster. The evaluation (inversion) of soil site layer properties was approached with refined theories (Tokimatsu et al., 1991), but the evaluation of pavement layer properties was still regarded as a quite complex issue (Martincek, 1994)."

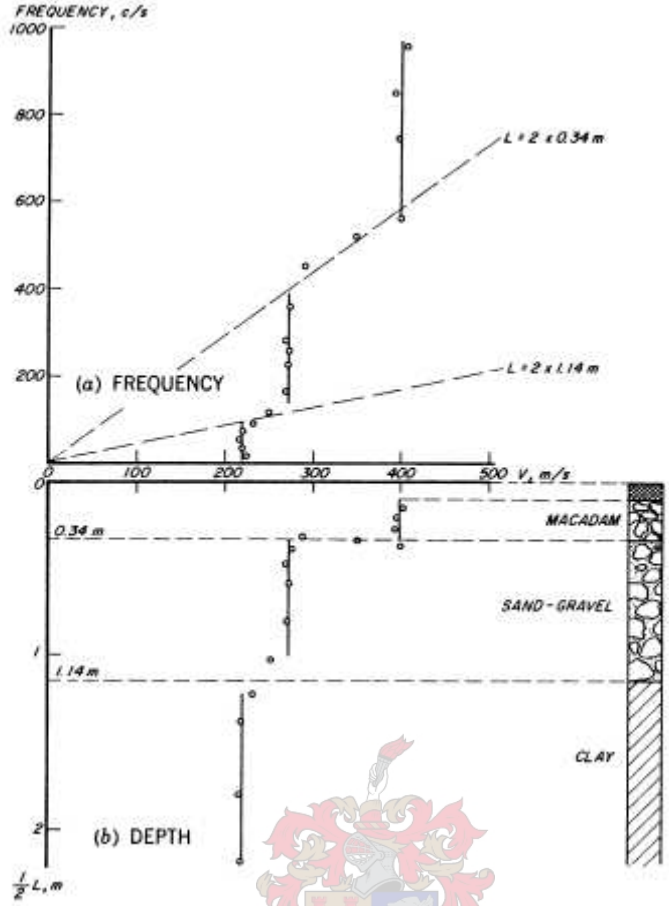

Figure A.9: Result from the steady state vibration method on a pavement profile. The depth to each layer interface has been correlated with the wavelength divided by 2, from Heukelum and Foster (1960).

A2.4 The Spectral Analysis of Surface Waves (SASW) method

"Heisey et al. (1982) first introduced the Spectral Analysis of Surface Waves (SASW) method. Since then a lot of research has been conducted, mainly at the University of Texas at Austin (Nazarian et al, 1983; Nazarian, 1984; Nazarian et al., 1987; Rix et al., 1991; Aouad, 1993; Stokoe et al, 1994; Fonquinos, 1995). Hiltunen and Gucunski (1994) presented an "Annotated bibliography on SASW" with 41 SASW abstracts, about half of these publications are focused on pavement testing. As described above the fundamental approach to measure surface wave phase velocity at different frequencies was already established in the steady state method (Jones, 1955). However the instruments

required for real time Fast Fourier Transformation (FFT) had not yet become available. The FFT made it feasible to measure a whole range of frequencies simultaneously. This revolution in digital data acquisition made the SASW method possible (Rix and Santamarina, 2000). Several publications in recent years have described the SASW method in detail (Aouad, 1993; Stokoe et al., 1994; Stokoe and Santamarina, 2000; Svensson, 2001). The essential elements in the field procedure are the measurement of surface waves between two receivers located a known distance apart on the pavement surface. Figure A.10 shows the principle set-up of the experimental arrangement for a SASW test."

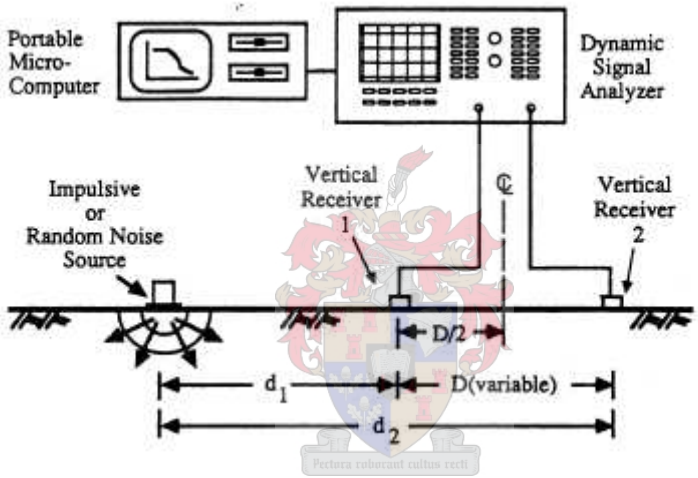

Figure A.10: Schematic of experimental arrangement for SASW tests, from Rix et al. (1991).

"In the SASW method, the phase difference (Δφ) between two receivers is measured for a number of frequencies, by means of a transient impulse applied to the pavement surface, see Figure A.10. The phase velocity (Vph) of a specific frequency of surface waves is calculated from the phase difference Δφ and the receiver spacing (D=Δx) with Equation A.3. Therefore, Δφ is the most critical parameter extracted from the measured data because it determines the accuracy of the dispersion curve constructed afterwards. The coherence function is a quality factor, used in the field to verify if the signals recorded at the receivers are descendent from the same source (Santamarina and Fratta, 1998). Good coherence results in a coherence value close to 1.0. Non-

coherent noise that enters the measurements results in a lower coherence value. This information is used to judge which frequency span that can be used when the dispersion curve is calculated from the measured phase difference.

Usually there is only a limited range of frequencies at each receiver spacing (D) that can be used for the dispersion curve calculation. This limitation is usually referred to originate from the near- and far-field effect. The SASW method assumes plane surface wave propagation (Figure A.8) between the receivers and a smooth continuous dispersion curve that can be determined through the wrapped phase difference spectrum. However, every surface wave frequency component needs to propagate a certain distance from the source before plane wave propagation can be assumed (Ganji et al., 1998). This near-field effect usually extends about one half wavelength from the source (Stokoe et al., 1994), but is site specific. There is also a far-field effect where high frequency surface waves are contaminated by body waves (Park et al., 1999c). The criteria that sets the limit of frequencies (or wavelengths) that can be used for the dispersion curve calculation from a given set-up geometry is often addressed as the "wavelength filter criteria".

To calculate the dispersion curve from the measured wrapped phase spectrum the unwrappping process must first be resolved correctly (Al-Hunaidi, 1992). As seen in Figure A.11 the measured phase difference is defined as a value between –180 and 180 degrees. When the phase difference becomes larger than 180 or -180 degrees it wraps around. The absolute phase difference for a specific frequency is often more than 180 degrees, i.e. the number of total "wrap arounds" needs to be determined in order to calculate a correct phase velocity.

After the phase unwrapping process has been conducted, the phase velocity at each frequency can be calculated. Figure A.12 shows the resulting dispersion curve from the data presented in Figure A.11. Several measurements recorded with different

spacing between the receivers are usually necessary to cover all frequencies (or wavelengths) of interest."

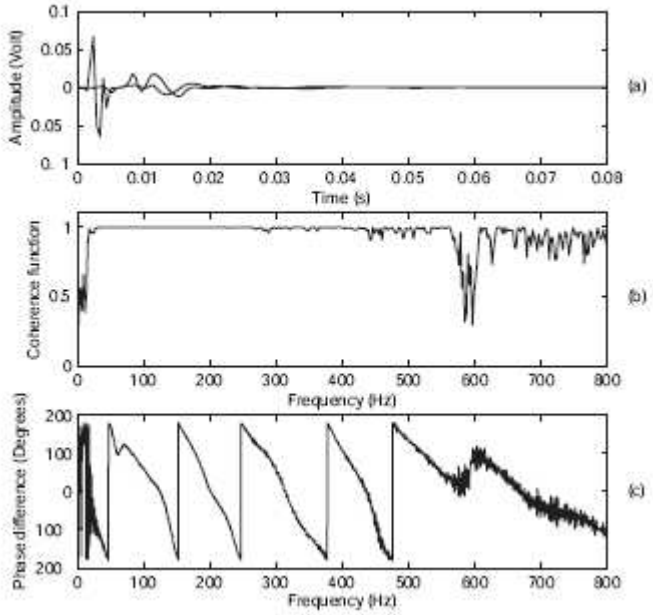

Figure A.11: Example from SASW field plots received instantly on site. In (a) time signals from both receivers, (b) the coherence function of the recorded signals, and (c) the wrapped phase of the cross power spectrum. The example is taken from a SASW test on a pavement construction with receiver spacing, D=1.3 meter.

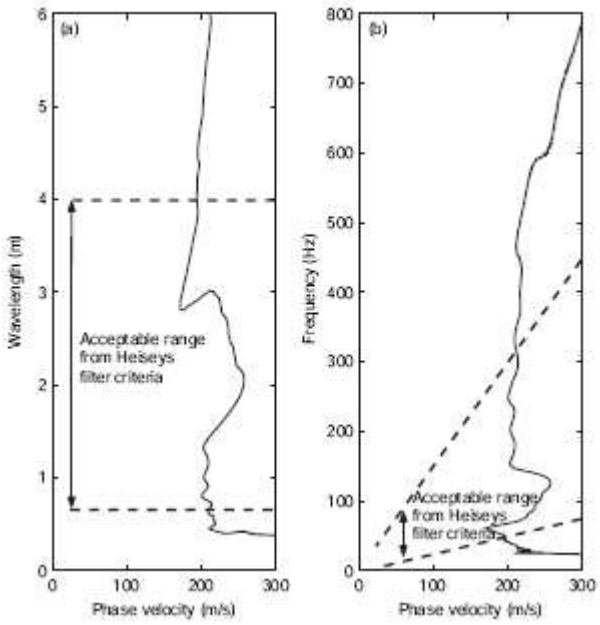

Figure A.12: Calculated dispersion curve from data in Figure A.11, (a) wavelength domain and (b) frequency domain. Marked line shows the usable range according to the wave filter criteria presented by Heisey et al. (1982).

"Finally a compact dispersion curve is constructed from the individual dispersion curves at each receiver spacing. The final dispersion curve assembled in this way has a broader frequency range compared to each individual dispersion curve, which is necessary for the inversion of a shear wave velocity with depth profile. The complete procedure, as presented by Wu et al. (2002), from SASW measurements to an inverted layer model is summarized in Figure A.13.

The inversion of pavement layer properties from the compact dispersion curve obtained with the SASW method has proved to be a challenging task. The initial procedure was based on a normal mode theoretical dispersion curve. The difference between the measured and theoretical dispersion curve was first minimized with a manual trial and error procedure (Nazarian, 1984). Hossain and Drnevich (1989) presented an automatic procedure based on a finite difference method to calculate the theoretical dispersion curve and a linearized optimization technique to minimize the

difference between the measured and theoretical dispersion curve".

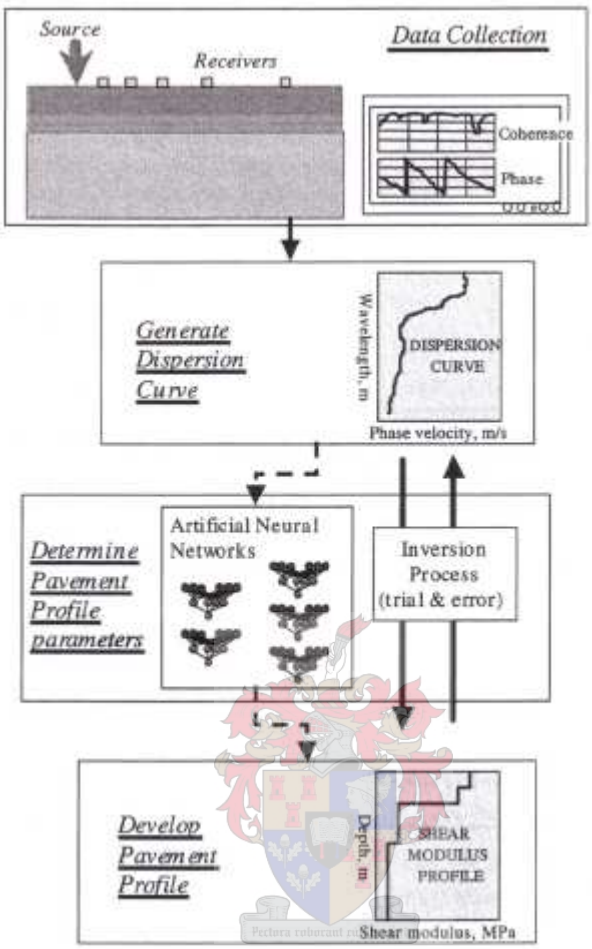

Figure A.13: SASW flow chart, from Wu et al., (2002).

"A similar method was later presented by Yuan and Nazarian (1993). These techniques are all based on a normal single mode dispersion curve. However, it was later found that the compact dispersion curve obtained from the SASW test on pavements is actually dependent on the receiver locations and formed by superposition of different modes of propagation (Roesset et al., 1990; Gucunski and Woods, 1992; Tokimatsu et al., 1992). To overcome this problem a new procedure based on a theoretical simulation of the complete test set-up was proposed (Williams and Gucunski, 1995). The main objective with this approach is to implicitly reproduce the same distortions in the theoretical dispersion curve as present in the measured dispersion curve.

This technique was first implemented with a neural network to find the best matching theoretical dispersion curve (Williams and Gucunski, 1995; Gucunski et al., 1998; Kim and Kim, 1998; Wu et al., 2002). Al-Hunaidi (1998) used the same procedure in combination with genetic algorithms, and Ganji et al., (1998) used a non-linear matrix based inversion technique for the optimization routine. Recently Rambod and Gucunski (2003) proposed to use simulated annealing to find the best matching theoretical dispersion curve."

A2.5 Experiences gained from seismic pavement testing

"Surface wave measurements have been continuously enhanced and proved to be useful for pavement testing (Aouad, 1993; Yuan et al., 1998; Nazarian et al., 1999). At normal soil sites, where the seismic velocity increases with depth, surface wave methods have proved successful in a number of applications (Matthews et al., 1996; Miller et al., 1999; Stokoe and Santamarina, 2000; Park et al., 1999a). In both soil mechanics (Abbis, 2001) and pavement design (Haegeman, 2002; Abdallah et al., 2003; Ekdahl et al., 2004) material models based on the result of surface wave measurements are starting to develop. However, difficulties with the measuring procedure in seismic pavement testing are still reported. In the millennium paper from the Transportation Research Board (TRB) on the characteristics of pavement sections, it was concluded that seismic wave based testing shows great potential but requires further work by the research community (Scullion et al., 2000).

Much of the work reported in this thesis originates from the reported and experienced difficulties with surface wave testing of pavements (Ryden, 1999). The evaluation of the top layer thickness and stiffness has proved to be most efficient and accurate (Roesset et al., 1990; Akhlaghi and Cogill, 1994). The inversion of deeper embedded layers has been the most challenging part in surface wave testing of pavements (Ganji et al., 1998; Gucunski et al., 2000). Particularly the embedded second

layer (base) underneath the asphalt layer has been difficult to resolve (Aouad, 1993; Wu et al., 2002). Reported difficulties and experience gained from the conventional methods are summarized below.

From the pioneer studies on seismic pavement testing, Van der Poel (1951), Heukelum and Foster (1960), and Vidale (1964) concluded that there existed discontinuities in the measurements of surface waves on pavements, manifested in two ways:

• Theoretically it was found that the dispersion curve from pavement profiles was not continuous, but was divided into several branches of dispersion curves.

• For some frequencies it was discovered that the phase velocity along the surface was not constant but sometimes changed from a lower to a higher velocity at a certain offset.

The branching phenomenon was studied by Jones (1962) and Vidale (1964). Both the theoretical calculations and field measurements were very time consuming which may explain why there was not much published in the 1970's on surface wave testing of pavements. The amount of studies increased significantly in the 1980's after the introduction of the much faster SASW method. However, some of the findings by the pioneers of the steady state method tended to be overlooked in the new studies. Almost all studies were conducted with the SASW approach using only two receivers. If the phase-distance relation is not constant and linear as in Figure A.11 it is evident that the phase difference measured between two receivers will be a tricky task.

Several authors have reported on limitations and difficulties related to the two receiver approach methods, at both soil and pavement sites. These problems include the influence of higher modes of surface waves (Rix et al., 1991; Tokimatsu, 1992; Stokoe et al., 1994), variation of phase velocity with distance from the source (Foti, 2000), near- and far-field effects (Fonquinos, 1995),

contamination from reflected surface waves (Sheu et al., 1988), contamination from reflected and direct body waves (Hiltunen and Woods, 1990; Tokimatsu, 1997), non-uniqueness (Ganji et al., 1998), difficulty with phase unwrapping (Al-Hunaidi, 1992), and time consuming testing procedures and data reduction (Hiltunen and Woods, 1990). Several researchers have been studying these limitations. They have proposed a variety of alternatives to minimize these influences.

The first and most simple solution was to use a phase velocity-wavelength domain filter criterion that maximizes the response from the fundamental mode surface wave (Sanchez-Salinero et al., 1987; Roesset et al., 1990), followed by more sophisticate solutions like numerical simulation of the complete test set-up (Gucunski and Woods, 1992; Ganji et al., 1998) and identification of particle orbits (Tokimatsu et al., 1991).

Nazarian and Desai (1993) proposed a method for faster data reduction. All these proposed alternatives improved, to a certain extent, overall performance of the seismic surface wave testing method based on two receiver measurements. However, the seismic phenomena of the pavement system and the distribution between different seismic events were still not clear."

References

Abbis, C.P., 2001, Deformation of landfill from measurements of shear wave velocity and damping, *Geotechnique,* Vol. 51, No. 6, pp 483-494.

Abdallah, I., Yuan, D., and Nazarian, S., 2003, Validation of software developed for determining design modulus from seismic testing, Research Report 1780-5, Center for Highway Materials Research, the University of Texas at El Paso, TX.

Akhlaghi, B.T., and Cogill, W.H., 1994, Application of the free plate analogy to a singlelayered pavement system, *INSIGHT,* Vol. 36, pp 514-518.

Al-Hunaidi, M.O., 1992, Difficulties with phase spectrum unwrapping in spectral analysis of surface waves nondestructive testing of pavements, *Can. Geotech. J.,* Vol. 29, pp 506-511.

Aouad, M.F., 1993, Evaluation of Flexible Pavements and Subgrades Using the Spectral-Analysis-of-Surface-Waves (SASW) Method, PhD thesis, Univ. of Texas at Austin, Texas.

Beaty, K.S., Schmitt, D.R. and Sacchi, M., 2002, Simulated annealing inversion of multimode Rayleigh wave dispersion curves for geological structure, *Geophys. J. Int.* Vol. 151, pp 622-631.

Bodare, A., 1997, Jord och Bergdynamik, Department for soil and rock mechanics, Royal Institute of Technology, Stockholm, Sweden.

Ekdahl, U., 1997, Kung Oscars bro, planskild korsning i Lund, Grundläggningsdagen 97, Swedish Geotechnical Society Publication.

Ekdahl, U., Bengtsson, P. E., and Ryden, N., 2004, A new framework for analytical pavement design based on systematic control during construction work, Proceedings of the 14th Nordic Geotechnical Meeting (NGM 2004), Ystad, Sweden, May 19-21.

Fonquinos Mera, R., 1995, Dynamic nondestructive testing of pavements, PhD thesis, Univ. of Texas at Austin, Texas.

Foti, S., 2000, Multistation methods for geotechnical characterization using surface waves, PhD thesis, Politecnico di Torino, Italy.

Ganji, V., Gucunski, N., and Nazarian, S., 1998, Automated inversion procedure for spectral analysis of surface waves, *J. Geotech. Engrg.,* ASCE, Vol. 124, No. 8, pp 757- 770.

Gordon, M.A., 1997, Application of field seismic geophysics to the measurement of geotechnical stiffness parameters, PhD thesis, Univ. of Surrey, UK.

Gucunski, N., and Woods, R.D., 1992, Numerical simulation of the SASW test, *Soil Dyn. and Earthquake Engrg. J.,* Vol. 11, No. 4, pp 213-227.

Gucunski, N., Krstic, V., and Maher, M.H., 1998, Backcalculation of pavement profiles
from the SASW test by neural networks, Chapter 8 in *Artificial Neural Networks for Civil
Engineers: Advanced Features and Applications*, I. Flood and N. Kartam Eds., ASCE, pp 191-222.

Haegeman, W., 2002, In situ assessment of stiffness of a road sand embankment, Proceedings of the BCRA 2002, Lissabon, Portugal. pp 629-635.

Heisey, J.S., Stokoe II, K.H., and Meyer, A.H., 1982, Moduli of pavement systems from Spectral Analysis of Surface Waves, *Transp. Res. Rec*., 852, Washington D.C, pp 22-31.

Heukelom, W., and Foster, C.R., 1960, Dynamic testing of pavements, *Journal of the Soil Mechanics and Foundations division*, ASCE, Vol. 86, No. SM1, Part 1, pp 2368-2372.

Hiltunen, D.R., and Woods, R.D., 1990, Variables affecting the testing of pavements by the surface wave method, *Transp. Res. Rec*., 1260, pp 42-52.

Hiltunen, D.R., and Gucunski, N., 1994, Annotated bibliography on SASW, in Geophysical characterization of sites. ISSMFE Technical Committee #10, edited by R.D. Woods, Oxford Publishers, New Delhi.

Hornych, P., Kazai, A., and Piau, J.M., 1998, Study of the resilient behaviour of unbound
granular materials, Proceedings of the 5th International Conference on the Bearing Capacity of Roads and Airfields (BCRA), Trondheim, Norway, pp 1277-1287.

Hossain, M.M., and Drnevich, V.P., 1989, Numerical and optimization techniques applied to surface waves for backcalculation of layer moduli, In ASTM special technical publication 1026, Nondestructive testing of pavements and backcalculation of moduli, Editors Bush III, A.J., and Baladi, G.Y., pp 649-669.

Huang, Y.H., 1993, *Pavement analysis and design*, Prentice Hall, New Jersey, ISBN 0-13-655275-7.

Ishibashi, I., and Zhang, X., 1993, Unified dynamic shear moduli and damping ratios of sand and clay, *Soils and Foundations*, Vol. 33, No. 1, pp 182-191.

Jamiolkowski, M., Leroueil, S., and Lo Presti, D.C.F., 1991, Design parameters from theory to practise, GEO-COAST 91, Yokohama, pp 877-916.

Jones, R., 1955, A vibration method for measuring the thickness of concrete road slabs in situ, *Magazine of Concrete Research,* Vol. 7, No. 20, pp 97-102.

Jones, R., 1958, In-situ measurement of the dynamic properties of soil by vibration methods, *Géotechnique*, Vol. 8, pp 1-21.

Jones, R., 1962, Surface wave technique for measuring the elastic properties and thickness of roads: Theoretical development, *British Journal of Applied Physics*, Vol. 13, pp 21-29.

Kim, Y., and Kim, Y.R., 1998, Prediction of layer moduli from FWD and surface wave measurements using artificial neural network, Transportation Research Board, 77th Annual Meeting, Washington D.C.

Larsson, R., 1994, Deformationsegenskaper i jord, Report B 1994:6, Department of Geotechnical Engineering, Chalmers University of Technology, Sweden.

Martincek, G., 1994, *Dynamics of pavement structures*, E & FN Spon and Ister Science Press, Slovak Republic.

Massarsch, K.R., 1999, Seismic field measurements applied to static geotechnical problems, Proceedings of the Environmental and Engineering Geophysical Society (EEGS), Se1.

Matthews, M.C., Hope, V.S., and Clayton, R.I., 1996, The use of surface waves in the determination of ground stiffness profiles, *Proc. Instn. Geotech. Engng.* Vol. 119, Apr., pp 84-95.

Miller, R.D., Xia, J., Park, C.B., and Ivanov, J.M., 1999, Multichannel analysis of surface waves to map bedrock, Kansas Geological Survey, *The Leading Edge*, December, pp 1392-1396.

Nazarian, S., Stokoe II, K.H., and Hudson, W.R., 1983, Use of spectral analysis of surface waves method for determination of moduli and thicknesses of pavement systems, *Transp. Res. Rec*. 930, Washington DC, pp 38-45.

Nazarian, S., 1984, In situ determination of soil deposits and pavement systems by spectral analysis of surface waves method. PhD thesis, Univ. of Texas at Austin, Texas.

Nazarian, S., Stokoe, II K.H., Briggs, R.C., and Rogers, R., 1987, Determination of pavement layer thicknesses and moduli by SASW method, *Transp. Res. Rec*. 1196, Washington DC, pp 133-150.

Nazarian, S., and Desai, M.R., 1993, Automated surface wave method: field testing. *J. Geotech. Engrg.*, ASCE, Vol. 119, No. 7, pp 1094-1111.

Nazarian, S., Yuan, D., and Tandon, V., 1999, Structural Field Testing of Flexible Pavement Layers with Seismic Methods for Quality Control, *Transp. Res. Rec*., 1654, pp 50-60.

Niekerk, A.A., Houben, L.J.M., and Molenaar, A.A.A., 1998, Estimation of mechanical behaviour of unbound road building materials from physical material properties,
Proceedings of the 5th International Conference on the Bearing Capacity of Roads and Airfields (BCRA), Trondheim, Norway, pp 1221-1223.

Park, C.B., Miller, R.D., and Xia, J., 1999a, Detection of near-surface voids using surface wave, Proceedings of the Symposium on the Application of Geophysics to Engineering and Environmental Problems (SAGEEP 1999), Oakland, CA, March 14-18, pp 281-286.

Park, C.B., Miller, R.D., and Xia, J., 1999c, Multichannel analysis of surface waves, Kansas Geological Survey, *Geophysics*, Vol 64, No 3, pp 800-808.

Pickett, G., 1945, Dynamic testing of pavements, *Journal of the American Concrete Institute,* Vol. 16, No. 5, pp 473-489.

Press, F., and Dobrin, M. B., 1956, Seismic wave studies over a high-speed surface layer, *Geophysics*, Vol. 21, No. 2, pp 285-298.

Rambod, H., and Gucunski, N., 2003, Inversion of SASW dispersion curve using numerical simulation, Proceedings of the Symposium on the Application of Geophysics to Engineering and Environmental Problems (SAGEEP 2003), San Antonio, Texas, SUR- 01.

Rix, G.J., Stokoe II, K. H., and Roesset, J.M., 1991, Experimental study of factors affecting the Spectral Analysis of Surface Waves method, Research report 1123-5, Center for Transportation Research, The University of Texas at Austin.

Rix, G.J., and Santamarina, J.C., 2000, Signals and inversion in geotechnical site characterization, EEGS Shortcourse, Symposium on the Application of

Geophysics to Engineering and Environmental Problems (SAGEEP 2000), Washington D.C, February 24.

Roesset, J.M., Chang, D.W., Stokoe II, K.H., and Auoad, M., 1990, Modulus and thickness of the pavement surface layer from SASW tests, *Transp. Res. Rec*., 1260, pp 53-63.

Ryden, N., 1999, SASW as a tool for non destructive testing of pavements, MSc thesis, Univ. of Lund, Sweden.

Ryden, N, 2004. Surface wave testing of pavement structures, PhD dissertation, University of Lund, Sweden.

Santamarina, J.C., and Fratta, D., 1998, *Introduction to discrete signals and inverse problems in civil engineering*, Georgia Institute of Technology, ISBN 0-7844-0311-2.

Santamarina, J.C., Klein, K.A., and Fam, M.A., 2001, *Soils and waves*, John Wiley & Sons, New York, ISBN 0-471-49058-X.

Sanchez-Salinero, I., Roesset, J. M., Shao, K. Y., Stokoe, K. H., and Rix, G. J., 1987, Analytical evaluation of variables affecting surface wave testing of pavements, *Transp. Res. Rec*., 1136, pp 86-95.

Scullion, T., Uzan, J., Nazarian, S., and Briggs, B., 2000, Future directions in characterizing strength and deformation properties of pavement layers, Tansportation Research Board (TRB), Millenium paper from the Committee on Strength and Deformation Characteristics of Pavement Sections.

Sezawa, K., 1938a, Anomalous dispersion of elastic surface waves, *Proc. Imp. Acad*, Vol. 14, pp 246-249.

Sezawa, K., 1938b, Anomalous dispersion of elastic surface waves II, *Bull. Earthq. Res. Inst.*, Vol. 16, pp 225-233.

Sheu, J.C., Stokoe II, K.H., and Roesset, J.M., 1988, Effect of Reflected Waves in SASW Testing of Pavements, *Transp. Res. Rec*., 1196, pp 51-61.

Stokoe II, K.H., Wright, S.G., Bay, J.A., and Roesset, J.M., 1994, Characterization of geotechnical sites by SASW method, in Geophysical characterization of sites. ISSMFE Technical Committee #10, edited by R.D. Woods, Oxford Publishers, New Delhi.

Stokoe II, K.H., and Santamarina, J.C., 2000, Seismic-wave-based testing in geotechnical engineering, Proceedings of the GeoEng 2000. Melbourne, Australia.

Svensson, M., 2001, Application of the SASW-technique in geotechnical in-situ testing, Ph.D. Thesis, LTH, Lund University, Sweden, ISRN LUTVDG/TVGT-1009-SE.

Tawfiq, K., Sobanjo, J., and Armaghani, J., 2000, Curvilinear behavior of base layer moduli from deflection and seismic methods, *Transp. Res. Rec.,* 1716, pp 55-63.

Tokimatsu, K., Kuwayama, S., Tamura, S., and Miyadera, Y., 1991, Vs determination from steady state Rayleigh wave method, *Soils and Found*, Vol. 31, No. 2, pp 153-163.

Tokimatsu, K., 1997. Geotechnical site characterization using surface waves, *Earthquake geotechnical engineering*, Ishihara (ed.), Balkema, Rotterdam.

Ullidtz, P., 1998, *Modelling flexible pavement response and performance*, Polyteknisk Forlag, Lyngby, Copenhagen.

Van der Poel, C., 1951, Dynamic testing of road constructions, *J. appl. Chem.,* Vol. 1, July, pp 281-290.

Vidale, R.F., 1964, The dispersion of stress waves in layered media overlaying a half space of lesser acoustic rigidity, Ph.D. Thesis, Univ. of Wisconsin.

Williams, T.P., and Gucunski, N., 1995, Neural networks for backcalculation of moduli from SASW test, *J. Comp. In Civ. Engrg,* ASCE, Vol. 9, No. 1, pp 1-8.

Wu, H., Wang, I., Abdallah, I., and Nazarian, S., 2002, A rapid approach to interpretation of SASW results, Proceedings of the 6th BCRA Conference 2002, Lisbon, Portugal. T8.18.

Xia, J., Miller, R.D., and Park, C.B., 1999, Estimation of near-surface shear-wave velocity by inversion of Rayleigh waves, Kansas Geological Survey, *Geophysics*, Vol. 64, No. 3, pp 691-700.

Xia, J., Miller, R.D., Park, C.B., and Ivanov, J., 2000a, Construction of 2-D vertical shear-wave velocity field by the Multichannel Analysis of Surface Wave technique, Proceedings of the Symposium on the Application of Geophysics to Engineering and Environmental Problems (SAGEEP 2000), Washington D.C, February 20-24, pp 1197-1206.

Yuan, D., and Nazarian, S., 1993, Rapid determination of layer properties from surface wave method, *Transp. Res. Rec*., 1377, pp 159-166.

Yuan, D., Nazarian, S., Chen, F., and Hugo, 1998, Use of seismic pavement analyser in monitoring degradation of flexible pavements under Texas Mobile Load Simulator (a case study), Transportation Research Board, Paper No. 981523, Washington DC.

PART 3

Excerpts from report MBTC – 2032 Development of Testing Protocol and Correlations for Resilient Modulus of Subgrade Soils

This appendix contains excerpts taken from the above mentioned report with the objective to explain the technical aspects of seismic pavement testing. Elastic and seismic waves, signal analysis and the development of the dispersion curve are presented in this section. These excerpts are quoted directly from the literature review of the research report since it gives an excellent explanation of the technical aspects of seismic pavement testing.

Non-destructive testing

> *"Non-destructive testing (NDT) techniques are commonly used to estimate the resilient moduli of materials used in pavement systems. Non-destructive testing offers several advantages over laboratory testing of resilient moduli. NDT tests can typically be carried out much faster, and at much less expense than can laboratory tests. NDT testing also offers the advantage of testing the materials in-situ, which gives a better representation of the material properties under field conditions. A larger volume of material is evaluated during NDT testing than during laboratory testing, which increases the accuracy of the obtained modulus values. Testing resilient modulus in-situ is especially beneficial as resilient modulus is heavily dependent upon both environmental conditions and state of stress. Considering all of these benefits, NDT testing may be considered a good tool to rapidly determine resilient modulus and to insure laboratory values are appropriate.*
>
> *One of the most popular NDT methods currently used to estimate resilient modulus is the Falling Weight Deflectometer (FWD). FWD testing allows for the resilient modulus of each layer of a pavement system to be estimated using a backcalculation procedure. However, results obtained from laboratory testing and FWD testing generally does not agree (Mikhail, 1999). Additionally, FWD testing suffers from several limitations including the attempt to model a*

dynamic load with an ill-conditioned static analysis procedure, which does not produce unique results.

An NDT that is gaining popularity for use in determining moduli of layered systems is spectral analysis of surface waves (SASW). SASW allows the resilient modulus and thickness of each layer of a pavement system to be estimated using a combination of elastic wave propagation theory and signal processing techniques. SASW testing offers a fast, economical and theoretically sound alternative to both laboratory resilient modulus and FWD testing. Additionally, if meaningful correlations can be established between the resilient modulus found using SASW and the resilient modulus found by laboratory triaxial testing, then the SASW method could potentially replace the laboratory triaxial method as the preferred technique for determining resilient modulus for roadway design procedures.

One of the primary difficulties in estimating appropriate values of resilient moduli for pavement design purposes is that the resilient modulus of a material is not a constant property. Resilient modulus changes as a function of both environmental and stress conditions. As such, resilient modulus is considered to be a seasonally variable material property, and this variability must be accounted for to appropriately design pavement systems. Currently the AHTD uses FWD testing to attempt to account for the seasonal variation in resilient modulus. SASW testing may prove to be a more useful field evaluation technique because of its ability to simultaneously estimate layer thicknesses and resilient moduli."

A3.1 Background

"The concept of using surface waves to evaluate properties of subsurface materials was first proposed in the 1950's in the form of the steady state Rayleigh wave technique (Rossett, 1990). This method was proposed for evaluation of the elastic properties of pavement systems, but never gained wide acceptance due to the amount of time required to perform the field testing and the non-portable nature of the equipment involved (Rossett, 1990). In the

1980's, a modification to the steady state Rayleigh wave technique was made which took advantage of the concepts of signal analysis and the properties of transient impacts (Foti, 2000). Utilization of these concepts as well as the availability of more sophisticated electronic equipment allowed for rapid testing using portable equipment. The method of using signal analysis techniques to analyze surface waves became known as spectral analysis of surface waves (SASW).

The SASW method is based on the dispersive behaviour of surface waves in a layered medium (Nazarian, 1995). Dispersion is the term used to describe the fact that the rate at which a Rayleigh wave travels through a medium depends upon the frequency of the wave, and this dependency can be used to determine mechanical properties of the medium through which the wave travels (Foti, 2000). Plotting Rayleigh wave velocity versus frequency (or wavelength) produces a graph called a dispersion curve. This dispersion curve can be used to develop a modulus versus depth profile through the use of a backcalculation procedure. Once the modulus versus depth profile is known, the resilient modulus and thickness of individual layers can be directly obtained.

To conduct SASW testing two receivers are placed on the pavement (or ground) surface. The receivers are connected to a digital signal analyzer (DSA). A transient impact is applied to the pavement surface which generates seismic surface waves. The particle motion associated with the passage of the surface waves is sensed by the receivers, and transformed into electrical signals. The DSA uses Fourier and spectral analysis procedures to determine the cross power and coherence values of the electrical signals as a function of frequency (Nazarian, 1995). From this information, Rayleigh wave velocity and wavelength can be calculated as a function of frequency. These two pieces of information allow for the dispersion curve previously mentioned to be constructed."

A3.2 Elastic waves

Wave Terminology

"In order for a wave to exist it must have a medium through which to travel. This literature study will be concerned with seismic waves and their properties when travelling through solid media such as asphalt, cement stabilised base material and soil. Two definitions relating to the medium through which seismic waves travel are important for developing the concepts of seismic wave propagation. The two definitions are relatively simple; however they are important in that they dictate the types of seismic waves that can be generated. Whole space is defined as a medium that has constant properties and extends infinitely in all directions. Half space is defined as a whole space that extends infinitely in only two directions and intersects a free surface in the third direction. A whole or half space can be called ideal if its material properties obey the theory of elasticity. The term layered ideal whole space or layered ideal half space will be used to describe a medium which is isotropic, consists of multiple layers each of which is homogenous, and the material contained in each layer is elastic in nature. A simple illustration of whole space, half space and layered half space is shown below".

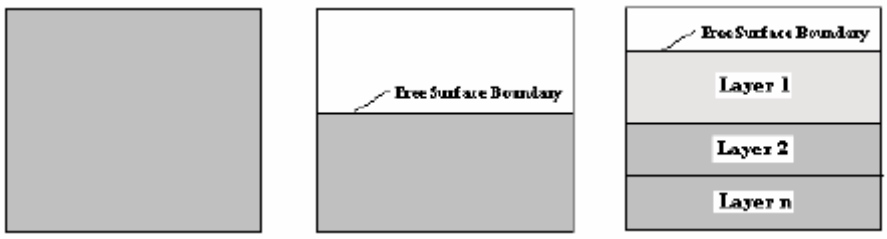

a) Whole space **b) Half space** **c) Layered halfspace**

Figure A.14: Illustration of whole space, half space and layered half space concepts

"Imagine that a seismic disturbance occurs within a whole space. The disturbance

will move away from the location of its origin in a spherical manner due to the fact that the material properties are uniform in all directions. The collection of points that define the disturbance at any given time is called the wavefront. A vector drawn normal to the wavefront is known as a ray or raypath. The raypath indicates the direction in which the wavefront is expanding (Burger, 1992).

This study will frequently discuss waves that are periodic and sinusoidal in shape.
Various terms are used to describe the properties of waveforms of this variety. Figure A.15 shows a periodic, sinusoidal waveform. Two variables can be used to define the shape of a sinusoidal waveform, λ and A. The wavelength (λ) is defined as the distance between two successive points on a wave that have similar displacements. Typically either the distance between successive crests or troughs is chosen to measure the wavelength. The amplitude (A) is the maximum displacement a particle will undergo as a result of the wave passing through a material (Burger, 1992)."

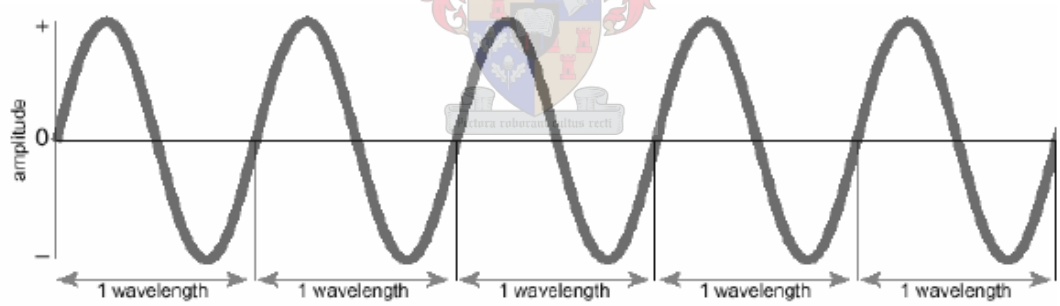

Figure A.15: Illustration of a sinusoidal waveform

"Two additional parameters are often used to describe the rate of propagation of sinusoidal waveforms. The period of a wave, T, is the amount of time it takes a wave to travel a distance of one wavelength (or cycle). Frequency (f) is the number of periods (cycles) that occur in a given amount of time. Therefore, the frequency is the reciprocal of the period, and can be shown in equation form as

$$f = \frac{1}{T} \qquad (A.5)$$

Hertz, or cycles per second, is the unit typically assigned to frequency.

Using the definitions above an important equation vital to seismic testing can be developed. Knowing both the frequency and the wavelength of a sinusoidal wave allows for the velocity of a wave in an elastic medium to be calculated using the equation"

$$V = f*\lambda \qquad (A.6)$$

A3.3 Seismic Waves

Body Waves

"Exact mathematical analysis based on the theory of elasticity can be used to derive equations of motion which show that two types of waves can exist in an ideal whole space due to a disturbance within the whole space; the reader is referred to Graff (1975) for further information on the subject. The results obtained from the derivation show that each type of wave has a characteristic particle motion and propagation velocity with which it is associated.

The first type of waveform is transmitted by particles that oscillate in a back and forth motion around their equilibrium position. This oscillation occurs in the same direction as the propagation direction of the wave. This type of wave is generally called a primary wave or P-wave because it travels the fastest of all the seismic waves, and thus appears first in seismic records (Bath, 1979). P-waves are also called volumetric waves because the push-pull motion of the P-wave causes the medium to undergo volumetric changes as the wave passes. The P-wave is also sometimes called an irrotational wave due to the fact that all of the particle motion occurs in the same direction as the wave is travelling (Graff, 1975). Other names such as compression wave,

dilation wave, or longitudinal wave may also be used to describe a P-wave.
P-waves are capable of travelling through all media which permit the passage of seismic waves including gasses, liquids, and solids. P-waves that travel in either gas or liquid are called acoustic waves.

The second type of waveform that can propagate in an elastic whole space is transmitted when particle motion occurs in a plane perpendicular to the direction in which the wave travels. This type of wave travels slower than a P-wave and is the reason it is termed the secondary, or S-wave (Bath, 1992). During the propagation of an S-wave no volume change occurs, and all of the particle motion occurs in the transverse direction which causes the S-wave to be called either an equivolumetric wave or a shear wave. S-waves are also occasionally referred to as rotational waves and transverse waves.
S-wave motion always occurs in the plane perpendicular to the direction the wave is travelling, however that plane may not be convenient for analysis purposes. For this reason, S-waves are often decomposed into horizontal and vertical components (relative to the ground surface) called SH-waves and SV-waves respectively (Bath, 1992).
This S-wave motion can only be transmitted in material that has shear strength. Thus, shear waves cannot be transmitted through gasses or liquids under normal circumstances.

Surface Waves

Seismologists in the 1800's discovered that records obtained from seismographs could not be completely explained using the types of waves known to them at the time (P and S waves). It was observed that the tremors experienced during an earthquake consisted of two minor tremors followed by a single significant tremor. The first minor tremor was known to correspond to the arrival of the P-wave, and the second minor tremor was attributed to the arrival of an S-wave. The third tremor, however, remained a

mystery until 1887 when it was explained by Lord Rayleigh (Graff, 1975).

Lord Rayleigh demonstrated mathematically that the third tremor was due to the arrival of a wave that propagated along the surface of the earth. This type of wave is now known as a Rayleigh wave. Elastic wave theory up to this time could not predict such a wave because wave theory had only been applied to the conditions of an ideal elastic whole space. Lord Rayleigh was able to prove the existence of this new type of wave by applying wave theory to an ideal elastic half space, meaning he imposed a free surface boundary condition onto a whole space. Refer to work by Graff (1975) for a full mathematical derivation of the existence of the Rayleigh wave in an ideal half space.

Like P and S waves, the Rayleigh wave can be characterized by both the particle motion it creates and the velocity at which it travels. The Rayleigh wave travels the slowest of all seismic waves, typically arriving slightly after the shear wave in a time history recording of a seismic event (Bath, 1979). The relationship between the Rayleigh wave velocity and the shear wave velocity is a very important relationship when performing spectral analysis of surface wave testing.
The propagation of the wavefront of a Rayleigh wave is unlike that of the body waves. Rayleigh waves are created by complex interactions of P and S-waves that occur at the free surface boundary of a half space when a disturbance occurs (Graff 1975).

As the surface wave name implies, a Rayleigh wave will travel only near the surface of the boundary at which it was created. The particle motion associated with the passage of a Rayleigh wave is a bit more complicated than it is for body waves. Rayleigh wave motion occurs in the vertical plane only. The planar particle motion that occurs when a Rayleigh wave passes consists of two separate displacement components, vertical and horizontal, which are exactly 90° out of phase with one another. The two components travel at the same velocity, however they attenuate according to

different exponential functions with depth. The vertical component of displacement is larger than the horizontal component of displacement at the free surface boundary which causes the particle motion to be a retrograde ellipse. However, the direction of particle motion changes to that of a prograde ellipse at a depth of approximately 1/2π of the wavelength because of the differing attenuation properties of the displacement components (Foti, 2000). Figure A.16 shows both of the displacement components of a Rayleigh wave as a function of depth."

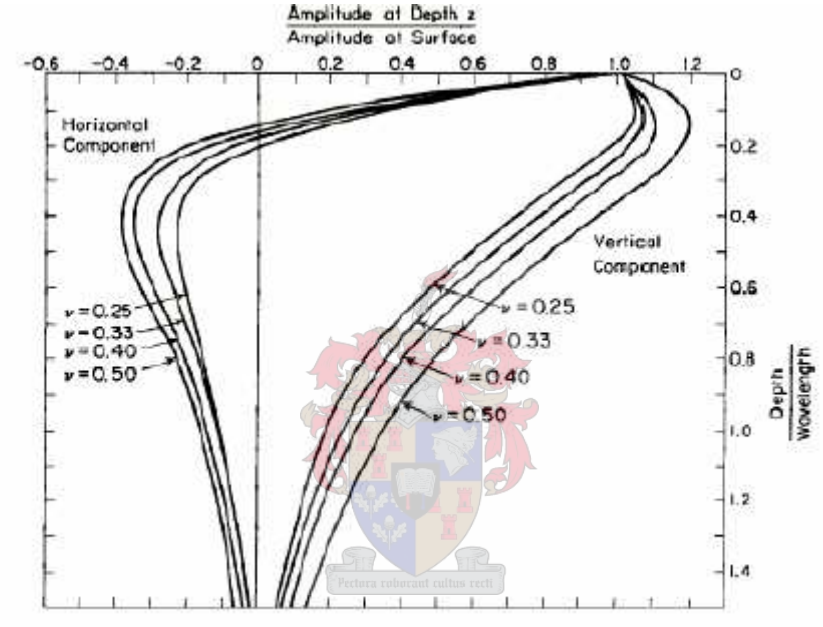

Figure A.16: Rayleigh wave amplitude as a function of depth for various values of Poisson's ratios (from Richart et al, 1970)

"The fact that the amplitude of the displacement components attenuates exponentially with depth is another very important property of Rayleigh waves when applying their usage to seismic analysis. Using Figure A.16 one can see that nearly all of the particle motion associated with the Rayleigh wave occurs at depths shallower than one and a half wavelengths. Practically speaking, this means that the properties of the medium below the zone in which the Rayleigh wave travels has no impact on the behaviour of the wave (Nazarian, 1984).

Figure A.17 shows the particle motion associated with the Rayleigh waves, P-waves, and S-waves."

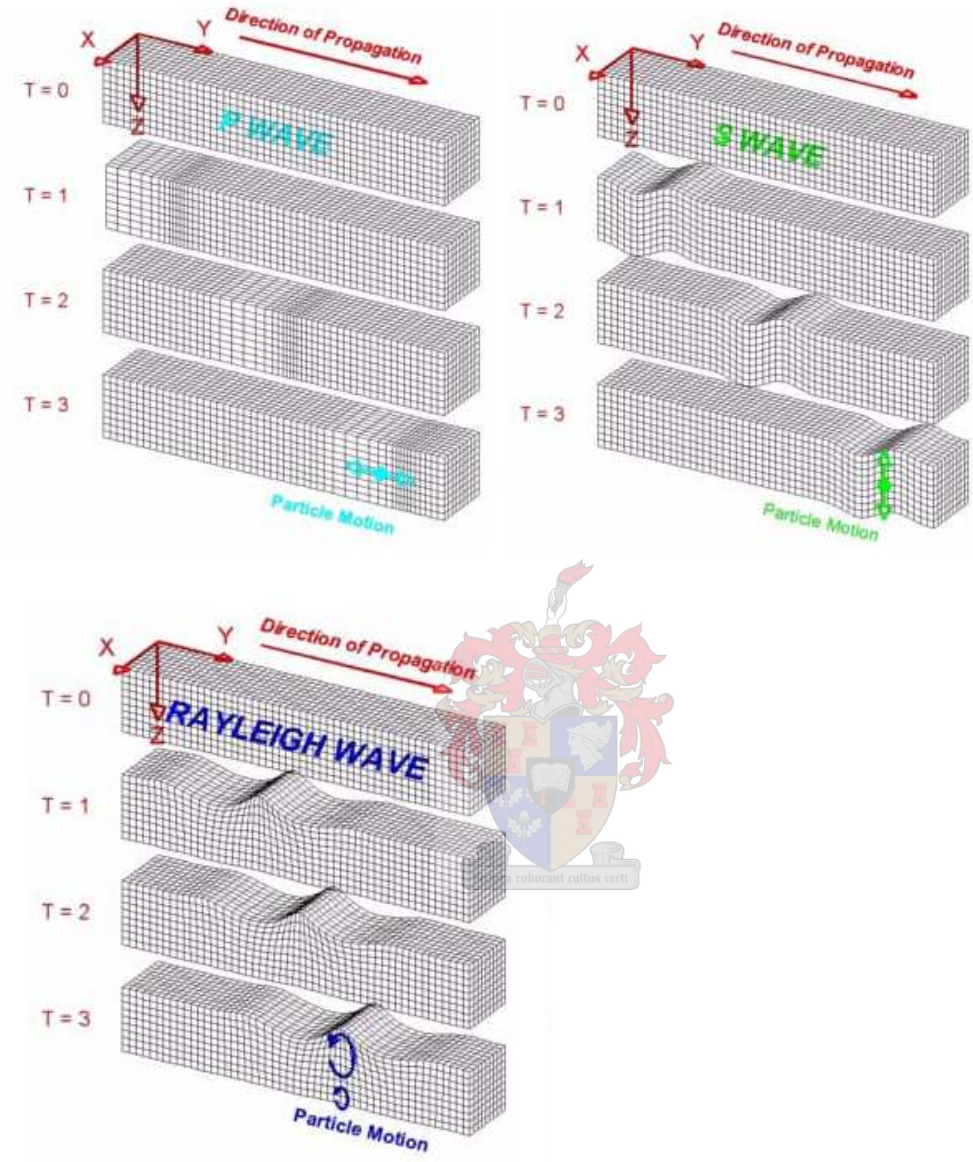

Figure A.17: Major types of seismic waves and their respective motions (from Braile, 2003)

A3.4 Properties of Seismic Waves in an Elastic Medium

Elastic Constants

"In classic elastic wave theory, wave velocities are typically derived using Lame's elastic constants, μ and λ. These two parameters are not commonly used in geotechnical engineering applications; therefore the first portion of this section will define the common elastic constants used in pavement engineering. Once these elastic constants and the relationships between them have been defined, it becomes possible to express wave velocity in terms of these commonly used engineering parameters.
According to Hooke's law a linear relationship exists between applied stress (σ) and the resultant strain (ε). For an axially applied stress Hooke's law is defined by

$$\sigma = E\varepsilon \qquad (A.7)$$

E is given the name Young's modulus, and is very commonly used to describe material behaviour. Another descriptor of material behaviour is Poisson's ratio (v). Poisson's ratio is used to quantify the phenomena that if a material is subjected to a compressive stress along a single axis it will shorten in the same direction in which the stress is applied, but will expand along axes perpendicular to the applied stress. In equation form

$$v = \frac{\varepsilon_{(transverse)}}{\varepsilon_{(longitudinal)}} \qquad (A.8)$$

Young's modulus predicts the relationship between stress and strain for a material that is subjected to axial compression or extension. If a material is deformed by simple shear a different modulus, called the shear modulus, is used to define the relationship between stress and strain behaviour. The equation that shows the linear relationship between shear stress (τ) and shear strain (γ) is

$$\tau = G\,\gamma \qquad (A.9)$$

where G is called the shear modulus. The shear modulus and Young's modulus are related to one another through Poisson's ratio by the equation shown below

$$G = \frac{E}{2(1+\nu)} \qquad (A.10)$$

Seismic Wave Velocity

Elastic wave theory predicts that the rate at which seismic waves move through a material is directly related to the elastic material properties (stiffness) of the material.
The significance of the previous statement is that if the propagation velocity of a seismic wave is known the elastic properties of the material can be calculated. One of the most commonly used relationships is the relationship between shear wave velocity and shear modulus. The relationship is a powerful link between seismic wave properties and elastic pavement properties. The significance of the relationship goes even further if Poisson's ratio is known, allowing Young's modulus to be obtained through the use of Equation A.10."

A3.5 Seismic Wave Energy

"As a wave travels outward from the source which caused the disturbance, energy is dissipated. Energy dissipated as a function of the distance the wave travels is called geometrical attenuation (Burger, 1992). Spectral analysis of surface waves analysis is based on the case of a point source acting on the ground surface. The P and S-waves generated due to the point source will attenuate differently than will the resulting Rayleigh wave due to their differing wave fronts. The body waves expand radially outward from the source, while the Rayleigh wave expands along

a cylindrical wave front. The Rayleigh wave front is cylindrical due to the fact that it travels solely near the ground surface. A geometrical spreading factor can be used to describe the rate at which the waves attenuate with distance from the source. Body wave attenuation along the ground surface has been found to be proportional to $1/r^2$, where r is the radial distance from the source. Rayleigh waves travelling along the ground surface attenuate much more slowly, proportional to $1/r^{0.5}$ (Foti, 2000).

Energy partitioning is the term used to describe how wave energy is transformed from one form to another. Miller and Pursey (1955) analyzed the case of a vertical harmonic point source acting on an ideal half space. They found that 67% of the input energy was transformed into the form of a Rayleigh wave, 26% transformed into shear waves, and the remaining 7% into primary waves. Figure A.18 shows the important properties associated with wave propagation away from a vertical harmonic point source."

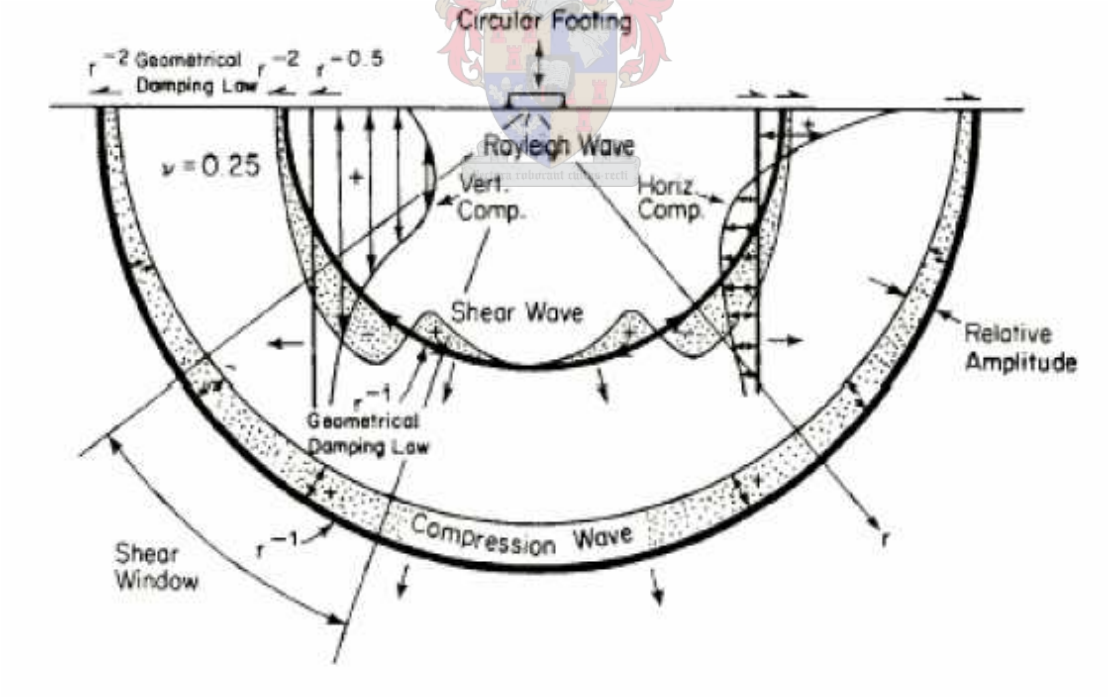

Figure A.18: Wave field generated due to a harmonic vertical point source acting on a homogenous isotropic, elastic halfspace (from Richard et al, 1970)

"When the fact that 67% of the input energy is converted into a Rayleigh wave is considered along with the fact that Rayleigh waves attenuate at a much slower rate than body waves, it becomes apparent that Rayleigh waves are the dominant waveform resulting from a vertical source. This fact is well illustrated by looking at work performed by Lamb in 1904. Lamb mathematically predicted the displacements that occur on the surface of an ideal half space due to a vertical point source acting on the surface at a distance r away. Figure A.19 shows a graphical depiction of the mathematical solution of the predicted particle motion. The dominance of the Rayleigh wave can clearly be seen in this example."

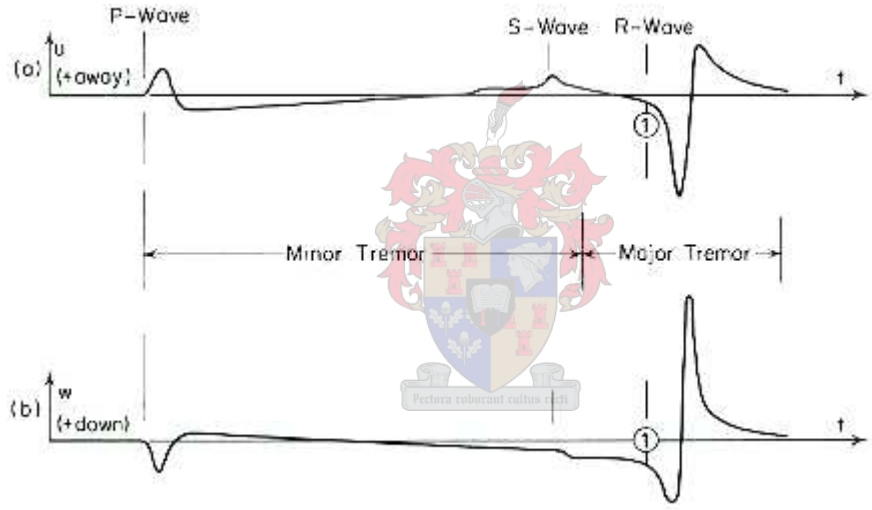

Figure A.19: Lamb's solution for a vertical point or line source acting on a homogenous, isotropic, elastic half space. Both radial motion (top) and vertical motion (bottom) are shown (from Richart et al, 1970, after Lamb 1904)

A3.6 Signal Processing

Signal processing is the area of engineering that involves the analysis of electric signals. In seismic testing the signal of interest is generated by the particle motion that occurs due to the passage of seismic waves. This particle motion is transformed into an electrical signal by means of velocity and acceleration transducers.

Properties of passing seismic waves can then be determined by properly analyzing the acquired signal.

Fourier analysis

One of the principle tools of signal processing is based on work published by
Baron Jean Baptiste Fourier in 1822 (Marven, 1996). Fourier analysis allows any signal (waveform) to be decomposed into a series of harmonic waves that have different frequencies. This concept is demonstrated by Figure A.20. The figure show a complex waveform decomposed into two sine waves as viewed from the time domain (b) and frequency domain (c). Each line on the frequency axis represents one sine wave of a given frequency and amplitude. A transient signal is defined as a signal that reduces to zero amplitude over a finite time interval. The frequency spectrum of a transient signal is continuous as shown in Figure A.21.

The first step in describing the mathematical forms of the Fourier transform is to present the signal as a phasor. A phasor is defined as a vector which rotates in the complex plane at a rotational speed of ω (radians/sec). Figure A.22 shows a phasor of magnitude A that has coordinates of a on the real axis and b on the imaginary axis. The angle θ represents the phase and can be expressed as the rotational speed multiplied by time."

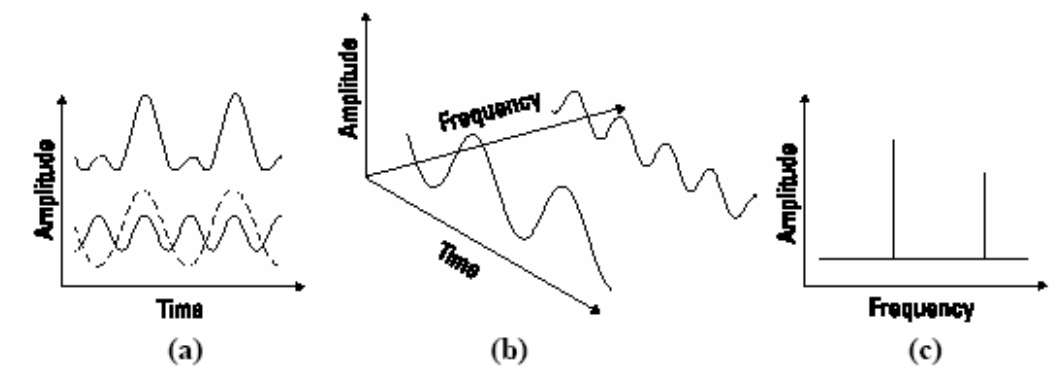

Figure A.20: Representation of a waveform in (a) time domain view, (b) 3-D view, and (c) frequency domain view (From Agilent Technologies, 2000)

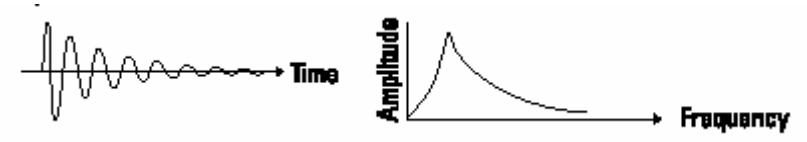

Figure A.21: A transient signal shown in time and frequency domains (From Agilent Technologies Application note 243, 2000)

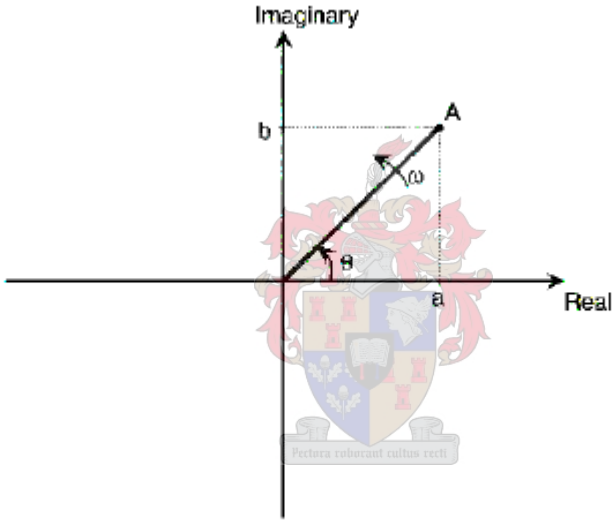

Figure A.22: Phasor model of signal (From Marven, 1996)

Fourier series

"Fourier's original theorem allows for a function x(t) to be decomposed into a group of sine waves by expanding into series form according to the equation

$$x(t) = A_0 + A_1 \sin(\omega_0 t + \theta_1) + A_2 \sin(2\omega_0 t + \theta_2) + \ldots A_3 \sin(n\omega_0 t + \theta_n) \quad (A.11)$$

and

$$\omega_0 = \frac{2\pi}{T} \qquad (A.12)$$

where T = period

The equations above basically state that a time dependent function can be rewritten as a series of terms that are dependent on frequency. A and θ still represent magnitude and phase respectively. An important characteristic of a series of this type is that x(t) must be a periodic function because each term contains a frequency component that is a multiple of the fundamental frequency f_0 which is related to ω_0 by

$$f_0 = \frac{\omega_0}{2\pi} \qquad (A.13)$$

Thus far Equation L.10 has been developed that allows any periodic function to be decomposed into a series of harmonic terms that are frequency dependent. The next step in developing Fourier analysis into a form suitable for SASW testing is to eliminate this limitation of periodicity.

The equations for the Fourier series and the Fourier coefficients developed above can be written in an equivalent form using the concept that a phasor can be represented in both rectangular and polar coordinates. Deriving the Fourier series using polar coordinates yields a complex representation of the series

$$x(t) = \sum_{k=-n}^{n} A_k e^{jk\omega_0 t} \qquad (A.14)$$

$$\text{where } A_k = \frac{a_k - jb_k}{2} \qquad (A.15)$$

Fourier Integral Transform

To extend Equation A.14 such that it is applicable to non-periodic time functions
(i.e. transient signals) the assumption that the frequencies that compose the series are harmonically related must be discarded. This is accomplished by taking the limit of Equation A.15 as the fundamental frequency f_0 approaches 0.

The Fourier integral transform is a powerful tool that allows a function to be "transformed" from a time function to a frequency function. The complex spectrum of a signal, consisting of the magnitude and phase for each frequency, can be found using this transform. The magnitude is the absolute value of the transform while the phase is the argument of the transform."

Spectral Analysis

"Up to this point this discussion has been concerned with a single signal that is recorded in the time domain, and then transformed into the frequency domain via Fourier analysis. When obtaining average values to describe signals, or comparing signals to one another, it becomes necessary to employ statistical methods. Spectral analysis is the title given to a set of statistical methods used to analyze signals in the frequency domain.

The first topic covered in this section is network analysis. Network analysis is the general analysis method employed to perform spectral analysis of surface waves. The spectral analysis functions used during network analysis are then described in subsections following network analysis. These spectral analysis functions are the foundation for SASW testing and are used extensively throughout this research."

Network Analysis

"Network analysis in its broadest definition is the process of determining how a system responds to a given input. 2 port network analysis evaluates the behaviour of a system by monitoring the response that occurs at a second port due to an input at the first port. Another way of writing this is that response x will occur due to input y. If the condition of linearity is imposed network analysis becomes even more powerful, allowing the principle of superposition to be employed. Now not only will response x occur due to input y, and response q occur to input p; but if y and p are input simultaneously the response will be equal to x + q. Now the response of a linear network can be said to be the sum of the responses to each component of the input (Agilent Technologies, 2000).

This type of analysis is directly analogous to the method used to perform SASW testing. In SASW testing the network is the pavement system and a seismic disturbance resulting from a vertical impact is the input. The properties of the pavement system are evaluated by comparing the output signal measured from one transducer to the input signal measured from another transducer. The pavement system is considered to behave linearly which allows the principle of superposition to apply. Figure A.23 shows the idealized network analysis system.
The actual system encountered in practice is shown in Figure A.23. This system takes into account the presence of background noise. To reduce the effect of background noise an averaging technique is often used. The reason that averaging is effective in eliminating the effects of background noise stems from the assumptions that background noise is random in nature and the input signal that is repeatable. The effects of an averaged repeatable input signal on a linear network will tend toward the true value of the input signal, while the effects of the random background noise averaged over time will tend towards zero."

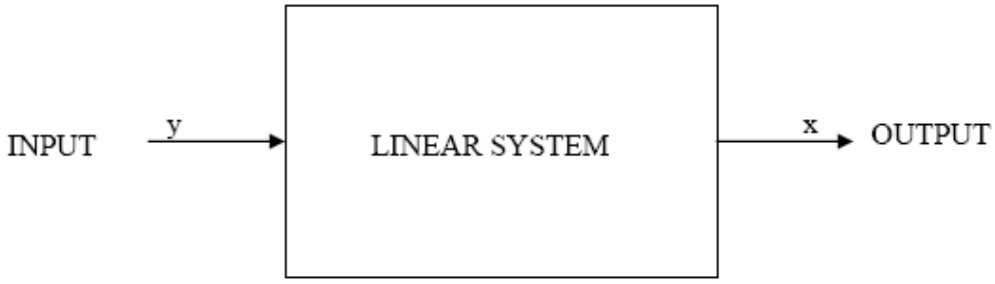

a) Idealized linear system

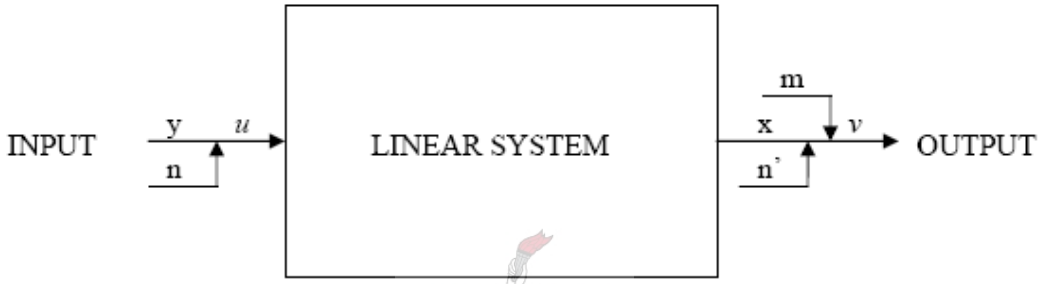

a) Actual linear system

y = Input from experiment
x = Output from experiment
n = Noise present at input
n' = Output caused by noise present at input
m = Noise present at output
u = y + n = Actual input
v = x + m + n = Actual output

Figure A.23: Idealized linear system (a) and actual linear system (b)

"Eliminating the effects of background noise by averaging allows the actual system being tested to be approximated using the idealized system (Nazarian, 1984)."

Linear Spectrum

"The basic information required to perform spectral analysis is the linear spectrum of an input signal, an output signal, or both an

input and an output signal. The linear spectrum is nothing more than the Fourier transform of a signal, and is called the linear spectrum because each frequency component is represented as a line in the frequency domain. The linear spectrum of a signal x(t) is typically denoted Sx(f) and is defined as

$$S_x(f) = \int_{-\infty}^{\infty} x(t)e^{-j2\pi ft} \cdot dt \qquad (A.16)$$

The linear spectrum contains both magnitude and absolute phase information for each of the frequency components of the frequency range (bandwidth) over which the measurement is taken (Heisey, 1982)."

Auto Spectrum

"The auto spectrum of a signal defines the power of a signal at each frequency over the measurement bandwidth. The auto spectrum is calculated by multiplying the linear spectrum by its complex conjugate. Multiplying the linear spectrum by its complex conjugate results in squaring the magnitude and negating the phase at each frequency.

Because of this, the auto spectrum is always real and all phase information is lost. Gxx(f) is the symbol used to define the auto spectrum of signal x(t), and is represented by the equation

$$Gxx(f) = Sx(f) \cdot S^{*}x(f) \qquad (A.17)$$

where $S^{*}x(f)$= complex conjugate of $S(f)x$

The auto spectrum measurement is performed on a single signal and can only be used when phase information is not required. However, an advantage of the auto spectrum measurement is that because no phase information is recorded no synchronizing trigger is necessary (Nazarian, 1984)."

Cross Spectrum

"A common goal in signal analysis is to investigate the amount of similarity that exists between two signals. To accomplish this task the cross spectrum measurement can be used. The cross spectrum is defined as the Fourier transform of the cross-correlation function performed between two signals x(t) and y(t). Mathematically, the cross spectrum Gxy is represented by the equation

$$Gyx = S\,y\,(\,f\,) \cdot S^{*}\,x\,(\,f\,) \qquad (A.18)$$

Equation A.18 states that the cross spectrum is found by multiplying the linear spectrum of output signal by the complex conjugate of the linear spectrum of the input signal. The cross spectrum is a complex function consisting of both magnitude and phase components. The magnitude of Gyx is the mutual power between the input and output signals and can be used to identify the predominant frequencies the two signals have in common. The phase of Gyx is a relative phase, or phase difference, between the two signals. Phase differences arise due to time delays, propagation delays, or varying wave paths between points of measurement (Heisey, 1982). Because the phase is a relative phase, a synchronized trigger does not have to be used to perform measurements."

Frequency Response

"The frequency response of a system is found by comparing the output signal from a system to the input signal applied to the system. The response of a linear system to a sine wave input can be shown to be a sine wave of the same frequency. The output sine wave will have a new amplitude that is proportional to the amplitude of the input sine wave, and the phase of the new sine wave will be shifted an amount that is dependent upon its

frequency (Agilent Technologies, 2000). This concept is shown in Figure A.24."

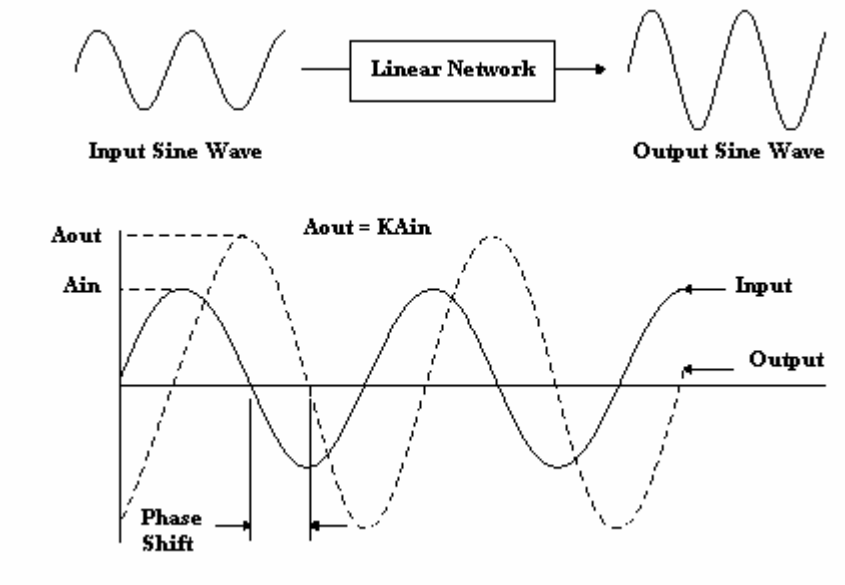

Figure A.24: Response of a linear network to a single sine wave input signal (From Agilent Technologies, 2000)

"To extend this concept, remember that any input signal x can be broken down into a series of sine waves. It has also been stated that the total response of a linear network is simply the sum of the responses of the linear network to the individual components of the input. These two facts lead to the conclusion that if the response of a network to each sine wave component of the input is known the output can be predicted. To find the response of the network to any given sine wave, the frequency of the sine wave shown in Figure A.24 is varied. As the frequency is varied the amplitude proportionality factor (gain) and amount of phase shift will change. The curves that represent the change of gain and phase shift as a function of the input frequency are called the frequency response function (Agilent Technologies, 2000). The frequency response is a property of a linear network that does not depend upon the stimulus. The frequency response can often be used to evaluate system properties such as impedance, dynamic stiffness, natural frequencies, and damping coefficients (Heisey, 1982)."

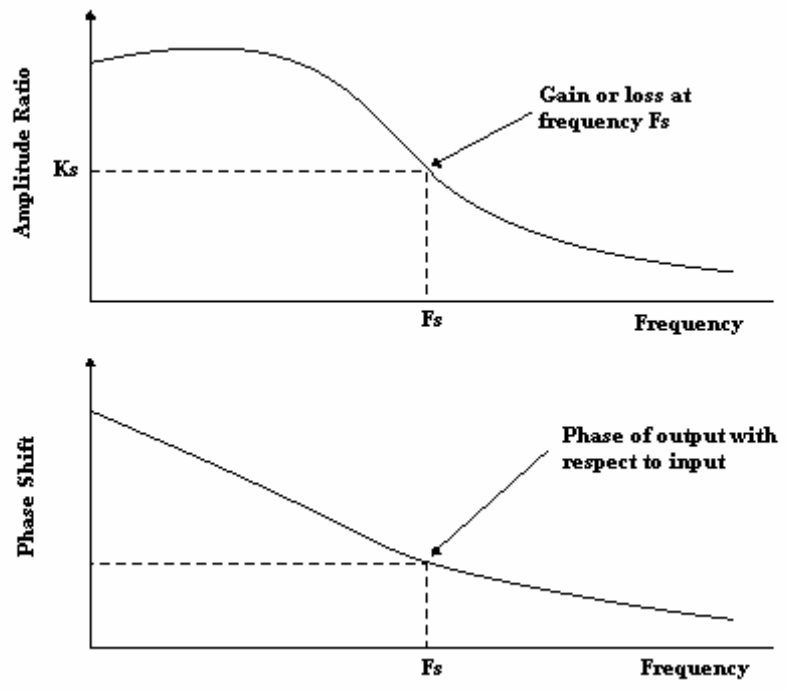

Figure A.25: Frequency response components of a linear network (From Agilent Technologies, 2000)

"Mathematically the frequency response function H(f) is defined as dividing the linear spectrum of the output by the linear spectrum of the input

$$H(f) = \frac{S_y(f)}{S_x(f)} \qquad (A.19)$$

The frequency response function can also be shown to be the cross spectrum between signals x(t) and y(t) that has been normalized by the auto spectrum of the input Gxx.
The frequency response function consists of both magnitude and phase components, as shown in Figure A.25. The magnitude is the magnitude of the cross spectrum normalized by the magnitude of the auto spectrum. The phase component contains exactly the same phase information as the cross spectrum (Nazarian, 1984)."

Coherence

"The purpose of the coherence function is to provide a method to check the validity of the frequency response function (Labview Measurements Manual, 2000). Coherence measures the power present in the output signal that is caused by the power in the input signal. The term coherence is used because it is the output power that is coherent with the input power.

If the coherence is equal to one then all of the output power at that frequency is due to the input power. If, however, the coherence is equal to zero none of the output power at that frequency is associated with the input power. Values of coherence close to one indicate that high quality measurements are being taken."

A3.7 Analysis Approach

"The purpose of this part of the literature review is to present how the spectral analysis of surface waves technique combines the seismic wave theory and the signal processing techniques, to allow for evaluation of the properties of layered pavement systems. SASW testing consists of three primary stages. The first stage of SASW testing is to measure the passage of seismic waves created by a transient impact on the surface of a pavement. The next stage of SASW testing is to construct a Rayleigh wave velocity versus wavelength plot, called a dispersion curve, from the field measurements performed during stage one.

The last stage taken in SASW testing is to create a dispersion curve that is a mathematical representation of the theoretical behaviour of Rayleigh waves in a layered system. The shape of the theoretical dispersion curve is influenced by the thickness and elastic properties of each of the layers in the pavement system. These properties are varied until the theoretical dispersion curve matches the measured dispersion curve to estimate the properties of each layer.

Experimental Dispersion Curve

It was shown that the velocity of Rayleigh waves propagating in a semi-infinite elastic medium can be used to estimate the elastic properties of the medium through which it travels. To apply this concept to the pavement systems of interest to this study, the discussion of Rayleigh wave propagation must be extended to include the effects of travelling through layered media. The first portion of this section addresses these effects, and how they change the relationships that exist between Rayleigh wave velocity and the elastic properties of the layered medium.

The second portion of this section describes two methods that can be used to measure Rayleigh waves travelling in a layered medium, allowing for the construction of an experimental dispersion curve. The first method is called the steady state vibration technique, and is conceptually simple but also very time consuming. The second method is the spectral analysis of surface waves technique, which is an improvement on the steady state technique that greatly reduces the required testing time by incorporating the aspects of signal analysis presented in this literature review.

Rayleigh Waves in Layered Media

Equation A.5 established that the velocity of any sinusoidal wave can be represented as the product of the wave's frequency and wavelength. In an ideal elastic half space material properties are constant as a function of depth. Therefore, the Rayleigh wave velocity predicted by Equation A.5 must remain constant regardless of the frequency of the Rayleigh wave.

When the elastic properties of a system do not remain constant with depth a phenomenon known as dispersion occurs. Dispersion is the term used to describe the fact that Rayleigh wave velocity changes as a function of frequency in a vertically layered system

(Foti, 2000). To understand why this phenomenon occurs, recall that Rayleigh waves travel along the surface of a half space and that the particle motion associated with the passage of the wave occurs at depths shallower than about one and a half wavelengths. Therefore, a Rayleigh wave that has a short wavelength (high frequency) will not travel through the same layers as a Rayleigh wave that has a long wavelength (low frequency) in a system that consists of horizontally stacked layers. Figure A.26 illustrates this concept."

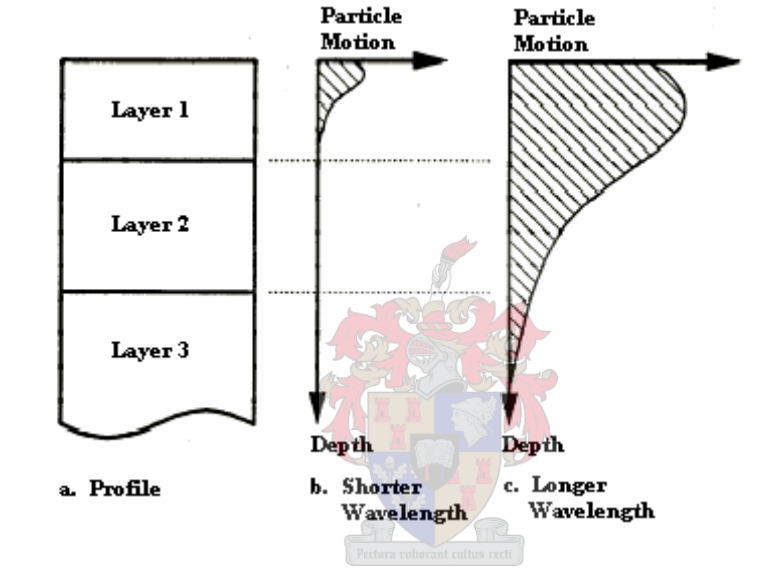

Figure A.26: Effect of wavelength in a layered medium (from Foti, after Rix 1988)

"A Rayleigh wave that has a short wavelength (high frequency) will only travel through the uppermost layer of a given profile. The velocity of these high frequency
waves is solely a function of the material properties of the uppermost layer, therefore the relationships between Rayleigh wave velocity and elastic medium constants established in part I remain applicable to the top layer. As the wavelength of the Rayleigh wave is gradually increased, it penetrates increasingly deeper into the system. These lower frequency waves travel through more than one layer, each of which has its own material properties. The velocity of a Rayleigh wave which travels through

more than one layer is a function of some average value of the material properties of the layers through which it travels. In this situation the Rayleigh wave velocity no longer maintains a direct relationship to the elastic properties of any given layer. If, however, the assumption is made that the bottommost layer in the system extends to infinite depth (common assumption in SASW testing) the velocity of very low frequency Rayleigh waves will approach the velocity predicted by the elastic properties of the bottom layer alone. This occurs because the majority of the low frequency Rayleigh wave travels through the bottom layer, which heavily weights the averaged material properties towards those of the bottom layer (Foti, 2000).

A plot of the change in Rayleigh wave velocity as a function of wavelength (frequency) is called a dispersion curve. The shape of the dispersion curve is closely related to the stiffness profile of the system (Nazarian, 1984). Two major types of dispersion curves are typically obtained, depending on the type of site under investigation. Sites that have profiles in which stiffness increases with depth are said to be normally dispersive. Many sites consisting of multiple soil layers exhibit this type of profile. Sites that have profiles in which stiffer layers are located above softer layers are called inversely dispersive. The pavement sites investigated during this study have profiles that are inversely dispersive because paving materials are stiffer than base course materials which are stiffer than subgrade materials. Figure A.27 shows the general shapes of dispersion curves obtained from sites with normally dispersive profiles (a) and from sites having inversely dispersive profiles (b).

Determination of the Experimental Dispersion Curve

"The simplest method used to experimentally determine the shape of the dispersion curve for a site is the steady state vibration technique. To perform this method at a pavement site, a sinusoidal wave generator is used to create a Rayleigh wave of known frequency. The wavelength of the Rayleigh wave is found by

moving receivers that detect vertical motion along the pavement surface to find the distance between successive troughs or peaks of the generated wave (Richart et. al, 1970)."

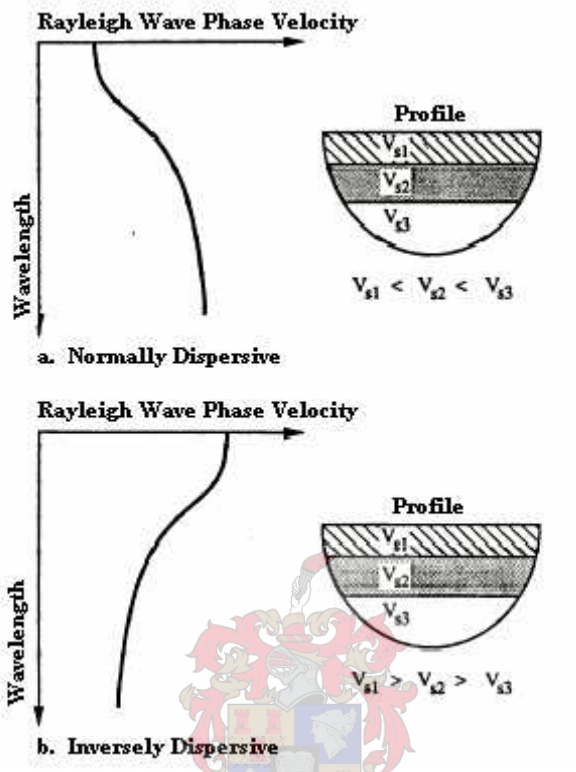

Figure A.27: Typical shape of dispersion curves obtained from normally and inversely dispersive profiles (From Foti, after Rix 1988)

"Once both the frequency and the wavelength are known, the velocity of the Rayleigh wave can be calculated using Equation A.5. The combination of the velocity calculated and the wavelength measured gives one point on the dispersion curve. If this procedure is repeated using a large number of input frequencies, a dispersion curve can be created. Figure A.28 is a depiction of the steady state technique."

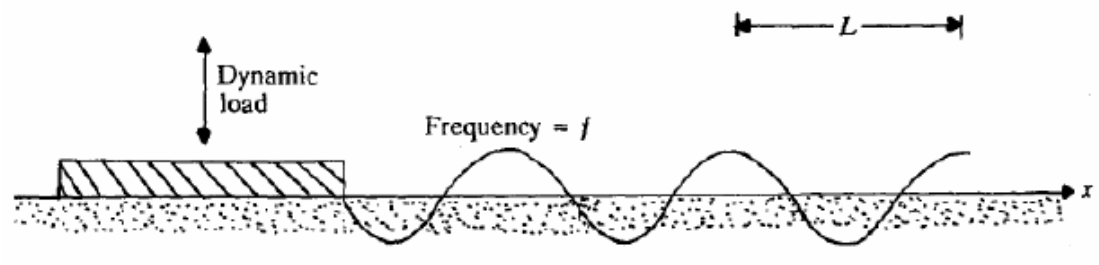

Figure A.28: Concept of the steady state vibration technique to construct a dispersion curve (from Das, 1992)

"Although the steady state method described above is a conceptually simple method that can be used to experimentally measure a dispersion curve, it is rarely utilized because it is very time consuming. A large number of frequencies have to be generated and measured to adequately define the dispersion curve at any given site (Richart et. a.1970). To develop the steady state method into a more practical testing procedure, concepts of signal processing are incorporated into the procedure. Combining signal processing with the steady state technique yields the spectral analysis of surface waves method.

Experimental determination of a dispersion curve using spectral analysis of surface wave testing is conceptually very similar to that of the steady state method. The primary difference is that a transient impact containing a large number of Rayleigh wave frequencies is used as the source instead of a single frequency sine wave from a sine wave generator. Fourier analysis allows the transient impact to be decomposed into a series of sine waves of various frequencies. The Rayleigh wave velocity and wavelength of each of these sine waves can be calculated from the results of spectral analysis measurements. The amount of time needed to develop a dispersion curve is greatly reduced because of the ability to analyze a wide range of frequencies simultaneously as opposed to testing each frequency individually.

To perform SASW testing a vertical transient impact generates a wavefield that is dominated by Rayleigh waves. The waves are transformed into electrical signals as they pass by two receivers spaced a known distance x apart. The electrical signals are then transmitted to a digital signal analyzer which transforms them into digital representations. Fourier analysis is then used to break both the input signal (first receiver) and output signal (second receiver) into a series of sine waves of varying frequencies. The cross power or frequency response function is calculated which provides the relative phase between the input and output signals for each frequency (Heisey, 1982). The relative phase is analogous to the amount of phase shift experienced by a sine wave of frequency (f) as it travels from the near receiver to the far receiver. This phase shift (φ) can be used to calculate the amount of time (t) taken by the sine wave to travel between the two receivers using Equation A.20."

$$t(f) = \frac{\phi(f)}{360 \cdot f} \tag{A.20}$$

The distance (x) between the receivers is a known value, so the velocity of the wave can now be calculated using the simple relationship

$$V_R = x / t \tag{A.21}$$

"The wavelength of a wave of frequency f is then calculated using Equation A.5. Using equations A.20, A.21, and A.5 for every frequency present in the transient impact yields the information necessary to create an experimental dispersion curve for the portion of the site located between the two receivers."

References

Bath, M, 1979. “Introduction to Seismology”, 2nd Ed. Natur och Kultur, Boston.

Burger, RH, 1992. “Exploration Geophysics of the Shallow Subsurface”, Prentice Hall, New Jersey.

Dennis, ND Jr and Bennett, K, 2005. Development of Testing Protocol and Correlations for Resilient Modulus fo Subgrade Soils, Research Report MBTC – 2023, Arakansas State Highway and Transportation Department, Little Rock, Arkansas.

Foti S, 2000. “Multistation Methods for Geotechnical Characterization using Surface Waves”, PhD Dissertation, Politecnico di Torino, Italy.

Graff, KF, 1975. “Wave Motion in Elastic Solids”, Dover, New York.

Heisey, J.S., Stokoe, K. H. II, Meyer, AH, 1982. “Moduli of Pavement Systems from Spectral Analysis of Surface Waves”, Transportation Research Record, vol 852, pp. 22-31.

Marven, C., Ewers, G. 1996. “A Simple Approach to Digital Signal Processing”, John Wiley and Sons, Inc., New York.

Nazarian, S, 1984. “In Situ Determination of Elastic Moduli of Soil Deposits and Pavement Systems by Specral Analysis of Surface Waves Method”, Ph.D. Diss., University of Texas at Austin.

Richart, F.E. Jr., Wood, R.D., Hall, J.R. Jr., 1970. “Vibration of Soils and Foundations”, Prentice-Hall, New Jersey.

“The Fundamentals of Signal Analysis.” Application Note 243. Agilent Technologies. 2 Feb. 2004 <http://we.home.agilent.com>.

Appendix B

Deflection performance plots

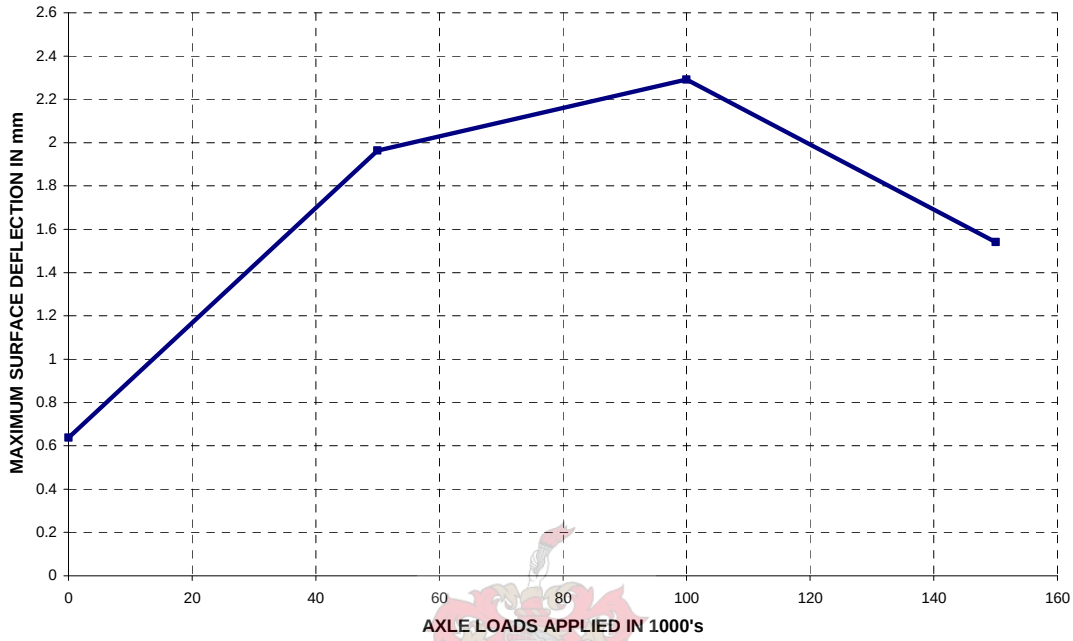

Figure B.1: Maximum Deflection at Slow Speed vs. Axle Load Application for Section 4B – 70 kN Axle Load

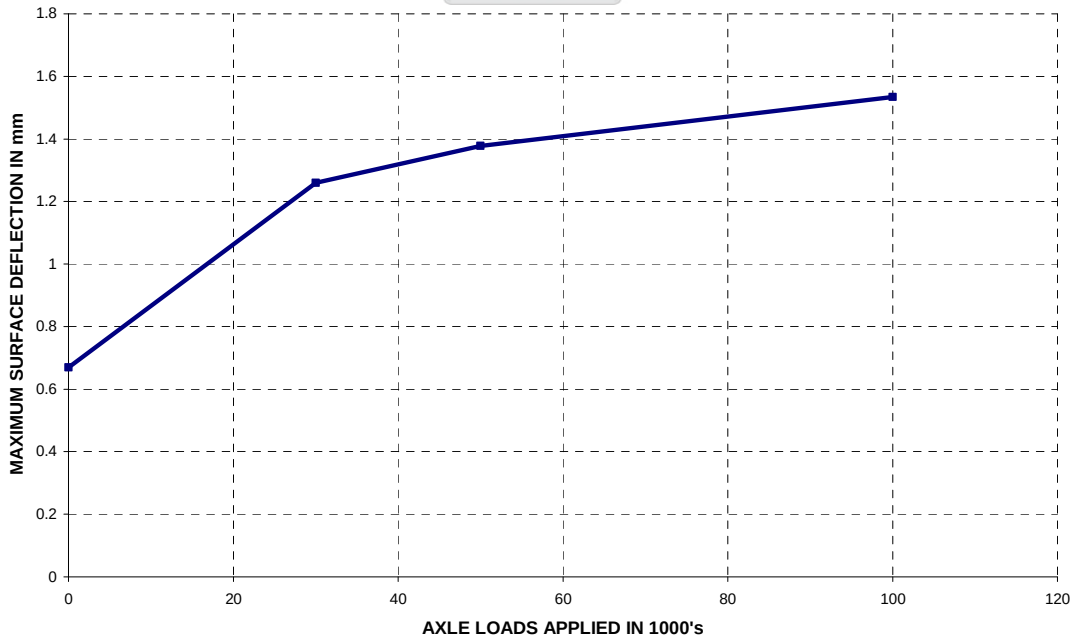

Figure B.2: Maximum Deflection at Slow Speed vs. Axle Load Application for Section 5A – 60 kN Axle Load

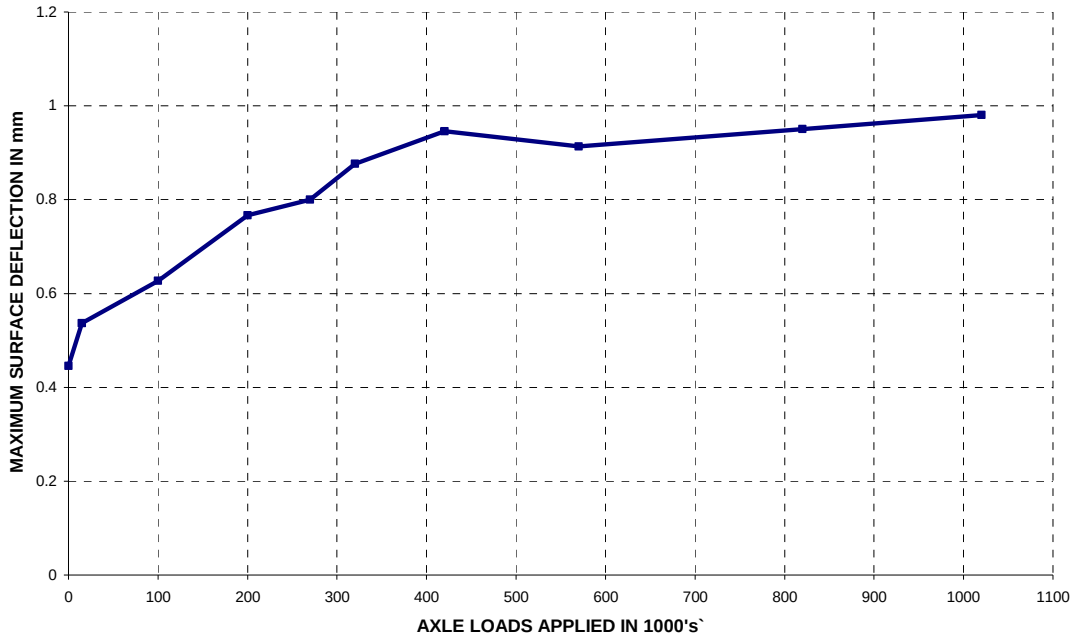

Figure B.3: Maximum Deflection at Slow Speed vs. Axle Load Application for Section 5B – 60 kN Axle Load

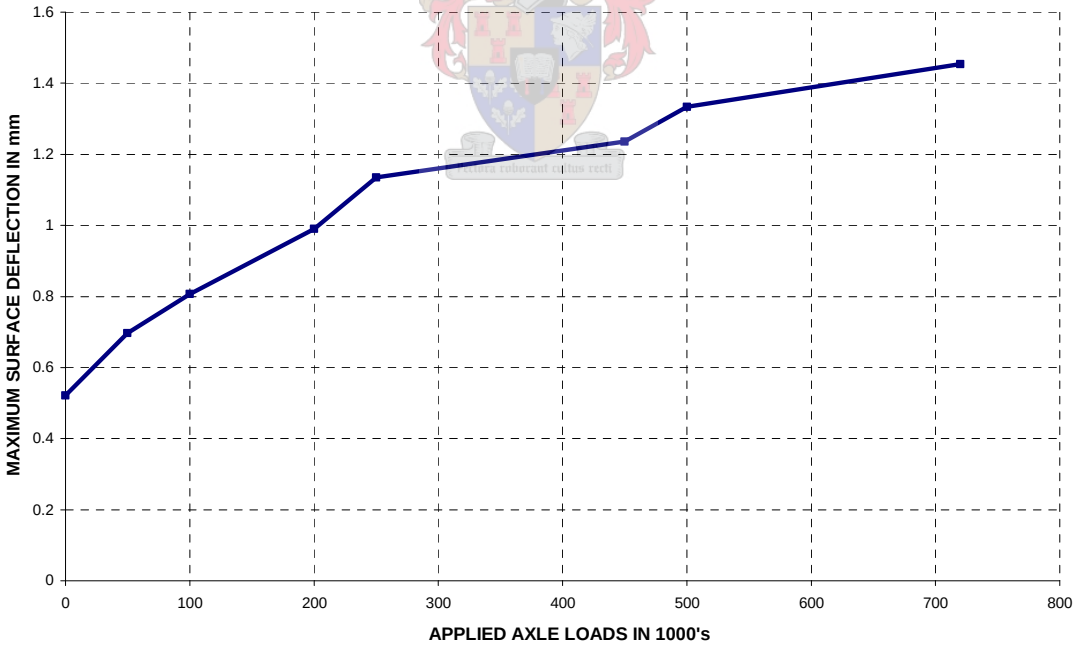

FIGURE A.4: Maximum Deflection at Slow Speed vs. Axle Load Application for Section 8 – 70 kN Axle Load

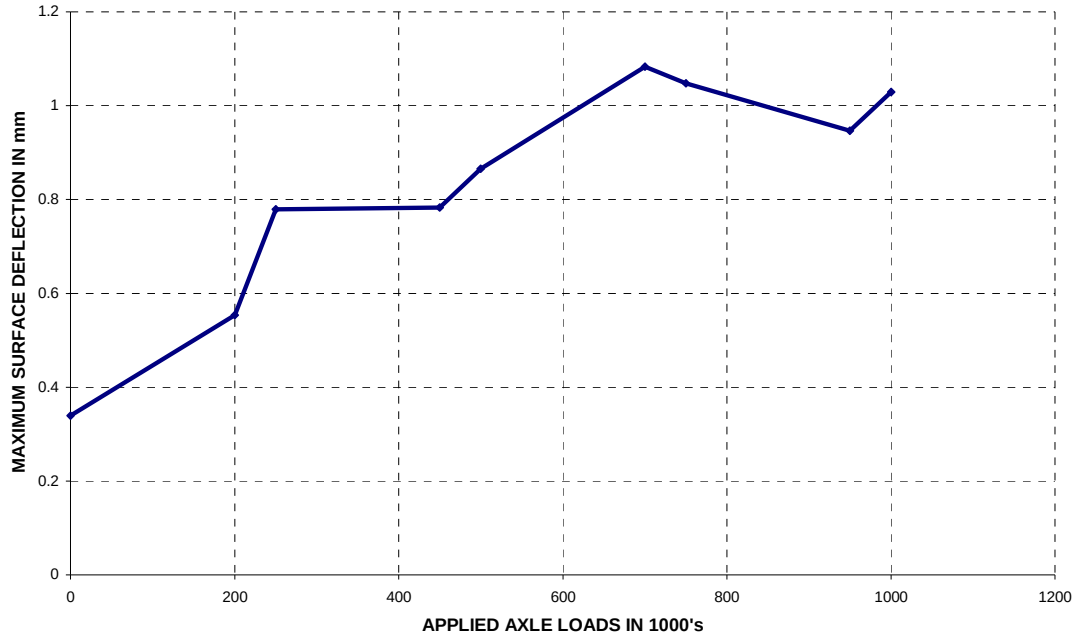

Figure B.5: Maximum Deflection at Slow Speed vs. Axle Load Application for Section 7 – 70 kN Axle Load

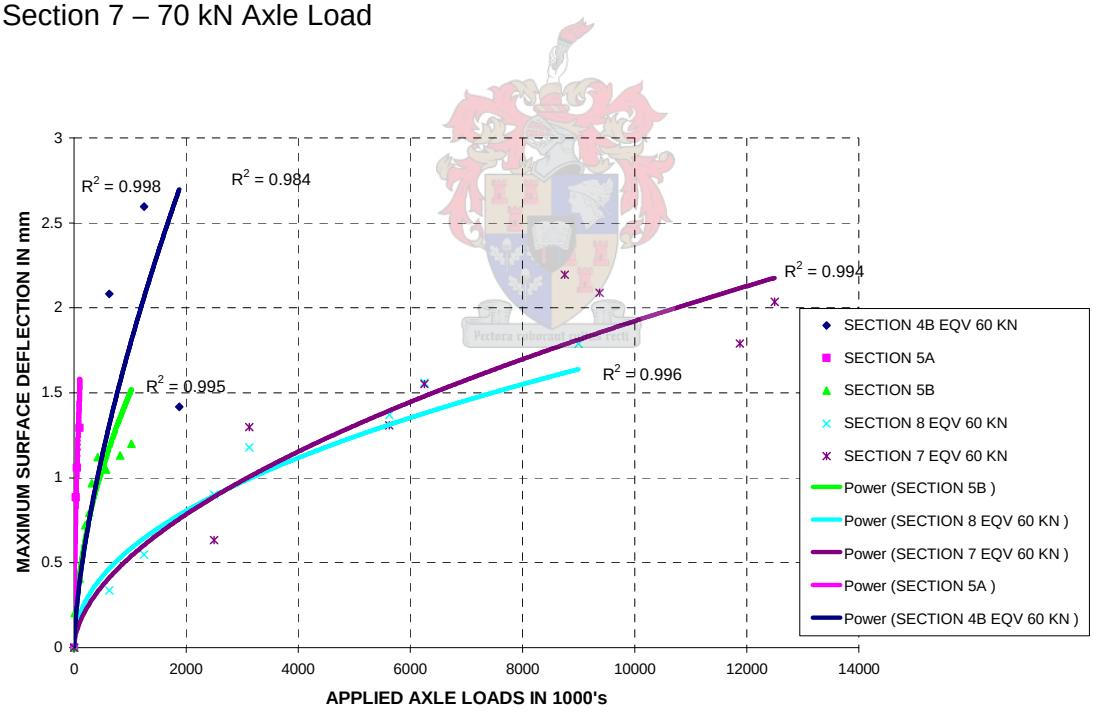

Figure B.6: Maximum Deflection Growth Trends with Equivalent 60 kN Axle Load Applications for Respective Test Sections

Appendix C

Stiffness performance plots

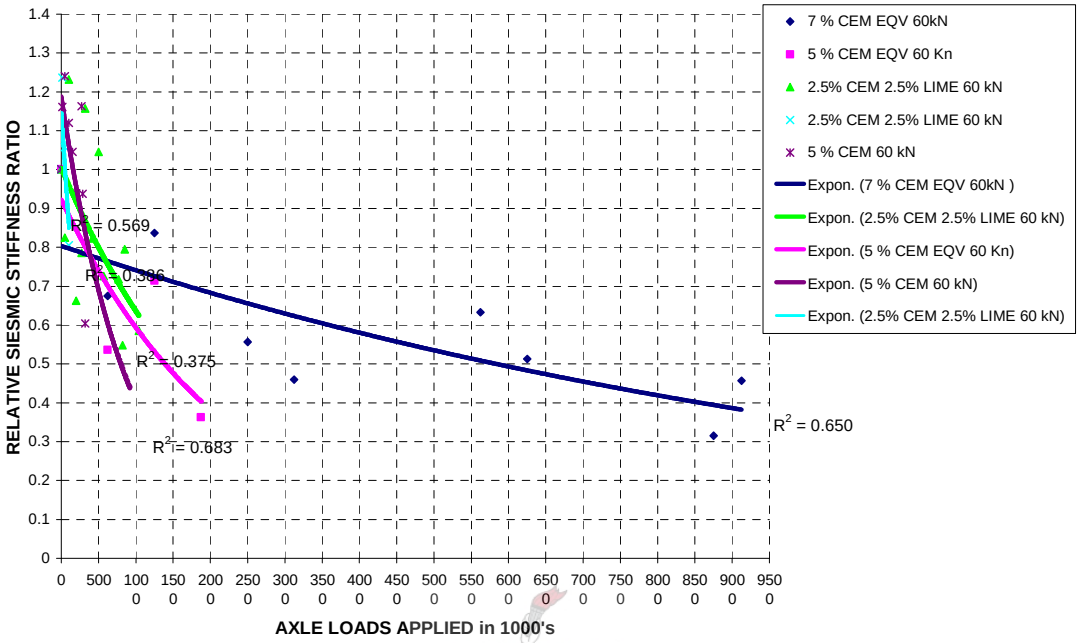

Figure C.1: Comparative Stiffness Performance Chart for Top of CTB in Longitudinal Direction for Equivalent 60 kN axle loads

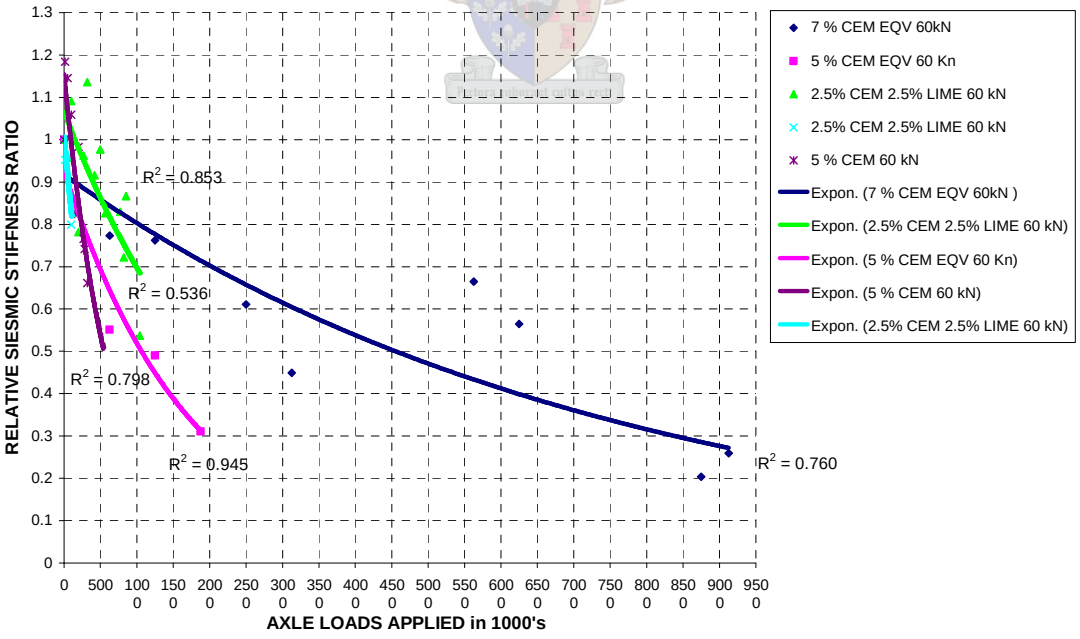

Figure C.2: Comparative Stiffness Performance Chart for Middle of CTB in Longitudinal Direction for Equivalent 60 kN axle load

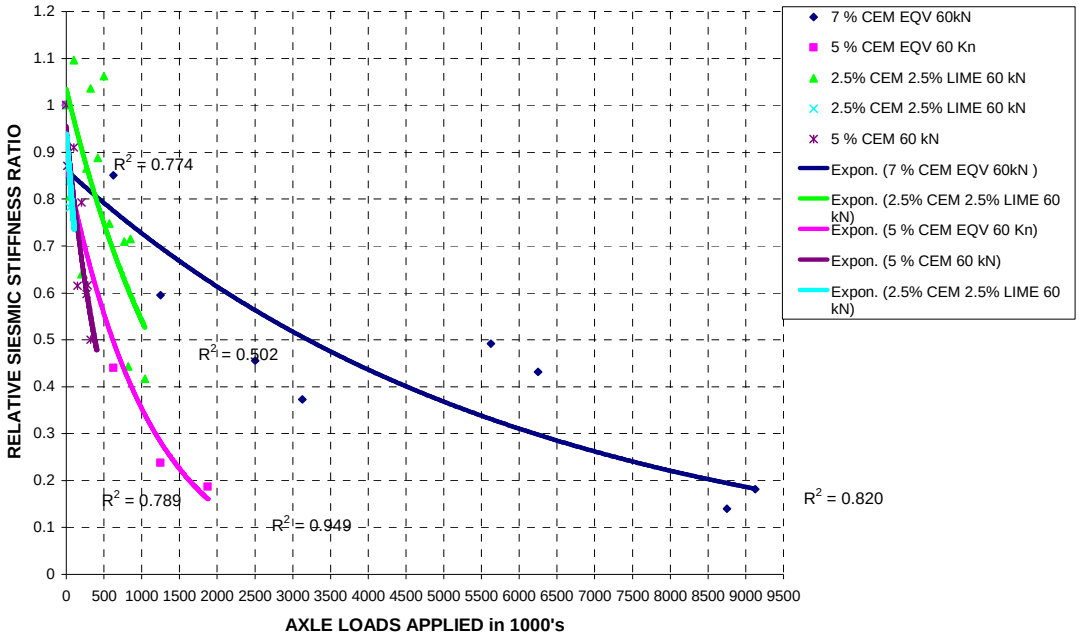

Figure C.3: Comparative Stiffness Performance Chart for Bottom of CTB in Longitudinal Direction for Equivalent 60 kN axle loads

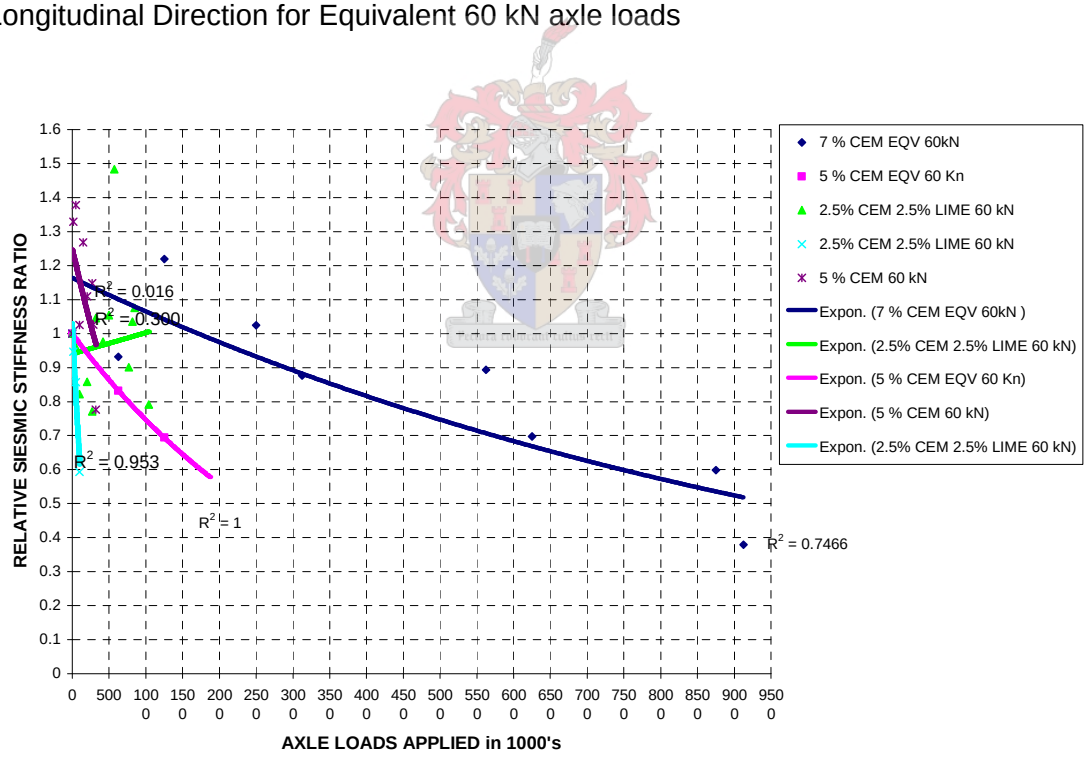

Figure C.4: Comparative Stiffness Performance Chart for Top of CTB in Transverse Direction for Equivalent 60 kN axle loads

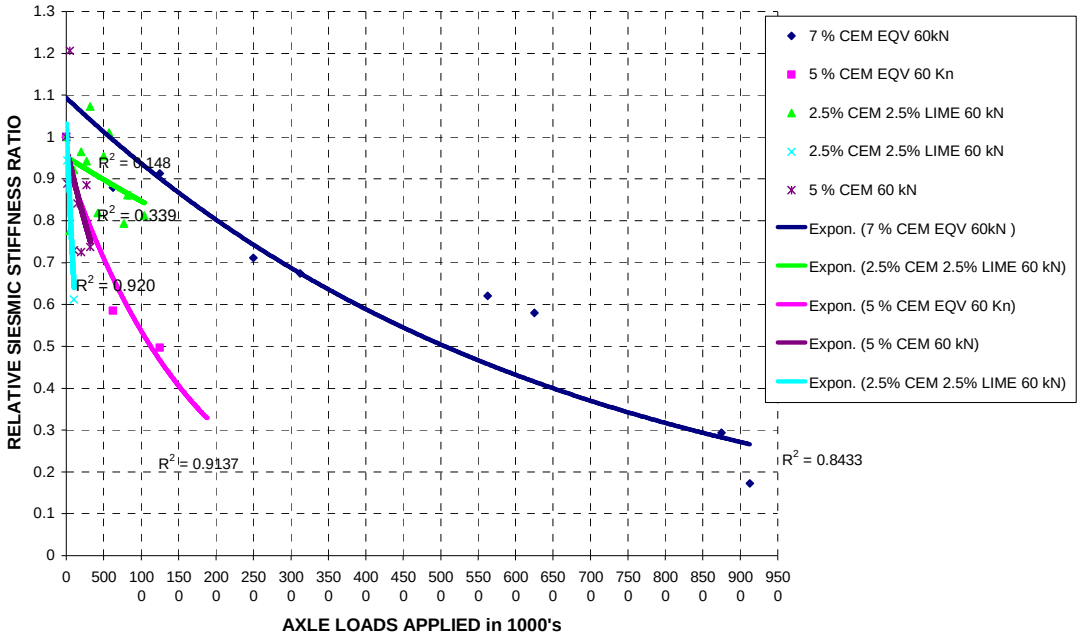

Figure C.5: Comparative Stiffness Performance Chart for Middle of CTB in Transverse Direction for Equivalent 60 kN axle loads

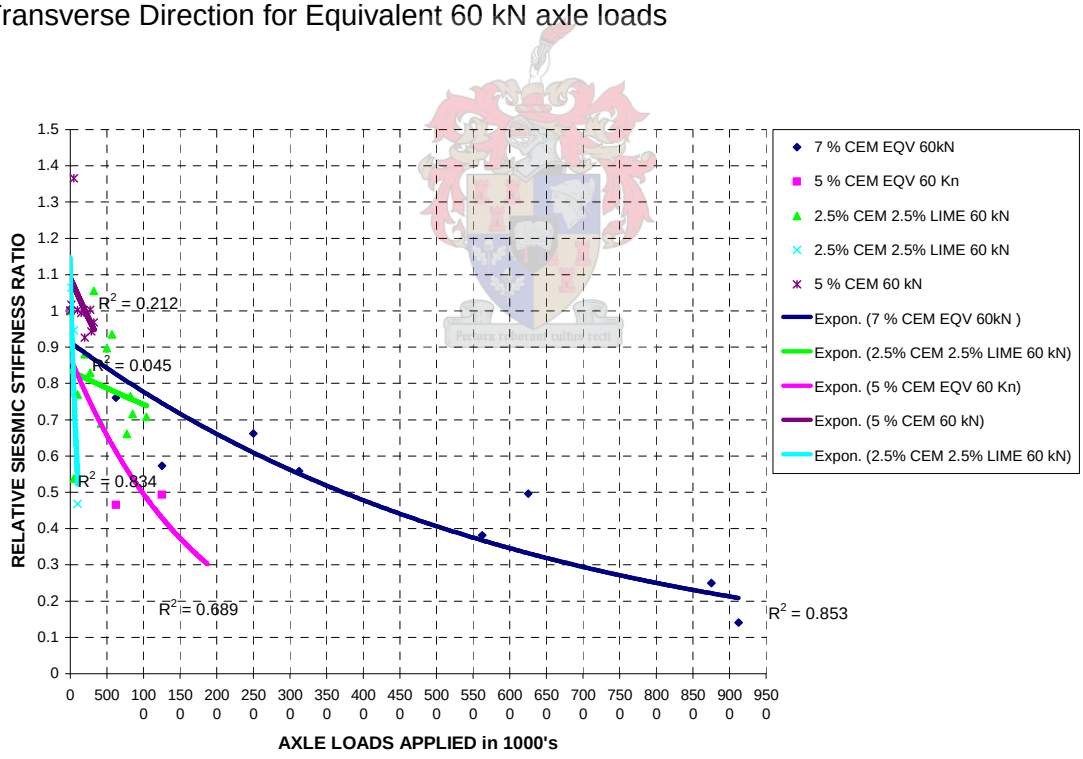

Figure C.6: Comparative Stiffness Performance Chart for Bottom of CTB in Transverse Direction for Equivalent 60 kN axle loads

Appendix D

Surface rut performance plots

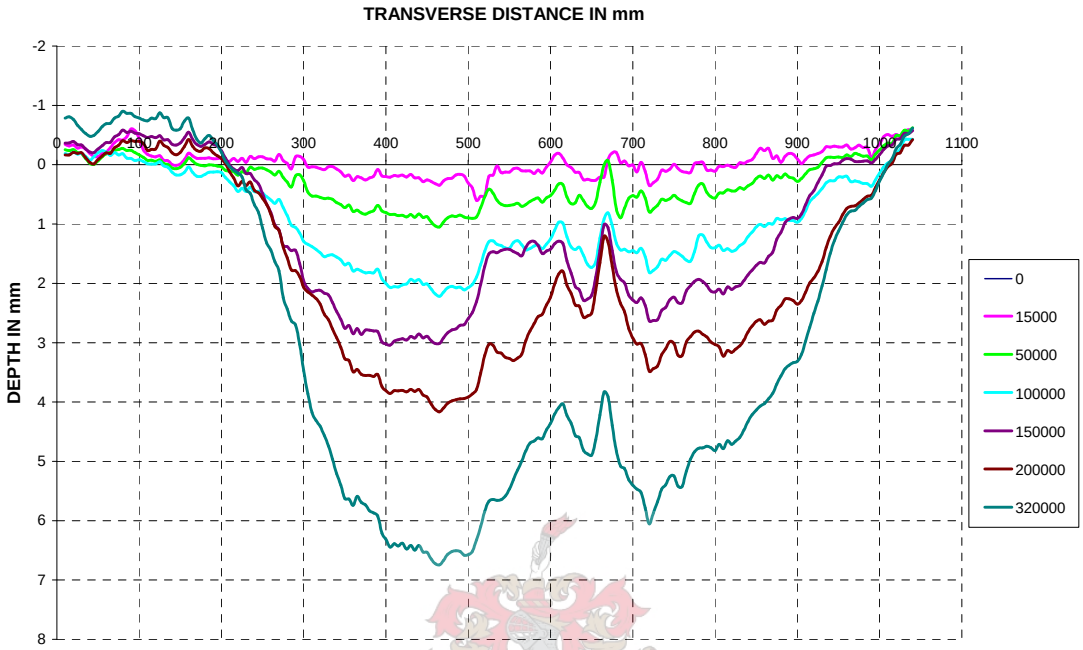

Figure D.1: Transverse rut profiles with load applications for Test Section 4A

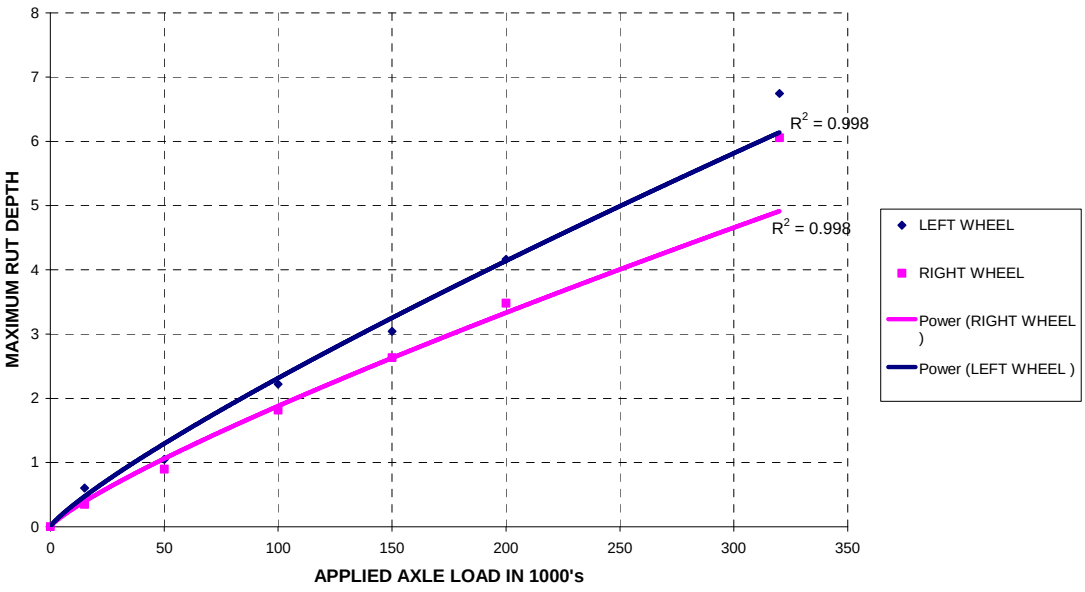

Figure D.2: Cumulative maximum rut depth for Test Section 4A

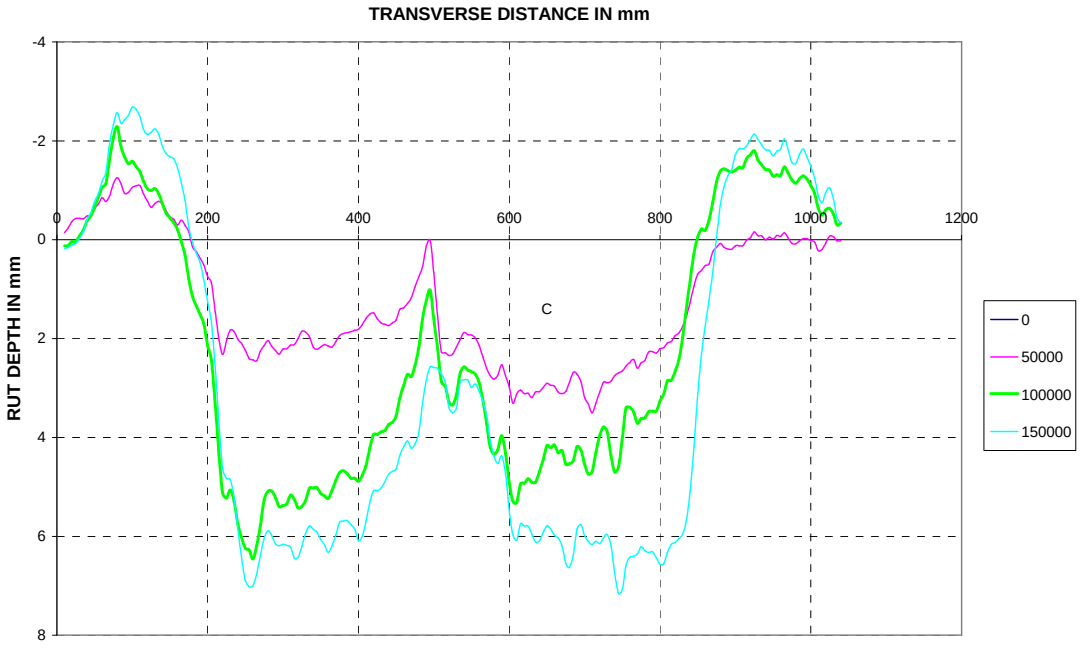

Figure D.3: Transverse rut profiles with load applications for Test Section 4B

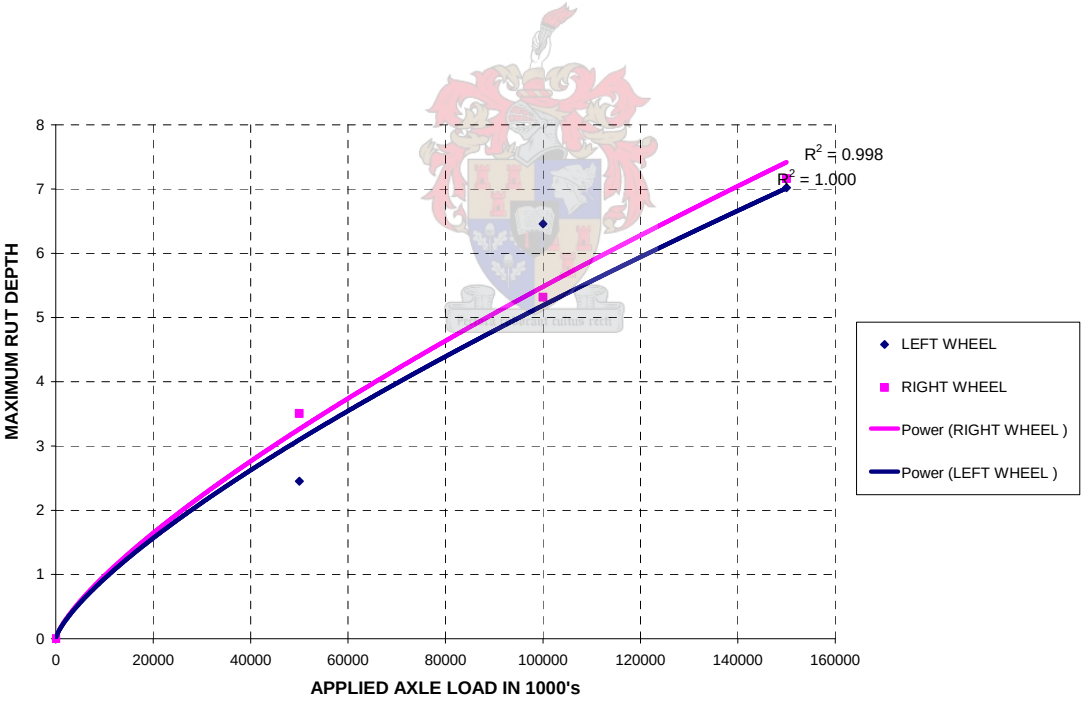

Figure D.4: Cumulative maximum rut depth for Test Section 4B

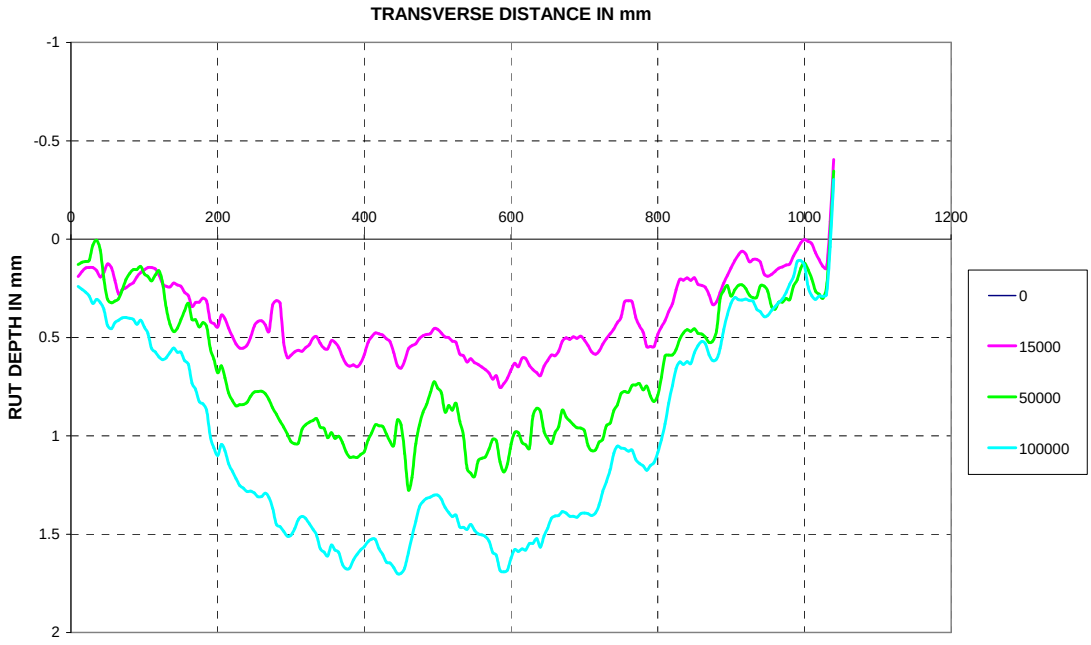

Figure D.5: Transverse rut profiles with load applications for Test Section 5A

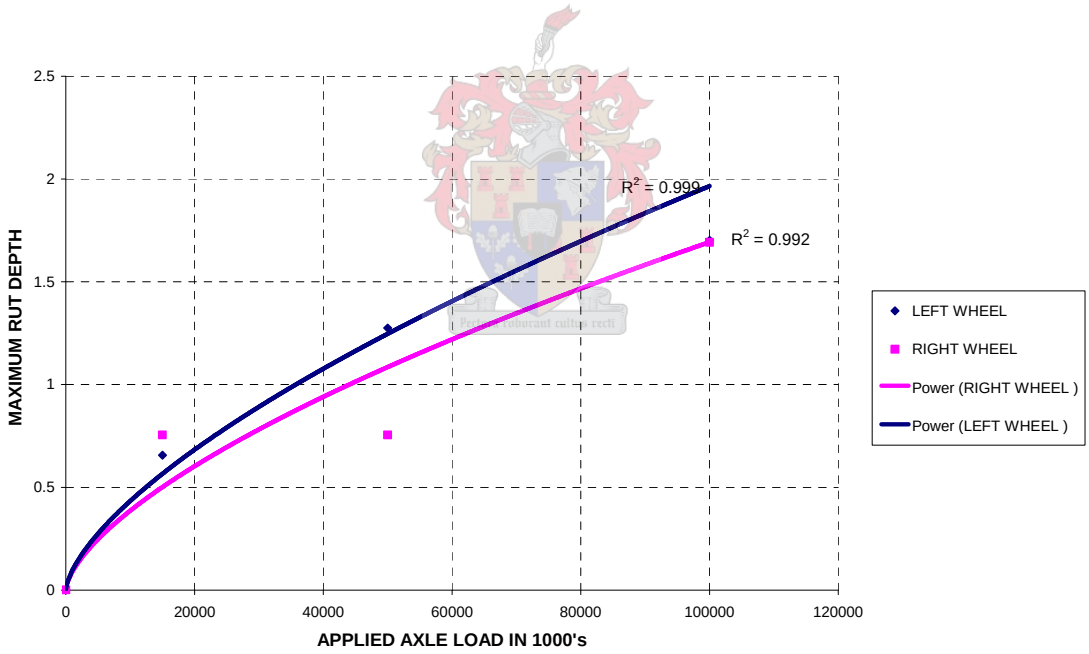

Figure D.6: Cumulative maximum rut depth for Test Section 5A

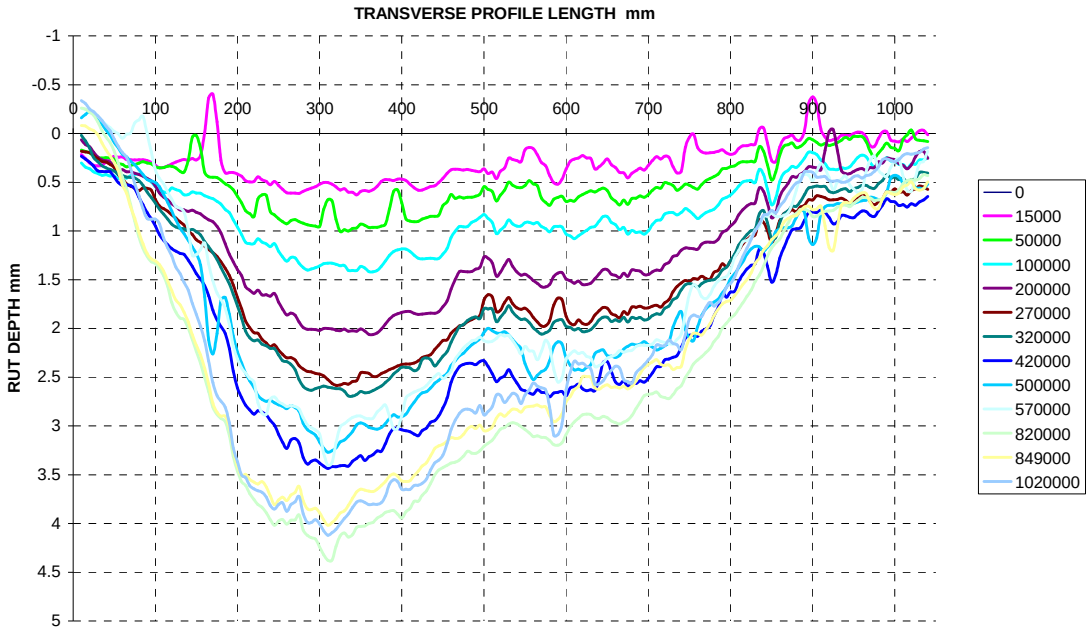

Figure D.7: Transverse rut profiles with load applications for Test Section 5B

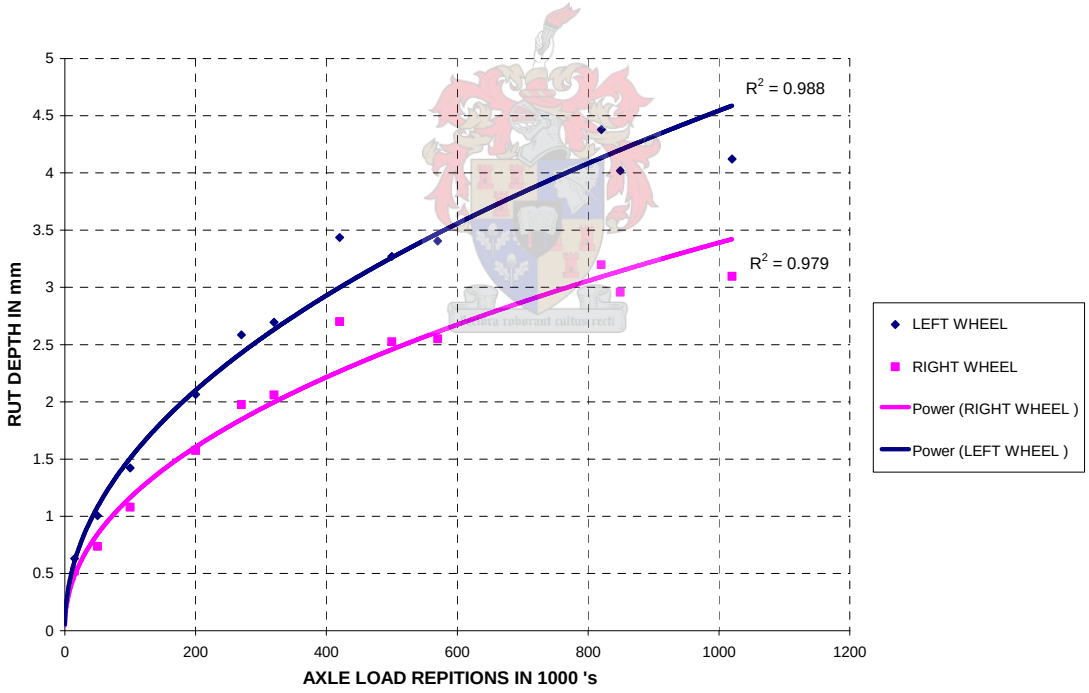

Figure D.8: Cumulative maximum rut depth for Test Section 5B

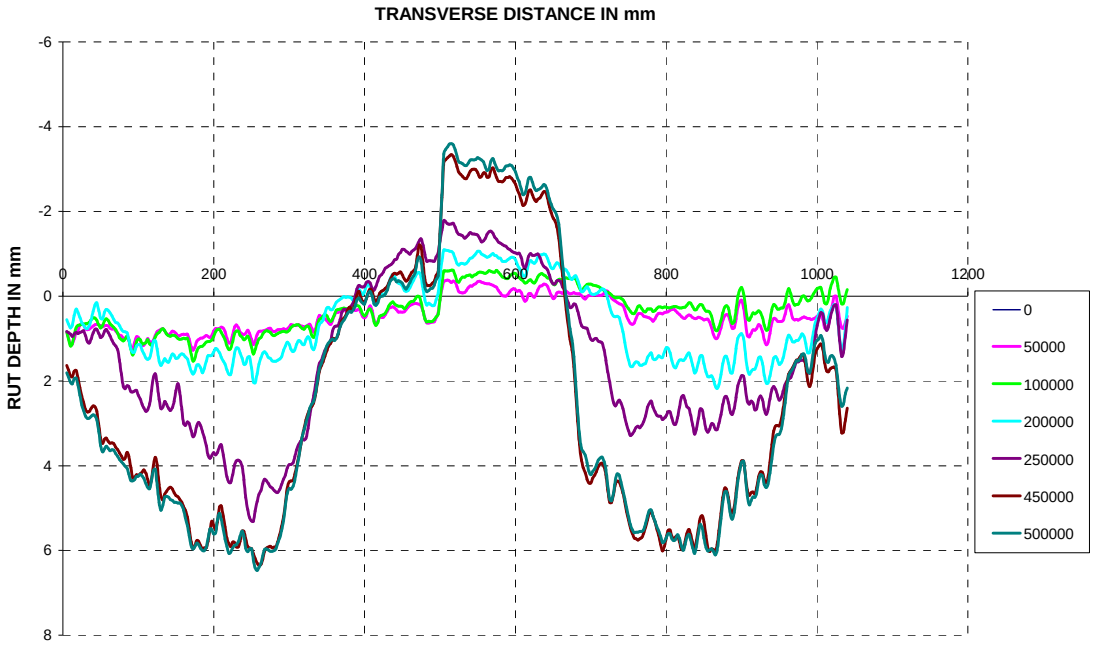

Figure D.9: Transverse rut profiles with load applications for Test Section 8

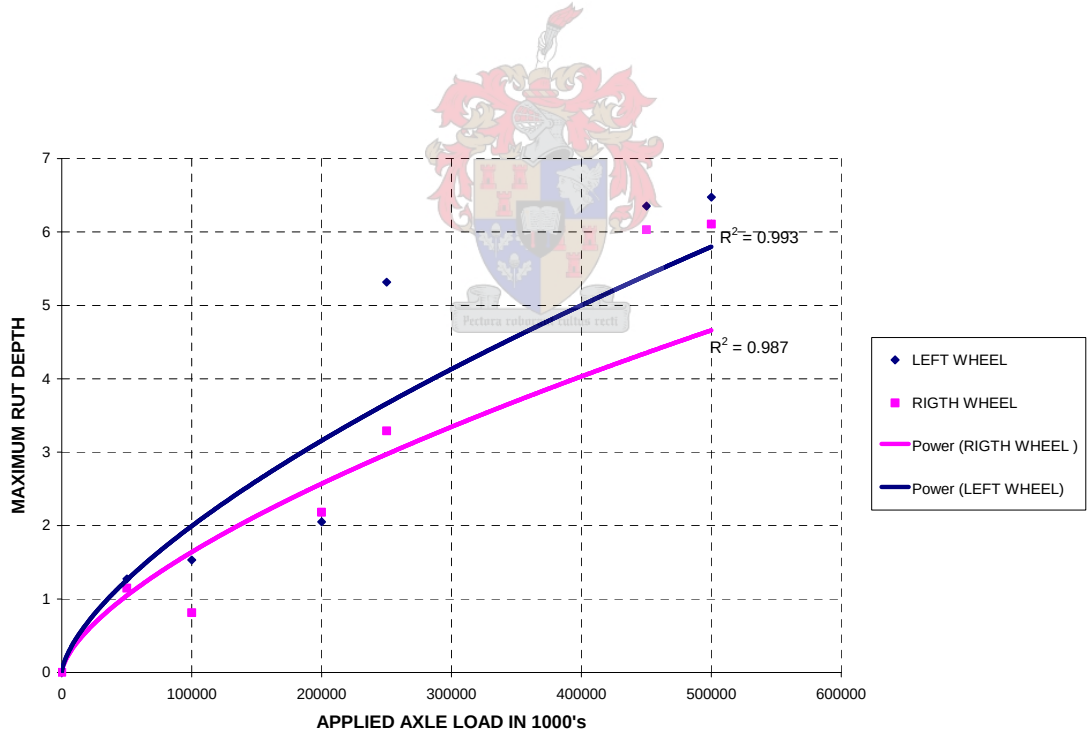

Figure D.10: Cumulative maximum rut depth for Test Section 8

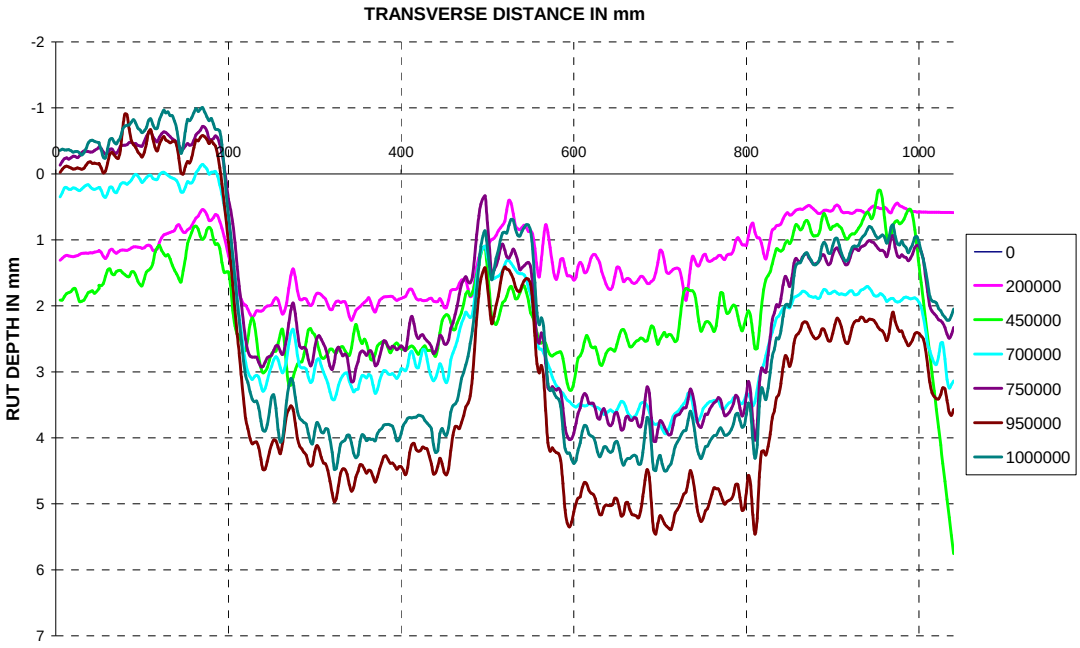

Figure D.11: Transverse rut profiles with load applications for Test Section 7

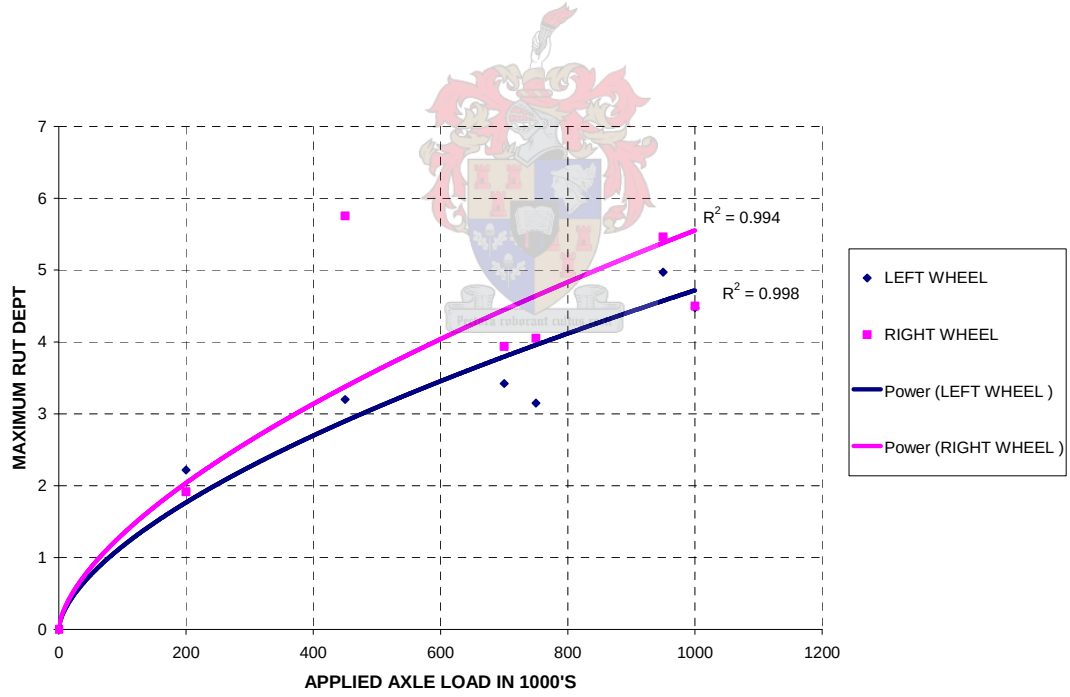

Figure D.12: Cumulative maximum rut depth for Test Section 7

Appendix E

SECTION 4A – MLS10

After 250 000 60 kN load applications


Surface crack initiation after 250 000 60 kN load applications


Surface crack initiation after 250 000 60 kN load applications


Surface crack initiation after 250 000 60 kN load applications

APPENDIX E

Surface crack initiation after 250 000 60 kN load applications

Diagonal shear crack development on outer edges of wheeltrack

Diagonal shear crack development on outer edges of wheeltrack

APPENDIX E

Diagonal shear crack development on outer edges of wheeltrack

After 270 000 60 kN load applications

Plan views of test section

Plan view of test section and illustration of the extent of rut formation

APPENDIX E

Transverse cracks in asphalt, still moist after wet trafficking

Transverse cracks in asphalt, still moist after wet trafficking and surface texture

After 285000 60 kN load applications

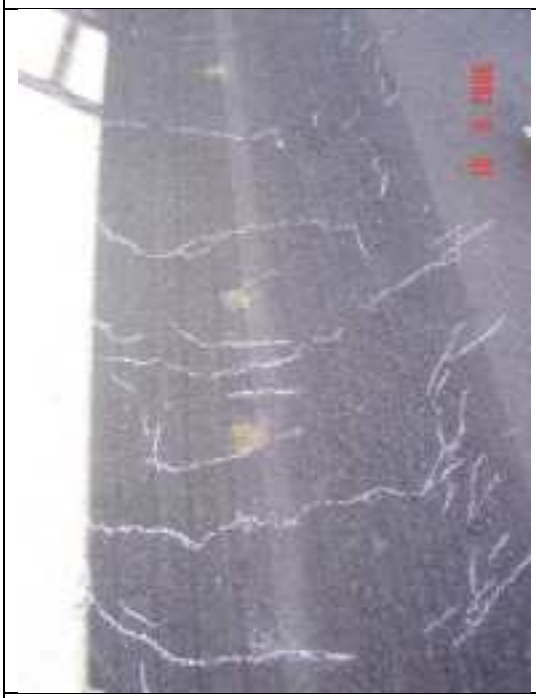

Plans views of test sections, with surface cracks marked

APPENDIX E


Transverse crack completed and material pumping

After 320 000 60 kN load applications

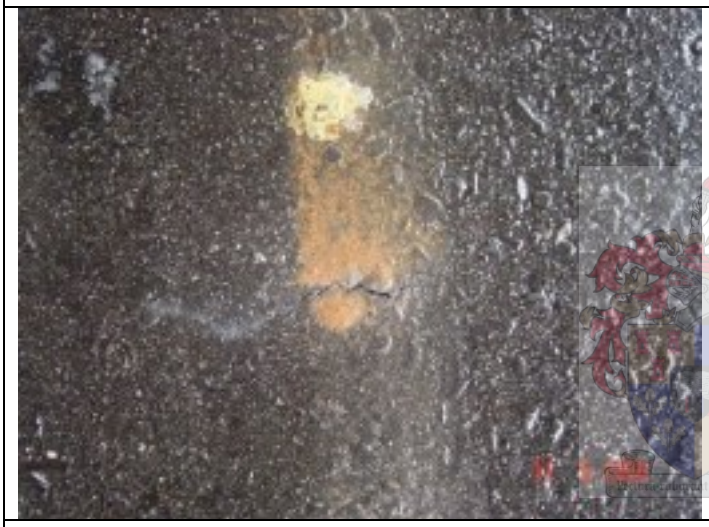
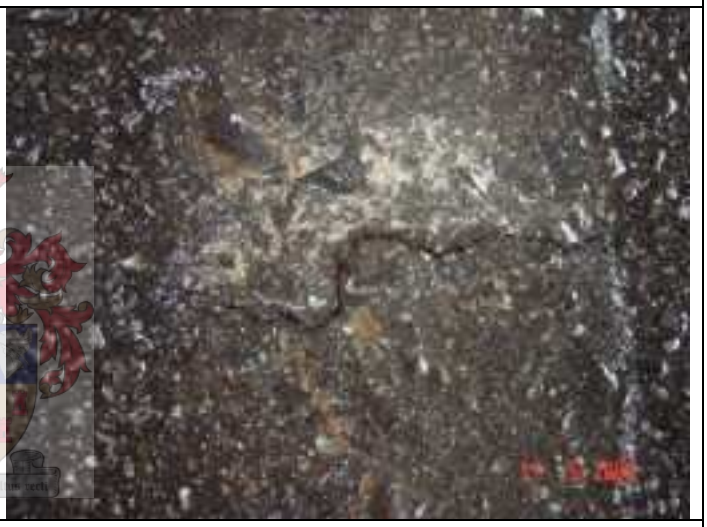

Sandy base material pumping through surface cracks


Surface crack pattern and texture after wet trafficking

APPENDIX E


Surface cracking pattern after wet trafficking, note completed transverse cracks, formation of longitudinal crack in left wheeltrack and material pumping.


Surface cracking pattern after wet trafficking, note completed transverse cracks, formation of longitudinal crack in left wheeltrack and material pumping.


Surface cracking pattern after wet trafficking, note completed transverse cracks, formation of longitudinal crack in left wheeltrack and material pumping.

APPENDIX E

After 320 000 60 kN load applications

Surface texture and visual rut profile

Plan views of test section with cracks drawn in with chalk

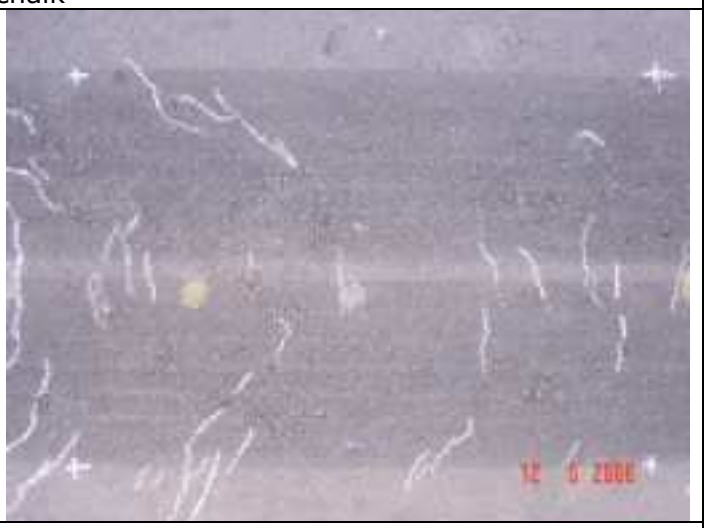

Plan views of test section with cracks drawn in with chalk

APPENDIX E


Plan and pictorial views of test section with cracks drawn in with chalk

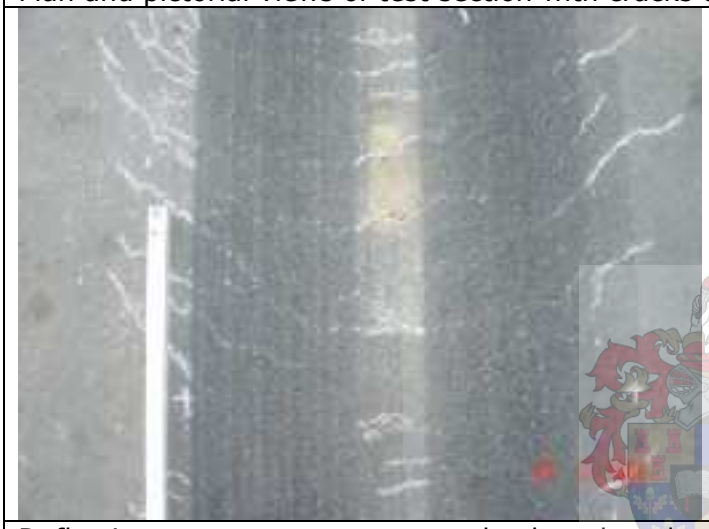


Deflection measurement next to wheel track and outline for diagnostic trenching


Underside of removed HMA surfacing block, note smooth surface due to interface distress

SECTION 4A – BLOCK PHOTOS

After 330 000 60 kN load applications

APPENDIX E

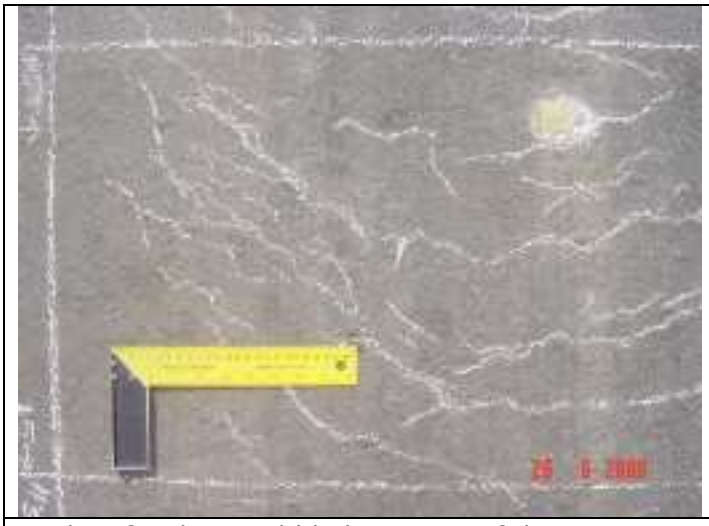

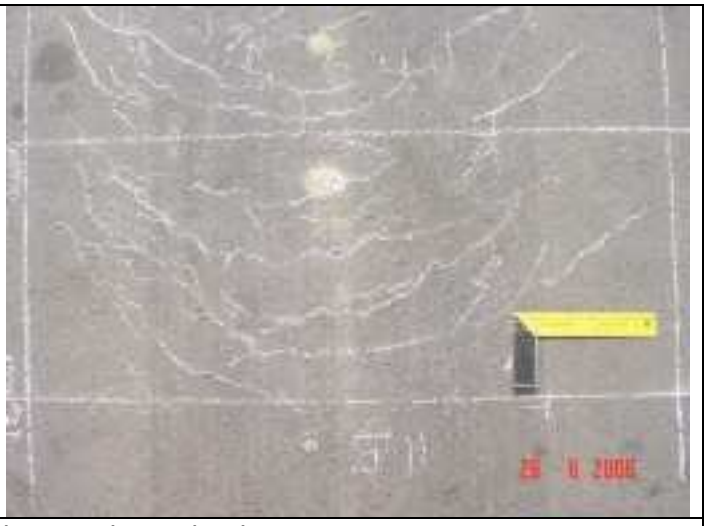

Outline for diamond blade cutting of diagnostic trenching with cracks drawn in

Underside of removed HMA surfacing block, note smooth surface due to interface distress

Underside of removed HMA slab and top view of CTB slab after removal of enclosed material

APPENDIX E

Longitudinal crack visible and top view of extraction operation

Longitudinal crack taken form the top side of the CTB block

Longitudinal crack taken form the top side of the CTB block as well as side view

APPENDIX E

Transverse crack in CTB, views taken from top of CTB block

Transverse crack in CTB, views taken from top of CTB block

Transverse crack in CTB, views taken from top of CTB block

APPENDIX E


Pictorial views of marco cracks found in CTB block during extraction


Pictorial views of marco cracks found in CTB block during extraction


Pictorial views of marco cracks found in CTB block during extraction

Appendix E

SECTION 4A – MLS10

After 250 000 60 kN load applications


Surface crack initiation after 250 000 60 kN load applications


Surface crack initiation after 250 000 60 kN load applications


Surface crack initiation after 250 000 60 kN load applications

APPENDIX E

Surface crack initiation after 250 000 60 kN load applications

Diagonal shear crack development on outer edges of wheeltrack

Diagonal shear crack development on outer edges of wheeltrack

APPENDIX E

Diagonal shear crack development on outer edges of wheeltrack

After 270 000 60 kN load applications

Plan views of test section

Plan view of test section and illustration of the extent of rut formation

APPENDIX E

Transverse cracks in asphalt, still moist after wet trafficking

Transverse cracks in asphalt, still moist after wet trafficking and surface texture

After 285000 60 kN load applications

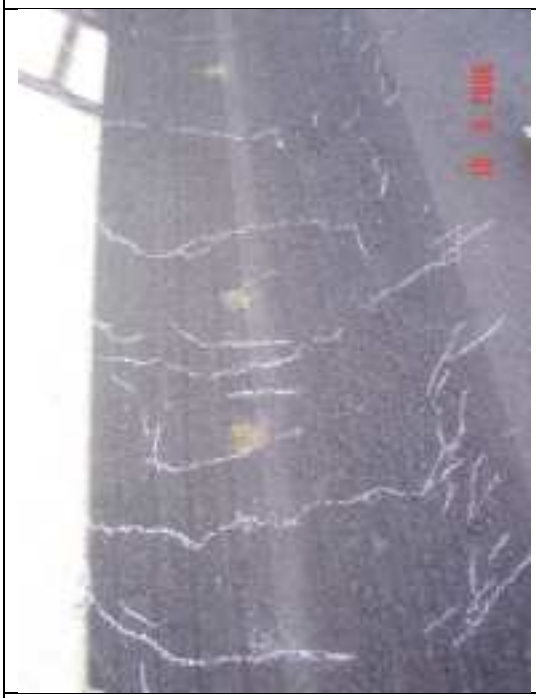

Plans views of test sections, with surface cracks marked

APPENDIX E


Transverse crack completed and material pumping

After 320 000 60 kN load applications

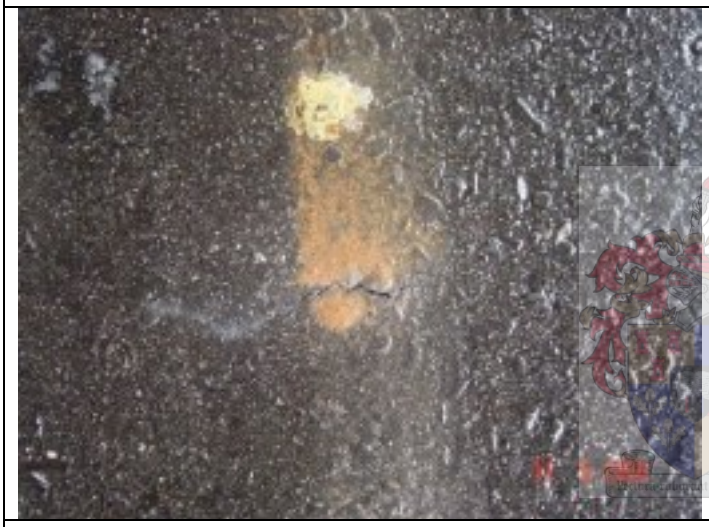
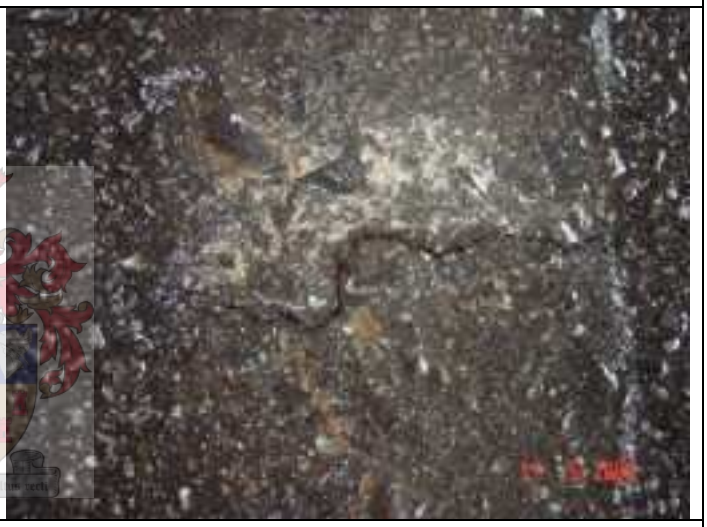

Sandy base material pumping through surface cracks


Surface crack pattern and texture after wet trafficking

APPENDIX E


Surface cracking pattern after wet trafficking, note completed transverse cracks, formation of longitudinal crack in left wheeltrack and material pumping.


Surface cracking pattern after wet trafficking, note completed transverse cracks, formation of longitudinal crack in left wheeltrack and material pumping.


Surface cracking pattern after wet trafficking, note completed transverse cracks, formation of longitudinal crack in left wheeltrack and material pumping.

APPENDIX E

After 320 000 60 kN load applications

Surface texture and visual rut profile

Plan views of test section with cracks drawn in with chalk

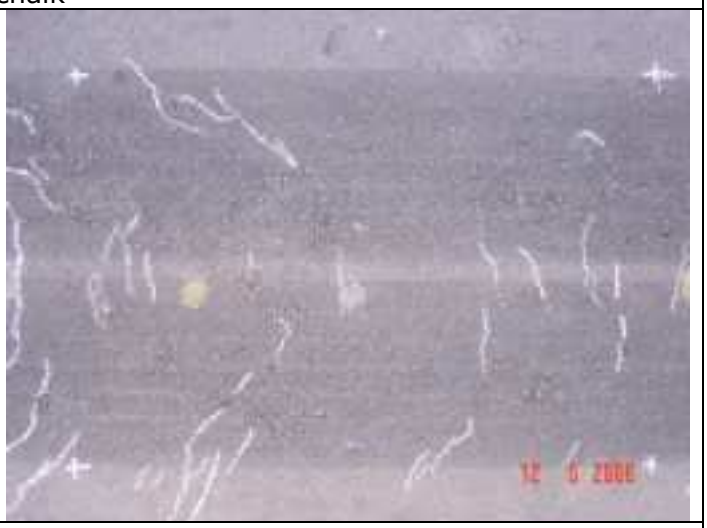

Plan views of test section with cracks drawn in with chalk

APPENDIX E


Plan and pictorial views of test section with cracks drawn in with chalk

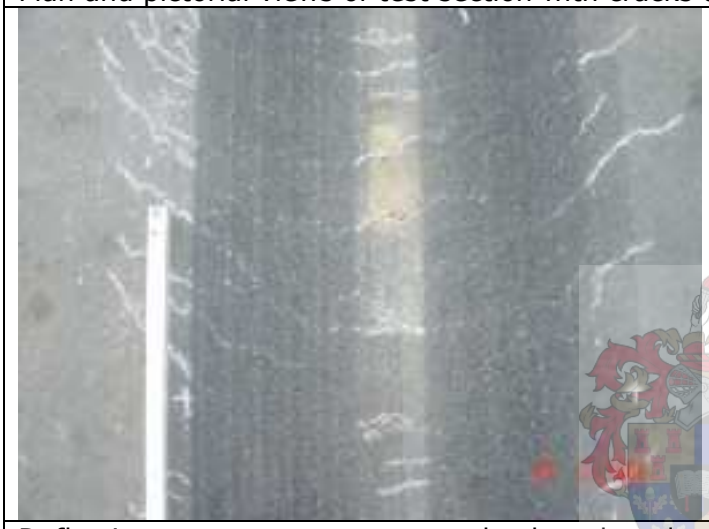


Deflection measurement next to wheel track and outline for diagnostic trenching


Underside of removed HMA surfacing block, note smooth surface due to interface distress

SECTION 4A – BLOCK PHOTOS

After 330 000 60 kN load applications

APPENDIX E

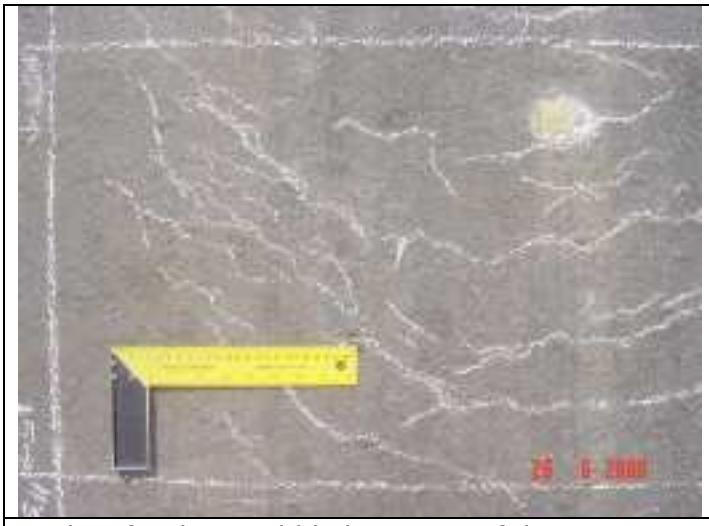

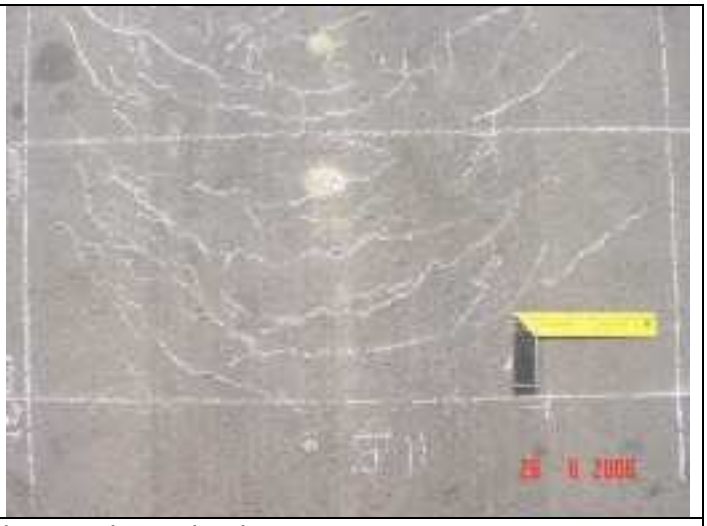

Outline for diamond blade cutting of diagnostic trenching with cracks drawn in

Underside of removed HMA surfacing block, note smooth surface due to interface distress

Underside of removed HMA slab and top view of CTB slab after removal of enclosed material

APPENDIX E

Longitudinal crack visible and top view of extraction operation

Longitudinal crack taken form the top side of the CTB block

Longitudinal crack taken form the top side of the CTB block as well as side view

APPENDIX E

Transverse crack in CTB, views taken from top of CTB block

Transverse crack in CTB, views taken from top of CTB block

Transverse crack in CTB, views taken from top of CTB block

APPENDIX E


Pictorial views of marco cracks found in CTB block during extraction


Pictorial views of marco cracks found in CTB block during extraction


Pictorial views of marco cracks found in CTB block during extraction

Appendix F

SECTION 4B – MLS10

Zero Axle Applications

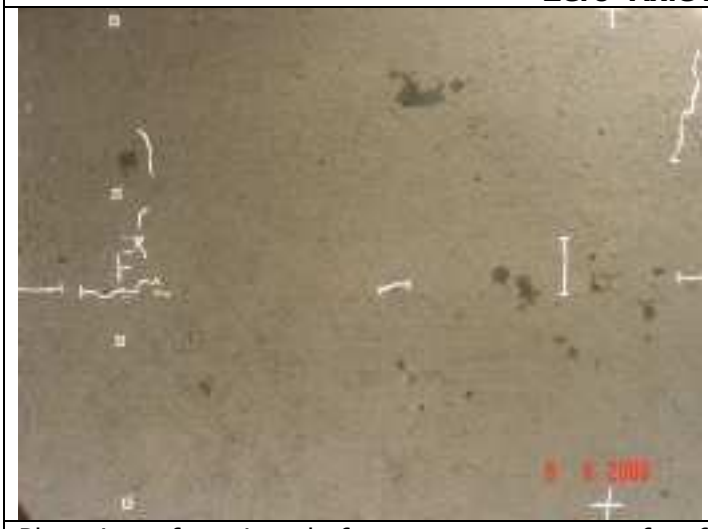

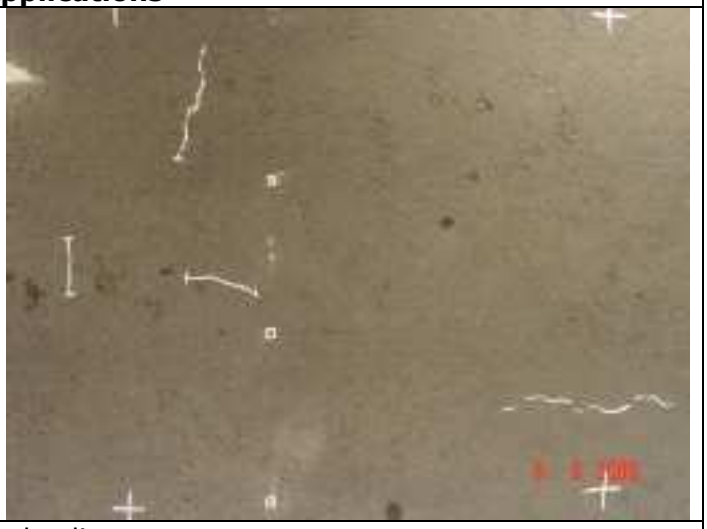

Plan view of sections before commencement of traffic loading

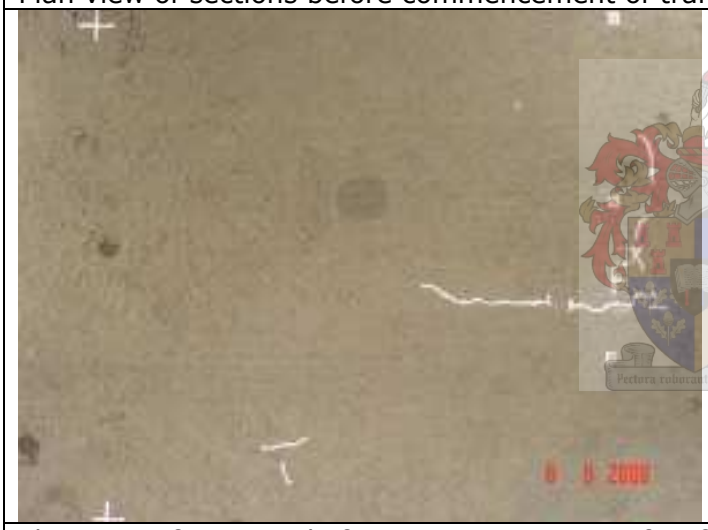

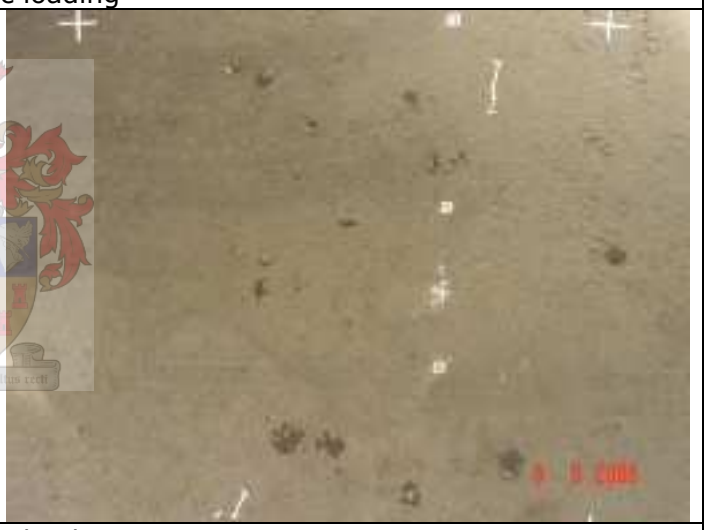

Plan view of sections before commencement of traffic loading

After 100 000 70 kN load applications

Plan view of sections after first 100 000 70 kN axles of traffic loading

After 100 000 70 kN Load Applications

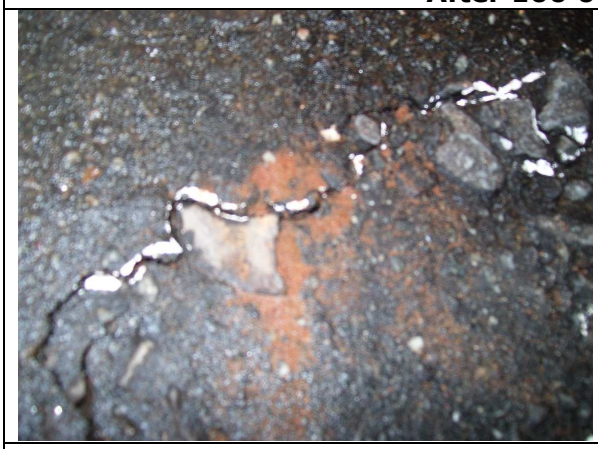


Asphalt cracks with fine base material pumping through


Asphalt cracks with fine base material pumping through


Plan view of test sections, note vertical asphalt and diagonal in plane shear cracking


Plan view of test sections, note vertical asphalt and diagonal in plane shear cracking

SECTION 4B – BLOCK PHOTOS
150 000k


Top of CTB after extraction of HMA and side view of vertical HMA shear


Side view of vertical HMA shear and plan view of CTB block before extraction


Pictorial view of extracted blocks

APPENDIX F

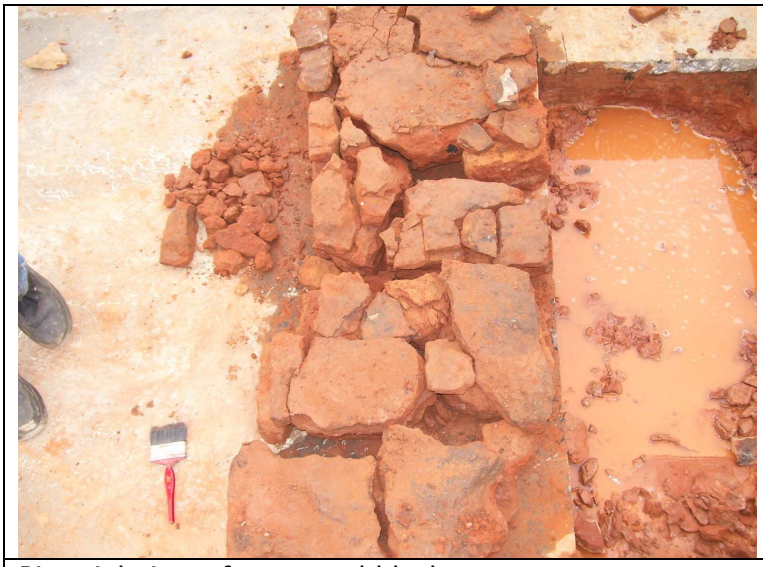

Pictorial view of extracted blocks

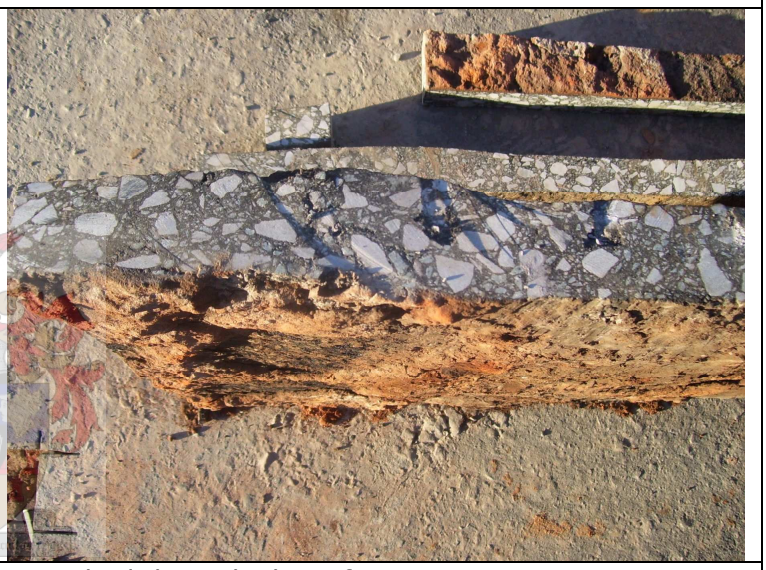

Side views of removed HMA mat note interface surfaces smoothed through shear fatigue

Plan view of HMA slab note smoothed surfaces. Top view of CTB block before extraction – Test pit 2

Plan view of HMA slab note smoothed surfaces. Test pit 3. Pictorial view of extraction of CTB blocks with hydraulic jacks

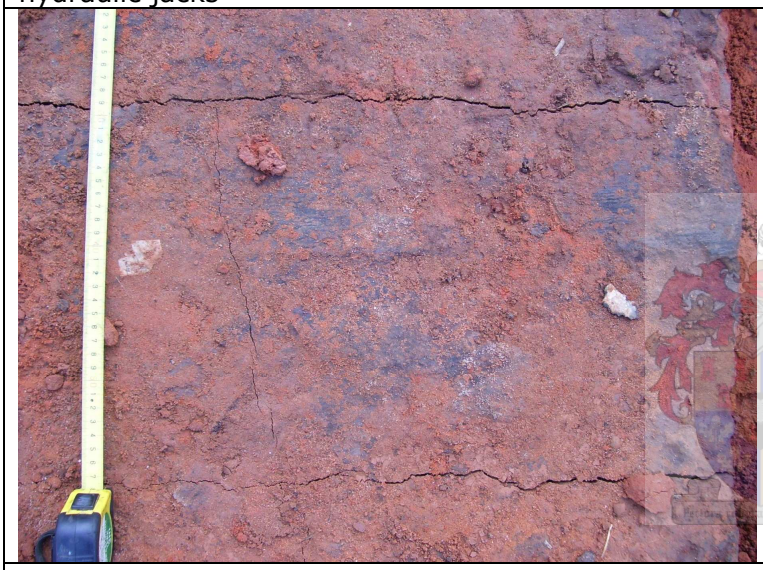

Plans views of CTB blocks from test pits 2 and 3 note longitudinal cracks

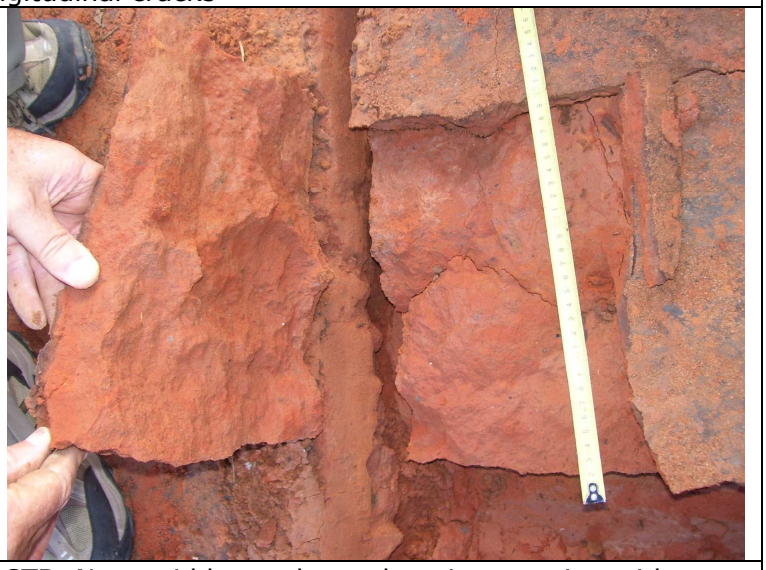

Pictorial overview of blocks and extraction of top part of CTB. Note mid layer shear plane intersecting with longitudinal and transverse cracks

APPENDIX F


Pictorial overview of extraction. Plan view of CTB block. Note smoothed top surface.


Plan view of CTB block. Note smoothed top surface.


Plan and side view of CTB block. Note smoothed top surface.

APPENDIX F


Pictorial views of diagnostic trench after excavation.


Pictorial views of diagnostic trench after excavation.


Removed CTB blocks from test pits 2 and 3. Note longitudinal cracks in direction of wheel travel and in plane shear cracking at the middle of the combined HMA and CTB structure.

APPENDIX F

Plan view of extracted CTB blocks.

Appendix G

SECTION 5A – MLS10
ZERO AXLES

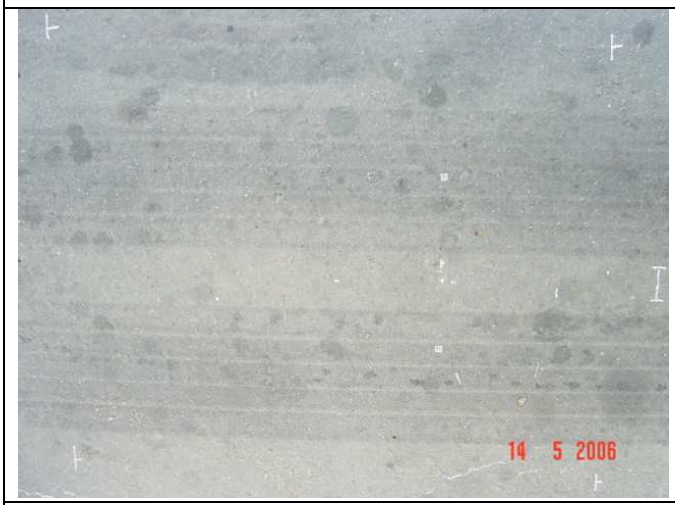

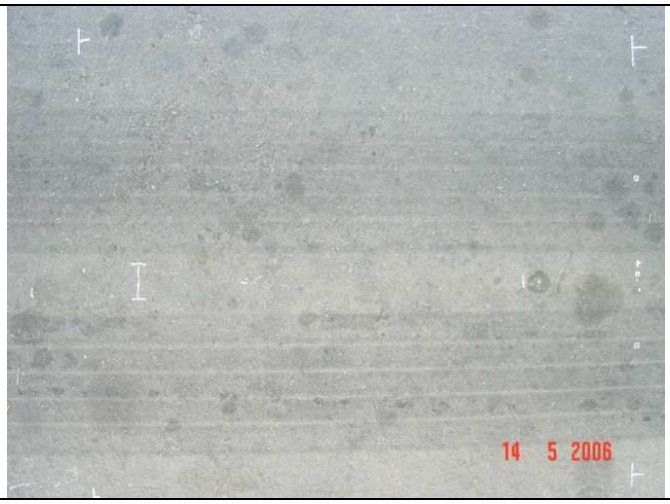

Plan views of section before commencement of axle load trafficking

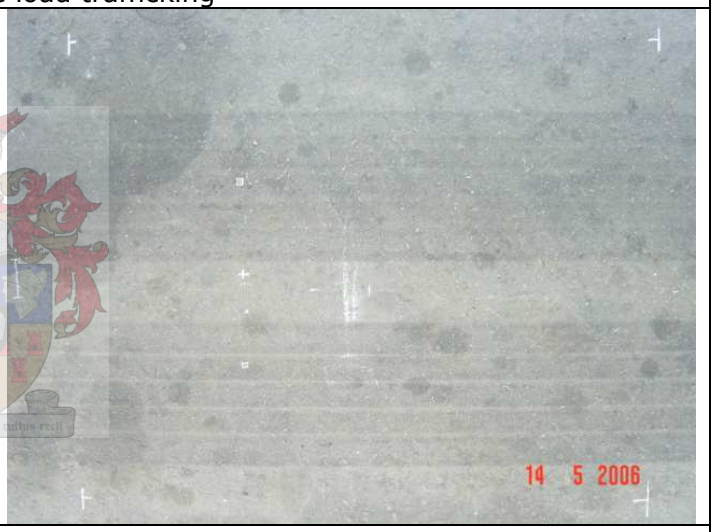

Plan views of section before commencement of axle load trafficking

Appendix H

SECTION 5B – MLS10

After 320 000 60 kN load applications


Pictorial overview of test section. HMA surface texture.


HMA surface texture. Note stripping of asphalt


Transverse crack formation


Asphalt surface texture. Plan view of test section

After 820 000 60 kN load applications


Plan views of test section with crack patterns marked with chalk


Plan views of test section with crack patterns marked with chalk

APPENDIX H

Pictorial overview of test section with crack patters marked with chalk.

Appendix I

SECTION 8C – MLS10

After 500 000 70 kn load applications

Plan views of test section with crack marked in white

Plan views of test section with crack marked in white

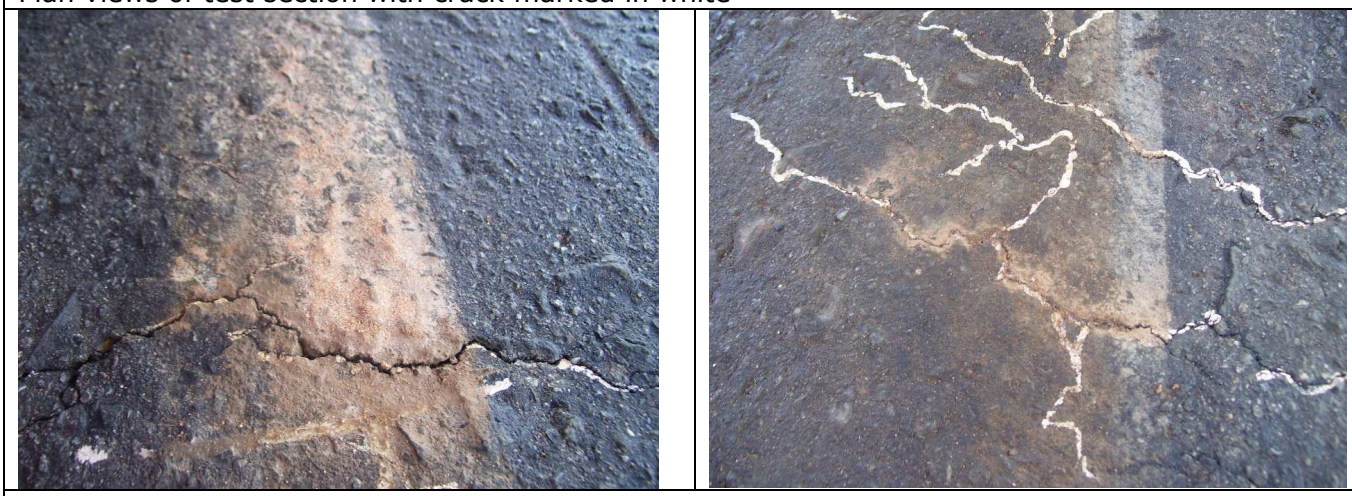

Close ups of material pumping through cracks in asphalt

After 600 000 70 kN load applications

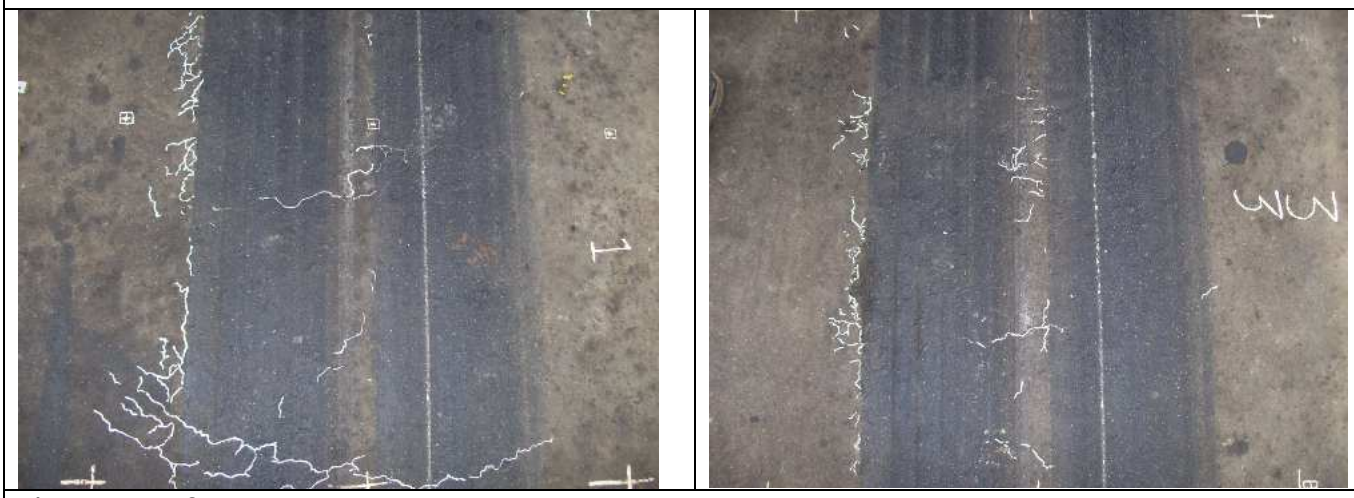

Plan views of test section

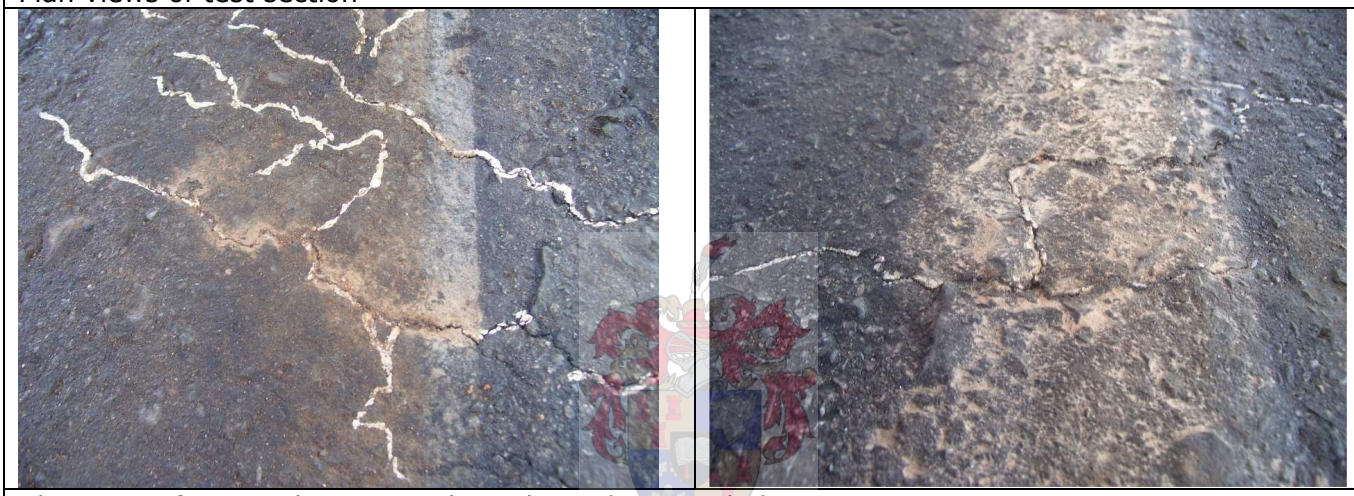

Close ups of material pumping through cracks in asphalt

After 700 000 70 kN load applications

Vertical shear and disintegration on the sides of the wheeltrack


HMA heaving and cracking on the side of the wheeltrack

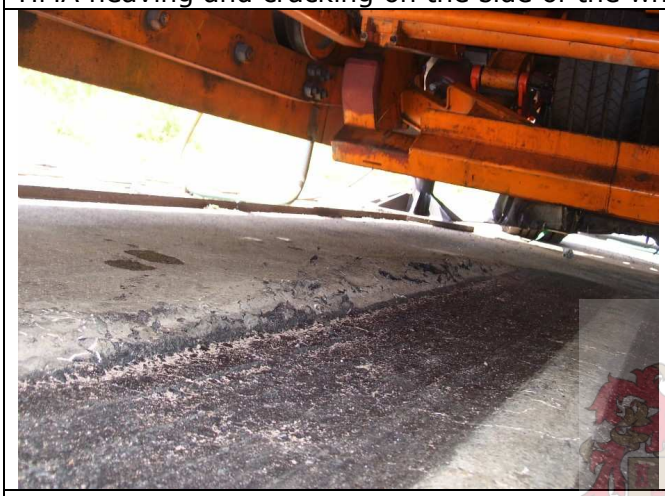


HMA heaving and cracking on the side of the wheeltrack

After 720 000 70 kN load applications


HMA heaving and cracking on the side of the wheeltrack. Note extensive crack pattern in wheeltrack


Heaved HMA on side of wheeltrack

After 790 000 70 kN load applications


Plan views of base material pumped out of test section. Note extensive crack patterns


Plan and pictorial views of base material pumped out of test section. Note extensive crack patterns

Plan views of test section before removal of HMA

Plan views of test section before removal of HMA

SECTION 8C – BLOCK PHOTOS

Underside of removed HMA mat. Note smoothed interface surface due to shear fatigue.

APPENDIX I

Plan view of CTB after removal of HMA mat

Close up of CTB surface after removal of HAM. Note smoothed surface texture.

Close up of CTB surface after removal of HAM. Note smoothed surface texture. Underside of HMA mat removed from test pit 2.

APPENDIX I

Close ups of HMA vertical shear

Underside of HMA mat after removal of test pit 3. Pictorial overview of all test pits with HAM removed.

Removal of CTB fractures.

APPENDIX I

Removal of CTB fractures. Plan view of test pit during removal of CTB fractures note the size ot the fractures.

Fractured CTB and plan view of test pit after removal of CTB fractures.

Pictorial overviews with fractures placed bedise test pit.

APPENDIX I

Removed CTB blocks and fractures. Overview of test pits.

After completion of diagnostic trenching note reconstituted CTB slab in front of picture.

Appendix J

SECTION 7A – MLS10

After 100 000 70 kN load applications

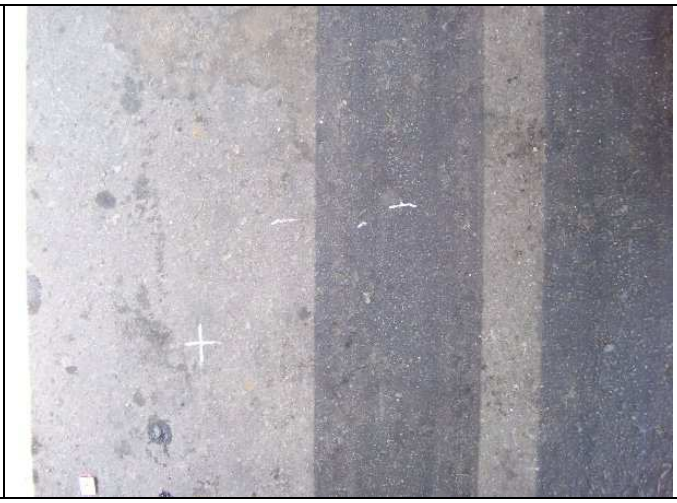

Plan views of test sections with cracks marked in white

Plan views of test sections with cracks marked in white

Plan views of test sections with cracks marked in white


Plan views of test sections with cracks marked in white


Plan views of test sections with cracks marked in white


Plan views of test sections with cracks marked in white


Plan views of test sections with cracks marked in white

After 1050 000 70 kN load applications

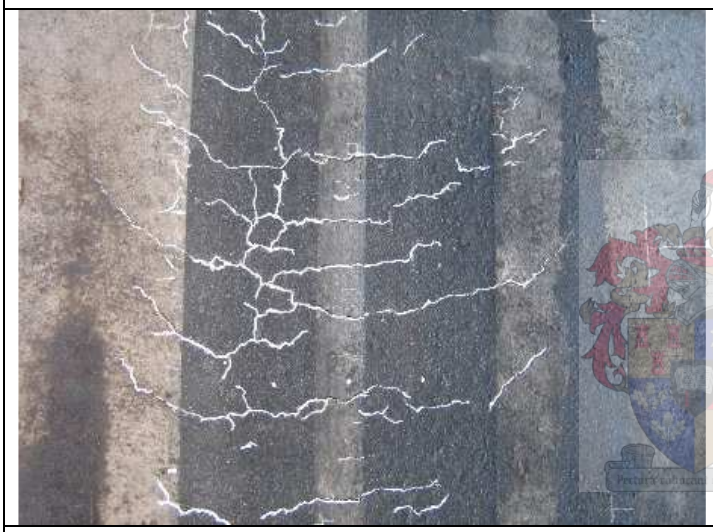


Plan views of test sections with cracks marked in white

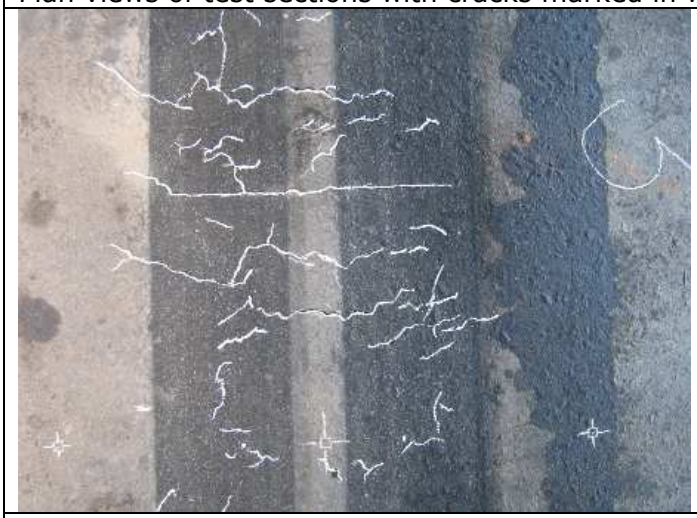


Plan views of test sections with cracks marked in white

APPENDIX J


Plan views of test sections with cracks marked in white


Pictorial overviews of test section with cracks marked in white.


Pictorial overviews of test section with cracks marked in white.

Appendix K

Stiffness – Deflection relation

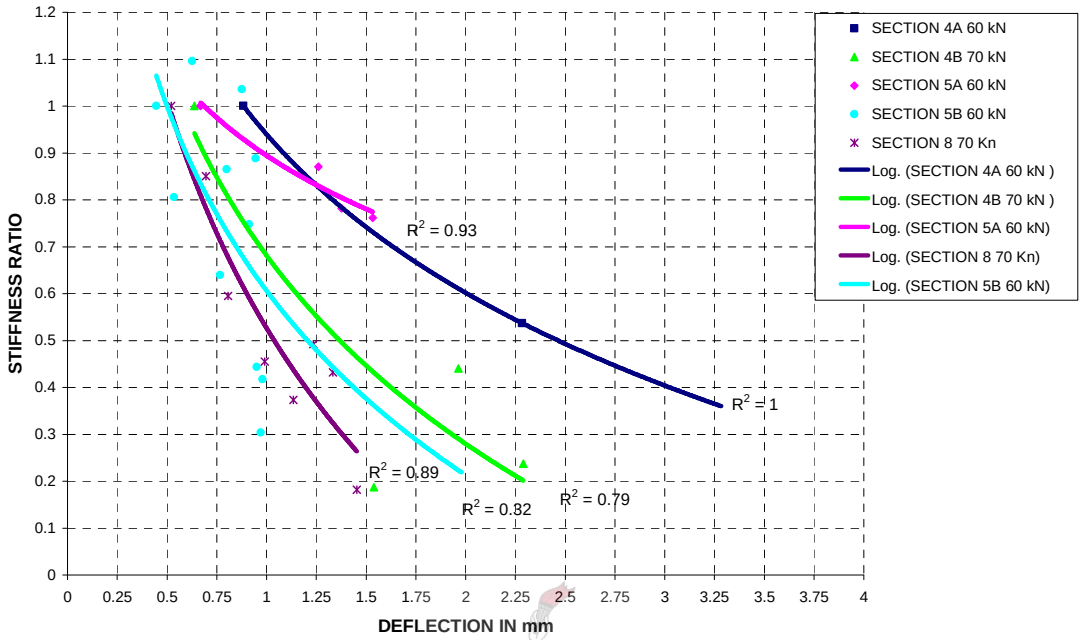

Figure K.1: Stiffness Deflection relations for base materials tested (Deflection in mm)

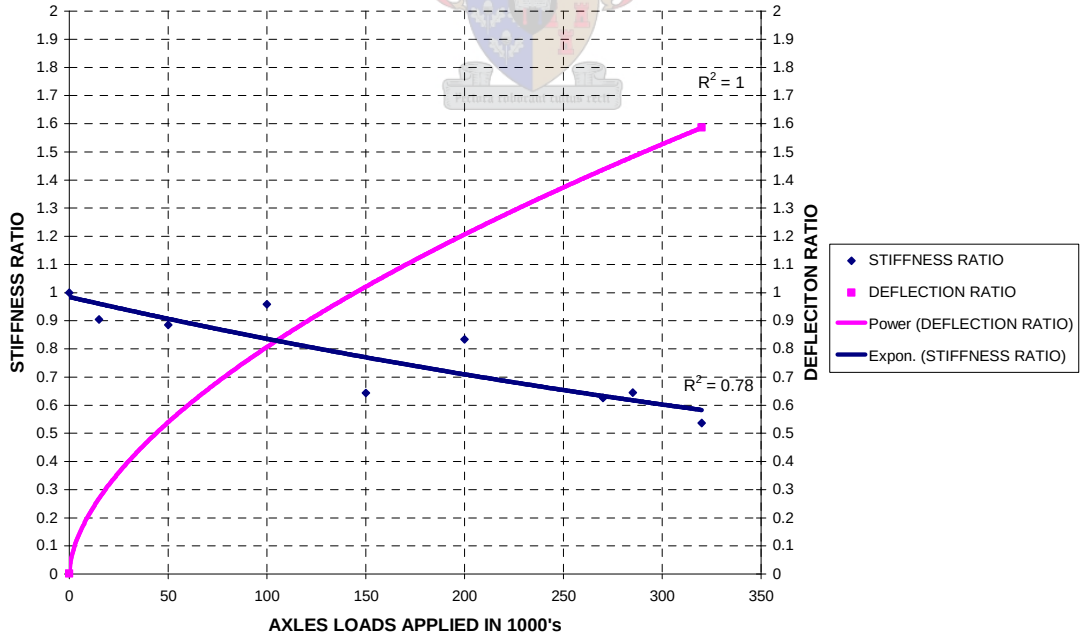

Figure K.2: Stiffness Deflectoin performacne of 5 % Cement stabilized Red base material under 60 kN axle laoding

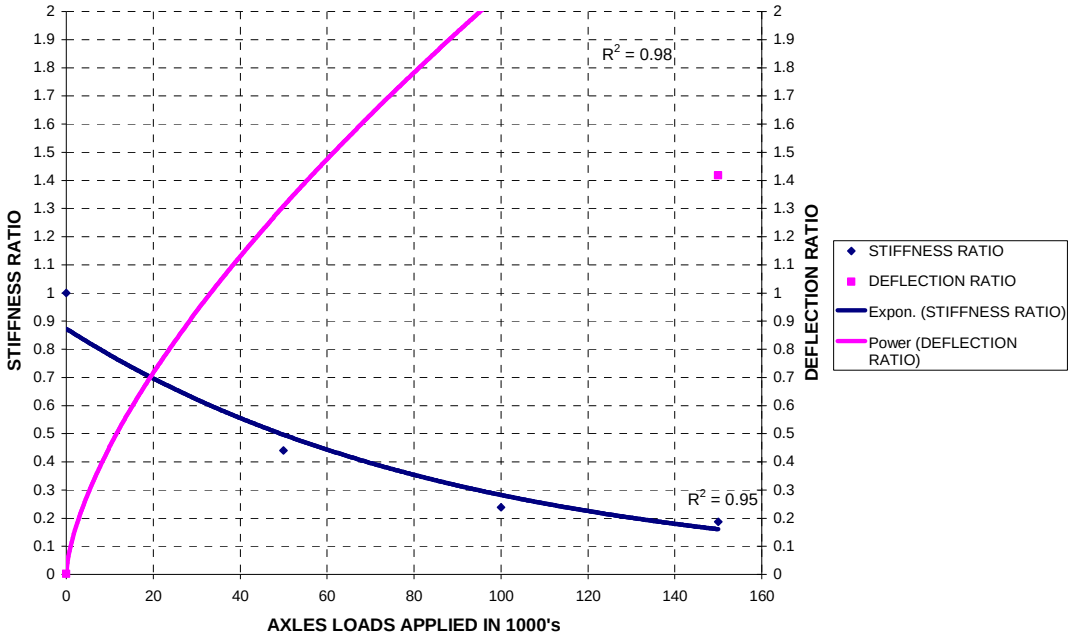

Figure K.3: Stiffness Deflectoin performacne of 5 % Cement stabilized Red base material under 70 kN axle laoding

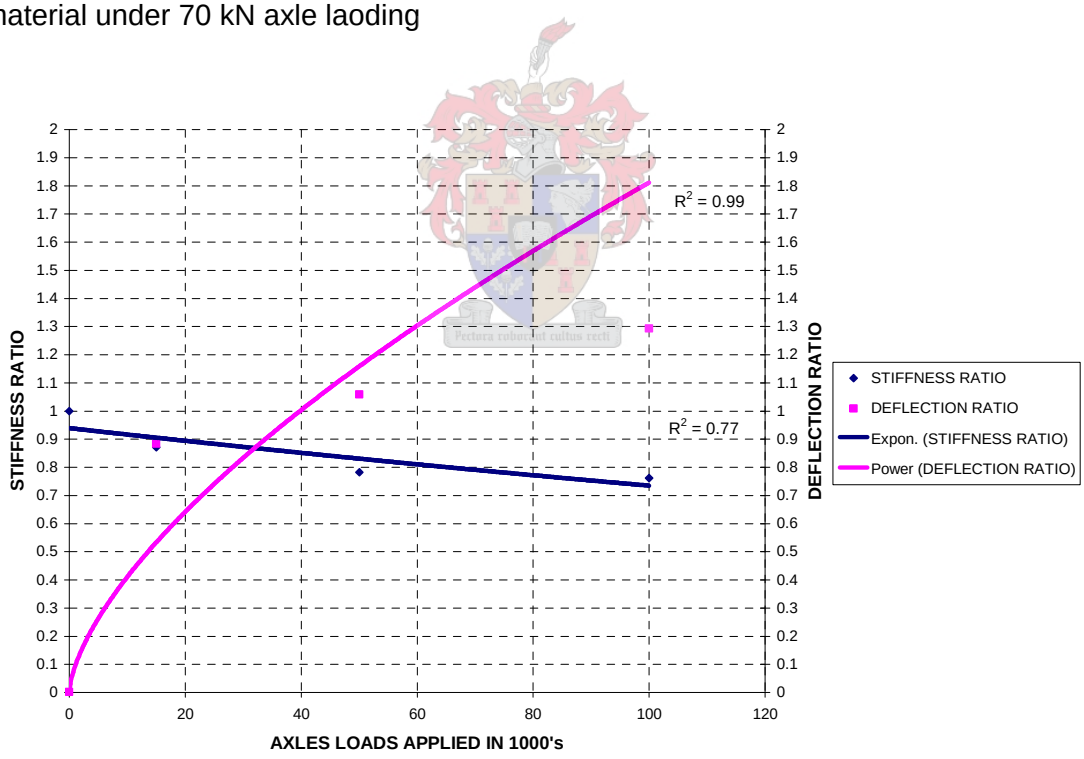

Figure K.4: Stiffness Deflectoin performacne trends of 2.5 % Cement and 2.5 % Lime stabilized Red base material under 60 kN axle laoding

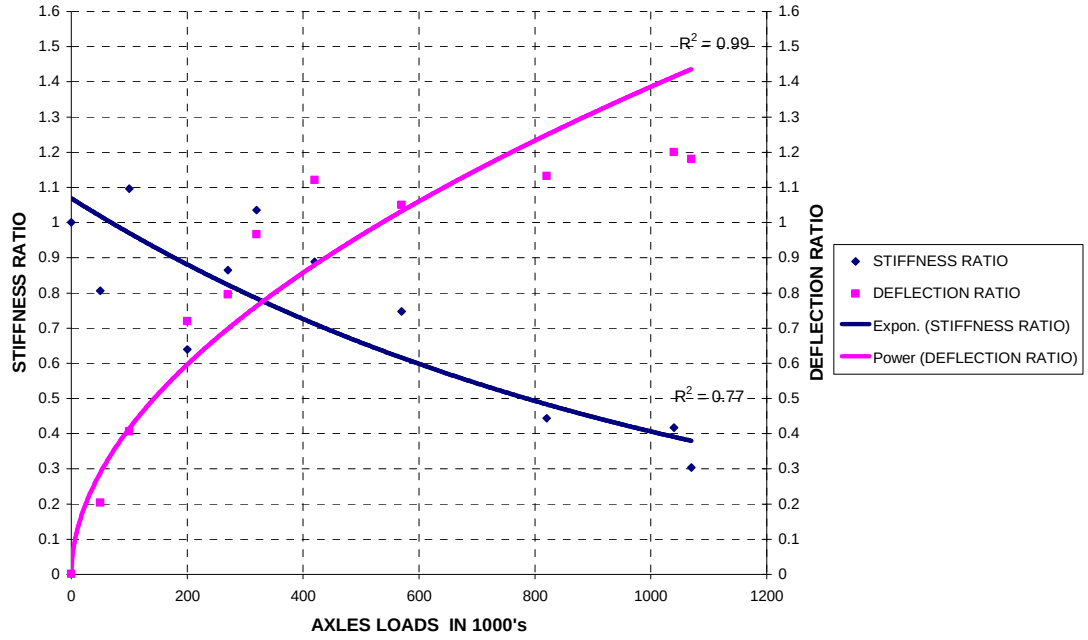

Figure K.5: Stiffness Deflectoin performacne of 2.5 % Cement and 2.5 % Lime stabilized Red base material under 60 kN axle laoding

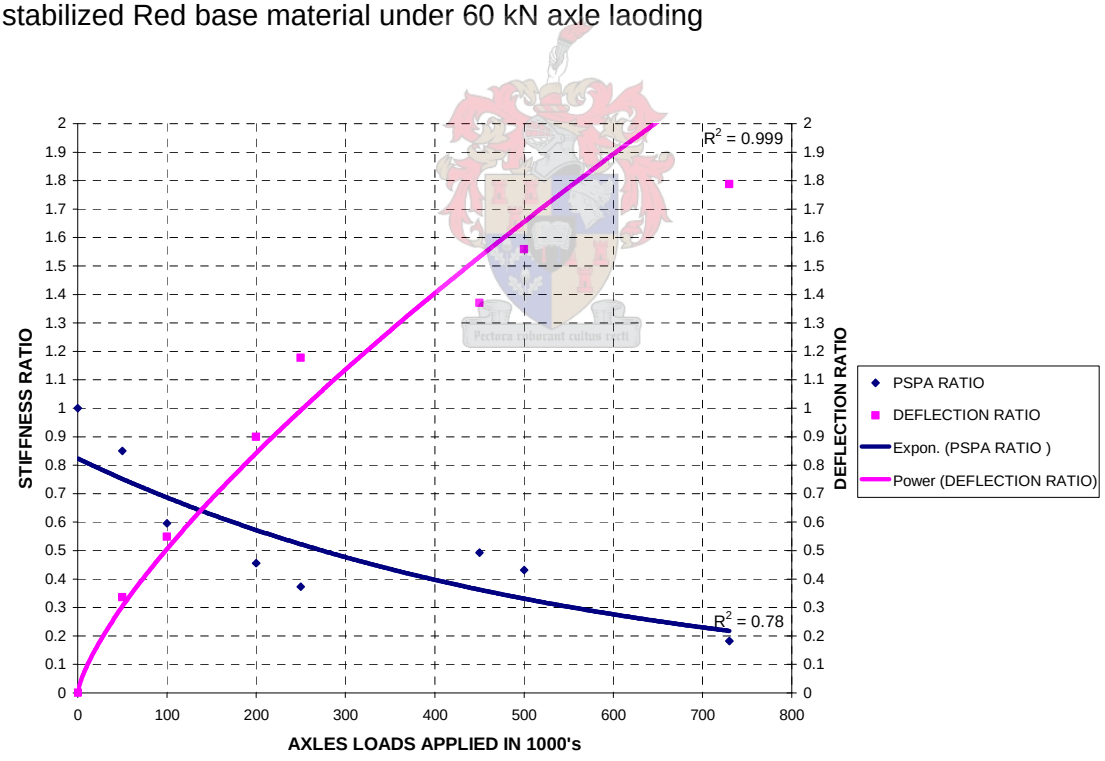

Figure K.6: Stiffness Deflectoin performacne trends of 7 % Cement stabilized Red base material under 70 kN axle laoding